NOTICE

The quality of this microform is heavily dependent upon the quality of the original thesis submitted for microfilming. Every effort has been made to ensure the highest quality of reproduction possible.

If pages are missing, contact the university which granted the degree.

Some pages may have indistinct print especially if the original pages were typed with a poor typewriter ribbon or if the university sent us an inferior photocopy.

AVIS

La qualité de cette microforme dépend grandement de la qualité de la thèse soumise au microfilmage. Nous avons tout fait pour assurer une qualité supérieure de reproduction.

S'il manque des pages, veuillez communiquer avec l'université qui a conféré le grade.

La qualité d'impression de certaines pages peut laisser à désirer, surtout si les pages originales ont été dactylographiées à l'aide d'un ruban usé ou si l'université nous a fait parvenir une photocopie de qualité inférieure.

NL-339 (r. 88/04) c

Canada

A FUNDAMENTAL STUDY OF THE EFFECT OF GRAVITY ON THE STATIC AND DYNAMIC BEHAVIOR OF ROBOTS

by

M. E. MAHJOUB

A Thesis

presented to the University of Ottawa

in partial fulfillment of the

requirement for the degree of

DOCTOR OF PHILOSOPHY

in

MECHANICAL ENGINEERING

September 1990

ISBN 0-315-68053-9

UNIVERSITÉ D'OTTAWA
UNIVERSITY OF OTTAWA

For her love and patience

dedicated to my mother

Abstract

The gravity induced force on revolute robot links is generally comparable to the dynamic induced forces at high operational speeds. At low speeds this force dominates over the dynamic forces. In the process of study of the static and dynamic behaviour of manipulators through the overall measures such as the force ellipsoid, the dynamic manipulability ellipsoid, and the generalized ellipsoid of inertia the effect of gravity is ignored due to the complexity that the inclusion of this force brings to the analysis.

This study presents a method to include the effect of gravity in the static and dynamic analysis of robot arms. Using the concept of fields, the gravity induced forces acting on individual links are replaced by a single force, called here the generalized weight of the arm. The generalized weight is a force that acts at the end effector and its magnitude and direction are functions of the configuration of the manipulator. Since the system is conservative, the generalized weight is considered to be the gradient of a potential field that will be called here the generalized gravitational field (GGF). This field alone can illustrate the overall effect of gravity on the manipulator throughout its work volume.

The generalized weight field is then integrated with the force ellipsoid to display the true force that a manipulator can apply to its environment. Based on the generalized weight field and the generalized inertia tensor the generalized gravitational acceleration field is introduced. The dynamic manipulability ellipsoid is then superimposed on this field to demonstrate the true acceleration capability of the end effector. The relation between the generalized weight and the generalized ellipsoid of

inertia is investigated.

Effect of change of physical parameters of the arm are also discussed. It is shown that for a particular design of manipulators the generalized gravitational field is absolutely flat, and in general the manipulators's physical parameters may be used to taylor the GGF for a particular application.

In Appreciation

I like to thank Dr. A. Fahim, my supervisor for his constant support, encouragement and guidance throughout the course of the research and in the writing of this thesis.

My thanks go also to several of my colleagues in room B203, specially Dr. Gordon Holloway with whom I had long discussions about the ideas that are developed to this work.

Appreciation should be extended to the staff of the department of mechanical engineering for their sincere cooperation.

Beyond the invaluable support accorded by numerous people in the course of writing these chapters, more personal obligations must be acknowledged. My immediate family demonstrated a great deal of confidence in this enterprise by their consistent patience and encouragement. Their understanding acceptance of a studious preoccupation with books, Journals, and computers, which has sometimes been accompanied by neglect of other duties, places the author deeply in their debt, a debt that can be repaid only in small part by the affectionate appreciation towards my wife and our daughters Maryam and Meregon.

Contents

List of Figures

List of Tables

Glossary of Terms

Roman Symbols

$\mathbf{A}$	Generalized acceleration vector.
$\mathbf{B}$	Base matrix of the force ellipsoid.
$\mathbf{C}$	Diagonalizing matrix, Coriolis forces.
C_i	Cosine of the angle θ_i.
$\mathbf{D}$	Base matrix of the acceleration ellipsoid.
$\mathbf{e_i}$	Unit vectors in joint space.
$\mathbf{F}$	Generalized task force.
g	Acceleration of gravity.
$\mathbf{G}$	Generalized gravitational acceleration vector.
h_i	Distance from joint i to center of mass of link i.
$\mathbf{i_i}$	Unit vectors in Cartesian space.
$\mathbf{I}$	Matrix of moments of inertia of the links.
I_i, I_{ii}	Longitudinal moment of inertia of the links.
$\mathbf{J}$	Jacobian matrix.

$\mathbf{K}$	Diagonalized matrix of joint motors constants.
K_{mi}	Motor constant of the joint i.
L_i	Length of the link i.
m_i	Mass of the link i.
m_p	Mass of the payload.
$\mathbf{M}$	Generalized inertia tensor.
p	Input power to the individual joint motors.
P	Total input power to the joint motors.
R_{min}, R_{max}	Minor and major radii of ellipsoids respectively.
S_i	Sine of the angle θ_i.
u, U	Normalized and actual potential energy of the arm respectively.
u_i	Coordinates of principal space.
$\mathbf{V}, \dot{\mathbf{V}}$	Velocity and acceleration vectors in task space respectively.
$\mathbf{w}, \mathbf{W}$	Normalized and actual vectors of generalized weigh respectively.
w_i, W_i	Normalized and actual components of generalized weight.
x_i	Coordinates of Cartesian space.
$\mathbf{Z}$	Base matrix of the dummy ellipsoid.

Greek Symbols

$\zeta_A, \zeta_B, \zeta_M$	Aspect ratios of the acceleration ellipsoid, force ellipsoid and generalized ellipsoid of inertia respectively.
η_d, η_m	Direction and magnitude indices respectively.
$\theta_i, \dot{\theta}_i, \ddot{\theta}_i$	Angular position, speed and acceleration of joint i respectively.
λ_i	Eigenvalues of the force ellipsoids.
μ	Lagrange multiplier.
ρ_i	Eigenvalues of the acceleration ellipsoids.
σ_i	Eigenvalues of the generalized ellipsoid of inertia.
τ_g	Vector of joint torques due to gravity.
τ_m	Output torque of a single joint motor.
τ_m	Vector of joint torques due to the work of the joint motors.
$\phi_A, \phi_B, \phi_M, \phi_Z$	Angular position of the acceleration ellipsoid, force ellipsoid, generalized ellipsoid of inertia, and the dummy ellipsoid respectively.
φ_g, φ_l	Global and local field indices.

Chapter 1

Introduction

1.1 Objectives and Outline of the Study

Unlike fast moving mechanisms the effect of gravity on the overall behavior of robot arms is significant. In fast moving mechanisms and machines the gravitational force is generally balanced or is negligible in comparison to the dynamic forces. In robotics, however, due to the relatively slow motion of the links and their large masses, the force of gravity is generally of the same order of magnitude as the dynamic forces even when the robot is operated at high speeds. At low operational speeds the force of gravity is significantly larger than the dynamic forces.

Generally speaking, revolute manipulators are more maneuverable, yet they are weaker than other types due to the nature of the revolute joints they employ. Furthermore, their dynamic behavior is more complex. Analysis of the behaviour of such manipulators requires a clear understanding of both their statics and dynamics, and

the factors that influence them. The structure of the linkage, as well as the masses of the links and the way they are distributed, are among the major parameters that influence the overall performance of revolute manipulators. Any improvement in performance of the manipulators has its roots in proper choice of these parameters.

The revolute manipulator of today is a crude imitation of the human arm. Its structure is that of an open chain linkage mechanism. Each link is supported at one end by the previous link down the chain and is free to move while carrying the next link at the other end. This arrangement renders flexibility and relatively good reach ability for the mechanism, however, it results in a disadvantaged structure which causes the weight and the inertia forces of the links as well as the forces which result from the interaction between them, to cascade down the chain through a cantilever arrangement.

Up to the present a large number of designs for the manipulators structure and the mass distribution of the links have been proposed. However, no unique design can claim optimum performance under all circumstances. This is due to the fact that a manipulator with several links has a variable configuration and a highly non-linear dynamic behavior. To overcome this complexity, attempts have been made to introduce measures that can be used to evaluate the overall static and dynamic performance of the system. However, it seems that a study that depicts a global view of the effect of gravity on manipulator links is still missing. Such a study will bring about a deeper understanding of the overall behavior of the system. It will also help to examine the effect of variation of the physical parameters of the links on behavior of the system as a whole.

The goal of this work is to study the effect of gravity on manipulators in the following respects:

- How it affects the system ,
- How it can be transformed into an abstract measure that would help in categorizing the characteristics of the manipulators, and
- How that measure can be utilized to study the static and dynamic behavior of manipulators.

In the remainder of this chapter an outline of the literature pertinent to this study is presented. In Chapter 2 the effect of gravity on joint torques of manipulators at various speeds is investigated. Towards that end a typical 6 DOF revolute-joint PUMA manipulator is used as a model and is made to move its end point along a typical spatial trajectory.

It is common practice to make use of the Jacobian matrix and its inverse in the forward and inverse kinematic analysis of the manipulators. In Sections 2.4 and 2.5 of this study the forward and inverse kinematic analysis are carried out without using the Jacobian matrix. The velocities and accelerations are directly calculated by differentiating the equations of position with respect to time.

The Newton-Euler equations for the dynamic analysis of the manipulators, are presented in a form that contains matrices and matrix operations only. This form gives a unified appearance to the equations. Suitable measures are taken to preserve the efficiency of the computation.

In Chapter 3 the concept of Generalized Gravitational Field (GGF) and the generalized weight fields are introduced. The notion of the field has proved to be extremely useful in conveying the underlying ideas in fundamental phenomena such as gravity. For this purpose a 3 link parallel drive manipulator is considered. Salient characteristics of the GGF such as its curl, divergence, and normal trajectories are discussed.

Static behavior of manipulators is the subject of Chapter 4. It starts with the review of the force ellipsoid that has been introduced by other researchers as a tool for the evaluation of the capability of the end effector in applying static force to its environment. It will be shown that the size and orientation of the force ellipsoids at various points of the work volume are closely related. The force ellipsoid, as introduced, does not take into account the effect of gravity. It will be shown in that chapter how the generalized weight field and the force ellipsoid can be integrated in order to display the true force that the end effector can exert on its surroundings.

In Chapter 5 the dynamic behavior of manipulators is discussed. The generalized ellipsoid of inertia and the dynamic manipulability ellipsoid which have been introduced by other researchers are reviewed. It is shown that similar to the force ellipsoid, these ellipsoids are also closely related across the working space of the manipulator. Utilizing the generalized weight field and the generalized tensor of inertia, the generalized gravitational acceleration field is introduced. The relation between the generalized weight field and the generalized gravitational acceleration and the generalized ellipsoid of inertia is explored. It is shown that the integration of the generalized gravitational acceleration and the dynamic manipulability ellipsoid can reveal the true acceleration capability of the end effector.

Effect of change of physical parameters of the manipulators on the conformation of their generalized gravitational field and generalized weight field, and on their static and dynamic behavior is discussed in Chapter 6. Manipulators are categorized based on the shape of their fields. The global and local field indices are defined to make the categorization possible. Manipulators with different values of indices are studied. It is shown that under a particular condition the GGF is similar to the ordinary gravitational field in every respect. The conclusion and future works appear in Chapter 7.

1.2 Literature Survey

The field of robotics, although still very young, enjoys a tremendous attention from the research community. During the last 10 years almost every area of this field has been deeply explored. The area of dynamics, and in particular the mass distribution of the links, has received wide attention. Some of the research has been devoted to prepare a better understanding of the overall behavior of the manipulators as well as the way they interact with their environment. Others have focused on improving the structural and physical elements of the system such that they comply with their particular tasks.

A number of researchers have concluded that decreasing the mass of the links makes it possible to improve the maneuverability of the robots as well as increasing the mass of the payload that they can carry. According to this group, manipulators need not have rigid links for accurate tracking and placement of their payload. Instead, they contend that the errors generated due to the flexibility of the links can

be compensated for by the manipulator's controller. Daniel (1985), Usoro (1986), Chedmail (1986), Biswas and Klafter (1989), and Kiedrzynski (1988) are among that group. A survey of pertinent works in the area of flexible manipulators can be found in Desoyer et al (1986).

Flexible link robots, however promising, have little application in industrial operations. Today's industrial applications of robots, in most cases, demand high accuracy in positioning. This, for the time being, requires that the industrial manipulator arms have rigid structures.

To reduce the effect of gravity on the robots, and hence increasing their accuracy in positioning of the end effector some researchers have considered the method of bracing of the manipulators near the endpoint as an additional external support. Book (1985), counting the lightweight arms advantages and disadvantages, explained the bracing concept as being similar to the strategy of human workers who steady their hand for precise work by bracing their arm against a work bench. Based on that strategy he concluded that if the coarse motions are assigned to joints which move the major links, and fine motions to other degrees of freedom which are referenced to the work piece rather than the base of the arm, then it is possible to employ the lightweight arms without suffering from their disadvantages in accurate small motions.

Asada and West (1986) designed a device they called jig hand. It is used to brace the endpoint of a manipulator against the work piece. They considered jig hands with active and passive joints and applied one to a commercial robot arm for grinding applications. They concluded that the jig hands can be fitted to conventional

robots to increase the effective stiffness at the end effector. The jig hand also reduces the backlash and enables the robot to measure the position of the tool relative to the work surface.

A group of researchers have investigated the idea of counterbalancing of the links such that the effect of gravity is partly or completely balanced. Currently the most widely utilized method of balancing robot links employs a fixed counterweight. This method works well for low velocity operation. However, at high velocities and accelerations, the increase in dynamic torque resulting from the added inertia of the counterweight become a major drawback.

Gvozdev (1983) designed a device that completely balances the robot links. The author claims that the device can also achieve complete balancing even when the payload has changed. Yang and Tzeng (1986) proposed a method for simplifying and linearizing the dynamic equations of manipulators by forcing the coefficients of the nonlinear terms in the Lagrangian of the system to become zero. This, in practice, requires the complete static counterbalancing of each link. Their study, however, deals only with the theoretical design, and no consideration was given to the physical realization of such a robot. Recently Gompertz and Yang (1989) have extended the idea of dynamic linearization to investigate the feasibility of kinematically redundant planar manipulators.

In a more realistic way Rivin (1988) argued that counterbalancing of the links using energy storage elements like springs, hydraulic or pneumatic cylinders, cannot result in the reduction or elimination of the configuration dependent terms in the dynamic equations of the system. However, proper mass counterbalancing of the

links leads to the reduction of joint torques as well as a large attenuation of torque variations. He then concluded that even a substantial addition of extra weight to the system in order to achieve balancing can be justified in many cases. For the cases such as material handling, where complete mass counterbalancing can not be achieved due to constant change in the payload, he suggests to assume a payload mass equal to 15 to 20 percent of that of the second link and to counterbalance the links as such. For a class of robots that handle a limited number of parts he suggests an adjustable counterbalance that allows approximate balancing for the range of the mass of the parts being handled.

The idea of utilizing an adjustable counterbalance has also been explored by other researchers. Chung et al. (1984) investigated the effect of two adjustable counterweights balancing the upper and lower arms of a PUMA type manipulator. As the robot picks up a payload, the counterweights are automatically moved to a proper location such that each link is statically balanced. The authors argue that with this system added to the robot the tracking or positioning error will be reduced and the control scheme will become simpler. Chung et al. (1986) carried out a more thorough dynamic study on the effect of adjustable counterweights on manipulators. They reported a significant reduction in on-line computation time for a computed torque control scheme simulation. They also concluded that for a given path the total variations in input torques of the unbalanced manipulator were about three times larger than those of the one equipped with the adjustable counterweights. However they mentioned that increasing the speed of the operation was accompanied by more increase in the torques of the joint drives for the case of the adjustable counterweights than for traditionally balanced manipulators.

Using the sensitivity theory, Chung and Cho (1988) studied the sensitivity of an unbalanced, a partially balanced and a completely balanced manipulator with respect to payload variations. They concluded that the sensitivity of the completely balanced manipulator is very low for payload variations. They also reported that even for the partially balanced robot the sensitivity is still lower than that of the unbalanced one.

Jumarie (1986) investigated the use of time-varying inertia links. In practice such a possibility can be reached only by using a moving counterbalance. However, the author did not elaborate on the method of physically obtaining the time varying inertia characteristics. He concluded that using such a link design makes it possible to control both joint torques and the inertia of the links to obtain a more versatile manipulator. The same author derived in 1988 the general equations governing the dynamic behavior of the manipulators with time-varying inertia links. He showed that the system can be described by a set of uncoupled Ricatti differential equations. He also considered the problems related to stabilization and structural parameter uncertainty.

Fahim and Fernandez (1988) built an active counterbalance for an ASEA robot and investigated the effect of adjustment of the center of mass of the upper link according to the motion of the end effector. The active counterbalance system comprise a quasistatic counterweight that adjusts to balance the arm at the beginning of the motion, and a dynamic counterweight that moves while the end effector travels on its path. Their analysis and experiments show a visible enhancement in load carrying capacity of their manipulator.

Attention has also been paid to the counterbalancing of the manipulators links by

means of springs. It is said that using this method, the links can be counterbalanced against the gravity without their masses being increased. Recently Jnifene (1989) investigated the dynamics and control of a spring counterbalanced manipulator. He reported an improvement in the joint torques of the manipulator with spring counterbalance with respect to its counterpart with mass balanced links.

Several researchers have concentrated on the system as a whole rather than on its individual elements. The advantage of this approach is that all aspects of the problem is considered. However, due to the complexity of the problem, there are times that many nonrealistic, even erroneous assumptions are made. Nevertheless the outcome can be used as guidelines in the design of manipulators for better dynamic performances.

Following this line of thought Asada and Youcef-Toumi (1984) designed a planar two degrees of freedom manipulator with invariant and decoupled inertia characteristics. In their design, no additional weight was used to counterbalance the effect of gravity on the links. Such a design makes the inertia perceived by each joint motor constant, regardless of the configuration of the manipulator. As a result the control problem is significantly simplified. Later in 1985 Youcef-Toumi and Asada presented a method for designing open loop manipulator arms that reduces the dynamic complexity to a great extent. The method is based on setting the off-diagonal terms of the inertia tensor equal to zero and/or forcing the diagonal members to become configuration independent. The first condition makes the inertia tensor decoupled, while the second condition makes it invariant. Under such circumstances the system is completely decoupled and linearized with constant parameters except for the gravity terms.

Tourassis and Neuman (1985) presented the coefficients of a general dynamic model of a manipulator in a way that their physical interpretation is facilitated. According to them, in order to accomplish a better controllability, it is necessary to integrate the mechanical design and the design of the controller. They concluded that to achieve such a state of design, the mass of the links must successively decrease and the first link should be oriented such that its axis of rotation is along the gravitational field.

In 1987 Tang and Tourassis showed that numerical simplification of the dynamic equations of a manipulator could lead to a totally erroneous dynamic models. The authors exemplified this by demonstrating a case where the quadratic form of the kinetic energy of the arm loses its positive-definite form.

Recently, Tourassis(1988) introduced the concept of robot dynamics emulation. He argued that the use of currently common model-based control strategies requires real-time evaluation of the dynamic parameters of the robot which dictates a simplified model. He proposed that instead of simplifying the dynamic equations, that might result in violation of physical principles (see his publication with Tang in 1987 briefed above), it is better to approximate the functional generator of the models, i.e. the Lagrangian of the manipulator, to a more simple form.

The influence of the mass properties of the links on the static and dynamic behavior of the manipulator has drastically complicated its dynamic behavior. As a result many researchers have sought a parameter or concept that helps visualize the static and/or the dynamic behavior of the manipulator as a whole and at the same time can fundamentally be used in the process of synthesis or design of robots.

Uchiyama et al. (1985) discussed the use of the manipulator's Jacobian as an index to evaluate the performance of the arm from the kinematic and static points of view. At any point in the work volume of the manipulator the performance index takes a special value which can be considered as a measure of dexterity of the manipulator. For example they showed that at singular points where the arm loses at least one degree of freedom, the performance index takes up its minimum value. An overall picture of the performance of the manipulator is then prepared by visualizing the value of the performance index for the whole working volume.

Yoshikawa (1983) introduced the concept of manipulability as a measure of the ability of the arm to position and orient the end effector. He proposed a manipulability measure defined as the square root of the determinant of a matrix resulted from the multiplication of the Jacobian and its transpose. He then defined the manipulability ellipsoid using the quadratic form resulting from the inverse of that matrix and the task velocity. He showed that the manipulability measure is proportional to the volume of the manipulability ellipsoid. He also defined the manipulating force ellipsoid based on the product of the Jacobian matrix and its transpose and showed that its volume is inversely proportional to that of the manipulability ellipsoid.

In 1985 Togai argued that the manipulability measure defined by Yoshikawa is not a proper measure of nearness of the Jacobian matrix to the singularity because it depends not only on the size of the Jacobian matrix but also the scaling factor such as the product of all singular values. He then proposed that the shape of the manipulability ellipsoid be considered rather than its volume, and defined the manipulability as the inverse of the condition number of the Jacobian matrix. He then referred to the work of Salisbury and Craig as another good reason to choose a

measure based on the condition number of the Jacobian matrix.

The work of Salisbury and Craig that was referred to by Togai was published in 1982. Considering the accuracy with which forces can be exerted at the arm tip, the authors noticed that the relative force error in the task space, is bounded by the product of the condition number of the Jacobian transpose matrix and the relative error in joint torques. They concluded that those points in the work volume that minimize the condition number of the Jacobian matrix are the best to minimize error propagation from input torques to the output forces. They indicated that the best conditioning possible occurs when the condition number becomes unity. This happens at those points where the column vectors of the Jacobian matrix are both orthogonal and equal in magnitude.

Reconsidering the velocity ellipsoid and force ellipsoid, Chiu (1988) argued that although the effective capability of a manipulator can be increased by adopting postures that align the eigenvectors of either of the ellipsoids with task directions, nevertheless it is not a sufficient criterion for determining the overall optimality of a posture. He then combined the two ellipsoids by defining the compatibility index as the weighted sum of squares of transmission ratios of both ellipsoids along any given direction. He then concluded that the maximization of this index can present an effective way of utilizing manipulator redundancy and that the index can also be applied to nonredundant manipulators as a criterion in work space design.

In 1984 Asada and Youcef-Toumi reported the development of a direct-drive arm using high torque brushless motors. They showed that for a given total input power to the joint motors, the force that can be applied by the tip of the arm can be

found from an ellipsoid called the force ellipsoid. The principal directions of the ellipsoid correspond to the directions of extremum values of the force. When the characteristics of all the joint motor are identical this ellipsoid is equivalent to that developed by Yoshikawa (1983). The authors also showed that while for an arm with parallel configuration the force ellipsoid appears to be isotropic in a wide region of the working volume, for a cross configuration arm the ellipsoid will degenerate into a line along its longest diameter.

Asada and Ro (1985) used the force ellipsoid and the voltage torque-speed linear characteristic of a DC motor to show that a new configuration design for the arm is necessary if the force developed at the endpoint is to be increased. They proposed a five-bar-link arm mechanism that has a better force-velocity characteristics.

Although the above mentioned research works have been dealing with the statics of the manipulators, nevertheless the effect of gravity on robot links is not included in the force ellipsoids introduced in them. As a result, the true force that the robot is capable of applying by its end point is not shown.

Asada (1983) was the first to take the dynamics of the manipulator into account. In his work he introduced the Generalized Ellipsoid of Inertia as a geometrical representation of the manipulator dynamics. For a single body, the ellipsoid of inertia which is an indication of the centroidal tensor of inertia, is solely a function of the distribution of the mass of the body. Therefore its dimensions and its orientation with respect to the body are fixed. In a system of rigid bodies the inertia tensor of the system is, in general, configuration dependant. The generalized ellipsoid, therefore, varies both in dimension and orientation as a result of any change in the configuration

of the system.

He explained the nonlinear forces that act on the arm due to the change in configuration, through the change in the dimensions and orientation of the ellipsoid. He then concluded that as the ellipsoid approaches the shape of a sphere, the nonlinear forces gradually disappear. The concept of GEI helps to visualize the complicated dynamic behavior of a three DOF manipulator, and serves as a tool for the synthesis of robot arms.

In 1985 Yoshikawa extended the concept of manipulability ellipsoid into dynamic manipulability ellipsoid to demonstrate the interrelation between the maximum acceleration of the end effector and the joint torques. He introduced several indices related to DME that could be used in the design and analysis of the manipulators. Application of the dynamic manipulability ellipsoid in the analysis and design of manipulators was exemplified by the same author in 1986.

In a similar work, the acceleration radius was introduced in 1988 by Graettinger and Krogh as a new measure for evaluation of the global performance of manipulators. The authors defined the acceleration radius as the maximum value that the acceleration of the end effector can reach at a given position and velocity. They illustrated the application of the acceleration radius in the design of a PUMA manipulator. They also showed that counterbalancing will improve the acceleration radius.

Chapter 2

Effect of Gravity on Joint Motors

2.1 Introduction

The subject of this chapter is to evaluate the role of gravity in dynamic models of manipulators. A systematic procedure to accomplish this is to determine the relative degree of importance of the gravity terms in the dynamic equations of the manipulator. No comprehensive appraisal has been carried out by the research community to determine this aspect of manipulators dynamics. Hollerbach(1984) showed that for a given mechanical design there are cases where both effects are equally important. The drawback of his work is that he employed a manipulator with only two links and limited the trajectory of the end point to a straight line. In a more exhaustive study Thomas and Tesar(1982), while propounding a dynamic model for serial manipulators, briefly demonstrated the static and dynamic effects through the simulation of a 6 DOF robot.

In the present study a typical PUMA manipulator with 6 degrees of freedom and physical parameters similar to those of commercially available manipulators is considered. Although all of the links are considered in the dynamic analysis, the focus will be on primary links as they are the most contributors to the dynamic behavior of a manipulator.

The manipulator is simulated for the case where its end point moves along a typical given trajectory. To preserve the generality of the simulation, the trajectory will be spatial and include both Cartesian and joint motions. Making use of the Newton-Euler set of equations, the joint torques are then calculated and plotted versus the distance traversed by the end point. Next, the robot is assumed to move along the same trajectory in a quasistatic manner. Once again the joint torques are calculated and plotted. The comparison of the plots will indicate the degree of importance of both gravity and dynamic terms.

2.2 Simulation of a 6 DOF PUMA Manipulator

Figure 2.1-a shows the schematic diagram of a typical 6 dof PUMA robot. Figure 2.1-b shows the secondary links in detail. The coordinate systems are assigned to each link based on Denavit-Hartenberg convention. According to that convention a coordinate frame must be attached to each link of the manipulator such that the z_i axis lies along the axis of rotation of the $(i+1)th$ link, the x_i axis is selected such that it is normal to both z_i and z_{i-1}, and the y_i axis completes the dexter coordinate frame.

According to D-H convention, the homogeneous transformation matrix that relates the successive link coordinate systems, is in the form

$$\mathbf{A}_i = \begin{bmatrix} cos\theta_i & -sin\theta_i cos\alpha_i & sin\theta_i sin\alpha_i & a_i cos\theta_i \\ sin\theta_i & cos\theta_i cos\alpha_i & -cos\theta_i sin\alpha_i & a_i sin\theta_i \\ 0 & sin\alpha_i & cos\alpha_i & d_i \\ 0 & 0 & 0 & 1 \end{bmatrix} \tag{2.1}$$

where θ_i is the joint angle about z_{i-1} axis,

α_i is the twist angle of the frame i about x_i axis,

a_i is the length of the common normal between z_i and z_{i-1},

and d_i is the distance from the origin of the coordinate system $i-1$ to the intersection of the z_{i-1} axis with x_i along z_{i-1}.

The first parameter, θ_i, is the joint variable and the other three are the constant link parameters. The joint variables and the link parameters for the PUMA manipulator under consideration, as well as the physical properties of the links are given in Appendix A.

The 4×4 homogeneous transformation matrix $\mathbf{T}$ which specifies the position and orientation of the end effector with respect to the base coordinate system, can be expressed as

$$\mathbf{T} = \begin{bmatrix} n_x & s_x & a_x & P_x \\ n_y & s_y & a_y & P_y \\ n_z & s_z & a_z & P_z \\ 0 & 0 & 0 & 1 \end{bmatrix} \tag{2.2}$$

In this matrix, the vector **P** specifies the position of the end effector with respect to the base frame and the unit vectors **n**, **a** and **s** represent the orientation of the end effector as shown in Figure 2.1-b. The orientation of the end effector can also be expressed as a set of Euler angles. Let ϕ, θ and ψ be the Roll, Pitch and Yaw angles about z, y and x axes respectively. The matrix **T** can then be written as

$$\mathbf{T} = \begin{bmatrix} C\phi C\theta & C\phi S\theta S\psi - S\phi C\psi & C\phi S\theta C\psi + S\phi S\psi & P_x \\ S\phi C\theta & S\phi S\theta S\psi + C\phi C\psi & S\phi S\theta C\psi - C\phi S\psi & P_y \\ -S\theta & C\theta S\psi & C\theta C\psi & P_z \\ 0 & 0 & 0 & 1 \end{bmatrix} \tag{2.3}$$

The relation between the **T** matrix and the **A** matrices can be expressed as

$$\mathbf{T} = \mathbf{A}_1.\mathbf{A}_2.\mathbf{A}_3.\mathbf{A}_4.\mathbf{A}_5.\mathbf{A}_6 \tag{2.4}$$

2.3 Path of the End Effector

To preserve the generality of the example, the end effector is made to traverse a spatial path. Starting from point P_1, the manipulator is assumed to pick up a tool and move it straight upward to point P_2 in Cartesian motion. At that point the robot is made to have a pause before heading towards the next point P_4. But due to the assumption that there is an obstacle, the gripper will move to point P_3 directly above the obstacle and then continue towards P_4. The travel from P_2 to P_4 will be in joint motion with a stop, but no pause, at P_3. Finally, after a pause at P_4, the manipulator is made to move to point P_5 in Cartesian motion to unload the tool.

The orientation of the end effector has also been subject to change from point to

POINT	X(m)	Y(m)	Z(m)	ROLL (deg)	PITCH (deg)	YAW (deg)
P_1	0.9	-0.5	0.2	-30.0	170.0	10.0
P_2	0.9	-0.5	0.8	-40.0	170.0	30.0
P_3	0.5	0.0	1.3	0.0	100.0	60.0
P_4	0.2	0.6	0.6	40.0	150.0	60.0
P_5	0.2	0.6	0.1	40.0	170.0	10.0

Table 2.1: A test path for the end effector of PUMA arm.

point. The coordinates of the points as well as the orientation angles, i.e. roll, pitch and yaw angles of the end effector at each point are given in Table 2.1. All values are with respect to the coordinate system x_o, y_o, z_o of Figure 2.1.

The VAL subset program (Shahinpoor 1987) has been implemented to provide the commands. The trajectory planning has been carried out by applying the method given in Paul (1983), chapter 5.

2.4 Forward Kinematics

Given the magnitude of the joint angles and their first and second time rates of change, the position and orientation of the end effector as well as its velocity and acceleration can be obtained through forward kinematic analysis. Substituting from Table A.2 in Equation 2.1 yields the six A matrices. Substituting for these matrices in Equation 2.4 and comparing the resulting matrix with Equation 2.2, gives the

elements of the T matrix as

$$\begin{aligned} n_x &= C_1\left[C_{23}(C_4C_5C_6 - S_4S_6) - S_{23}S_5C_6\right] - S_1(S_4C_5C_6 + C_4S_6) \\ n_y &= S_1\left[C_{23}(C_4C_5C_6 - S_4S_6) - S_{23}S_5C_6\right] + C_1(S_4C_5C_6 + C_4S_6) \\ n_z &= -S_{23}(C_4C_5C_6 - S_4S_6) - C_{23}S_5C_6 \end{aligned} \tag{2.5}$$

$$\begin{aligned} s_x &= -C_1\left[C_{23}(C_4C_5S_6 + S_4C_6) - S_{23}S_5S_6\right] + S_1(S_4C_5S_6 - C_4C_6) \\ s_y &= -S_1\left[C_{23}(C_4C_5S_6 + S_4C_6) - S_{23}S_5S_6\right] - C_1(S_4C_5S_6 - C_4C_6) \\ s_z &= S_{23}(C_4C_5S_6 + S_4C_6) + C_{23}S_5S_6 \end{aligned} \tag{2.6}$$

$$\begin{aligned} a_x &= C_1(C_{23}C_4S_5 + S_{23}C_5) - S_1S_4S_5 \\ a_y &= S_1(C_{23}C_4S_5 + S_{23}C_5) + C_1S_4S_5 \\ a_z &= -S_{23}C_4S_5 + C_{23}C_5 \end{aligned} \tag{2.7}$$

$$\begin{aligned} P_x &= C_1\left[(C_{23}C_4S_5 + S_{23}C_5)d_6 + S_{23}d_4 + C_2a_2\right] - S_1(S_4S_5d_6 + d_2) \\ P_y &= S_1\left[(C_{23}C_4S_5 + S_{23}C_5)d_6 + S_{23}d_4 + C_2a_2\right] + C_1(S_4S_5d_6 + d_2) \\ P_z &= (C_{23}C_5 - S_{23}C_4S_5)d_6 + C_{23}d_4 - S_2a_2 \end{aligned} \tag{2.8}$$

In the above expressions

$$S_i = sin\theta_i, \qquad C_i = cos\theta_i, \qquad S_{ij} = sin(\theta_i + \theta_j), \qquad C_{ij} = cos(\theta_i + \theta_j).$$

To obtain the orientation angles of the end effector, the corresponding elements of the matrices given in Equations 2.2 and 2.3 are set equal. This results in

$$\begin{aligned} \phi &= \arctan\left(\frac{n_y}{n_x}\right) \\ \theta &= \arctan\left(\frac{-n_z}{n_xC\phi + n_yS\phi}\right) \\ \psi &= \arctan\left(\frac{s_x}{a_x}\right) \end{aligned} \tag{2.9}$$

Furthermore, it should be noted that the unit vectors n, s and a are orthonormal. Consequently, out of nine equations obtained from the comparison of the two matrices, six equations are dependent. The remaining three will suffice to find the 3 orientation angles. Substituting from the Equations 2.5, 2.6 and 2.7 for the components of unit vectors in Equation 2.9 results in the orientation angles.

The common approach for obtaining the velocity and acceleration of the end effector is to use the Jacobian matrix. In this study, however, Equations 2.8 and 2.9 are differentiated twice with respect to time. The resulting equations will be prohibitively long to be expressed in the text, however, a simple subroutine is prepared in the computer analysis that performs the differentiation recursively.

2.5 Inverse Kinematics

In the inverse kinematic analysis the joint angles as well as the joint velocities and accelerations are found as functions of the position and orientation of the end effector and their time rates of change. The joint angles are given by Lee(1982) as followings

$$
\begin{aligned}
\theta_1 &= \arctan\left(\frac{P_y\sqrt{P_x^2+P_y^2-d_2^2}-d_2P_x}{P_x\sqrt{P_x^2+P_y^2-d_2^2}+d_2P_y}\right)\\
\theta_3 &= \arctan\left(\frac{P_x^2+P_y^2+P_z^2-d_2^2-d_4^2-a_2^2}{\sqrt{4a_2^2d_4^2-\left[P_x^2+P_y^2+P_z^2-d_2^2-d_4^2-a_2^2\right]^2}}\right)\\
\theta_2 &= \arctan\left(\frac{-P_x(d_4S_3+a_2)+d_4C_3\sqrt{P_x^2+P_y^2-d_2^2}}{P_xd_4C_3+(d_4S_3+a_2)\sqrt{P_x^2+P_y^2-d_2^2}}\right)\\
\theta_4 &= \arctan\left(\frac{C_1a_y-S_1a_x}{C_1C_{23}a_x+S_1C_{23}a_y-S_{23}a_z}\right)\\
\theta_5 &= \arctan\left(\frac{(C_1C_{23}C_4-S_1S_4)a_x+(S_1C_{23}C_4+C_1S_4)a_y-S_{23}C_4a_z}{C_1S_{23}a_x+S_1S_{23}a_y+C_{23}a_z}\right)\\
\theta_6 &= \arctan\left(\frac{-(C_1C_{23}S_4+S_1C_4)n_x-(S_1C_{23}S_4-C_1C_4)n_y+S_{23}S_4n_z}{-(C_1C_{23}S_4+S_1C_4)s_x-(S_1C_{23}S_4-C_1C_4)s_y+S_{23}S_4s_z}\right)
\end{aligned}
\tag{2.10}
$$

The first and second derivative of these equations with respect to time give the joint velocities and accelerations respectively.

2.6 Dynamic Analysis

The joint torques are obtained from the dynamic analysis using the recursive Newton-Euler formulation. In this study the Newton-Euler equations are derived from basic dynamic principles in order to cast them in a unified form that contains only matrices and matrix operations. The derivation process is presented in Appendix B.

2.7 Results of Simulation

The results of simulation are presented through the plots of the joint torques against the distance traversed by the end point in meters. In order to illustrate the effect of the speed of the end effector, the simulation is carried out for three speed categories. At low speeds the maximum linear speed of the end point in each direction and the maximum joint speed are assumed to be $1m/s$ and $\frac{\pi}{2}r/s$ respectively. At moderate speeds these values are increased to $1.5m/s$ and $\frac{3\pi}{4}r/s$, and at high speeds to $2.0m/s$ and $\pi r/s$ respectively. The plots are shown in Figures 2.2 to 2.10. In these figures the solid lines refer to the total torque while the dashed lines refer to the gravitational effect only, i.e. to the case where the motion is quasistatic.

As it is shown in Figures 2.2 to 2.4 the torque of the first joint in quasistatic simulation is zero throughout the arm's travel. This is due to the fact that the first

link is always oriented along the direction of the effect of gravity. In the first and the last segment of the path, i.e. along the lines P_1 P_2 and P_4 P_5 the end point is moving in a vertical plane. In these segments the first motor does not have to apply any torque for the positioning task. However, according to Figure 2.2 the torque of the first joint in the above segments is not zero. This is due to the fact that the orientation of the gripper is changing during the motion along those two lines. As a result the reaction of the torques applied by the secondary link motors is reflected on the first motor.

The torques of the second and third joints are normalized with respect to their corresponding absolute values when the arm is fully extended. This is the position in which the Static Load Carrying Capacity (SLCC) of robots is defined. (Wang and Ravani - 1988).

These figures show that at low speeds the effect of gravity dominates over the dynamic effects throughout the operation. At high speeds, as indicated in the last run for each link, the effect of gravity is seen to be of the same order of magnitude as that of the mean of the dynamic effects.

It should, however, be noted that the state of balancing of the arm has a dramatic effect on the joint torques. As indicated in Appendix A, in present example the links are partially balanced.

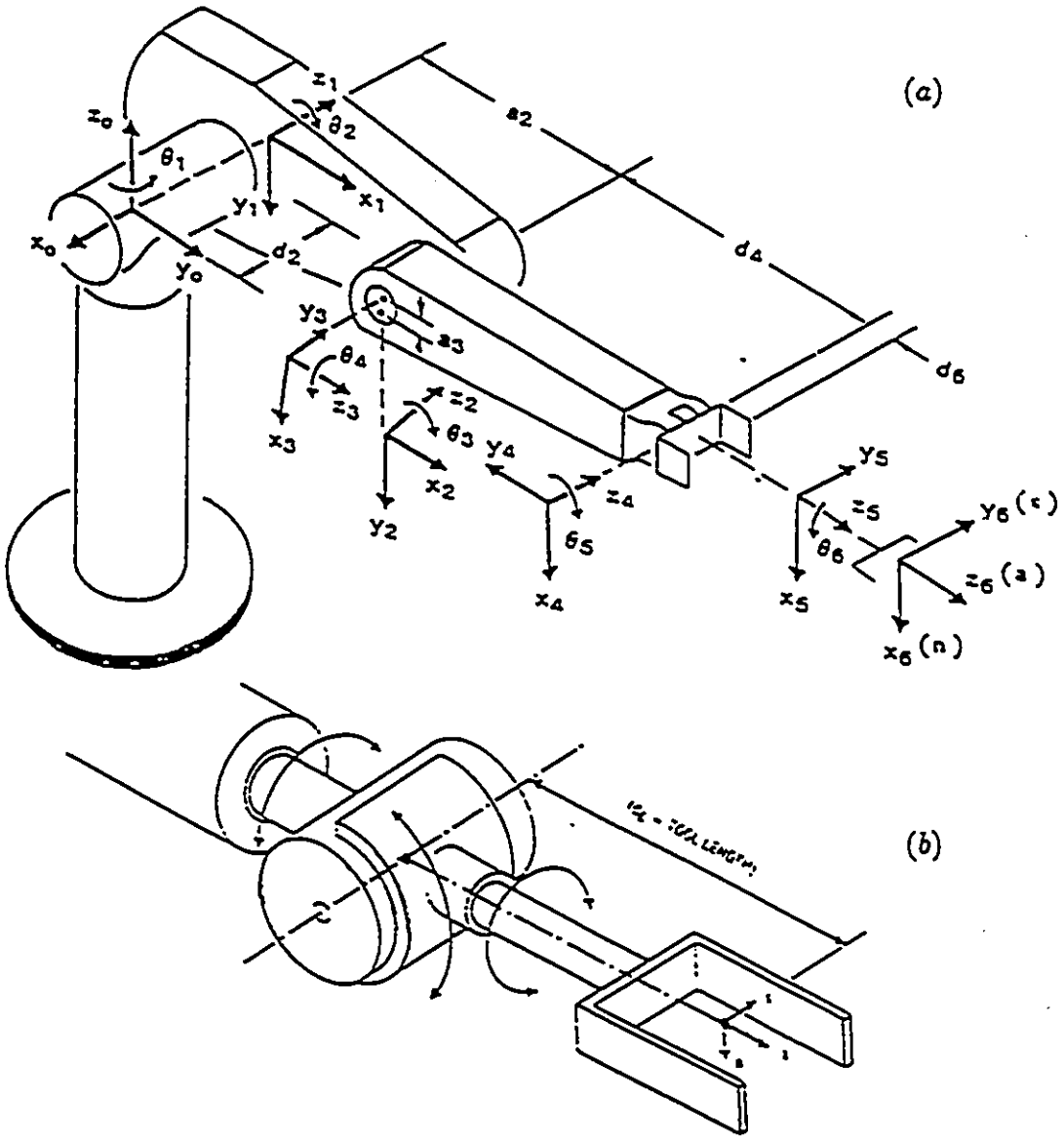

Figure 2.1: Schematic diagram of a typical PUMA manipulator, Lee(1982).

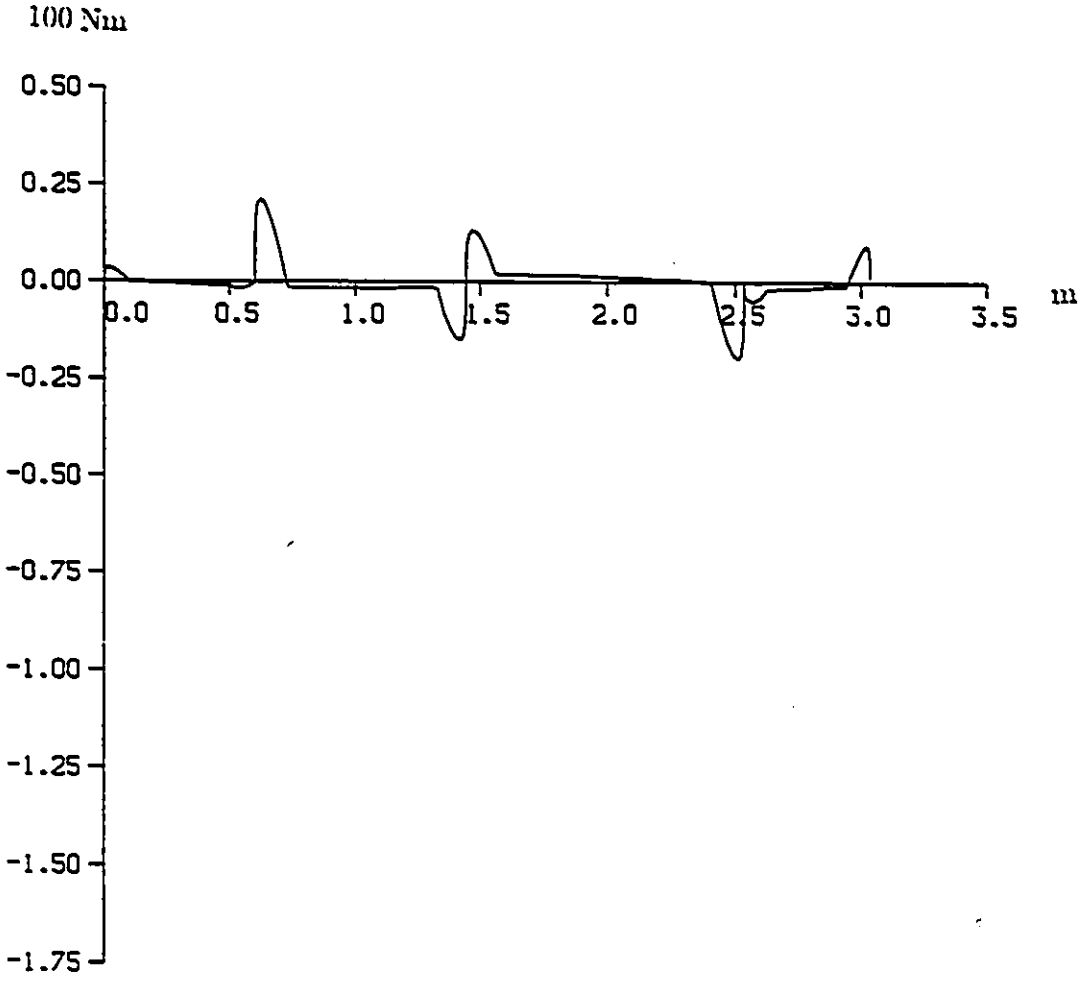

Figure 2.2: Normalized torque of joint 1 versus the distance traversed by the end effector at low speeds.

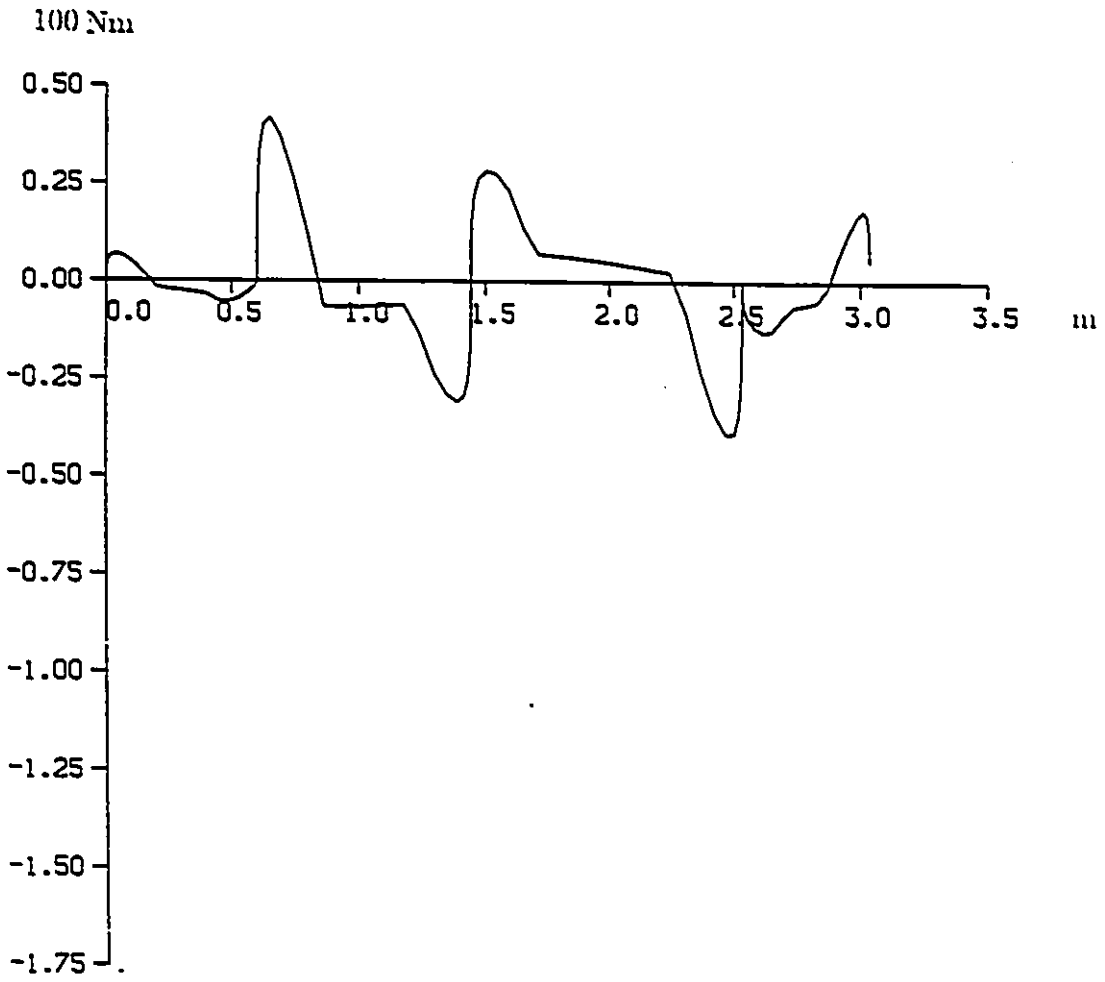

Figure 2.3: Normalized torque of joint 1 versus the distance traversed by the end effector at moderate speeds.

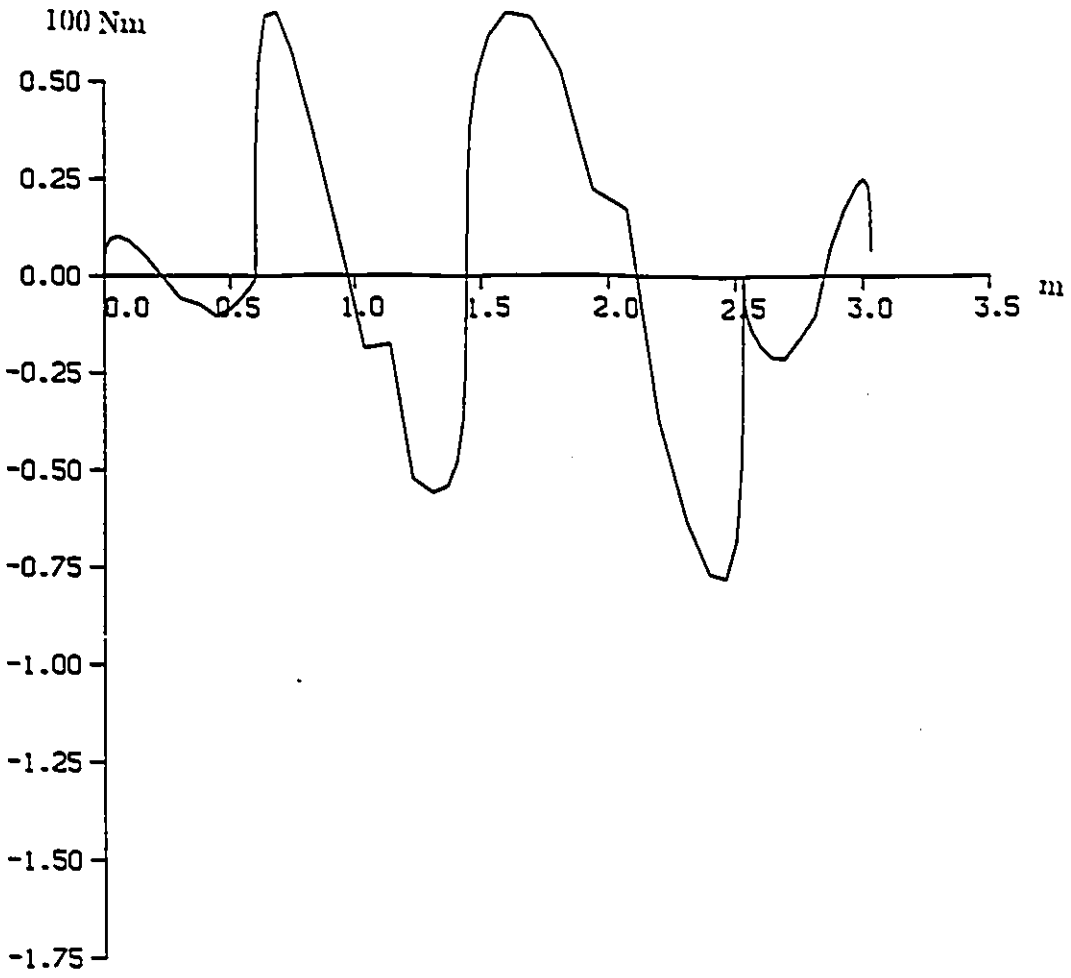

Figure 2.4: Normalized torque of joint 1 versus the distance traversed by the end effector at high speeds.

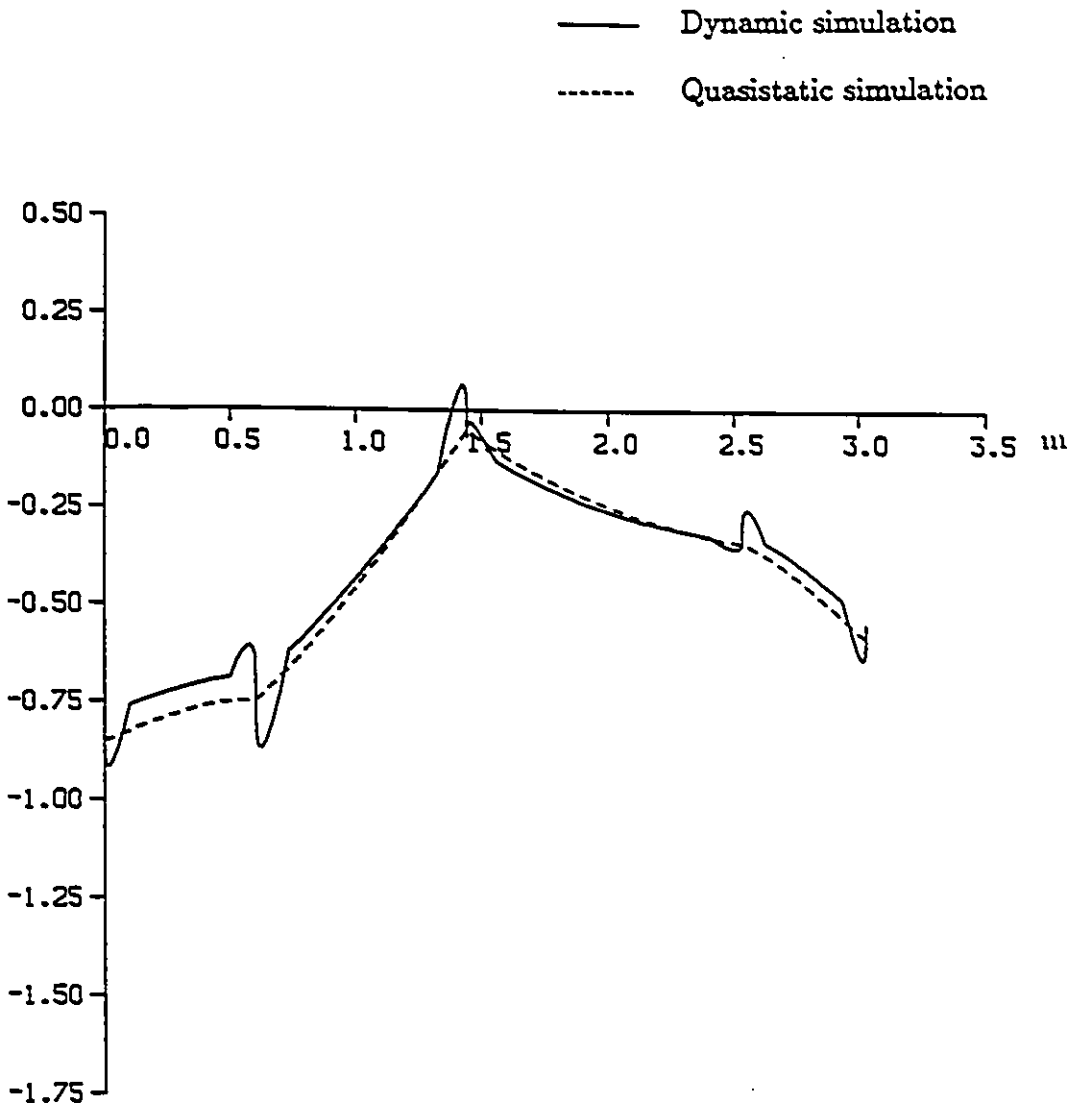

Figure 2.5: Normalized torque of joint 2 versus the distance traversed by the end effector at low speeds.

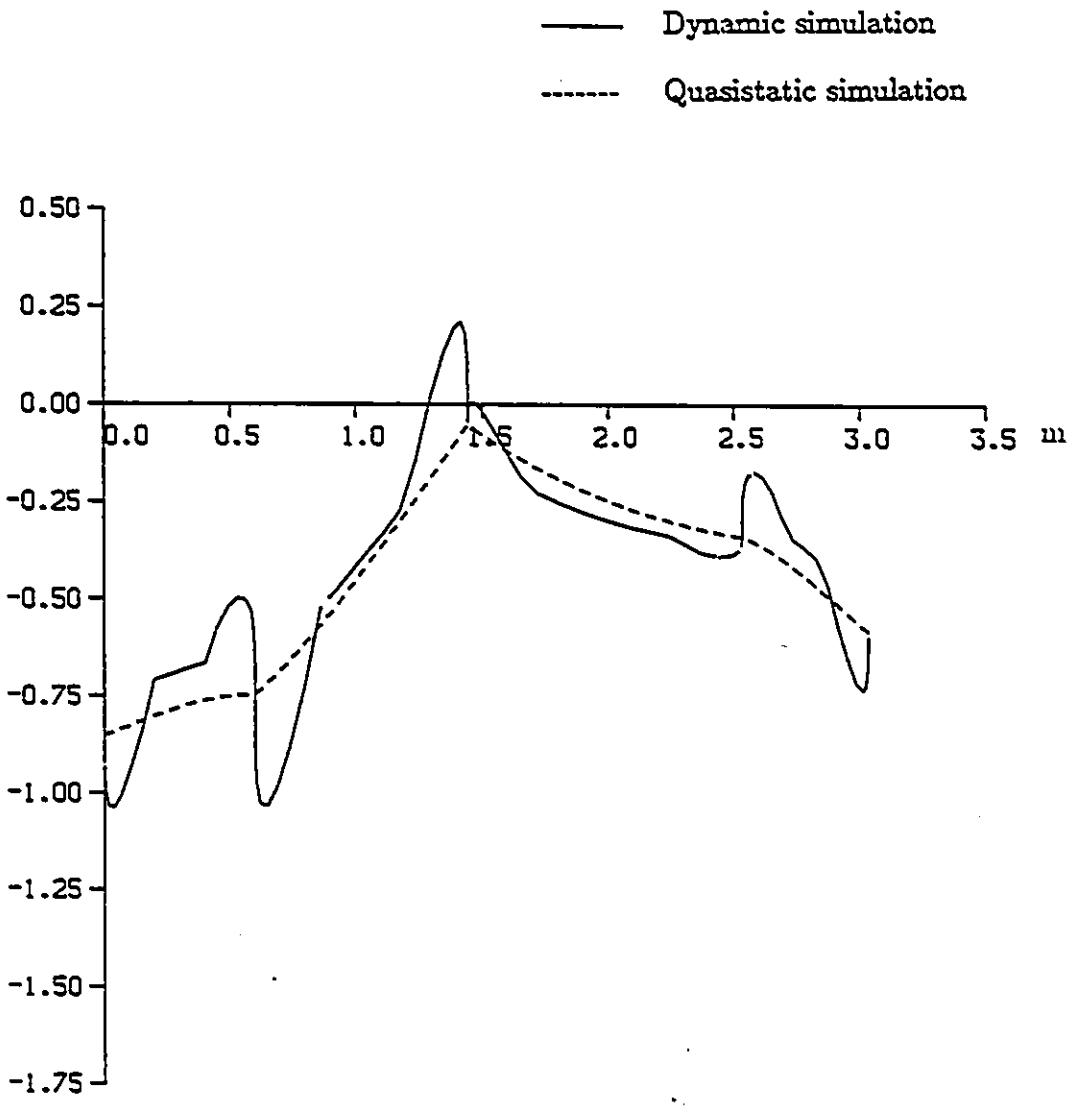

Figure 2.6: Normalized torque of joint 2 versus the distance traversed by the end effector at moderate speeds.

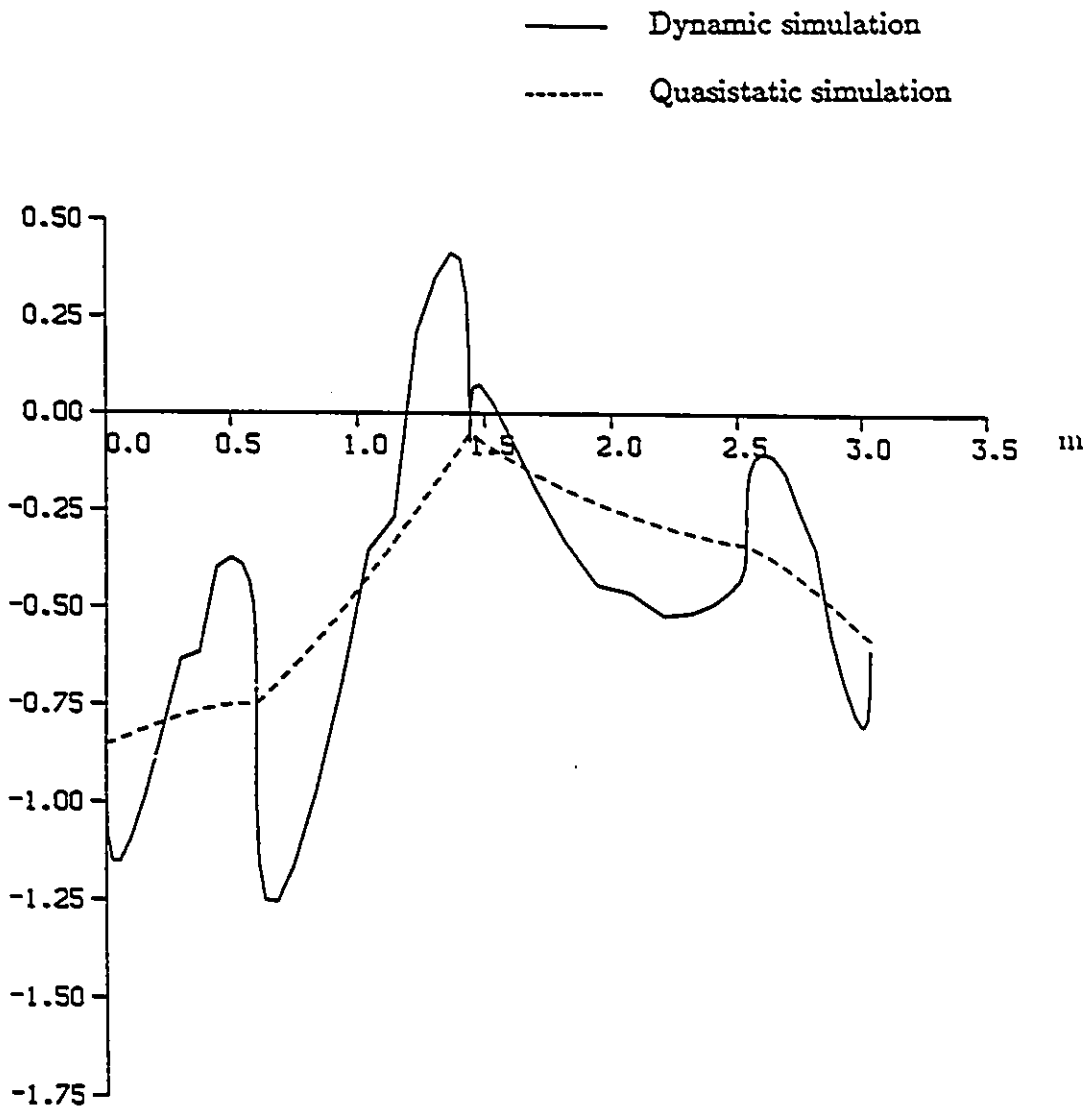

Figure 2.7: Normalized torque of joint 2 versus the distance traversed by the end effector at high speeds.

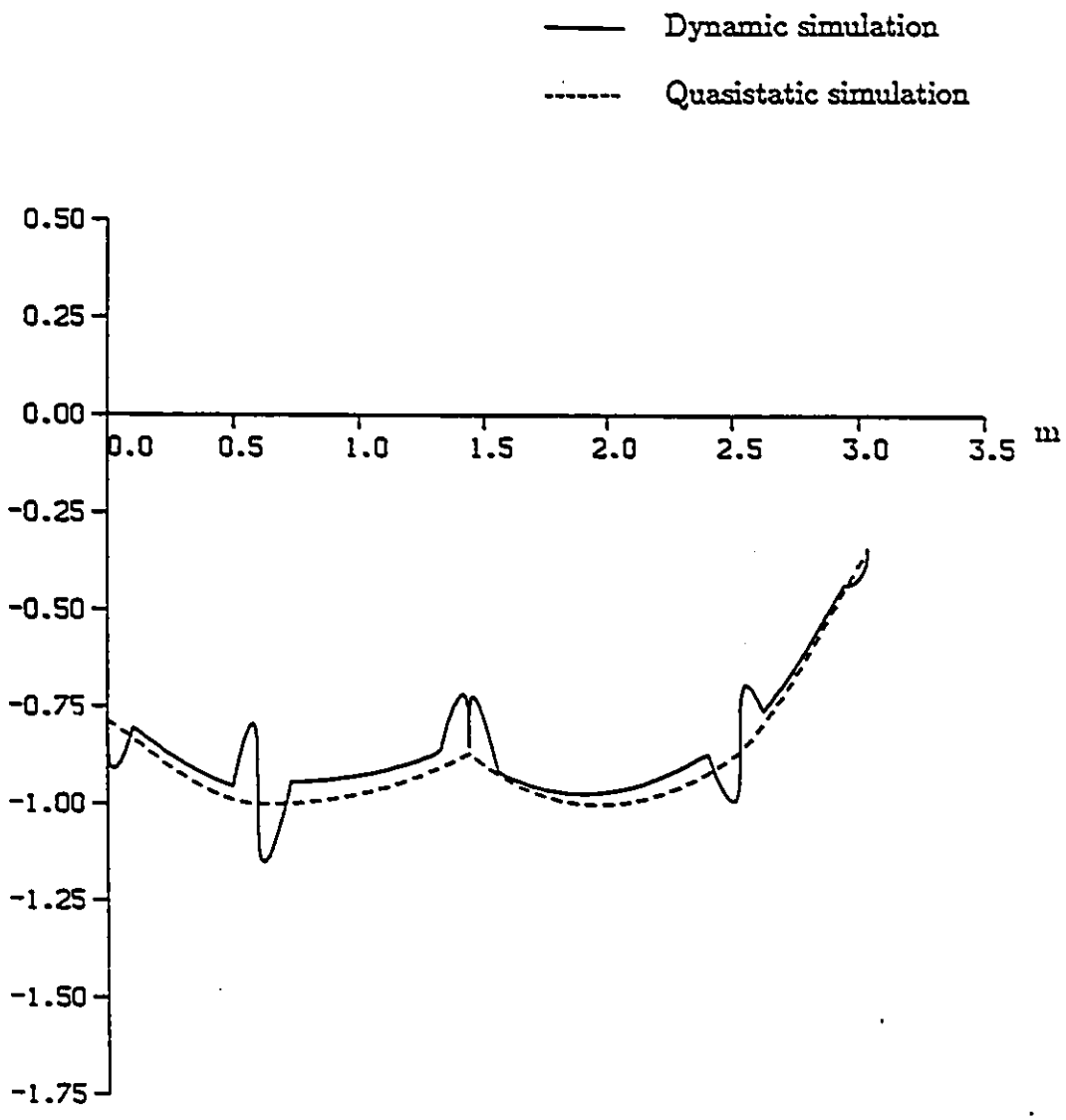

Figure 2.8: Normalized torque of joint 3 versus the distance traversed by the end effector at low speeds.

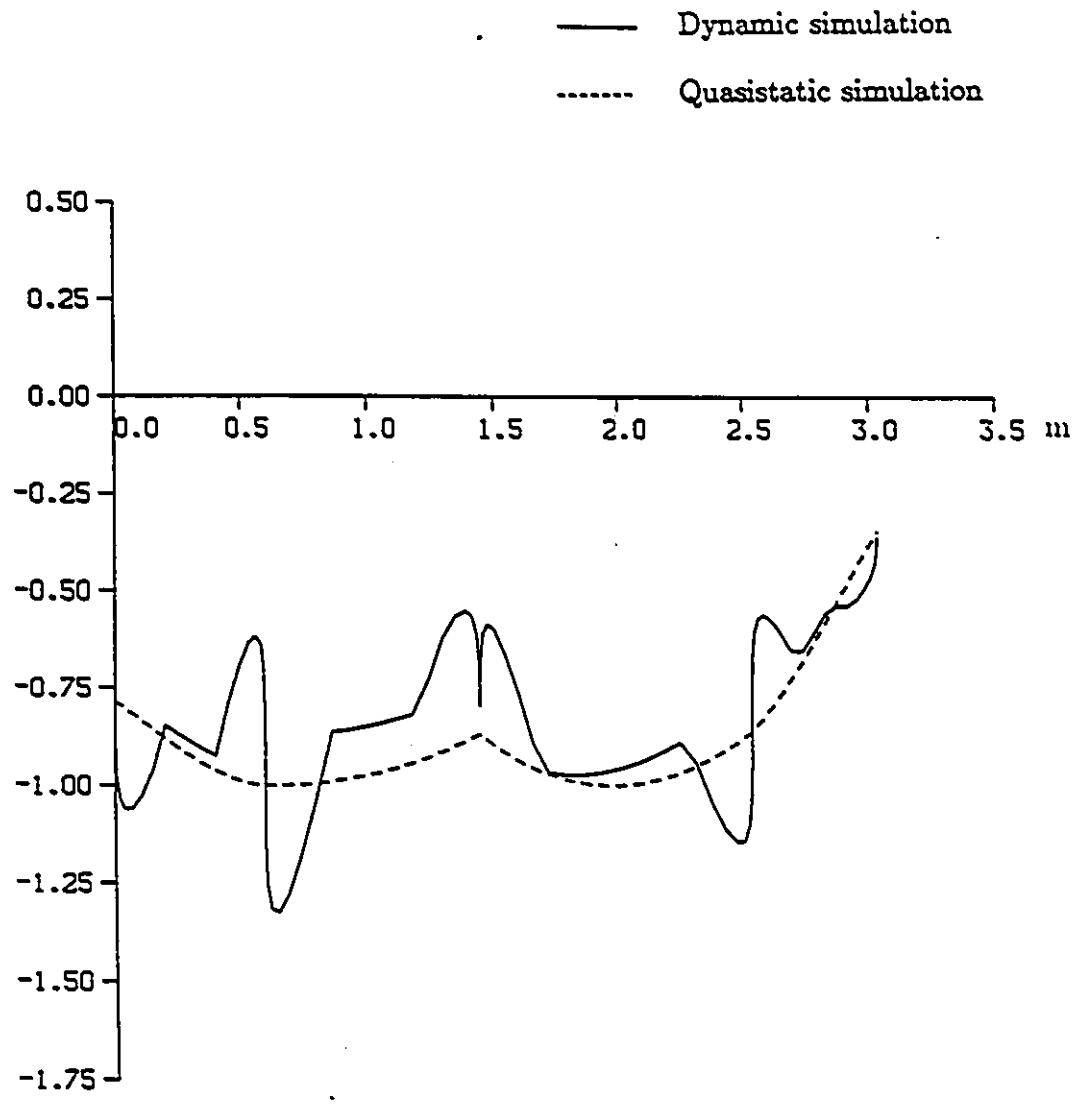

Figure 2.9: Normalized torque of joint 3 versus the distance traversed by the end effector at moderate speeds.

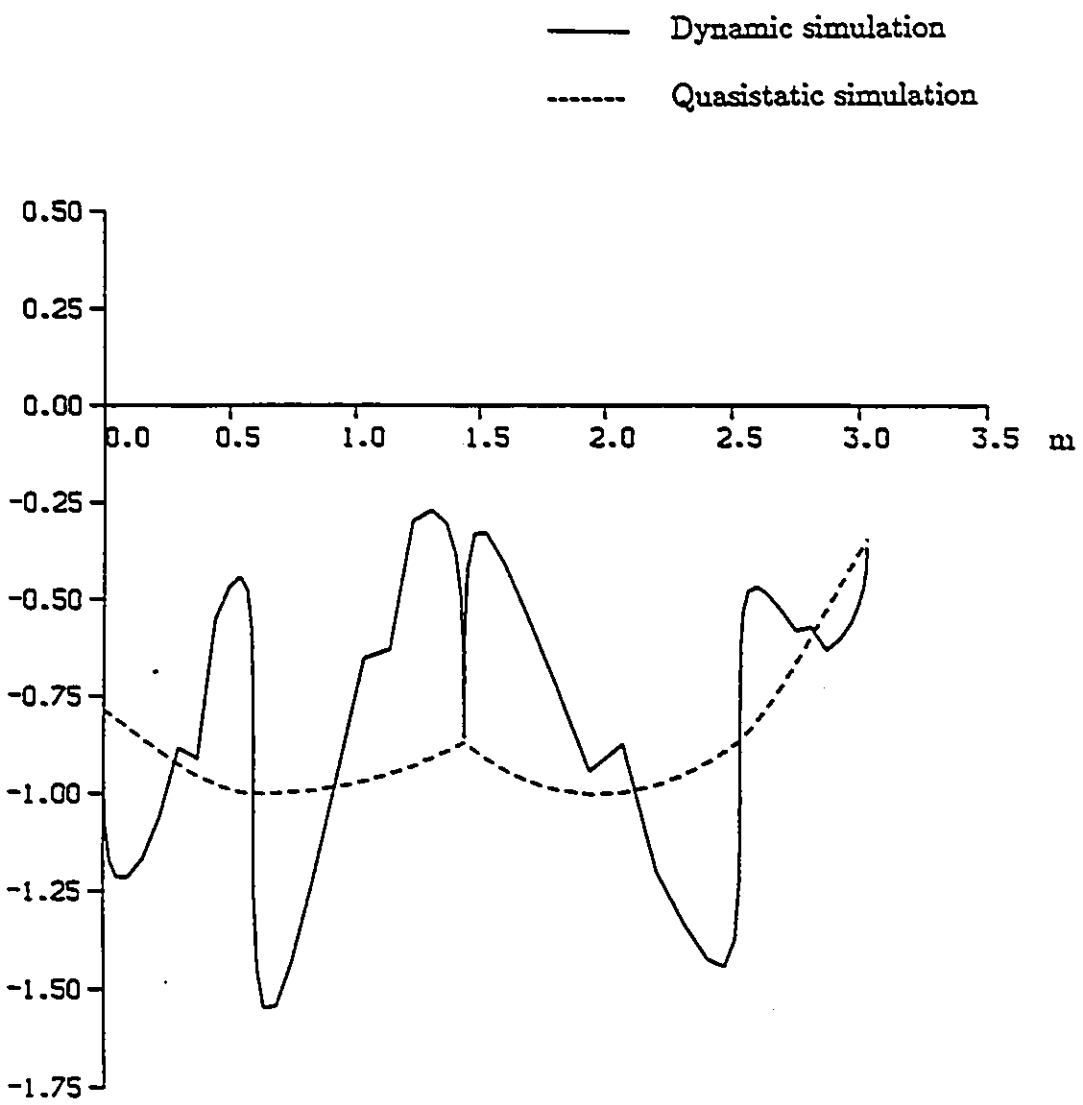

Figure 2.10: Normalized torque of joint 3 versus the distance traversed by the end effector at high speeds.

Chapter 3

Generalized Gravitational Field (GGF)

3.1 Introduction

The joint motors of a robot arm provide the necessary torques to counteract both the dynamic and the gravitational effects on the links and on the payload. Part of the joint torques that balance the force of gravity can be related through the manipulator's Jacobian to a force acting at the endpoint of the robot arm. This force in essence can replace the effect of gravity on each individual link, and therefore can be thought of as the generalized weight of the arm.

If a force field that acts on a system is conservative, then it can be represented by the gradient of a scalar potential field which is a function of the configuration of the system. The total gravitational potential energy of a manipulator is also

only a function of the configuration. This makes it possible to define a Generalized Gravitational Field (GGF) such that its gradient equals the generalized weight of the manipulator.

The GGF possesses all the fundamental characteristics of fields encountered in other diciplines of science and engineering. It is single valued, bounded, continuous, and differentiable. However, the GGF as defined here cannot be extended to include more than 3 degrees of freedom. This is due to the fact that the moment potentials, in general, do not exist (Simmonds -1984). In other words, although it is possible to replace the gravitational forces that act on all individual links of the robot by a single generalized force acting on the end effector, nevertheless this generalized force can not, necessarily, be defined as the gradient of a scalar potential field.

This limitation does not distract from the importance of the current study since it is common practice in the mechanical analysis and design of the primary links of the manipulators to either neglect the effect of secondary links, or lump them as a point mass at the end of the third link. The works of Dubowsky and Des Forges (1979), Liegeois et al (1980), Thomas and Tesar (1982), and Gosiewski (1986). are examples of such an approach. Furthermore, the error involved in this simplification is negligible even at high speeds. This can be verified by repeating the simulation carried out in Chapter 2 at high speed, this time with the secondary links lumped at the end of the third link. The results are shown in Figures 3.1 through 3.3. The corresponding joint torques obtained for the 6 dof arm in the previous analysis are also plotted for comparison.

The dashed curves show the magnitude of the joint torques for the case when the

minor links are lumped at the end of the third link. An overall examination of the curves for all cases reveals that the two curves are very close throughout the path such that the difference between them for all three links is insignificant and in fact negligible. As a result, it would be reasonable to assume that it is valid to treat the secondary links as a point mass lumped at the end effector. This approach greatly simplifies the process of modelling, analysis and design of the primary links without introducing any significant inaccuracy.

A proper selection of the orientation of the manipulator with respect to the direction of the gravitational acceleration makes the study of the GGF even more simplified. For instance if the manipulator is oriented such that the axis of rotation of the first link is parallel to the gravitational field, then the total potential energy of the system will be insensitive to the orientation of the first link. According to Tourassis and Neuman (1985) such an orientation will also help in improving the controllability of the arm. Taking this fact into account throughout this work the generalized gravitational field under consideration will have two dimensions. Such a field can be created by the upper two links of the a three link robot with its first link being vertical. Furthermore this study will focus on a manipulator with a parallel drive mechanical configuration.

3.2 Equipotential Surfaces

Figure 3.4 shows a schematic diagram of a parallel drive manipulator. [1] With the exception of the positions where the second and third links are collinear, all other points within the robot work volume may be reached through two different configurations. Throughout this work only the configurations where θ_2 is smaller than θ_1 will be considered. From a practical standpoint, some parallel drive robot arms such as the ASEA robot have the upper arm mechanically constrained such that θ_2 can never exceed θ_1.

With reference to Figure 3.4 and using θ_1 and θ_2 as the coordinates of the configuration space, the potential function is given by

$$U(\theta_1, \theta_2) = A_1 sin\theta_1 + A_2 sin\theta_2 \tag{3.1}$$

where

$$\begin{cases} A_1 = [m_1 h_1 + (m_2 + m_p) L_1] g \\ A_2 = (m_2 h_2 + m_p L_2) g \end{cases} \tag{3.2}$$

In the above expressions m_1 and m_2 are the masses of the links 1 and 2 respectively, m_p is the lumped mass of the payload at the end of the link 2, and g is the acceleration of gravity.

The maximum potential energy of the arm corresponds to the configuration where both links are vertical, i.e. where $\theta_1 = \theta_2 = 90°$, and is given by

$$U_{max} = A_1 + A_2$$

[1] A detailed definition for the parallel drive and serial drive manipulators is given in appendix C.

The total potential energy given by Equation 3.1 is normalized with respect to the maximum potential energy U_{max} as follows

$$u(\theta_1, \theta_2) = \frac{U(\theta_1, \theta_2)}{U_{max}} = a_1 sin\theta_1 + a_2 sin\theta_2 \tag{3.3}$$

where

$$\begin{cases} a_1 = \frac{A_1}{A_1 + A_2} \\ a_2 = \frac{A_2}{A_1 + A_2} \end{cases} \tag{3.4}$$

The bounds on the normalized potential energy are $-1 \leq u \leq 1$.

The potential function can be expressed as a function of x_1 and x_2 by finding θ_1 and θ_2 from the transformation relations

$$\begin{cases} x_1 = L_1 cos\theta_1 + L_2 cos\theta_2 \\ x_2 = L_1 sin\theta_1 + L_2 sin\theta_2 \end{cases} \tag{3.5}$$

and substituting them into Equation 3.3. The result will be

$$u(x_1, x_2) = \frac{a_2}{L_2} x_2 + (a_1 - \frac{L_1}{L_2} a_2) \frac{r x_2 + x_1 \sqrt{{x_1}^2 + {x_2}^2 - r^2}}{{x_1}^2 + {x_2}^2} \tag{3.6}$$

where

$$r = \frac{x_1^2 + x_2^2 + L_1^2 - L_2^2}{2L_1}$$

Figure 3.5 shows the generalized gravitational field in Cartesian space for the arm shown in Figure 3.4. The equipotential surfaces for a 3 DOF manipulator can be generated by simply rotating the equipotential lines of Figure 3.5 about the vertical axis.

The equipotential lines may also be constructed for a configuration space with the joint angles as its coordinates. Figure 3.6 shows these lines. The dashed lines represent the equipotential lines of the complementary configurations, i.e. configurations at which $\theta_1 \leq \theta_2$, and are shown here for completeness.

The followings are some salient points pertaining to the equipotential lines represented in Cartesian space shown in Figure 3.5.

- The equipotential lines of the GGF for a robot arm are distorted with varying space between them. This indicates that the strength of the field is nonhomogeneous and is a function of the configuration of the arm.
- The GGF has two singularity loci: the outer circle, and the inner circle. These circles correspond to the physical limits when both links are colinear.
- The equipotential lines may be divided into two distinct groups. The first group, associated with energy levels from zero to a certain energy level designated by u_{dis}, lose their continuity at the inner singularity circle. The second group are continuous from one end on the outer singularity circle to the other end on the same circle. The discontinuity in the first group is due to the physical constraint on the linkages that prevents the endpoint from passing through the inner circle. The lines stop at a point on the inner circle and continue from another point horizontally opposite to the stopping point.
- All equipotential lines are tangent, at their extrema, to the outer singularity circle. The two points of tangency have the same ordinates.
- The inner and outer singularity circles are envelopes of the family of the equipo-

tential lines. The proof for this statement will be carried out after the gradient field is defined.

the case where the links of the arm have equal lengths, the inner singularity circ will shrink to a point. In that case all equipotential lines will be continuous at that oint, however, they will not be smooth.

rominent points pertaining to the equipotential lines in the joint space shown in F ure 3.6 are

- The outer singularity circle in the Cartesian space maps onto the line $\theta_1 = \theta_2$, and the inner singularity circle maps onto the lines $\theta_1 - \theta_2 = \pm\pi$.

- Those equipotential lines with discontinuity in Cartesian space are also discontinuous in joint space, except that in the latter case the lines are not tangent to the singularities. This discrepancy in behaviour is due to the fact that the mapping is not conformal. However, all of the discontinuous lines meet the singularities at equal angles. With reference to the Cartesian and the joint space mapping in Figures 3.5 and 3.6, the equipotential line ABC ($u = 0.8$) is an example of a continuous energy line in both maps. The line DEFG ($u = 0.2$) is an example of a discontinuous energy line. It is discontinuous at points E and F.

3.3 Gradient Field

The gradient of the GGF in Cartesian space is a force field. The strength of this field at each point is a vector which is referred to as the generalized weight of the arm. The gradient field in Cartesian space can be expressed as

$$\nabla u(x_1, x_2) = w_1 \mathbf{i}_1 + w_2 \mathbf{i}_2$$

where $\mathbf{i}_1$ and $\mathbf{i}_2$ are unit vectors along x_1 and x_2 directions.

Applying the chain rule to differentiate Equation 3.3 with respect to x_1 and x_2, and using Equation 3.5, the components of the gradient are found as

$$\begin{cases} w_1 = -\frac{\partial u}{\partial x_1} = \frac{\frac{a_1}{L_1} - \frac{a_2}{L_2}}{tan\theta_1 - tan\theta_2} \\ w_2 = -\frac{\partial u}{\partial x_2} = -\frac{\frac{a_2}{L_2} tan\theta_1 - \frac{a_1}{L_1} tan\theta_2}{tan\theta_1 - tan\theta_2} \end{cases} \tag{3.7}$$

It should be noted that w_1 and w_2 are the normalized components of the gradient field. The actual components can be found by multiplying them by the normalization factor $A_1 + A_2$. Performing the multiplication and substituting for a_1 and a_2 from Equation 3.4 yields

$$\begin{cases} W_1 = \frac{\frac{A_1}{L_1} - \frac{A_2}{L_2}}{tan\theta_1 - tan\theta_2} \\ W_2 = -\frac{\frac{A_2}{L_2} tan\theta_1 - \frac{A_1}{L_1} tan\theta_2}{tan\theta_1 - tan\theta_2} \end{cases} \tag{3.8}$$

where A_1 and A_2 are given by the Equation 3.2.

Figure 3.7 shows the gradient field corresponding to the generalized gravitational field of Figure 3.5. The slope of the gradient vector at any point can be found from Equation 3.7 as

$$\frac{w_2}{w_1} = \frac{\frac{a_2}{L_2} tan\theta_1 - \frac{a_1}{L_1} tan\theta_2}{\frac{a_2}{L_2} - \frac{a_1}{L_1}} \tag{3.9}$$

The gradient vector is normal to the equipotential lines at any point, including those at which the equipotential lines meet the singularity circles. The equation of the outer and inner singularity circles are $\theta_1 - \theta_2 = 0$ and $\theta_1 - \theta_2 = \pi$ respectively. Substituting these relations into Equation 3.9 yields the slope of the gradient vector at those points as $tan\theta_1$ (or $tan\theta_2$). This slope coincides with the slope of the radii of the singularity circles. This indicates that at those points the gradient vector is perpendicular to the singularity circles, and therefore proves the observation stated earlier that the equipotential lines meet the singularity circles tangentially.

In joint space, the gradient of the field is a vector field whose components along the coordinate axes of the configuration space are torques that act on the corresponding joints. The equation of this field can be found by applying the ∇ operator to the energy function given by the Equation 3.3. The result will be

$$\nabla\, u(\theta_1, \theta_2) = \tau_1 \mathbf{e}_1 + \tau_2 \mathbf{e}_2$$

where $\mathbf{e}_1$ and $\mathbf{e}_2$ are unit vectors along the coordinate axes of joint space. Differentiating Equation 3.3 with respect to θ_1 and θ_2 gives

$$\begin{cases} \tau_1 = -\frac{\partial u}{\partial \theta_1} = -a_1 cos\theta_1 \\ \tau_2 = -\frac{\partial u}{\partial \theta_2} = -a_2 cos\theta_2 \end{cases}$$

The torques obtained from the above equations are normalized with respect to $A_1 + A_2$.

3.4 Curl and Divergence of the Field

The gradient field derived in the preceding section show the direction and magnitude of the maximum rate of change of the total potential energy of the arm. This field completely represents the effect of gravity on the whole arm and according to Equation 3.7 it is a function of the space only. In other words the generalized weight of the arm, as can be seen from the Figure 3.7, varies from point to point both in magnitude and direction.

In any vector field, the curl and divergence can be utilized as a measure of the space rate of change of the strength of the field. On the other hand, a vector field that can be expressed as the gradient of a scalar field is conservative. Consequently, the generalized gravitational field is conservative both in joint and Cartesian spaces. This observation can be analytically verified by taking the curl of the vector fields and showing that they identically vanish.

The Laplacian of the GGF in Cartesian space can be expressed as

$$\nabla^2 u(x_1, x_2) = \frac{\partial w_1}{\partial x_1} + \frac{\partial w_2}{\partial x_2} \tag{3.10}$$

Solving Equations 3.10 and 3.7 together with Equation 3.5 gives

$$div\mathbf{w} = -\nabla^2 u(x_1, x_2) = (\frac{L_2}{L_1})^2 (a_1 - \frac{L_1}{L_2} a_2) \frac{x_1}{(x_1^2 + x_2^2 - r^2)^{3/2}} \tag{3.11}$$

The divergence of the field for the joint space can be obtained from the Equation 3.3 as

$$div\tau = -\nabla^2 u(\theta_1, \theta_2) = u(\theta_1, \theta_2) \tag{3.12}$$

As Equations 3.11 and 3.12 show, the generalized gravitational field is not

solenoidal in either the joint or the Cartesian space. In other words the divergence of the gradient field (or the Laplacian of the gravitational field), in general, does not vanish anywhere in the space. The nonsolenoidal GGF is similar, in nature, to an electrostatic field in a charged medium with the density of the charge being a function of the space; or to a gravitational field in a massive medium with a variable mass density. The differential equations of such fields have the form of Poisson's partial differential equation rather than Laplace's equation.

3.5 Force Lines

A scalar field may be portrayed graphically with the aid of constant value surfaces. Such a representation is not meaningful for portraying a vector field. The conventional method for graphically portraying a vector field is to draw force lines which are tangent to the vector field at all points. The force lines form a system of orthogonal trajectories to the family of equipotential surfaces. In a solenoidal field the force lines represent the direction, and the inverse of the spacing between them represent the magnitude of the field. Since the GGF is nonsolenoidal, the spacing between the force lines can not be taken as representative of the strength of the field. Instead, the spacing between the equipotential lines should be taken as a rough quantitative measure of the strength of the field. The smaller the spacing between two consecutive equipotential lines at a point, the stronger the field will be at that point, and vice versa.

Referring to Equation 3.9 the differential equation of the force lines in Cartesian

space is given by

$$\frac{dx_2}{dx_1} = \frac{w_2}{w_1} = \frac{\frac{a_2}{L_2}tan\theta_1 - \frac{a_1}{L_1}tan\theta_2}{\frac{a_2}{L_2} - \frac{a_1}{L_1}} \tag{3.13}$$

For the differential in Equation 3.13 to be exact, the divergence of the field must vanish. However, it was shown previously that this is not the case. It should be noted here that the divergence of a field at a point P is a measure of the strength of the source (or sink) at that point. If, within an infinitesimal surface surrounding the point, no force lines start or stop, then the divergence is said to be zero at that point. On the other hand, if the net flux of lines is different from zero, then depending on the sign of the divergence, that point acts as a source or a sink. A positive divergence indicates a source at P, while a negative divergence indicates a sink. Figure 3.S shows some typical force lines for the field shown in Figure 3.5.

Equation 3.11 shows that in Cartesian space the sign of the divergence is determined by a_1, a_2 and x_1. Along the vertical axis the divergence vanishes irrespective of the magnitude of a_1 and a_2. For values of a_1 and a_2 that make the factor $(a_1 - \frac{L_1}{L_2}a_2)$ nonzero, the vertical axis will divide the configuration space into two halves. For positive values of the factor, all points in the right half plane will act as sources, and points in the left half will act as sinks. Thus, moving from higher potential levels towards lower ones in the right half plane, force lines will continuously be generated. Their rate of generation, however, will not be uniform. For negative values of the factor, the situation of sources and sinks is reversed. When the factor equals zero the field will be solenoidal. This condition will be examined in detail in a later section.

In the joint space the differential equation of the normal lines is given by

$$\frac{d\theta_2}{d\theta_1} = \frac{a_2 cos\theta_2}{a_1 cos\theta_1}$$

Separating the variables and integrating yields the general solution as follows

$$\left(\frac{1+sin\theta_1}{cos\theta_1}\right)^{a_2}-\left(\frac{cos\theta_2}{1+sin\theta_2}\right)^{a_1}=C$$

where C is the constant of integration. Assigning different values to C gives the equation of normal lines. Figure 3.9 shows some typical normal lines of the joint space.

Equation 3.12 shows that the divergence of this field at any point is equal to the value of the potential at that point. This means that the rate of creation of normal lines is proportional to the level of energy. All points of the field associated with positive energy will act as sources and all points with negative energy levels will act as sinks. For points lying on the zero energy line, equal number of normal lines will be created and vanish.

3.6 Strength Distribution of the Field

The strength of the field in both Cartesian and joint spaces is not uniform. However, the shape of the equipotential lines in Figures 3.5 and 3.6 indicate that they possess some ordered trends. In Cartesian space, all equipotential lines originate at the outer singularity circle with infinitesimally small spacing between them. The spacings then gradually increase up to a maximum somewhere along the line before starting to decrease. The equipotential lines then terminate at some other points of the singularity circle, again with an infinitesimally small spacing between them. In order to find the points associated with minimum field strength along the equipotential lines, the magnitude of the force vector

$$f(x_1, x_2) = \sqrt{{w_1}^2 + {w_2}^2} = \sqrt{(\frac{\partial u}{\partial x_1})^2 + (\frac{\partial u}{\partial x_2})^2} \tag{3.14}$$

must be minimized subject to the equality constraint

$$g(x_1, x_2) = u(x_1, x_2) - const. = 0$$

Applying the method of Lagrange multipliers gives the set of auxiliary equations as

$$\nabla f(x_1, x_2) = \mu \nabla g(x_1, x_2)$$

which leads to the set of equations

$$\begin{cases} \frac{\partial f(x_1,x_2)}{\partial x_1} = \mu \frac{\partial u(x_1,x_2)}{\partial x_1} \\ \frac{\partial f(x_1,x_2)}{\partial x_2} = \mu \frac{\partial u(x_1,x_2)}{\partial x_2} \end{cases}$$

Dividing both sides of the first equation by the second and substituting for the partial derivatives of f from Equation 3.14 leads to

$$\frac{\frac{\partial^2 u}{\partial x_1^2} - \frac{\partial^2 u}{\partial x_2^2}}{\frac{\partial^2 u}{\partial x_1 \partial x_2}} = \frac{(\frac{\partial u}{\partial x_1})^2 - (\frac{\partial u}{\partial x_2})^2}{\frac{\partial u}{\partial x_1}\frac{\partial u}{\partial x_2}}$$

The first partial derivatives of $u(x_1, x_2)$ are given by the set of Equations 3.7. Applying the chain rule to the same set will give the second partial derivatives of $u(x_1, x_2)$. Substituting for these values in the above equation results in

$$\frac{\frac{a_2}{L_2}cos\theta_2 - \frac{a_1}{L_1}cos\theta_1 cos(\theta_1 - \theta_2)}{\frac{a_1}{L_1}cos\theta_1 - \frac{a_2}{L_2}cos\theta_2 cos(\theta_1 - \theta_2)} = \frac{a_2 cos^2\theta_2}{a_1 cos^2\theta_1} \tag{3.15}$$

This is the equation of the locus of the minimum generalized weight, i.e. the locus of the weakest points of the field in Cartesian space. Combining this equation

with Equation 3.5 gives the equation of this locus as a function of x_1 and x_2 in Cartesian space. Figure 3.10 shows the plot of this locus with a chain dot curve. The corresponding locus in joint space is shown in Figure 3.11.

The points associated with maximum generalized weight lie on the two singularity circles. The magnitude of the generalized weight at those points is infinitely large.

In a similar way the loci of the points at which the strength of the field, in joint space, is a minimum or a maximum, can be found at the extrema of the magnitude of the torque vector

$$\tau(\theta_1, \theta_2) = \sqrt{\tau_1^2 + \tau_2^2}$$

subject to the equality constraint

$$h(\theta_1, \theta_2) = u - a_1 sin\theta_1 - a_2 sin\theta_2 = 0$$

The following solutions are obtained.

$$\theta_1 = 90°, \qquad \theta_1 = 270°, \qquad \theta_2 = 90°, \qquad \theta_2 = 270°, \qquad a_1 sin\theta_1 = a_2 sin\theta_2$$

Figure 3.12 shows the locus, in Cartesian space, of the points associated with minimum and maximum values of the torque vector by a chain dot and a solid line respectively. The corresponding loci in joint space are shown in Figure 3.13. All the above results and observations are summarized in Table 3.1.

LOCUS	CURVE SECTION	GOVERNING EQUATIONS
minimum force	$ABCD$ (chain dot)	Equation 3.15
maximum force	singularities (solid)	$\theta_1 - \theta_2 = 0, \pi$
minimum torque	$A'BCD$(chain dot)	$\theta_1 = 90, \theta_2 = 270$
maximum torque	DE and GEF(solid)	$\theta_2 = 90, a_1 sin\theta_1 = a_2 sin\theta_2$

Table 3.1: Loci of the points with extremum field strength

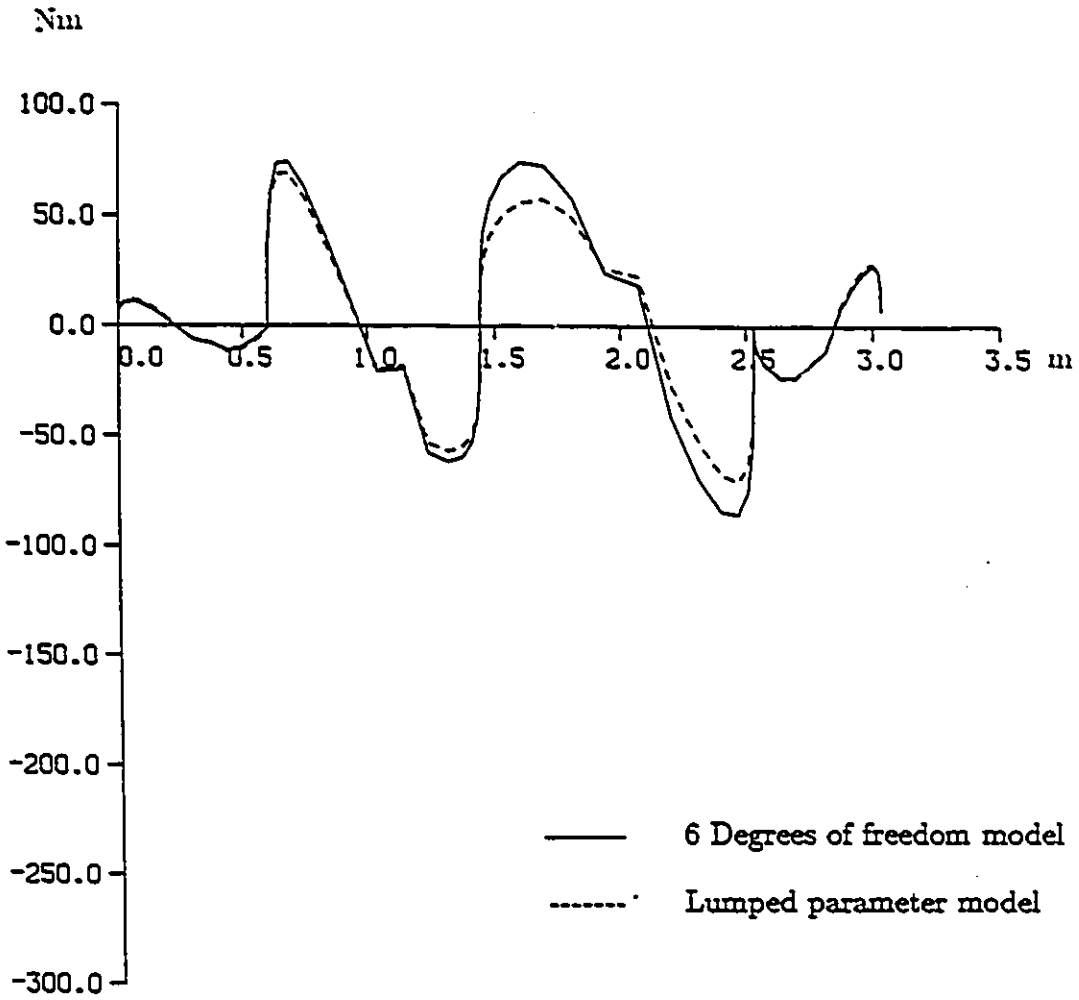

Figure 3.1: Torque of joint 1 versus the distance traversed by the end effector for the case when the secondary links are lumped at the end of the third link.

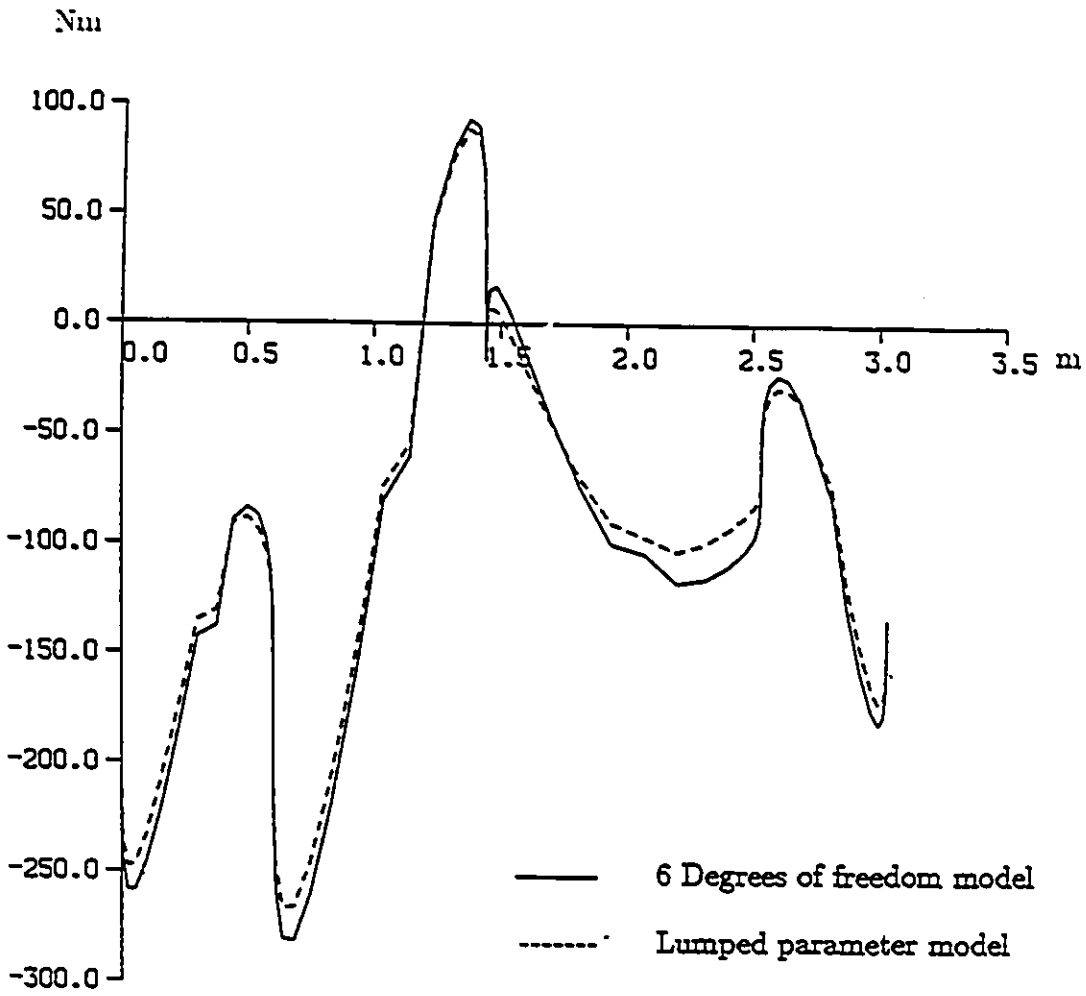

Figure 3.2: Torque of joint 2 versus the distance traversed by the end effector for the case when the secondary links are lumped at the end of the third link.

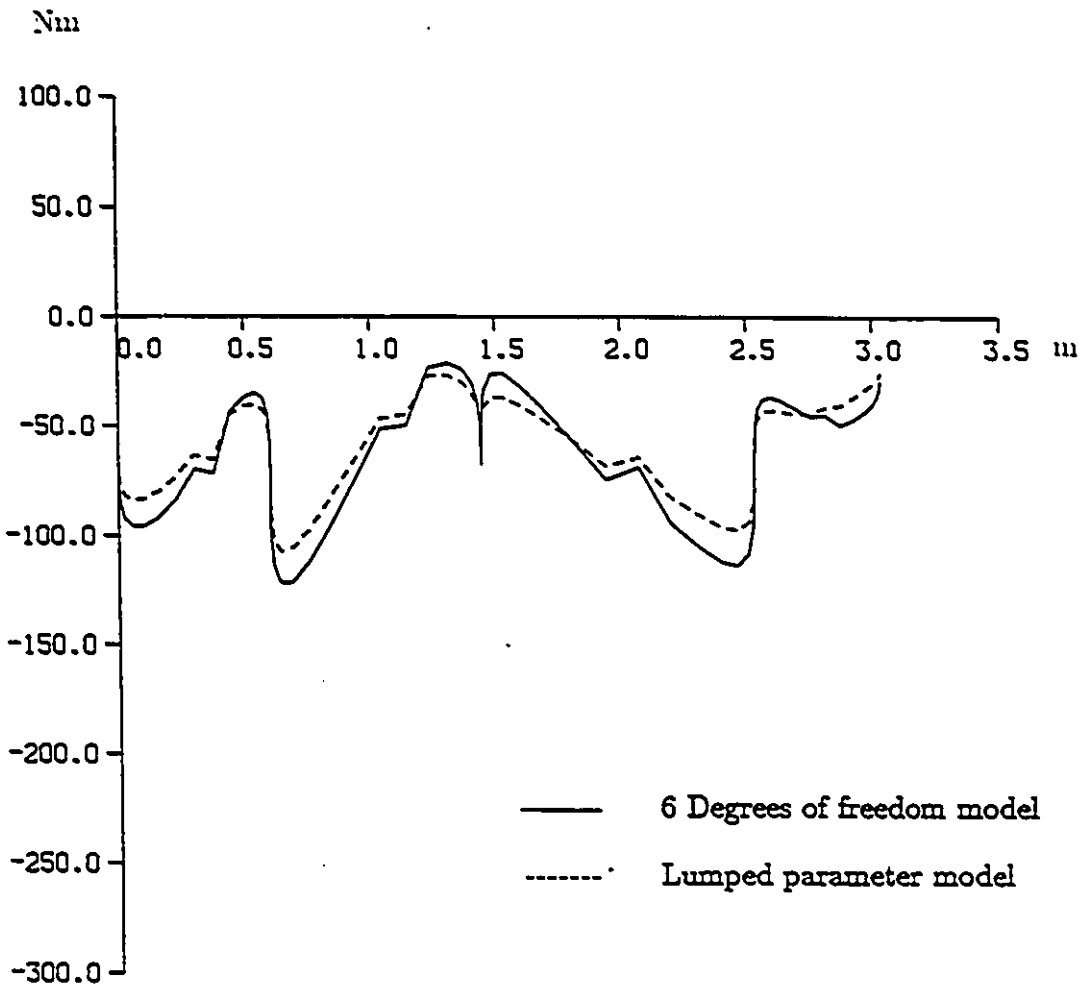

Figure 3.3: Torque of joint 3 versus the distance traversed by the end effector for the case when the secondary links are lumped at the end of the third link.

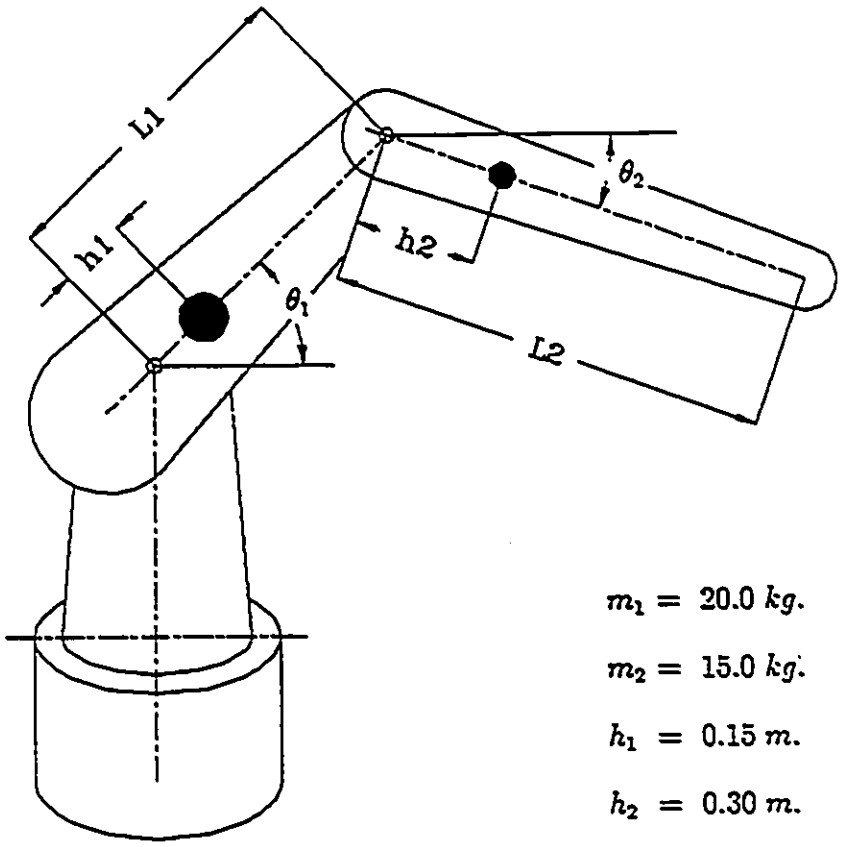

$m_1 = 20.0\ kg.$

$m_2 = 15.0\ kg.$

$h_1 = 0.15\ m.$

$h_2 = 0.30\ m.$

$L_1 = 0.50\ m.$

$L_2 = 0.70\ m.$

Figure 3.4: Parallel drive manipulator with primary links only.

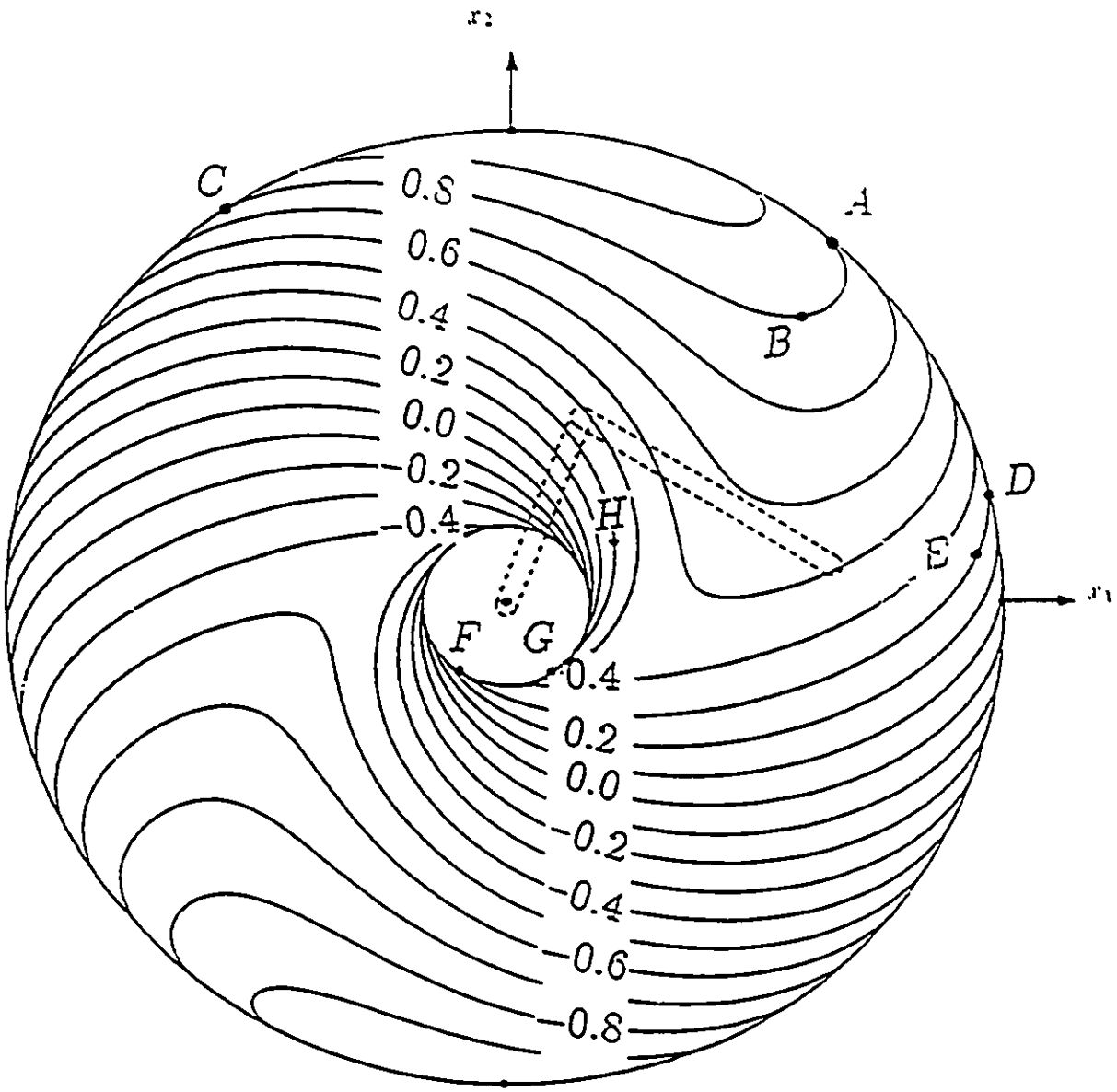

Figure 3.5: Generalized Gravitational Field in Cartesian space for a manipulator with primary links only.

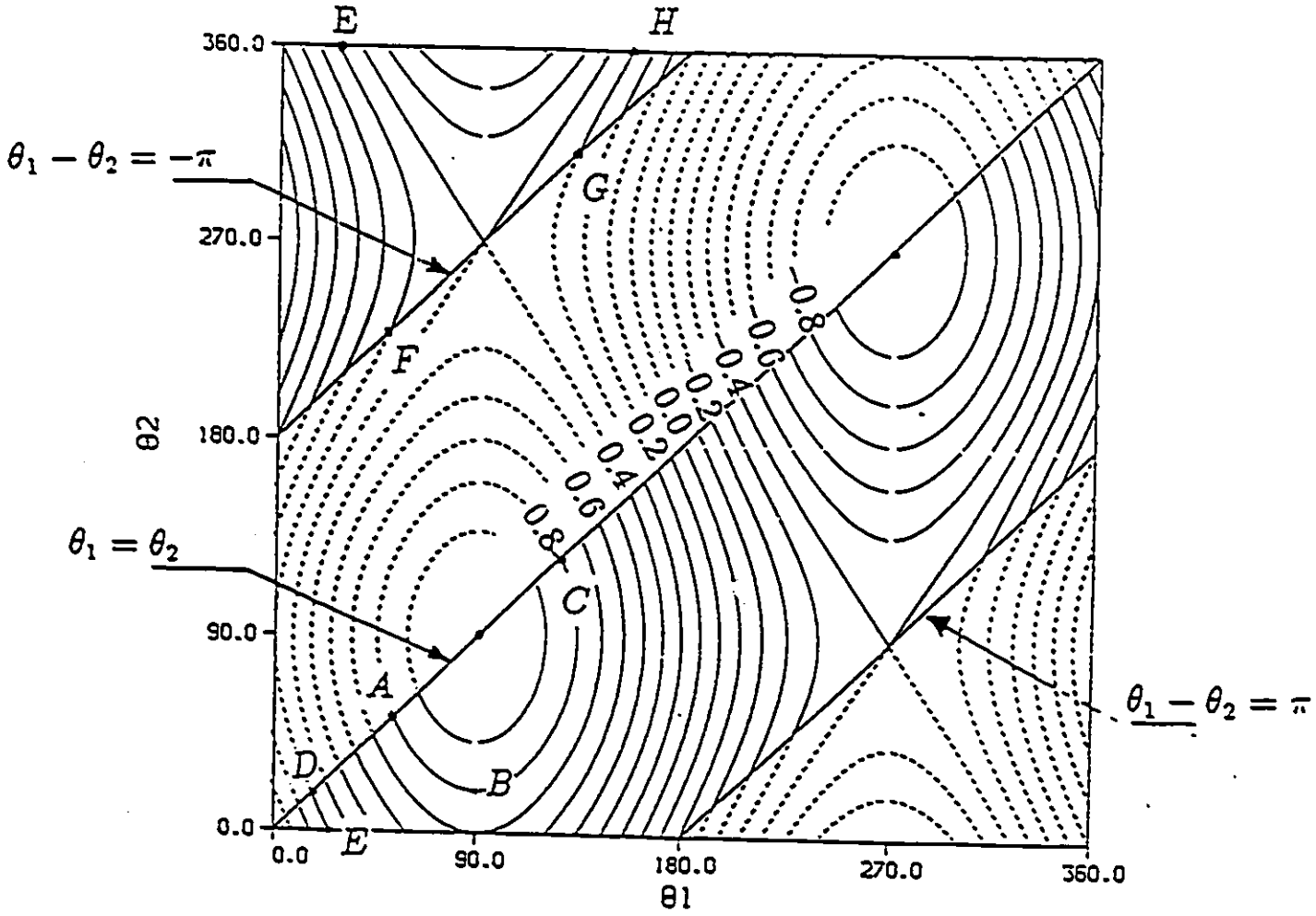

Figure 3.6: Generalized Gravitational Field in joint space for a manipulator with primary links only.

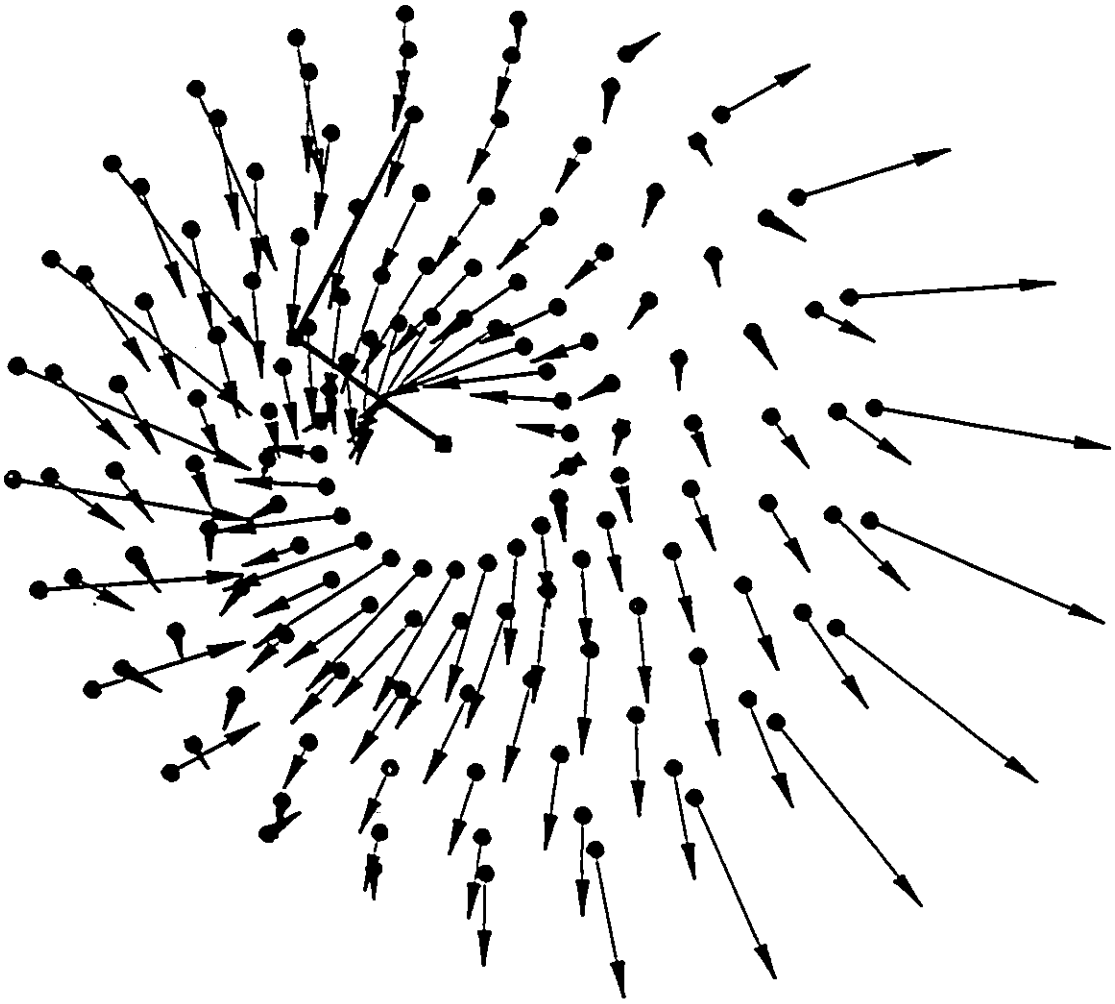

Figure 3.7: Generalized weight field for a manipulator with primary links only.

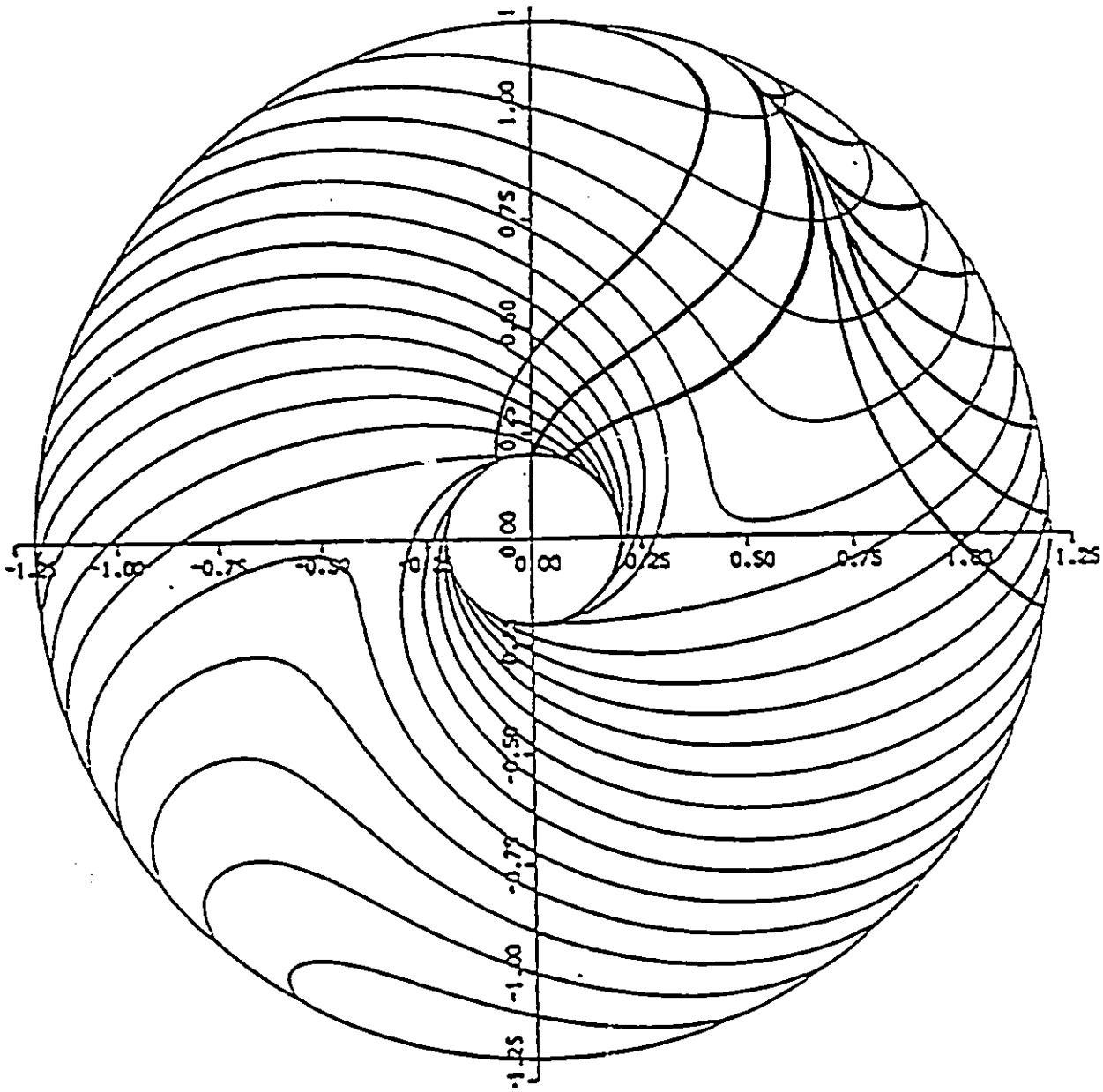

Figure 3.8: Typical force lines in Cartesian space.

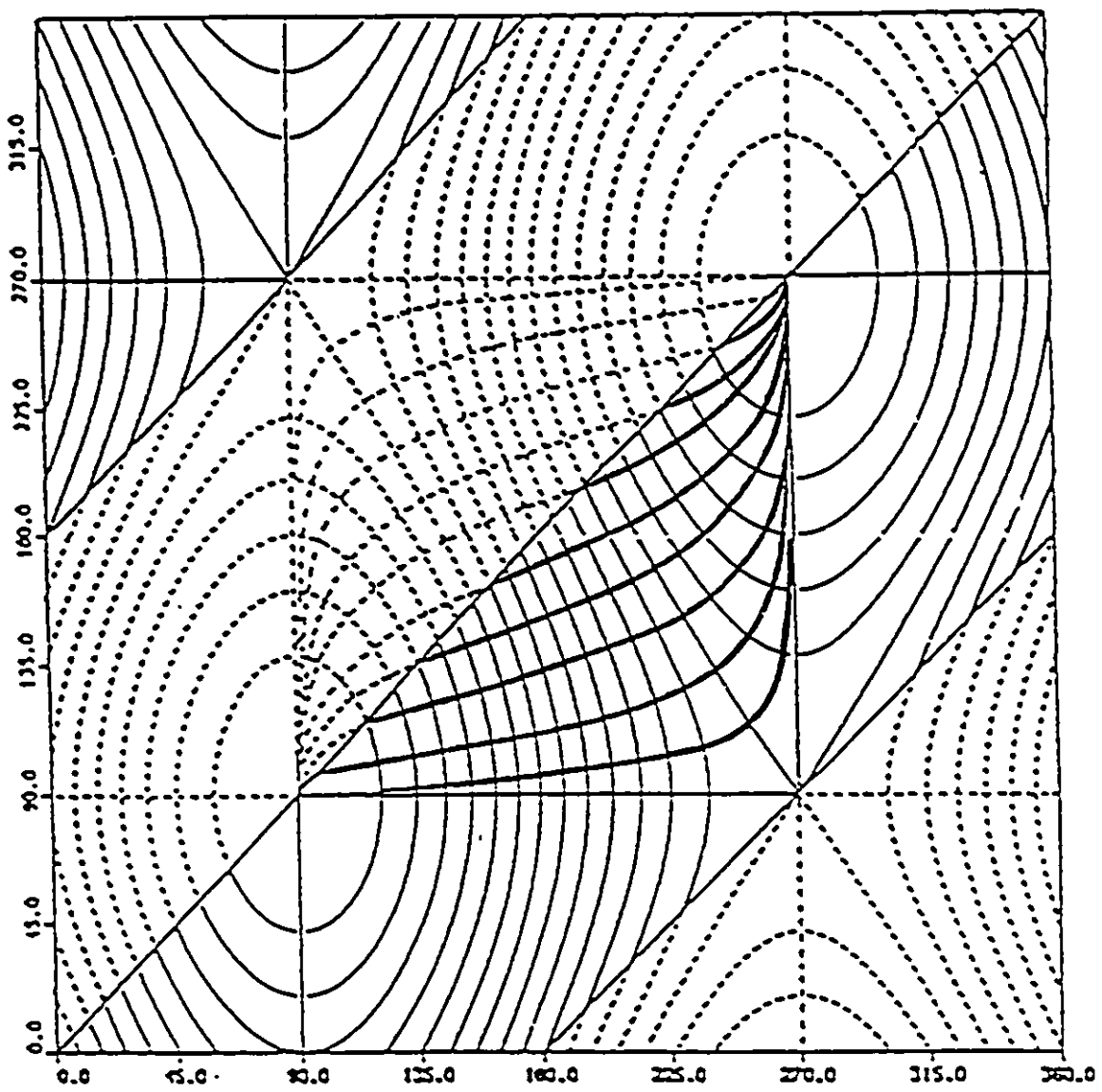

Figure 3.9: Typical force lines in joint space.

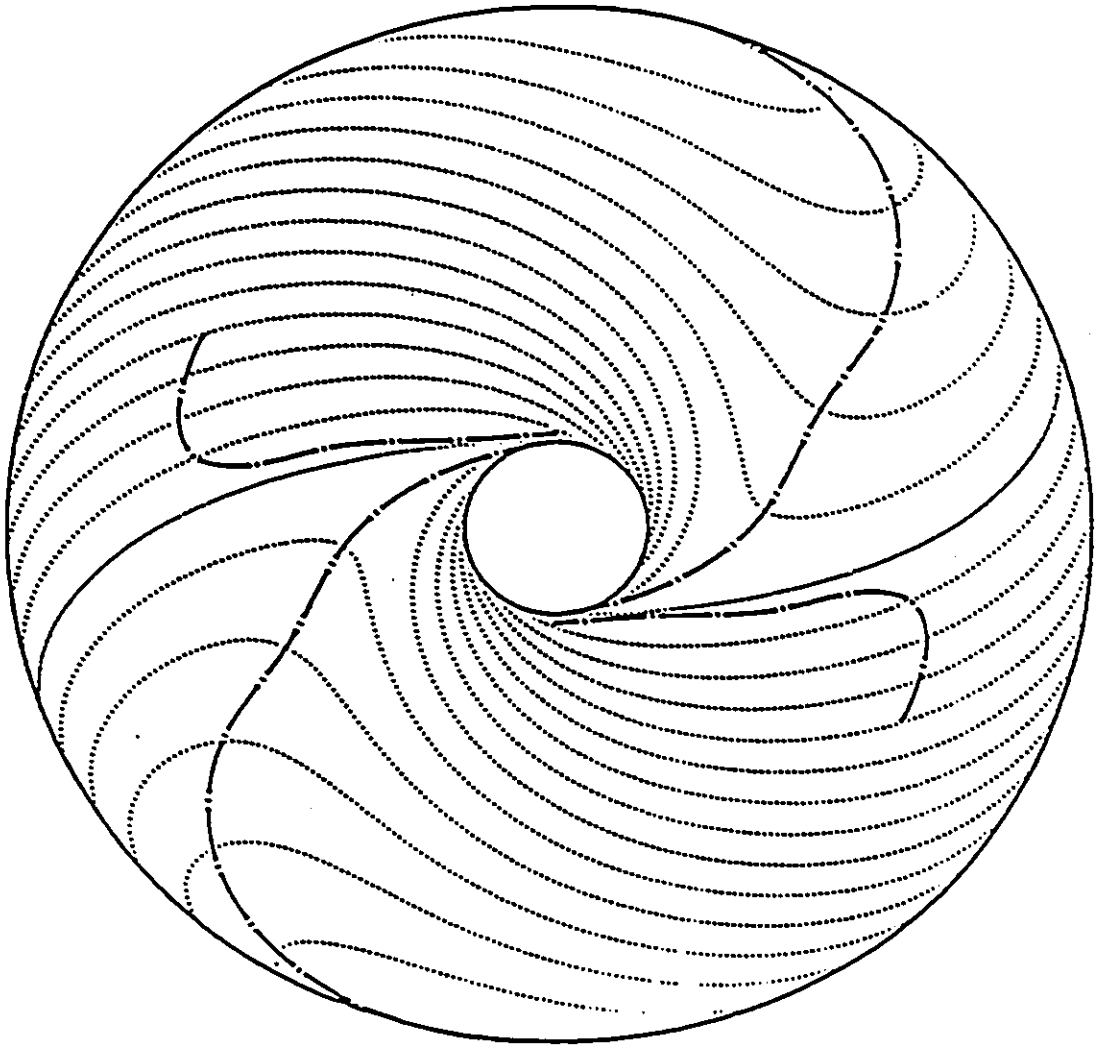

Figure 3.10: Loci of extremum force in Cartesian space.

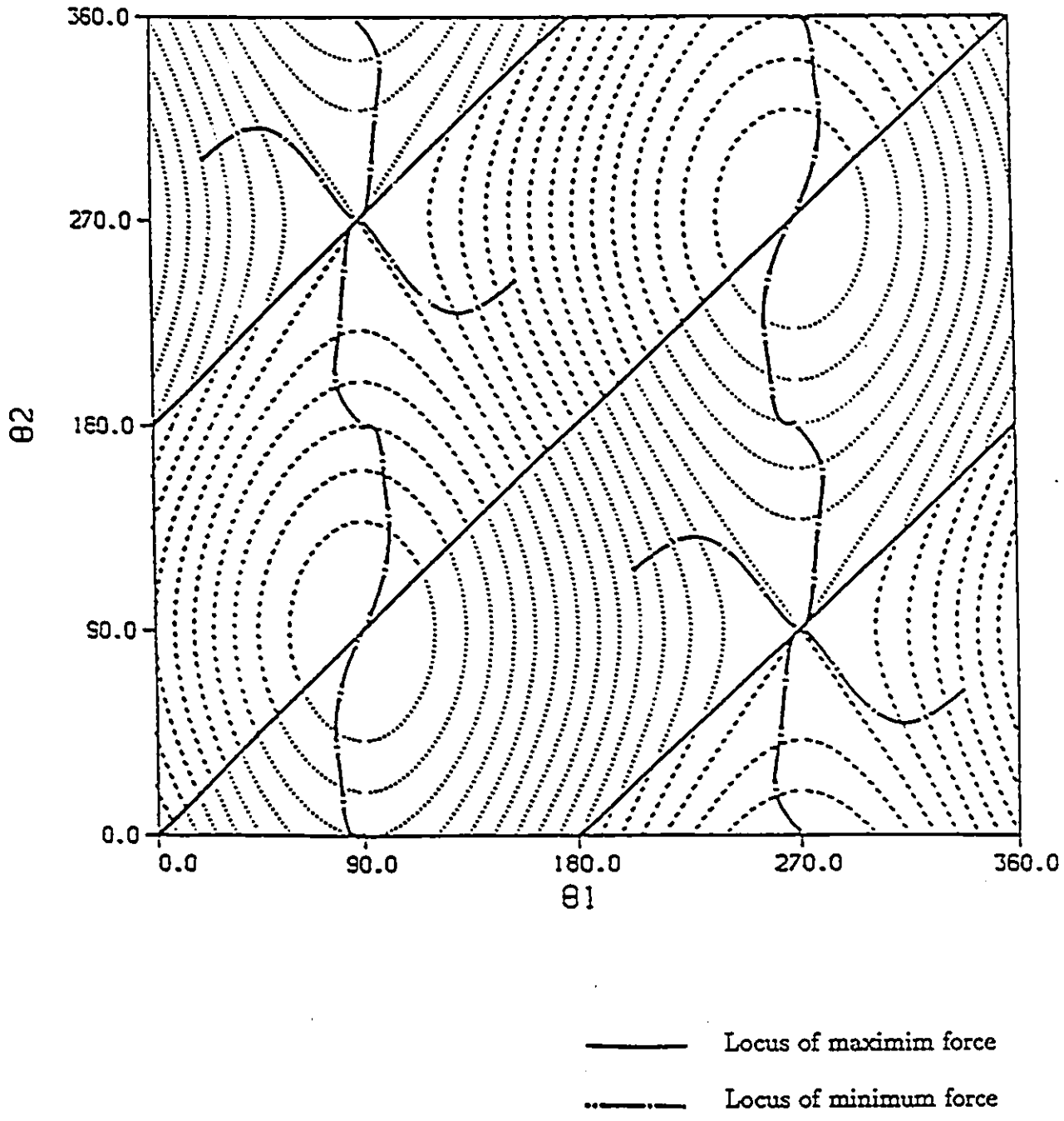

Figure 3.11: Loci of extremum force in joint space.

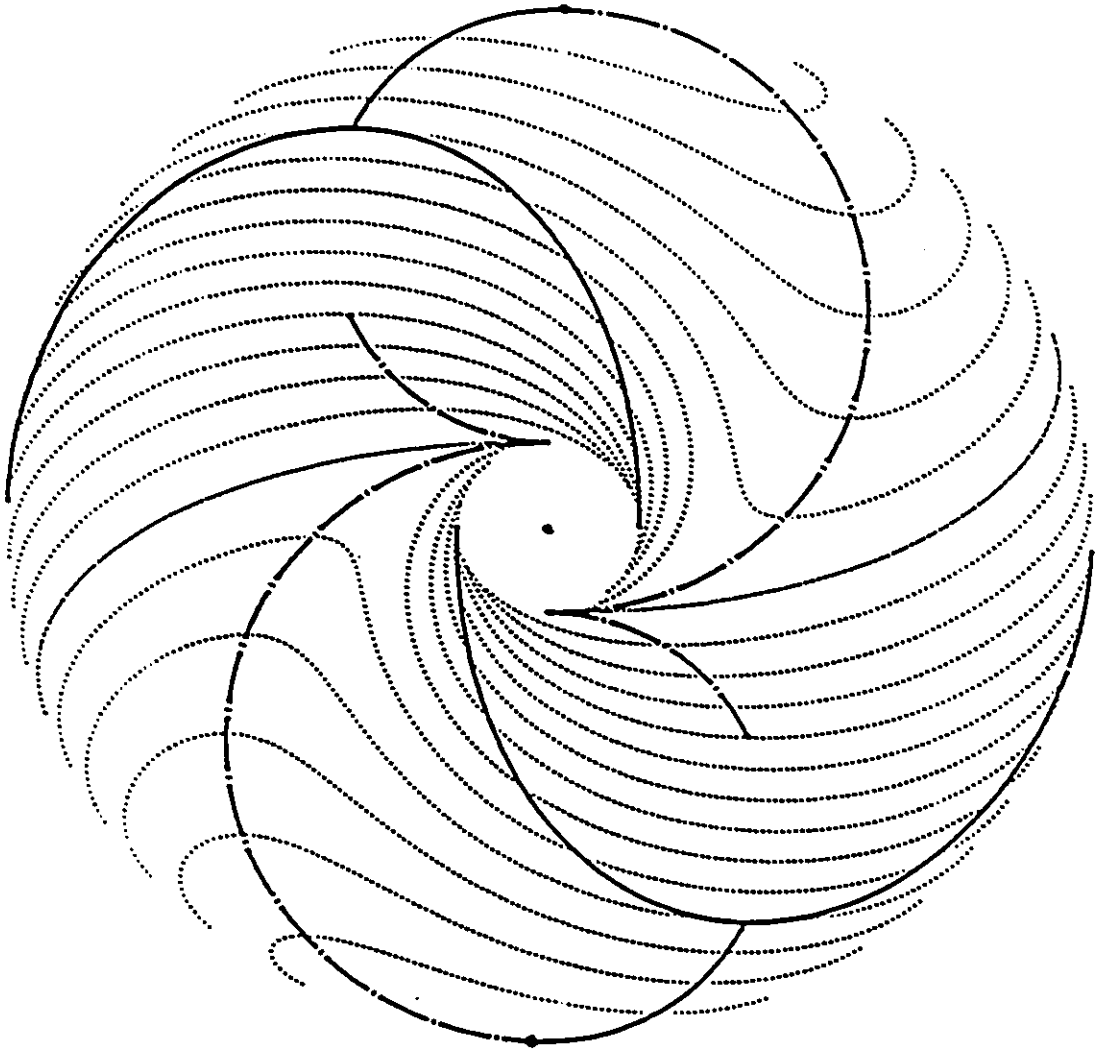

Figure 3.12: Loci of extremum torque in Cartesian space.

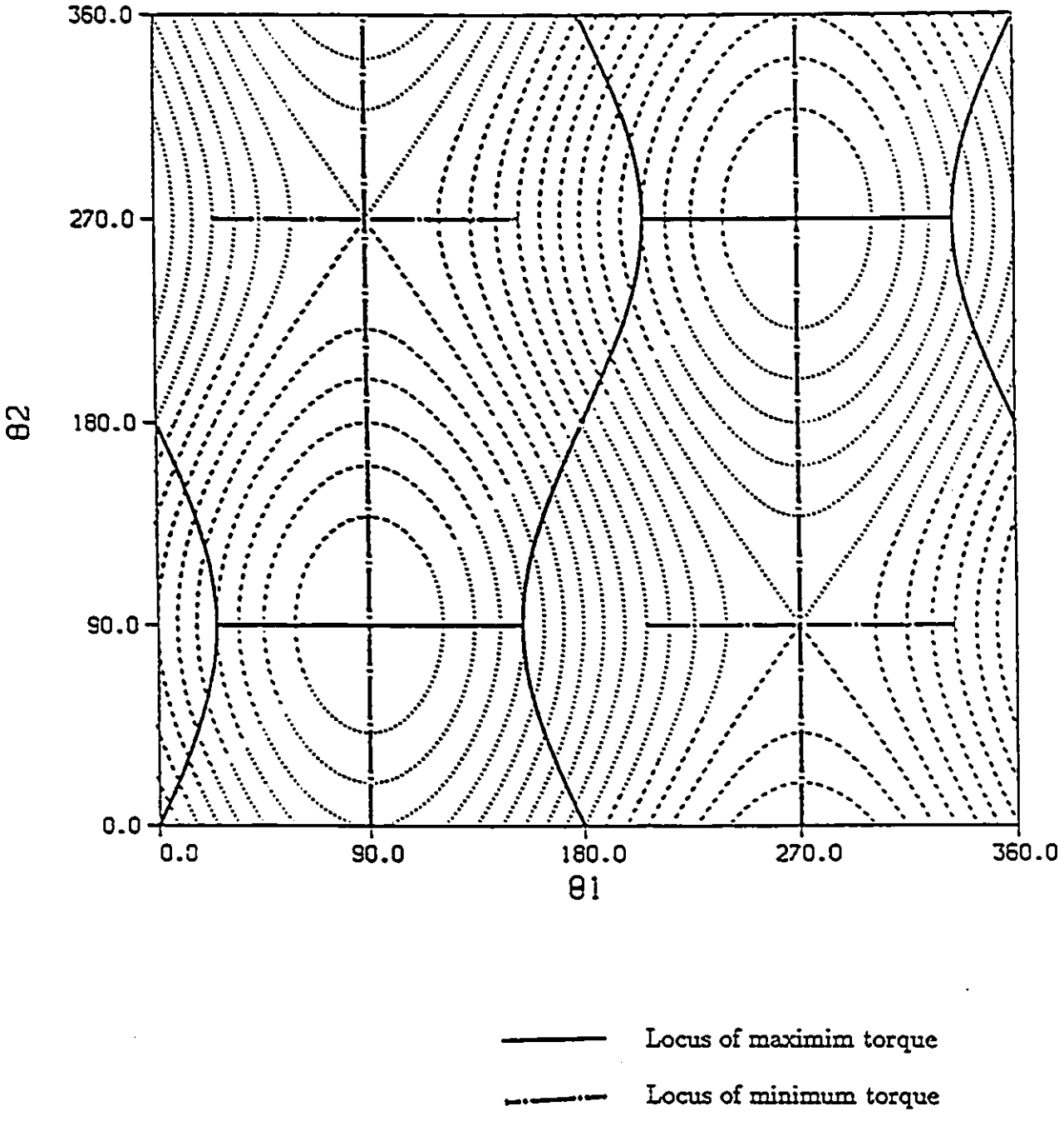

Figure 3.13: Loci of extremum torque in joint space.

Chapter 4

Static Behavior of the Manipulator

4.1 Introduction

An important issue in the design of any mechanical system is the study of the characteristics of its output and that of the demand, i.e. the load that the system is designed to carry. The system reaches its operating condition only when its output meets the demand. In case of a manipulator the output of the system is some mechanical force or torque developed by the axes drives, and the demand or load that acts on the system is a combination of the inertial, gravitational and frictional forces or torques.

Yoshikawa (1983), and Asada and Youcef-Toumi (1984) have shown that for a given value of the total power supplied to the joint motors under stall condition, the capability of a manipulator's end effector in applying static force to its surroundings can be represented by an ellipsoidal surface in the task space. In other words if the

tip of the vectors of the force that the end effector can apply to the external world in any direction are connected, an ellipsoid will be formed. They called this ellipsoid the force ellipsoid.

The generalized weight of the arm, defined in Chapter 3, will be considered here as the demand force. However, it should be mentioned that although the generalized weight may act as the demand force in one direction, in the opposite direction it will tend to augment the output of the axes drives.

In this chapter the quadratic function that expresses the analytical form of the force ellipsoid will first be obtained. Then, for the robot arm shown in the Figure 3.4, the force ellipsoids will be plotted for several configurations of the arm throughout its work volume. It will be shown that there is a strong relationship between the size as well as the orientation of the ellipsoids at various points of the work volume. In order to establish a thorough representation of the output-demand relationship for the manipulator, the force ellipsoid will be related to the generalized weight of the arm both in magnitude and direction. It will also be shown that the true capability of the end effector in applying static force to the environment is revealed only when the force ellipsoid at each point of the work volume is shifted to the tip of the vector of the generalized weight at that point. As a result, the maximum and minimum values of the task force must be modified accordingly.

4.2 Output Characteristics of the Arm

A large number of robots use iron core permanent magnet DC motors in their drive system. The relation between the power supplied to a DC motor and its output torque under stall condition can be written as (Saner 1987)

$$p = \frac{\tau_m^2}{K_m^2} \tag{4.1}$$

where p is the input power to the motor, τ_m represents the output torque of the motor, and K_m is the motor constant.

The total power (P) supplied to all of the joint motors is then given by

$$P = \frac{\tau_{m1}^2}{K_{m1}^2} + \frac{\tau_{m2}^2}{K_{m2}^2} + \cdots + \frac{\tau_{mn}^2}{K_{mn}^2}$$

This equation can be expressed in matrix form as

$$P = \left\{ \tau_m \right\}^T \left[\mathbf{K} \right] \left\{ \tau_m \right\} \tag{4.2}$$

where

$$\left[\mathbf{K} \right] = \left[\frac{1}{K_{mi}^2} \right] \tag{4.3}$$

The torque (force) τ developed by the joint motors is transformed through the manipulator's mechanism into a generalized force $\mathbf{F}$ at the end effector. This force can be applied to the external environment and is called the *task force*. Using the principle of virtual work it has been shown by many authors (see for example Shahinpoor 1987) that the relationship between the joint torques and the task force is given by

$$\left\{ \tau \right\} = \left[\mathbf{J} \right]^T \left\{ \mathbf{F} \right\} \tag{4.4}$$

where J represents the Jacobian matrix of the transformation. J is the matrix that relates infinitesimal variations in the joint space of the robot arm to infinitesimal displacements of the end effector in the task space.

It should be noted that the effect of gravity is not included in the above equation. The vector τ represents only the net torque at the joint motors that balances the external forces, or moments, applied to the end effector by the environment. Therefore the vector τ in the above equation may be replaced by the vector of the torques of the joint motors τ_m. Substituting for this vector from Equation 4.4 into Equation 4.2 yields

$$P = \{\mathbf{F}\}^T [\ \mathbf{J}\ ][\ \mathbf{K}\ ][\ \mathbf{J}\ ]^T \{\mathbf{F}\} \tag{4.5}$$

Let

$$[\ \mathbf{B}\ ] = [\ \mathbf{J}\ ][\ \mathbf{K}\ ][\ \mathbf{J}\ ]^T \tag{4.6}$$

Equation 4.5 then becomes

$$\{\mathbf{F}\}^T [\ \mathbf{B}\ ] \{\mathbf{F}\} = P \tag{4.7}$$

Equation 4.7 is a quadratic form. It represents an ellipsoidal hypersurface if the matrix $\mathbf{B}$ is positive definite, i.e. if all of its eigenvalues are of the same sign (Fraleigh 1987). As long as the Jacobian matrix $\mathbf{J}$ in Equation 4.6 is nonsingular the matrix $\mathbf{B}$ is congruent to the diagonal matrix $\mathbf{K}$ (Lipschutz 1987). On the other hand, according to the Sylvester's law of inertia, in a congruence transformation the signs of eigenvalues are preserved (Strang 1976). Therefore, the eigenvalues of the matrix $\mathbf{B}$ have the same sign as those of the matrix $\mathbf{K}$. Thus the matrix $\mathbf{B}$ is also positive definite and the quadratic form given by the Equation 4.7 represents an

ellipsoidal hypersurface in the task space. This quadratic form can be diagonalized through the transformation

$$\left\{\mathbf{F}\right\} = \left[\ \mathbf{C}\ \right]\left\{\mathbf{U}\right\} \tag{4.8}$$

where $\mathbf{C}$ is an $n \times n$ orthogonal matrix called the diagonalizing matrix. The jth column vector of $\mathbf{C}$ is a normalized eigenvector of the matrix $\mathbf{B}$ which corresponds to its jth eigenvalue λ_j. The column vectors of $\mathbf{C}$ form an orthonormal basis. The diagonalized form appears as

$$\lambda_1 u_1^2 + \lambda_2 u_2^2 + \cdots + \lambda_n u_n^2 = P \tag{4.9}$$

where the λ_j are the eigenvalues of the matrix $\mathbf{B}$.

The eigenvalues indicate the efficiency with which the input power to the joint motors is converted into the task force. A large eigenvalue λ_i indicates that a large share of the total power will be dissipated in the process of producing the task force F_i in the direction of the corresponding eigenvector. More precisely, for a given amount of total input power, the magnitude of the task force in any direction is inversely proportional to the square root of the corresponding eigenvalue. As a result, for a given amount of input power, the magnitude of the task force will be a maximum along the major axis of the force ellipsoid which is associated with the smallest eigenvalue. Conversely, the magnitude of the task force will be a minimum along the minor axis of the force ellipsoid which is associated with the largest eigenvalue.

To evaluate the overall efficiency of the power-force conversion, Asada and Youcef-Toumi(1984) have defined the power dissipation ratio λ_m as the mean of the eigen-

values. It is given as

$$\lambda_m = \frac{1}{n} trace\left[\ \mathbf{B}\ \right] \tag{4.10}$$

For the example robot at hand the output characteristics can be represented by a quadratic form whose equation in principal space is

$$\lambda_1 u_1^2 + \lambda_2 u_2^2 = P \tag{4.11}$$

To obtain λ_1 and λ_2 the matrix $\mathbf{B}$ should first be set up. The Jacobian matrix associated with the arm's links can be expressed as

$$\left[\ \mathbf{J}\ \right] = \begin{bmatrix} -L_1 sin\theta_1 & -L_2 sin\theta_2 \\ L_1 cos\theta_1 & L_2 cos\theta_2 \end{bmatrix} \tag{4.12}$$

Substituting for the matrix $\mathbf{J}$ from above, and for the matrix $\mathbf{K}$ from Equation 4.3 in Equation 4.6 yields

$$\left[\ \mathbf{B}\ \right] = \begin{bmatrix} q_1^2 S_1^2 + q_2^2 S_2^2 & -(q_1^2 S_1 C_1 + q_2^2 S_2 C_2) \\ -(q_1^2 S_1 C_1 + q_2^2 S_2 C_2) & q_1^2 C_1^2 + q_2^2 C_2^2 \end{bmatrix} \tag{4.13}$$

where

$$\begin{aligned} q_1 &= \frac{L_1}{K_{m1}} \\ q_2 &= \frac{L_2}{K_{m2}} \end{aligned} \tag{4.14}$$

and $S_i = sin\theta_i$, $C_i = cos\theta_i$

The eigenvalues of the matrix $\mathbf{B}$ are

$$\begin{aligned} \lambda_1 &= \tfrac{1}{2}\left(q_1^2 + q_2^2 - \sqrt{q_1^4 + q_2^4 + 2q_1^2 q_2^2\ cos2(\theta_1 - \theta_2)}\right) \\ \lambda_2 &= \tfrac{1}{2}\left(q_1^2 + q_2^2 + \sqrt{q_1^4 + q_2^4 + 2q_1^2 q_2^2\ cos2(\theta_1 - \theta_2)}\right) \end{aligned} \tag{4.15}$$

From Equations 4.10 and 4.13 the mean power dissipation ratio can be found as

$$\lambda_m = \frac{1}{2}(q_1^2 + q_2^2) = \frac{1}{2}\left(\frac{L_1^2}{K_{m1}^2} + \frac{L_2^2}{K_{m2}^2}\right) \tag{4.16}$$

The above equation indicates that although the individual eigenvalues are, in general, functions of the configuration of the manipulator, the mean of their sum remains the same throughout the work volume. It can further be concluded that for manipulators with shorter links and larger motor constants, the value of λ_m is smaller. Consequently, the power to force conversion for these kind of manipulators would be more efficient. This result was first obtained by Asada and Youcef-Toumi (1984).

The equation of the force ellipsoid can be found by substituting for λ_1 and λ_2 from Equation 4.15 in Equation 4.11. Figure 4.1 shows the force ellipsoids for several configurations of the arm. In order to draw information from this figure it is convenient to divide the work volume of the manipulator into concentric circles created by the end effector travelling while $\theta_1 - \theta_2$ is kept constant. These circles will be referred to as the *solid configuration circles*. In particular the solid configuration circle associated with $\theta_1 - \theta_2 = 90°$ will be called the *home circle*.

Regarding the size and the orientation of the force ellipsoids the following observations can be made.

- The size and orientation of the force ellipsoids at any configuration of the arm depend on the length of the links and the motor constant of the joint drives. Variation of other physical parameters of the arm such as the mass of the links or their center of masses will not cause any change in force ellipsoids.

- From Equation 4.15 it can be concluded that both eigenvalues are only functions of $\theta_1 - \theta_2$. As a result it can be said that the size of the force ellipsoid at any point of the work volume is only a function of the relative orientation of the upper arm with respect to the lower arm rather than a function of the absolute orientation of both links. This can be verified by noticing in Figure 4.1 that all the ellipsoids whose centers are located on the circumference of the same solid configuration circle are of the same size.

- A special case arises when the end effector is on the circumference of the home circle. The expression under the radical sign in Equation 4.15 assumes its smallest value. This makes the difference between the eigenvalues a minimum. As a result the ellipsoids take up a shape which, in comparison with the other configurations of the manipulator, is closest to a sphere. In particular, if the manipulator is designed such that $q_1 = q_2$, then from Equation 4.14

$$\frac{K_{m1}}{K_{m2}} = \frac{L_1}{L_2} \tag{4.17}$$

and the force ellipsoid will converge to a sphere. The power to force conversion efficiency will then be the same in all directions. Yoshikawa (1983) has referred to this case as the best posture from the manipulability point of view. This observation motivates the introduction of a measure that takes into account the lengths of the axes of the ellipsoid. The ratio of the length of the minor axis to the that of the major axis, which is inversely proportional to the square root of the condition number of the matrix $\mathbf{B}$ is a convenient candidate. This measure will be called here the *aspect ratio* and will be given by

$$\zeta_B = \frac{R_{min}}{R_{max}} = \sqrt{\frac{\lambda_1}{\lambda_2}}$$

The aspect ratio varies from zero at the singularity circles to its maximum at the home circle. The larger this measure is at a point in the work volume, the more isotropic will be the static performance of the manipulator at that point, and vice versa.

It was mentioned earlier that the size of the force ellipsoids along the solid configuration circles do not vary. Consequently the aspect ratio will remain constant along these circles. Figure 4.2 depicts the loci of the points at which the aspect ratio has constant values. The minor deviation of the contour lines from perfect circles at some points is due to the approximations made by the contour drawing software, rather than due to the actual destortion in the contours.

- It is interesting to note that at any point on the circumference of the solid configuration circles in Figure 4.1, the orientation of the force ellipsoids with respect to the manipulator is constant. In other words, if the end effector moves along the circumference of a solid configuration circle the force ellipsoid will also move along, without any change in its size, as if it is rigidly attached to the end effector. Unlike the case of the size of the force ellipsoids, this fact is not immediately apparent from Equation 4.15. Appendix D provides the relationships needed for this condition to be satisfied for a general ellipsoid with defining matrix **Z**. For the force ellipsoid with defining matrix **B** as given in Equation 4.13, the necessary conditions become

$$\frac{\partial B_{11}}{\partial \theta_1} = -2B_{12}$$

$$\frac{\partial B_{12}}{\partial \theta_1} = B_{11} - B_{12}$$

Differentiating B_{11} and B_{12} from Equation 4.13 and combining the results with the above equation shows that the matrix **B** satisfies the conditions given in Appendix D.

- The orientation of the force ellipsoids on the circumference of the home circle depends on the relative values of q_1 and q_2. Appendix D gives the orientation of a general ellipsoid with defining matrix **Z**, as

$$\phi_2 = tan^{-1}\left(\frac{\xi_1 - Z_{11}}{Z_{12}}\right)$$

where ξ_1 represents the smallest eigenvalue of the matrix **Z**. Substituting for the corresponding terms in the above equation from the matrix **B** given by Equation 4.13 gives the angle that the major axis of the force ellipsoid makes with the horizontal as

$$\phi_B = tan^{-1}\left(\frac{q_1^2 S_1^2 + q_2^2 S_2^2 - \lambda_1}{q_1^2 S_1 C_1 + q_2^2 S_2 C_2}\right) \tag{4.18}$$

If $q_1 < q_2$ then for the points on the home circle where $\theta_1 - \theta_2 = 90°$ Equation 4.15 gives $\lambda_1 = q_1^2$. Substituting for this value of λ_1 in the above equation gives $\phi_B = \theta_2$. This means that the major axis of the force ellipsoid will fall along the longitudinal axis of the upper arm of the manipulator as shown in the Figure 4.3-a. Similarly, it can be shown that if $q_1 > q_2$ then the minor axis of the ellipsoid will coincide with the longitudinal axis of the upper arm. This case is portrayed in the Figure 4.3-b.

For the majority of manipulators, the upper and the lower arm joint motors are identical and have the same motor constants. Consequently the ratio $\frac{q_1}{q_2} = \frac{L_1}{L_2}$. For such manipulators, if the upper arm is longer than the lower arm, then

in the vicinity of the home circle it will be capable of applying force along the longitudinal axis of its upper arm more than in any other direction. Conversely, if the upper arm is shorter than the lower arm, then the force capability of the arm will be better in a direction normal to that of the upper arm. If both the upper and the lower arms are of the same length then in the neighborhood of the home circle the force ellipsoids converge into circles. In consequence, the static capability of the manipulator becomes the same in all directions.

- In the neighborhood of the outer singularity circle where θ_1 approaches θ_2, and in the neighborhood of the inner singularity circle where θ_1 approaches $\theta_2 + \pi$, Equation 4.15 indicates that λ_1 approaches zero. Substituting for this condition in Equation 4.18 results in $\phi_B = \theta_1 = \theta_2$ (or $\theta_2 + \pi$). Therefore it can be concluded that, in the vicinity of the singularity circles, the force ellipsoid is very long and slender and is oriented such that its major axis falls along the radius of the singularity circles. Asada and Youcef-Toumi (1984) have shown that for certain mechanical designs the force characteristics would be a finite line instead of an ellipsoid throughout the work volume.

4.3 Static Output-Demand Relation

It was pointed out earlier in this chapter that under the stall condition the output characteristics of a manipulator in any direction can be represented by the radius of the force ellipsoid in that direction. Under such condition the only load that the joint motors are obliged to carry is the weight of the links and the payload. In Chapter 3 it was shown that all of these forces are reflected in a single vector called the generalized

weight of the arm. It is therefore convenient to consider the generalized weight as the demand force. The aim of this section is to examine the output of the system against the demand. Since both the output and the demand are vectors, the task of comparison must be carried out both in magnitude and in direction. In that respect two parameters will be defined, the *magnitude index* and the *direction index*.

4.3.1 Magnitude Index

The ratio of the magnitude of the generalized weight at any robot configuration, to the radius of the force ellipsoid along the generalized weight at that configuration indicates the relative degree of importance of the effect of gravity. This ratio will be called here the magnitude index and will be designated by η_m. Referring to Figure 4.4 this ratio can be expressed as

$$\eta_m = \frac{|\mathbf{W}|}{|\mathbf{F}|} = \frac{|\vec{OA}|}{|\vec{OB}|}$$

where $|\mathbf{W}|$ indicates the magnitude of the generalized weight and $|\mathbf{F}|$ represents the task force in the direction of the generalized weight. Substituting for $\{\mathbf{F}\}$ from the above expression into the Equation 4.7 gives

$$\left\{\frac{1}{\eta_m}\mathbf{W}\right\}^T \begin{bmatrix} \mathbf{B} \end{bmatrix} \left\{\frac{1}{\eta_m}\mathbf{W}\right\} = P$$

The magnitude index can now be expressed as

$$\eta_m = \sqrt{\frac{\{\mathbf{W}\}^T \begin{bmatrix} \mathbf{B} \end{bmatrix} \{\mathbf{W}\}}{P}} \tag{4.19}$$

The numerator under the radical sign in the above equation is the power consumed by the joint motors in order to compensate for the effect of gravity. Denoting this power by P_g the magnitude index can simply be presented as

$$\eta_m = \sqrt{\frac{P_g}{P}} \tag{4.20}$$

Since both $\mathbf{W}$ and $\mathbf{F}$ have been shown to be configuration dependent, then the magnitude index is a function of the configuration of the arm. At the points of the work volume where the magnitude index is relatively small the power dissipation due to the effect of gravity will also be small, and vice versa.

In order to provide a global view for the magnitude index, a contour map of its values throughout the work volume is portrayed in Figure 4.5 for the manipulator shown in Figure 3.4. From a design perspective, the magnitude of the total power supplied to the joint motors must be selected such that the value of the magnitude index does not exceed unity. Figure 4.5 shows that in some areas of the work volume the value of the magnitude index is close to one. This indicates that in those regions most of the power of the joint motors is used to carry the manipulator's own weight and the force that is available at the end effector to carry out useful work is very small.

It is enlightening to compare this figure with Figure 3.5 which shows the generalized gravitational field for the same manipulator and Figure 3.7 which portrays the generalized weight. The comparison reveals that a strong resemblance exists between the contour map of the magnitude index and the GGF. In the lower right quadrant of the work volume where the field is strong, the value of the magnitude index is close to its maximum. Conversely, in the upper right quadrant where the GGF is generally

weak, the magnitude index is relatively small. Even the locus of the minimum field strength which is highlighted in the Figure 3.10 seems to be matching the contour line associated with minimum value of the magnitude index. The conclusion to this observation is that for a typical PUMA robot like the one exemplified in this study, operation in the upper right quadrant, specially in the vicinity of the weakest region of the field, is associated with the least amount of power used by the joint motors to overcome the effect of gravity. Conversely, in the lower right quadrant the power consumption by the joint motors due to gravitational forces is the most.

4.3.2 Direction Index

In order to quantize the relative orientation of the force ellipsoid with respect to the direction of the generalized weight, the direction index η_d is introduced. With reference to the Figure 4.6, this measure is defined as the cosine of the angle between the vector of the generalized weight and the direction of the major axis of the force ellipsoid. To calculate this measure it will suffice to obtain the unit vectors associated with each direction and find their dot product.

To obtain the unit vector along the major axis of the force ellipsoid, the diagonalizing matrix $\mathbf{C}$ which was introduced in Equation 4.8 must first be set up. It was mentioned there that the column vectors of the matrix $\mathbf{C}$ are the same as normalized eigenvectors of the matrix $\mathbf{B}$. The eigenvectors of the dummy matrix $\mathbf{Z}$ is given in Appendix D as

$$\begin{bmatrix} 1 & \frac{\xi_2 - Z_{22}}{Z_{21}} \\ \frac{\xi_1 - Z_{11}}{Z_{12}} & 1 \end{bmatrix}$$

where ξ_1 and ξ_2 represent the eigenvalues of the dummy matrix $\mathbf{Z}$. Replacing the matrix $\mathbf{Z}$ and its eigenvalues by the matrix $\mathbf{B}$ and its eigenvalues and normalizing the column vectors gives the matrix $\mathbf{C}$ as

$$\left[\ \mathbf{C}\ \right] = \begin{bmatrix} \frac{B_{12}}{\sqrt{B_{12}^2+(\lambda_1-B_{11})^2}} & \frac{\lambda_2-B_{22}}{\sqrt{B_{21}^2+(\lambda_2-B_{22})^2}} \\ \frac{\lambda_1-B_{11}}{\sqrt{B_{12}^2+(\lambda_1-B_{11})^2}} & \frac{B_{21}}{\sqrt{B_{21}^2+(\lambda_2-B_{22})^2}} \end{bmatrix} \tag{4.21}$$

Since the matrix $\mathbf{C}$ is orthonormal its column vectors represent the unit vectors along the principal directions of the force ellipsoid. The first column of this matrix is associated with the smallest eigenvalue of the matrix $\mathbf{B}$. As a result the vector $\mathbf{C}_{i1}$ represents the unit vector along the major axis of the force ellipsoid. The direction index can therefore be expressed as

$$\eta_d = \frac{\mathbf{C}_{1j} \circ \mathbf{W}}{\| \mathbf{W} \|}$$

where $\| \mathbf{W} \|$ is the norm of the vector of generalized weight. The unit vector in the direction of the generalized weight of the manipulator is given by

$$\begin{Bmatrix} \frac{W_1}{\sqrt{W_1^2+W_2^2}} \\ \frac{W_2}{\sqrt{W_1^2+W_2^2}} \end{Bmatrix}$$

where W_1 and W_2 are the normalized components of the generalized weight and are given by the Equation 3.8. The inner product of this unit vector and the one given in the first column of the diagonalizing matrix $\mathbf{C}$ gives

$$\eta_d = \frac{1 + \frac{\lambda_1-B_{11}}{B_{12}}\frac{w_2}{w_1}}{\sqrt{\left[1+\left(\frac{\lambda_1-B_{11}}{B_{12}}\right)^2\right]\left[1+\left(\frac{w_2}{w_1}\right)^2\right]}} \tag{4.22}$$

Substituting for $\frac{w_2}{w_1}$ from the Equation 3.9, for λ_1 from the Equation 4.15, and for B_{11} and B_{12} from the Equation 4.13 gives the value of the direction index as a

function of the physical specifications of the manipulator as well as its instantaneous configuration.

For a given robot arm the direction index is a function of the configuration of the arm and varies between -1 and $+1$. The contour lines of the Figure 4.7 show the loci of the points of the work volume of the example manipulator which are associated with the same value of the direction index.

A comparison between the contour lines shown in Figures 4.5 and 4.7, and the generalized gravitational field depicted in Figure 3.5 shows that, in regions such as the central part of the upper right quadrant where the field is generally weak, both η_m and η_d are relatively small. A small η_d indicates that the direction of the generalized weight is almost along the minor axis of the force ellipsoid. The condition under which the absolute value of the direction index reaches its minimum value of $\eta_d = 0$ is obtained from Equation 4.22 and is given by

$$1 + \frac{\lambda_1 - B_{11}}{B_{12}} = -\frac{w_1}{w_2}$$

On the other hand, Figures 4.5 and 4.7 show that in the lower right quadrant of the work volume both indices are close to their maximum values. As can be seen from Figure 3.5, the field is relatively strong in that region. A high value for η_d indicates that the generalized weight almost coincides with the major axis of the force ellipsoid. The direction index reaches its maximum value when

$$1 + \frac{\lambda_1 - B_{11}}{B_{12}} = \frac{W_2}{W_1}$$

4.4 Effect of Gravity on the Output

The output characteristics of the arm, as described in Section 4.2, does not take into account the effect of gravity. Furthermore, the total task force that the gripper can apply to the environment can not be displayed by the force ellipsoid as described by Yoshikawa (1983), and Asada and Youcef-Toumi (1984). In this section it will be shown that the integration of the force ellipsoid with the generalized weight can help to overcome this drawback.

For any configuration of the manipulator the radius of the force ellipsoid in any direction indicates the magnitude of the force that the end effector is capable of applying to the environment in that direction. This force is created by virtue of the electrical power supplied to the joint motors. On the other hand, the generalized weight indicates the force that the end effector can exert to its surroundings by virtue of the effect of gravity on the links. Therefore the total force that the end effector can apply to the external world is the vector sum of the two. This makes the force ellipsoid shift, with no rotation, such that its new center is located at the tip of the vector of the generalized weight.

The analytical proof to this conclusion can be established by considering the vector of the joint torques in Equation 4.4 as the combination of the vector of the torque of the joint motors τ_m , and the vector of the torques induced through the effect of gravity τ_g , as follows

$$\left\{ \tau_m \right\} + \left\{ \tau_g \right\} = \left[\mathbf{J} \right]^T \left\{ \mathbf{F} \right\} \tag{4.23}$$

Using Equation 4.4, the vector τ_g can be related to the generalized weight of the

arm $\mathbf{W}$ defined in Section 3.3, through the transformation

$$\left\{ \tau_g \right\} = \left[\mathbf{J} \right]^T \left\{ \mathbf{W} \right\}$$

Substituting for τ_g from the above equation into Equation 4.23 and rearranging gives

$$\left\{ \tau_m \right\} = \left[\mathbf{J} \right]^T \left\{ \mathbf{F} - \mathbf{W} \right\}$$

If the vector τ_m in Equation 4.2 is replaced by the one given in the above equation the following quadratic form results

$$\left\{ \mathbf{F} - \mathbf{W} \right\}^T \left[\mathbf{B} \right] \left\{ \mathbf{F} - \mathbf{W} \right\} = P$$

which is clearly the equation of an ellipsoid whose center is located at the end of the vector $\mathbf{W}$. Figure 4.8 displays this transformation for some configurations of the arm. The shifted ellipsoid portrays the net capability of the end effector in applying force to the environment. With reference to the Figure 4.8 the following conclusions can be drawn.

- In presence of gravity the task force is not symmetrical with respect to the tip of the arm. In particular, the task force in the positive direction of the generalized weight is increased by an amount which is exactly equal to the magnitude of the generalized weight. In the opposite direction, however, the task force is decreased by the same amount.

- If at any configuration of the arm, the end effector falls on the outside of the

shifted ellipsoid, then it can be concluded that the selected motors are not capable of supporting the arm's weight at that configuration.

- The eigenvalues of the matrix B given by the Equation 4.13 no longer indicate the maximum and the minimum values of the task force. The new maximum and minimum will be the longest and the shortest vectors drawn from the arm's tip to the surface of the ellipsoid. The magnitude and direction of these vectors will be calculated analytically in the following section.

4.5 Maximum and Minimum Values of the Task Force

Determination of the extreme values of the task force is in essence the same problem as that of finding the extreme values of the distance between a fixed point A with coordinates $\{\mathbf{x}_A\} = (x_{1A}, x_{2A}, \cdots, x_{nA})^T$ and a general point P with coordinates $\{\mathbf{x}\} = (x_1, x_2, \cdots, x_n)^T$ on the surface of an ellipsoid. In other words the extrema of the function

$$s(x_1, x_2, \cdots, x_n) = \sqrt{(x_1 - x_{1A})^2 + (x_2 - x_{2A})^2 + \cdots + (x_n - x_{nA})^2} \qquad (4.24)$$

must be found subject to the constraint

$$g(x_1, x_2, \cdots, x_n) = \lambda_1 x_1^2 + \lambda_2 x_2^2 + \cdots + \lambda_n x_n^2 - const. = 0 \qquad (4.25)$$

Applying the method of Lagrange multipliers yields a set of auxiliary equations as

$$\nabla\, s(x_1, x_2, \cdots, x_n) = \mu\, \nabla\, g(x_1, x_2, \cdots, x_n)$$

where μ represents the Lagrange multiplier. For the present example the above set will reduce to two equations. Solving out μ between the two equations and substituting for the partial derivatives from Equations 4.24 and 4.25 gives the equation of the locus of the point P on the ellipsoid as

$$\frac{x_1 - x_{1A}}{x_2 - x_{2A}} = \frac{\lambda_1 x_1}{\lambda_2 x_2} \tag{4.26}$$

Equation 4.26 represents a rectangular hyperbola known as the hyperbola of Apollonius (Robson 1949 page 297). The intersection of this hyperbola with the ellipsoid given by the two dimensional form of Equation 4.25 locates the point P. The algebraic equation that gives the intersection points has a quartic form given by

$$\left(\frac{1}{\lambda_1^2} - \frac{1}{\lambda_2^2}\right)^2 x^4 - \frac{2x_{1A}}{\lambda_1^2}\left(\frac{1}{\lambda_1^2} - \frac{1}{\lambda_2^2}\right) x^3 + \frac{1}{\lambda_1^2}\left(\frac{x_{1A}^2}{\lambda_1^2} + \frac{x_{2A}^2}{\lambda_2^2} - \left(\frac{1}{\lambda_1^2} - \frac{1}{\lambda_2^2}\right)^2\right) x^2$$

$$+ \frac{2x_{1A}}{\lambda_1^4}\left(\frac{1}{\lambda_1^2} - \frac{1}{\lambda_2^2}\right) x - \frac{x_{1A}^2}{\lambda_1^6} = 0 \tag{4.27}$$

The above equation has four roots. This indicates that there may be as many as four locations on the ellipsoid for the point P. It should be noted that the coordinates of the center of the ellipsoid satisfies Equation 4.26. This means that at least one branch of the hyperbola passes through the center of the ellipsoid which, in turn, means that the hyperbola intersects the ellipsoid at least at two distinct points. In other words Equation 4.27 has at least two real roots. If the other two roots are also real then the other branch of the hyperbola will also intersect the ellipsoid, and if they are imaginary then the other branch of the hyperbola will fall on the outside of the ellipsoid. In any case the smallest and the largest roots will represent, respectively, the true magnitude of the minimum and maximum force that the end effector can

apply to its environment. Figure 4.9 shows a typical force ellipsoid together with the corresponding hyperbola of Apollonius. It can be shown that, any line drawn from point A to any intersection point of the hyperbola and the ellipsoid, is perpendicular to the surface of the ellipsoid at the point of intersection (Tuckey and Armistead 1953 page 170). Consequently, in order to find the net maximum and minimum forces that the end effector is capable of applying to the environment, it will suffice to draw a normal from the point where the end effector is located to the surface of the force ellipsoid. The longest and the shortest normals will respectively represent the maximum and the minimum task forces.

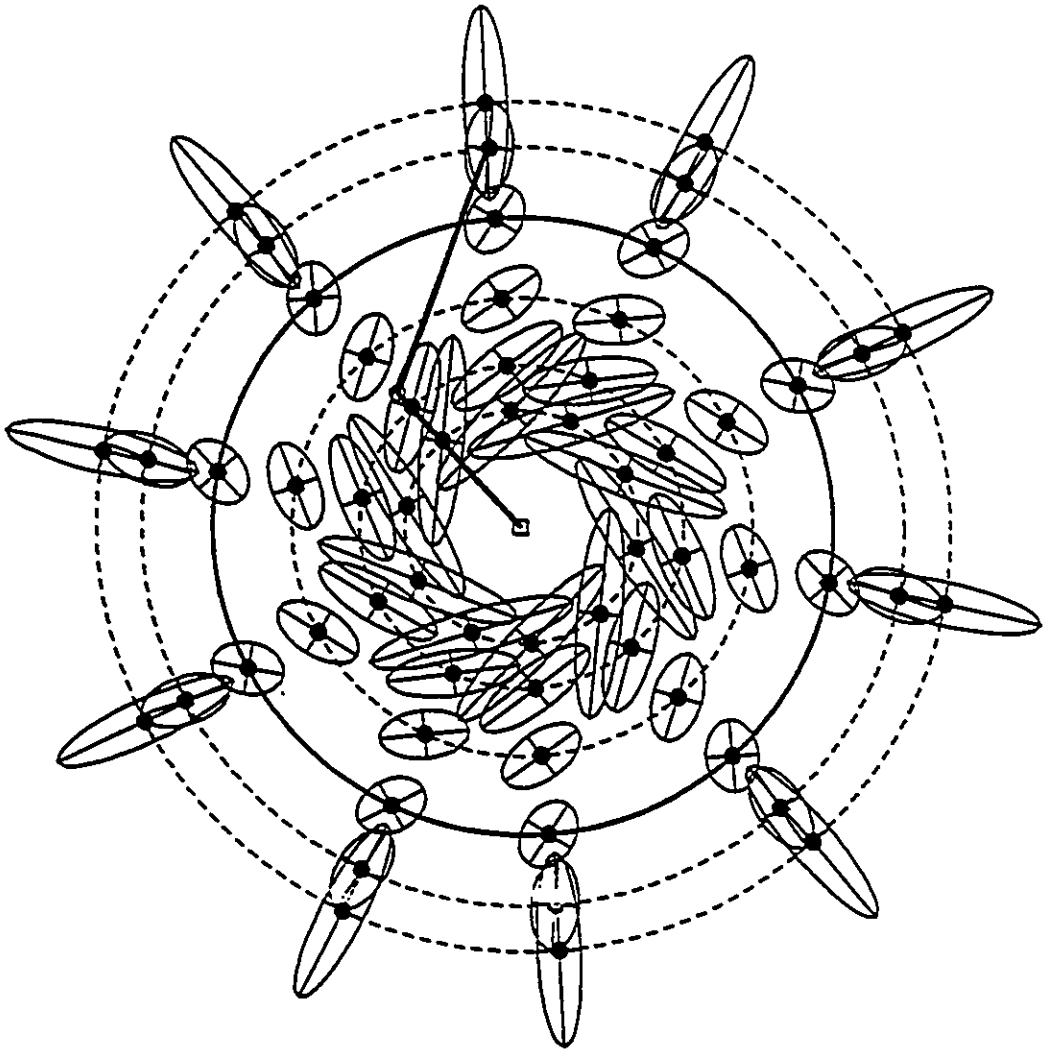

Figure 4.1: Force ellipsoids.

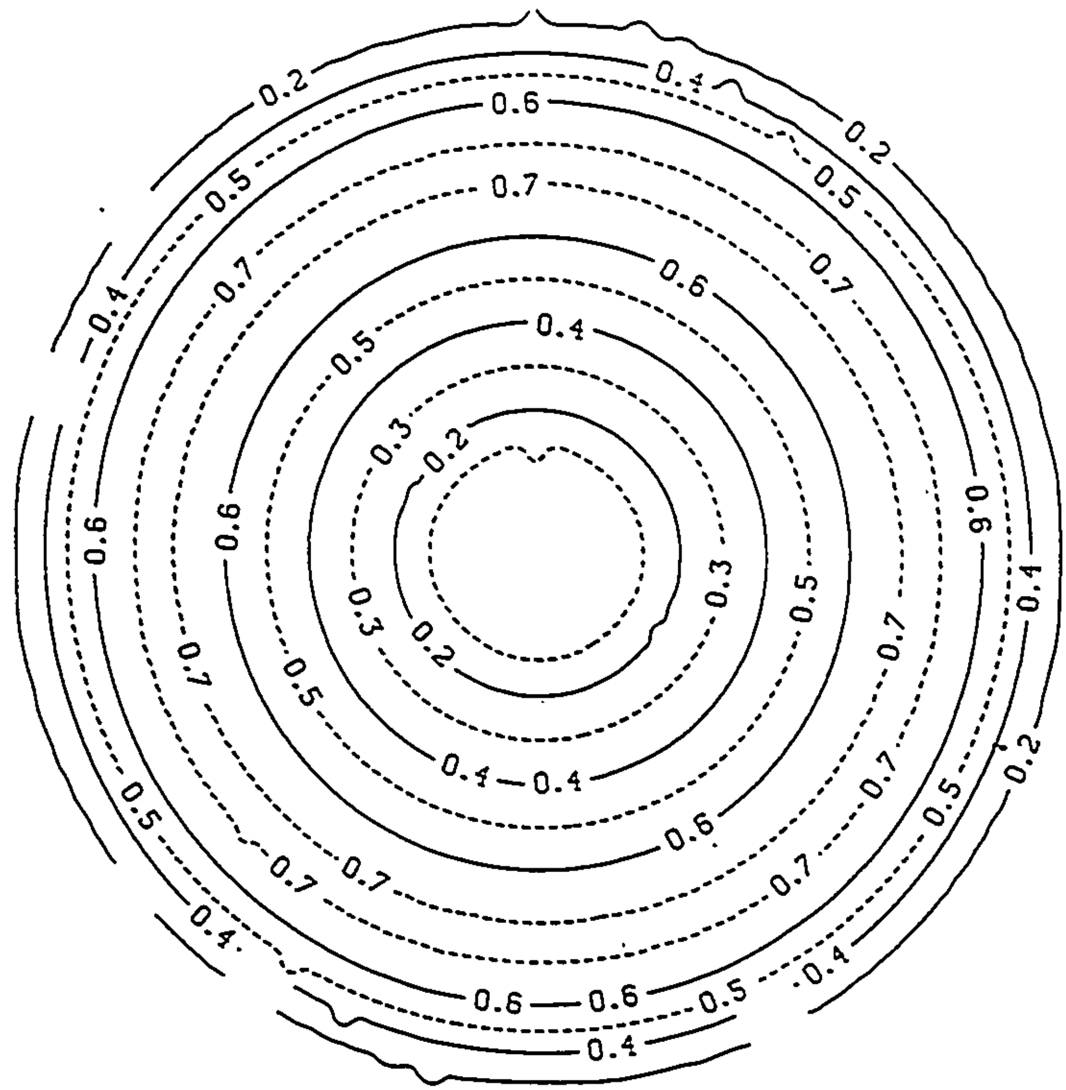

Figure 4.2: Contour map of aspect ratio for the force ellipsoids.

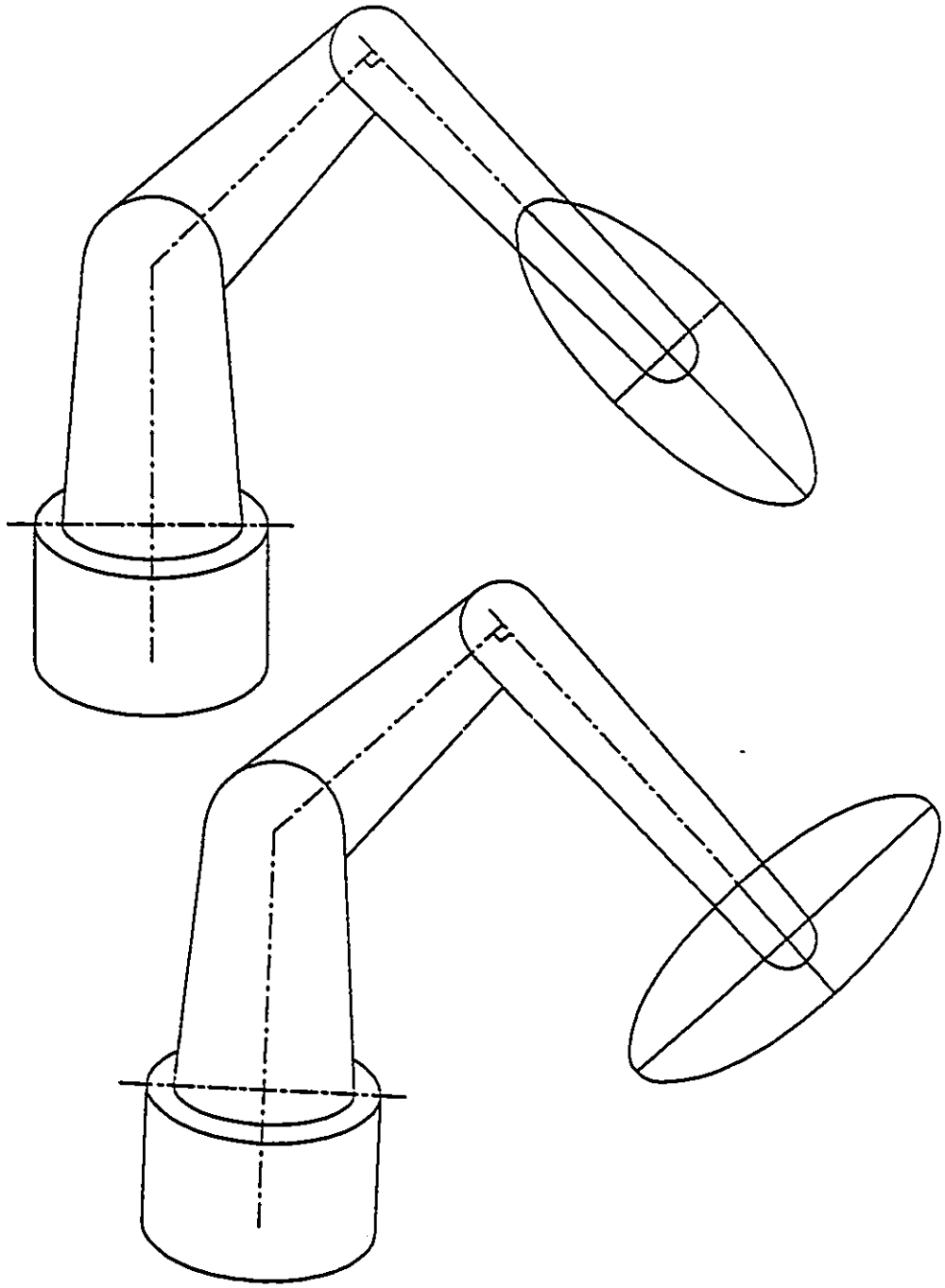

Figure 4.3: Orientation of a dummy ellipsoid on the home circle for two special cases.

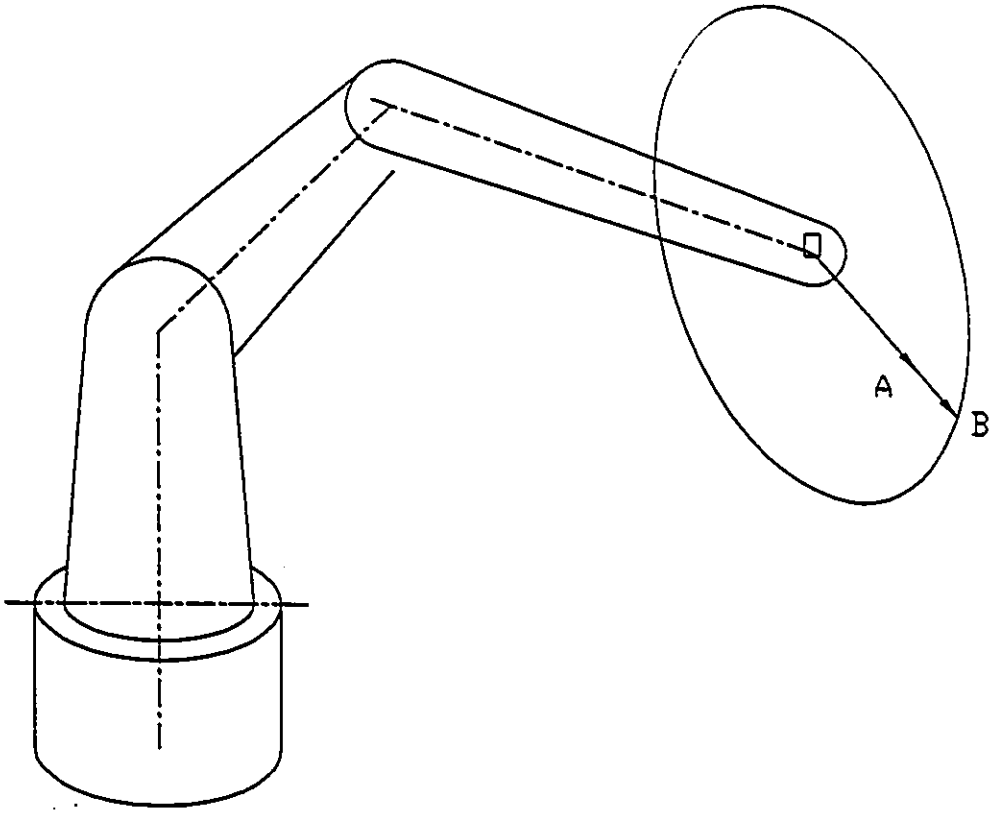

$$\eta_m = \frac{|W|}{|F|} = \frac{|\bar{OA}|}{|\bar{OB}|}$$

Figure 4.4: Description of the magnitude index.

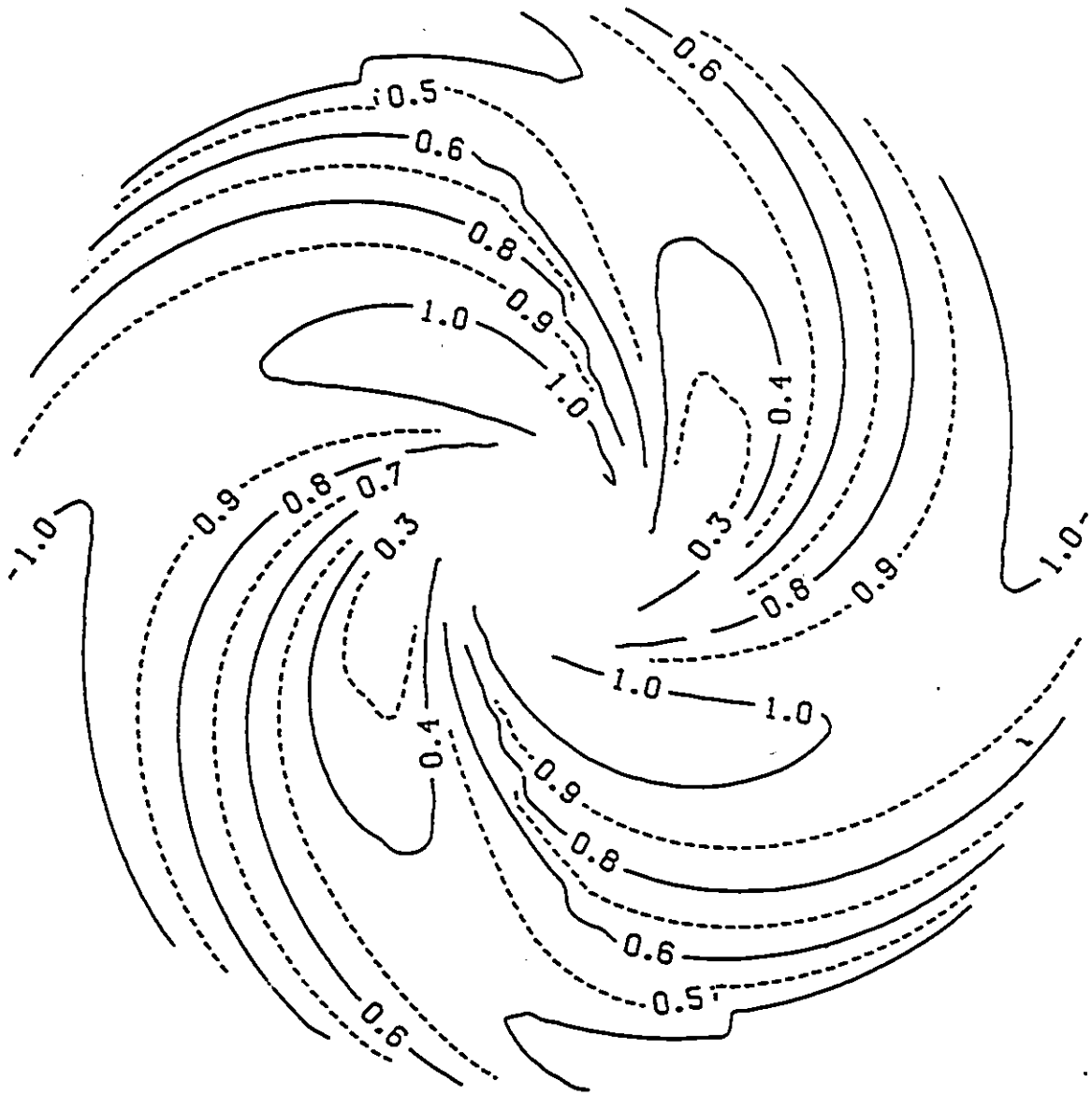

Figure 4.5: Contour map of magnitude index for static output-demand model.

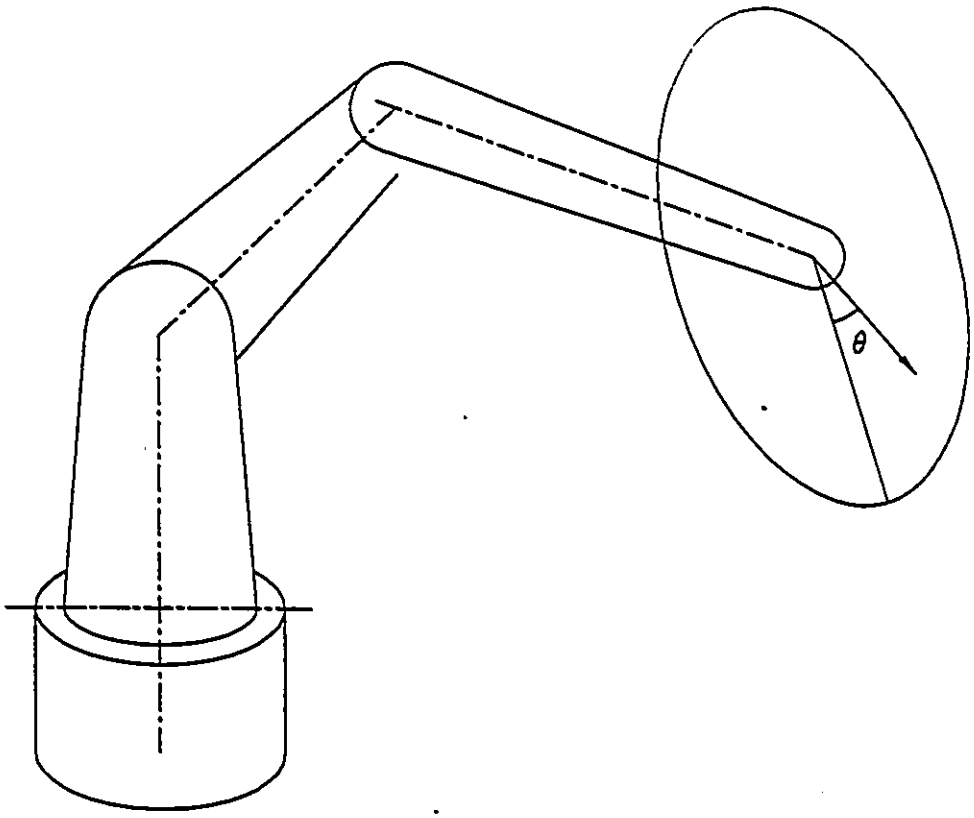

$$\eta_d = cos\theta$$

Figure 4.6: Description of the direction index.

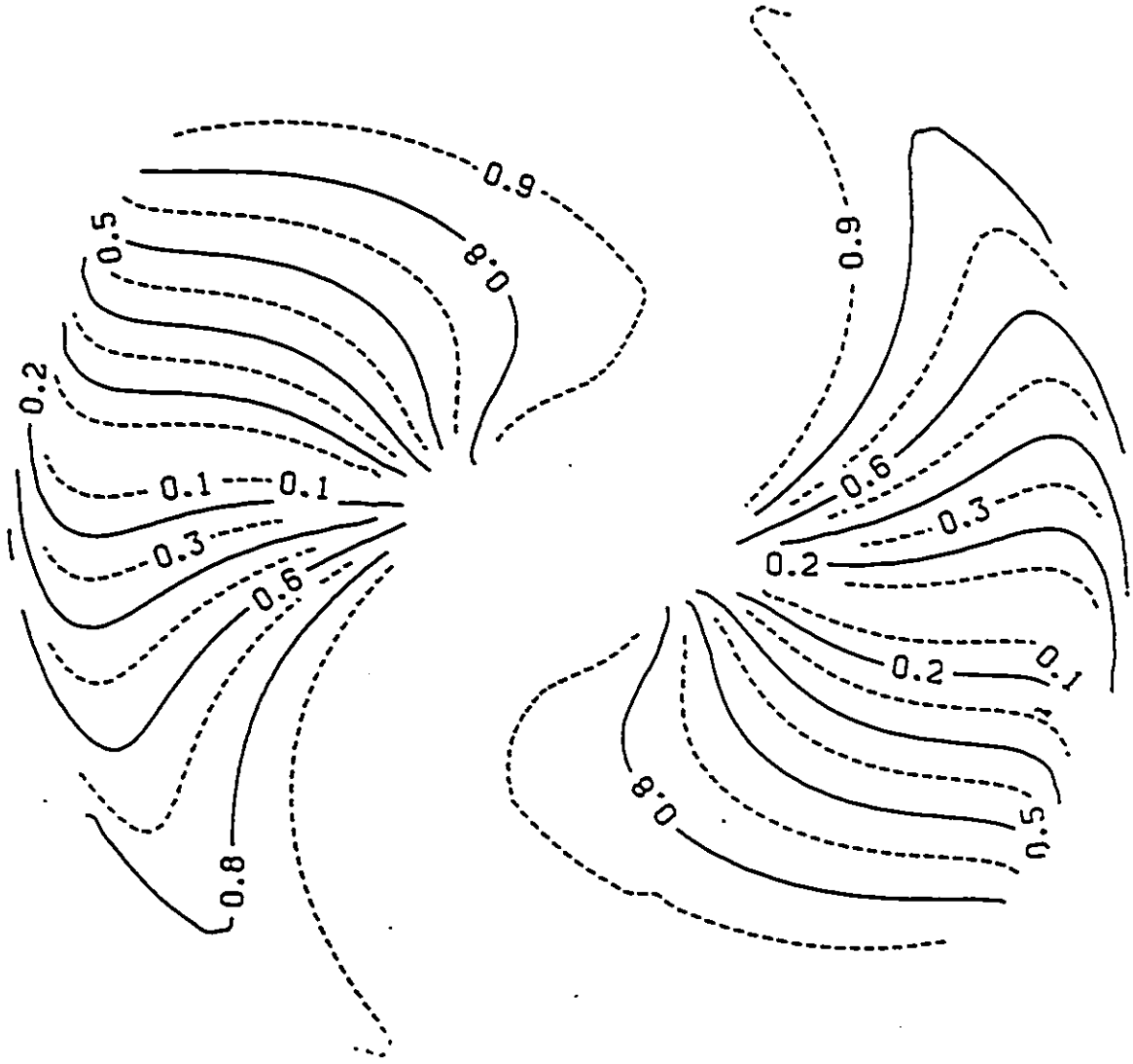

Figure 4.7: Contour map of direction index for static output-demand model.

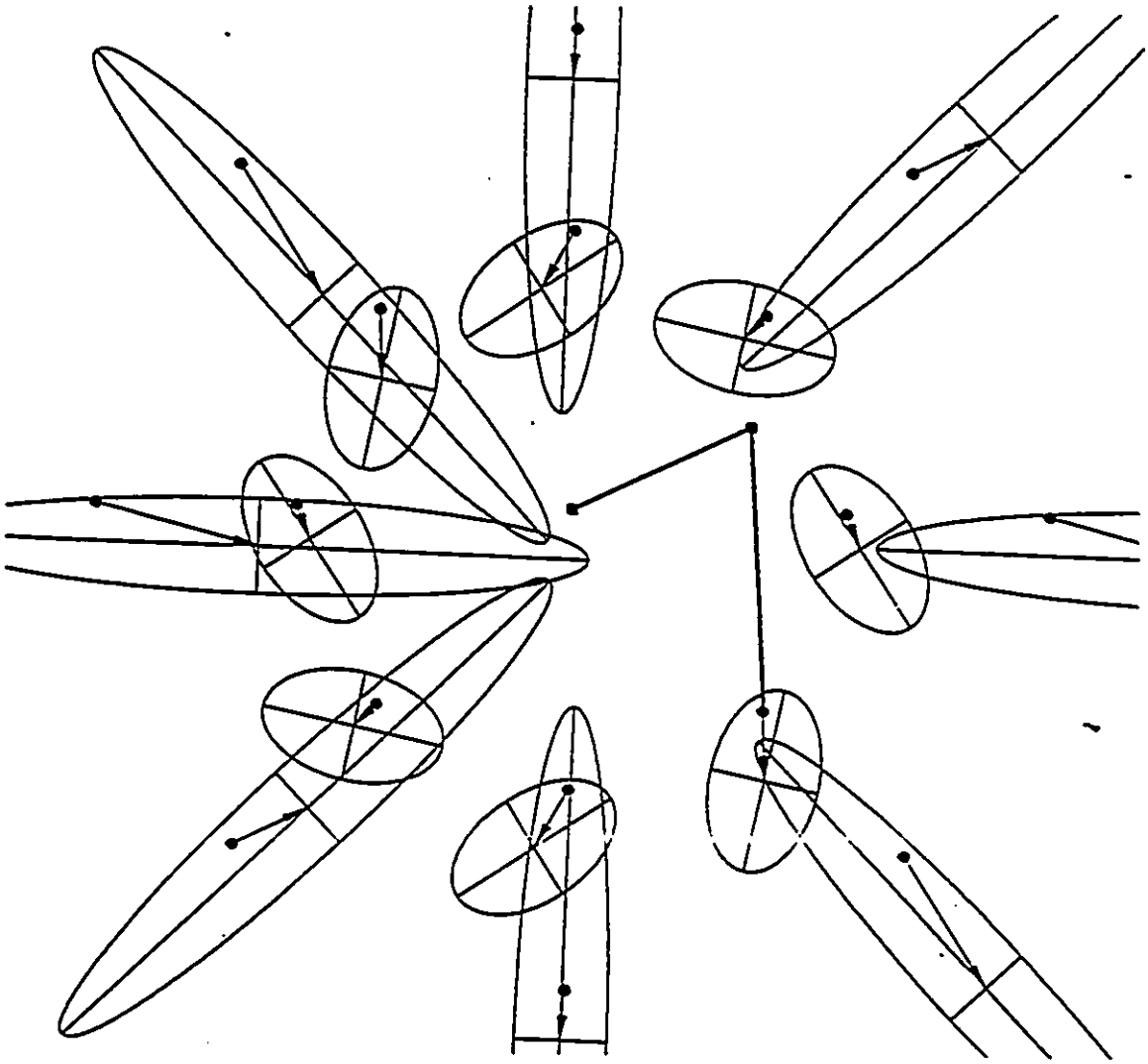

Figure 4.8: Force ellipsoids in shifted positions.

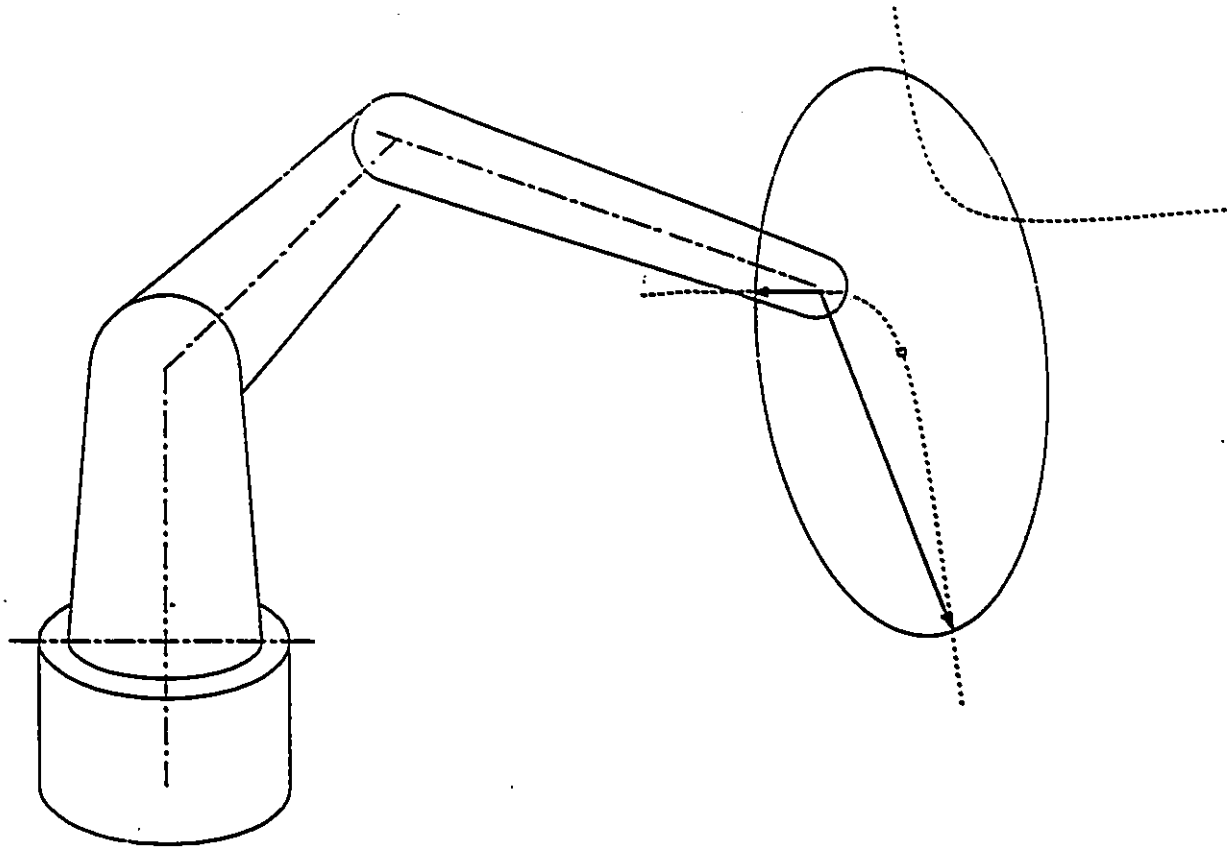

Figure 4.9: Maximum and minimum task forces.

Chapter 5

Dynamic Behavior of the Manipulator

5.1 Introduction

Dynamic performance of manipulators has been the subject of many research works. The goal of some of these works has been to find some global measures that uniquely explain the dynamic behavior of the arm at any point of the work volume. Among the most noticeable works in this category is the generalized ellipsoid of inertia introduced by Asada in 1983. He extended the ellipsoid of inertia defined in classical dynamics for single rigid bodies, to the case of a system of rigid bodies such as a manipulator. The generalized ellipsoid of inertia determines the limits of the speed that the end effector of a manipulator will attain in any direction with a given amount of kinetic energy. Another important concept that was introduced by Yoshikawa in 1985, is the dynamic manipulability ellipsoid. For a manipulator under stall conditions with

a given amount of input energy, the dynamic manipulability ellipsoid indicates the acceleration that the end effector can assume in various directions.

In this chapter the concept of the generalized weight that was defined in Chapter 3 will be utilized to develop the generalized inertia tensor and the generalized gravitational acceleration. The generalized inertia tensor was first introduced by Asada through the energy method in his above cited work. Neither Asada(1983), nor Yoshikawa(1985) have considered the relationship that was shown in Chapter 4 to govern the size and orientation of the force ellipsoid throughout the work volume. The work of the two researchers will be briefly reviewed here. Then it will be shown that the above mentioned relationship also holds true for both the generalized ellipsoid of inertia and the dynamic manipulability ellipsoid.

The output-demand model that was developed in Chapter 4 to study the static performance of manipulators will be extended in this chapter to include the dynamic behavior. For this purpose the dynamic manipulability ellipsoid will be considered as the output of the system and the generalized gravitational acceleration as the demand. The generalized gravitational acceleration field will be investigated in connection with the generalized weight of the manipulator. The relation between these two and the generalized ellipsoid of inertia will then be determined. Finally, the effect of gravity on the dynamic manipulability ellipsoid will be investigated. It will be shown that, similar to the case of the force ellipsoid, the true acceleration capability of the end effector can only be demonstrated by the dynamic manipulability ellipsoid when the center of that ellipsoid is shifted to the tip of the generalized gravitational acceleration vector.

5.2 Generalized Inertia Tensor

The Newton law for the motion of a particle is

$$\mathbf{f} = m\mathbf{a}$$

where $\mathbf{f}$ is the total external force acting on the particle, m is the mass of the particle and $\mathbf{a}$ is the acceleration that the particle can attain due to the action of the force f.

Considering $\mathbf{f}$ and $\mathbf{a}$ as single element vectors and m as a single element matrix, the Newton law of motion can be extended to the motion of a system of rigid bodies such as a manipulator as following

$$\left\{\mathbf{F}\right\} = \left[\ \mathbf{M}\ \right]\left\{\mathbf{A}\right\} \tag{5.1}$$

In the above equation the vector $\mathbf{F}$ is the generalized force that acts on the arm in the task space, the matrix $\mathbf{M}$ represents the generalized inertia tensor of the manipulator, and the vector $\mathbf{A}$ is the acceleration that the end effector can attain by virtue of the application of the force $\mathbf{F}$. The general equation of motion for a manipulator can be expressed as

$$\left[\ \mathbf{I}\ \right]\left\{\ddot{\theta}\right\} + \left\{\ C(\theta,\dot{\theta})\ \right\} = \left\{\ \tau\ \right\} \tag{5.2}$$

where $\ddot{\theta}$ is the joints acceleration vector, $C(\theta,\dot{\theta})$ represents the Coriolis and centrifugal effects, and τ is the combination of the joint torques and the effect of gravity. The matrix $\mathbf{I}$ in this equation represents the matrix of moment of inertia of

the links. For the example at hand this matrix is given by (Asada and Slotine 1986).

$$\left[\ \mathbf{I}\ \right] = \begin{bmatrix} I_1 + m_1 h_1^2 + m_2 L_1^2 & m_2 h_2 L_1 cos(\theta_1 - \theta_2) \\ m_2 h_2 L_1 cos(\theta_1 - \theta_2) & I_2 + m_2 h_2^2 \end{bmatrix} \tag{5.3}$$

The velocity vector in the joint space can be mapped onto the task space through the transformation

$$\left\{\mathbf{V}\right\} = \left[\ \mathbf{J}\ \right]\left\{\dot{\theta}\right\}$$

where $\mathbf{V}$ is the velocity vector in the task space, $\mathbf{J}$ is the Jacobian matrix given in Equation 4.12, and $\dot{\theta}$ is the velocity vector in the joint space.

Differentiating the above equation with respect to time gives

$$\left\{\dot{\mathbf{V}}\right\} = \left[\ \mathbf{J}\ \right]\left\{\ddot{\theta}\right\} + \left[\ \dot{\mathbf{J}}\ \right]\left\{\dot{\theta}\right\}$$

where $\dot{\mathbf{V}}$ represents the acceleration of the end effector in the task space. Calculating θ from the above equation and substituting the results in Equation 5.2 leads to

$$\left[\ \mathbf{I}\ \right]\left[\ \mathbf{J}\ \right]^{-1}\left(\left\{\dot{\mathbf{V}}\right\} - \left[\ \dot{\mathbf{J}}\ \right]\left\{\dot{\theta}\right\} + \left[\ \mathbf{J}\ \right]\left[\ \mathbf{I}\ \right]^{-1}\left\{C(\theta,\dot{\theta})\right\}\right) = \left\{\tau\right\} \tag{5.4}$$

The generalized acceleration can now be expressed as

$$\left\{\mathbf{A}\right\} = \left\{\dot{\mathbf{V}}\right\} - \left[\ \dot{\mathbf{J}}\ \right]\left\{\dot{\theta}\right\} + \left[\ \mathbf{J}\ \right]\left[\ \mathbf{I}\ \right]^{-1}\left\{C(\theta,\dot{\theta})\right\}$$

The second and third terms in the right hand side of the above equation are proportional to the dual products of the joint speeds. When the joint speeds are relatively

low, and specially at $t = 0$ where the speeds are virtually zero, these terms vanish. Consequently the vector $\mathbf{A}$ becomes equal to the acceleration of the end effector in the task space. Combining the above equation with Equation 5.4 gives

$$\left[\mathbf{I} \right]\left[\mathbf{J} \right]^{-1}\left\{\mathbf{A}\right\} = \left\{ \tau \right\} \tag{5.5}$$

Substituting for τ from Equation 4.4 in the Equation 5.5 and rearranging the result yields

$$\left\{\mathbf{F}\right\} = \left[\mathbf{J} \right]^{-T}\left[\mathbf{I} \right]\left[\mathbf{J} \right]^{-1}\left\{\mathbf{A}\right\} \tag{5.6}$$

Comparing the above equation with Equation 5.1 gives the generalized inertia tensor of the manipulator as

$$\left[\mathbf{M} \right] = \left[\mathbf{J} \right]^{-T}\left[\mathbf{I} \right]\left[\mathbf{J} \right]^{-1} \tag{5.7}$$

In a manner similar to that used for Equation 4.6, it can be shown here that the generalized inertia tensor $\mathbf{M}$ is congruent to the matrix of moment of inertia $\mathbf{I}$. As a result, since $\mathbf{I}$ is symmetric and positive definite, the generalized inertia tensor also possesses the same properties.

Asada (1983) obtained this matrix through the energy method. Liegeois(1985) has also obtained this matrix by taking into account only the inertia terms in the equation of motion at the outset of the motion of the arm. The inverse of the Jacobian matrix can be found from Equation 4.12 as

$$\left[\mathbf{J} \right]^{-1} = \frac{1}{L_1 L_2 sin(\theta_1 - \theta_2)} \begin{bmatrix} -L_2 cos\theta_2 & -L_2 sin\theta_2 \\ L_1 cos\theta_1 & L_1 sin\theta_1 \end{bmatrix} \tag{5.8}$$

For the present example the generalized inertia tensor can be found by substituting for $\mathbf{J}^{-1}$ from the above equation, and for $\mathbf{I}$ from Equation 5.3, in Equation 5.7.

This results in

$$\left[\begin{array}{c} \\ \mathrm{M} \\ \\ \end{array}\right] = \left[\begin{array}{cc} q_{11}C_2^2 - 2q_{12}C_1C_2 + q_{22}C_1^2 & q_{11}S_2C_2 - q_{12}S_{1+2} + q_{22}S_1C_1 \\ q_{11}S_2C_2 - q_{12}S_{1+2} + q_{22}S_1C_1 & q_{11}S_2^2 - 2q_{12}S_1S_2 + q_{22}S_1^2 \end{array}\right] \quad (5.9)$$

where

$$\begin{aligned} q_{11} &= \frac{I_{11}}{L_1^2 S_{1-2}^2} \\ q_{12} &= \frac{I_{12}}{L_1 L_2 S_{1-2}^2} \\ q_{22} &= \frac{I_{22}}{L_2^2 S_{1-2}^2} \end{aligned} \quad (5.10)$$

and $S_i = sin\theta_i$, $C_i = cos\theta_i$, $S_{1-2} = sin(\theta_1 - \theta_2)$, $S_{1+2} = sin(\theta_1 + \theta_2)$

5.3 Generalized Ellipsoid of Inertia

In 1983 Asada introduced the generalized ellipsoid of inertia based on the generalized inertia tensor. The generalized ellipsoid of inertia, as the name implies, is the extension of the concept of the ellipsoid of inertia, defined in classical dynamics for rigid bodies, to the case of a system of rigid bodies such as a manipulator. However, unlike the case of a single rigid body in which the size and the orientation of the ellipsoid with respect to the body is time invariant, both the size and orientation of the generalized ellipsoid of inertia are functions of time. In case of a single rigid body the ellipsoid of inertia is constructed in a space whose dimensions are the components of the angular velocity of the body. Therefore it represents the rotational inertia characteristics of the body. The radii of the ellipsoid of inertia in any direction indicate the magnitude of the angular speed that the body can attain if it is made to rotate about that direction with a given amount of kinetic energy. The directions along which the angular speed of the body is an extremum for a given value of the

kinetic energy are indicated by the principal axes of the ellipsoid.

The generalized ellipsoid of inertia is constructed based on the generalized inertia tensor in a space whose dimensions are the components of the velocity of the end effector. Hence it characterizes the general inertia of the manipulator undergoing a general motion. For a given total kinetic energy of the system, the principal axes of the generalized ellipsoid of inertia indicate the directions along which the speed of the manipulator is an extremum. For the example at hand the principal axes of the generalized ellipsoid of inertia can be obtained from the eigenvalues of the matrix $\mathbf{M}$ which are given as

$$\begin{aligned}\sigma_1 &= \tfrac{1}{2}\left\{q_{11}+q_{22}+2q_{12}C_{12}-\sqrt{(q_{11}+q_{22}+2q_{12}C_{12})^2-4(q_{11}q_{22}-q_{12}^2)S_{12}^2}\right\}\\ \sigma_2 &= \tfrac{1}{2}\left\{q_{11}+q_{22}+2q_{12}C_{12}+\sqrt{(q_{11}+q_{22}+2q_{12}C_{12})^2-4(q_{11}q_{22}-q_{12}^2)S_{12}^2}\right\}\end{aligned} \tag{5.11}$$

Figure 5.1 shows the generalized ellipsoid of inertia for several configurations of the example at hand. With reference to that figure the following remarks can be made.

- The ellipsoids on the circumference of any of the solid configuration circles are of the same size. This observation can be analytically validated by noticing in Equation 5.11 that the eigenvalues of the matrix $\mathbf{M}$ (and therefore the lengths of the principal axes of the ellipsoids) at any configuration of the manipulator, are only functions of $\theta_1 - \theta_2$.

- On the circumference of the solid configuration circles the relative orientation of the ellipsoids with respect to the manipulator remains unchanged. This can be verified by proving that the members of the matrix $\mathbf{M}$ satisfy the conditions

which are presented in Appendix A. For the matrix M these conditions can be written as

$$\frac{\partial M_{11}}{\partial \theta_1} = -2M_{12}$$

$$\frac{\partial M_{12}}{\partial \theta_1} = M_{11} - M_{12}$$

Substituting for members of the matrix M from Equation 5.9 and performing the mathematical work involved proves that for the generalized ellipsoid of inertia the above conditions are satisfied.

- The shape of the generalized ellipsoid of inertia at any point on the home circle is closest to a sphere than any other point. This is due to the fact that for $\theta_1 - \theta_2 = 90°$, as Equation 5.11 indicates, the difference between the eigenvalues of the matrix M is a minimum. In particular, if the physical properties of the manipulator are selected such that $q_{11} = q_{22}$, i.e.

$$\frac{I_1 + m_1 h_1^2 + m_2 L_1^2}{I_2 + m_2 h_2^2} = \left(\frac{L_1}{L_2}\right)^2 \tag{5.12}$$

then the two eigenvalues will become equal and the ellipsoid converges to a sphere. In that case, for a given amount of kinetic energy, the capability of the manipulator in attaining velocity will be the same in all directions. Asada(1983) has shown that under such circumstances the effect of nonlinear forces such as Coriolis will disappear. The aspect ratio, defined in Chapter 4 for the force ellipsoid can also be employed here to indicate the relative degree of importance of the effect of the nonlinear forces at various points of the work volume. This ratio can be given as

$$\zeta_M = \frac{R_{min}}{R_{max}} = \sqrt{\frac{\sigma_1}{\sigma_2}}$$

For the generalized ellipsoid of inertia the aspect ratio varies from zero at the singularity circles to its maximum at the home circle. The larger this measure is the better will be the dynamic performance of the manipulator and vice versa. It was mentioned earlier that the size of the ellipsoids along the solid configuration circles do not vary. Consequently the aspect ratio will remain unchanged along the circumference of those circles. Figure 5.2 portrays the loci of the points at which the aspect ratio is constant. Here again the minor deviation of the contour lines from perfect circles at some points of the work volume is due to the approximations made by the contour drawing software.

- The orientation of the generalized ellipsoid of inertia on the circumference of the home circle depends on the magnitude of q_{11} and q_{22}. Referring to Equations 5.3 and 5.10, it can be shown that for the points on the circumference of the home circle $q_{12} = 0$. The slope of the major axis of the generalized ellipsoid of inertia can be obtained by replacing the members of the dummy matrix $\mathbf{Z}$ and its first eigenvalue in Equation D.3 with those of the matrix M. The result would be

$$\phi_M = tan^{-1}\left(\frac{\sigma_1 - M_{11}}{M_{12}}\right)$$

Substituting for the members of the matrix M from the Equation 5.9 gives

$$\phi_M = tan^{-1}\left(\frac{\sigma_1 - q_{11}C_2^2 - q_{22}C_1^2}{q_{11}S_2C_2 + q_{22}S_1C_1}\right) \qquad (5.13)$$

If $q_{11} < q_{22}$ then for the points on the home circle Equation5.11 yields $\sigma_1 = q_{11}$. Substituting for this value of σ_1 in the above equation gives $\phi_M = \theta_2$. This means that the major axis of the generalized ellipsoid of inertia falls along the

longitudinal axis of the upper arm of the manipulator as shown in Figure 4.3-a. Similarly it is possible to show that if $q_{11} > q_{22}$ then the minor axis of the generalized ellipsoid of inertia will coincide with the longitudinal axes of the upper arm. This case is shown in the Figure 4.3-b.

Equation 5.3 shows that I_{11} equals the moment of inertia of the lower arm about its joint with the upper arm considered as a point mass lumped at its end. In addition, I_{22} is the moment of inertia of the upper arm with respect to its own joint. With reference to Equation 5.10 for a typical PUMA manipulator it is usual to accept that $q_{11} > q_{22}$. Consequently it can be concluded that in the vicinity of the home circle, the capability of these kind of manipulators in converting their kinetic energy into the velocity of the end effector, is the most in a direction perpendicular to the direction of the longitudinal axis of the upper arm.

- Equations 5.11 and 5.13 indicate that at any point on the singularity circles the generalized ellipsoid of inertia degenerates into a line which is infinitely long and is oriented along the tangent to the singularity circles.

5.4 Generalized Gravitational Acceleration

For a body of mass m exposed to a uniform gravitational field, the Newton law of motion takes up a special form which is given by

$$\mathbf{w} = m\mathbf{g}$$

where w represents the force applied on the body by the field, commonly known as the weight of the body, and g represents the local strength of the field and is called the gravitational acceleration. The generalized form of this equation for a manipulator can be expressed as

$$\left\{\mathbf{W}\right\} = \left[\ \mathbf{M}\ \right]\left\{\mathbf{G}\right\} \tag{5.14}$$

In this equation the vector **W** is the generalized weight of the arm defined in Section 3.3, the matrix **M** denotes the generalized inertia tensor of the arm defined in previous section, and the vector **G** represents the acceleration that the end effector can attain by virtue of the effect of gravity. This vector will be called here the *generalized gravitational acceleration*.

Substituting for **M** from Equation 5.7 into the above equation gives the generalized gravitational acceleration as

$$\left\{\mathbf{G}\right\} = \left[\ \mathbf{J}\ \right]\left[\ \mathbf{I}\ \right]^{-1}\left[\ \mathbf{J}\ \right]^{T}\left\{\mathbf{W}\right\} \tag{5.15}$$

For the example at hand the generalized gravitational acceleration vectors at various points of the work volume are depicted in Figure 5.3. As it can be seen in that figure, the acceleration field is more or less uniform both in magnitude and direction. The strength of the field approaches zero at the points associated with maximum and minimum potentials. This is due to the fact that the strength of the generalized gravitational field is zero at those points (Compare Figure 5.3 with Figure 3.7). Although the generalized weight, as shown in Figure 3.7 assumes various directions, the direction of the generalized acceleration, except at the points near the boundary of the work volume, is almost downward everywhere.

Referring to Equation 5.14, the generalized weight field can be thought of as a vector field resulting from the application of the transformation matrix M on the generalized acceleration field G. The two fields are shown together in Figure 5.4. The invariant lines of this transformation fall along the eigenvectors of the generalized tensor of inertia M. It was shown in the previous section that the eigenvectors of the matrix M are along the principal axes of the generalized ellipsoid of inertia. Consequently it can be concluded that

$$\frac{W_i}{G_i} = \sigma_i$$

where W_i and G_i are respectively the components of the generalized weight and generalized gravitational acceleration along the principal axes of the generalized ellipsoid of inertia, and σ_i is the corresponding eigenvalue of the matrix M. In particular, if the generalized weight lies along the principal axes of the generalized ellipsoid of inertia, then the generalized acceleration will also fall along the same direction. The ratio of the former to the latter will be equal to the corresponding eigenvalue. In the special case when the manipulator is designed such that the condition given by the Equation 5.12 is satisfied, the two fields will completely coincide along the home circle. This case is depicted in the Figure 5.5.

5.5 The Acceleration Ellipsoid

If the effect of gravity is ignored then the acceleration that the end effector can attain will be due to the effect of the joint motors only. Consequently Equation 5.5 can be expressed as

$$\left[\ \mathbf{I}\ \right]\left[\ \mathbf{J}\ \right]^{-1}\left\{\mathbf{A}\right\} = \left\{\ \tau_m\ \right\}$$

where τ_m represents the vector of the torques applied by the joint motors to the system. Substituting for this vector from the above equation in the Equation 4.2 yields

$$\left\{\mathbf{A}\right\}^T\left[\ \mathbf{J}\ \right]^{-T}\left[\ \mathbf{I}\ \right]^T\left[\ \mathbf{K}\ \right]\left[\ \mathbf{I}\ \right]\left[\ \mathbf{J}\ \right]^{-1}\left\{\mathbf{A}\right\} = P \qquad (5.16)$$

The matrix **K** in the above equation is given by Equation 4.3. Defining the matrix **D** as

$$\left[\ \mathbf{D}\ \right] = \left[\ \mathbf{J}\ \right]^{-T}\left[\ \mathbf{I}\ \right]^T\left[\ \mathbf{K}\ \right]\left[\ \mathbf{I}\ \right]\left[\ \mathbf{J}\ \right]^{-1} \qquad (5.17)$$

makes it possible to recast Equation 5.16 as

$$\left\{\mathbf{A}\right\}^T\left[\ \mathbf{D}\ \right]\left\{\mathbf{A}\right\} = P \qquad (5.18)$$

Equation 5.17 represents a congruence transformation. Therefore the matrix **D** is positive definite. As a result the quadratic form given by Equation 5.18 represents an ellipsoid called here the acceleration ellipsoid. [1] The acceleration ellipsoid has the property of indicating the capability of the manipulator in transforming the input power under the stall condition to the acceleration of the end effector. The principal axes of this ellipsoid indicate the direction and magnitude of the maximum and minimum accelerations that the end effector can achieve.

[1]This is the same ellipsoid that has been introduced by Yoshikawa in 1985 as the dynamic manipulability ellipsoid. The name acceleration ellipsoid is more suitable than the one employed by Yoshikawa. Thus it will be used throughout the rest of this work.

Using some geometrical properties of the acceleration ellipsoid such as its volume and its condition number, Yoshikawa introduced several measures that are useful for the assessment of the dynamic manipulability of the arm. For the manipulator under discussion the matrix $\mathbf{D}$ can be obtained by substituting for $\mathbf{J}^{-1}$ from Equation 5.8, for $\mathbf{I}$ from Equation 5.3, and for $\mathbf{K}$ from Equation 4.3 in Equation 5.18. The result is

$$\left[\begin{array}{c} \\ \mathbf{D} \\ \\ \end{array}\right] = \left[\begin{array}{cc} r_{11}C_2^2 - 2r_{12}C_1C_2 + r_{22}C_1^2 & r_{11}S_2C_2 - r_{12}S_{1+2} + r_{22}S_1C_1 \\ r_{11}S_2C_2 - r_{12}S_{1+2} + r_{22}S_1C_1 & r_{11}S_2^2 - 2r_{12}S_1S_2 + r_{22}S_1^2 \end{array}\right] \tag{5.19}$$

where

$$\begin{aligned} r_{11} &= \frac{1}{L_1^2 S_{1-2}^2}\left(\frac{I_{z1}^2}{k_{m1}^2} + \frac{I_{z2}^2}{k_{m2}^2}\right) \\ r_{12} &= \frac{1}{L_1 L_2 S_{1-2}^2}\left(\frac{I_{11} I_{12}}{k_{m1}^2} + \frac{I_{12} I_{22}}{k_{m2}^2}\right) \\ r_{22} &= \frac{1}{L_2^2 S_{1-2}^2}\left(\frac{I_{z2}^2}{k_{m1}^2} + \frac{I_{z2}^2}{k_{m2}^2}\right) \end{aligned} \tag{5.20}$$

and $S_i = sin\theta_i$ $C_i = cos\theta_i$ $S_{1-2} = sin(\theta_1 - \theta_2)$ $S_{1+2} = sin(\theta_1 + \theta_2)$

The eigenvalues of the $\mathbf{D}$ matrix are

$$\begin{aligned} \rho_1 &= \tfrac{1}{2}\left\{r_{11} + r_{22} + 2r_{12}C_{12} - \sqrt{(r_{11} + r_{22} + 2r_{12}C_{12})^2 - 4(r_{11}r_{22} - r_{12}^2)S_{12}^2}\right\} \\ \rho_2 &= \tfrac{1}{2}\left\{r_{11} + r_{22} + 2r_{12}C_{12} + \sqrt{(r_{11} + r_{22} + 2r_{12}C_{12})^2 - 4(r_{11}r_{22} - r_{12}^2)S_{12}^2}\right\} \end{aligned} \tag{5.21}$$

Figure 5.6 shows the acceleration ellipsoids at several points of the work volume. With reference to that figure and similar to the case of the generalized ellipsoid of inertia the following remarks can be made.

- Equation 5.21 indicates that the eigenvalues of the matrix $\mathbf{D}$ at any configuration of the manipulator are only functions of $\theta_1 - \theta_2$. The consequence is that on the circumference of the solid configuration circles the acceleration ellipsoids are all of the same size.

- The orientation of the acceleration ellipsoids with respect to the manipulator does not vary along the circumference of the solid configuration circles. This can be verified by proving that the members of the matrix $\mathbf{D}$ satisfy the conditions given in Appendix D. For the matrix $\mathbf{D}$ these condition are

$$\frac{\partial D_{11}}{\partial \theta_1} = -2D_{12}$$
$$\frac{\partial D_{12}}{\partial \theta_1} = D_{11} - D_{12}$$

Substituting for the members of the matrix $\mathbf{D}$ from Equation 5.19 and performing the involved mathematical work proves that for the acceleration ellipsoid the above conditions are satisfied.

- Equation 5.21 shows that for configurations at which $\theta_1 - \theta_2 = 90°$ the difference between the eigenvalues of the matrix $\mathbf{D}$ is a minimum. As a result, it can be said that along the circumference of the home circle the shape of the acceleration ellipsoid is closest to a sphere. In particular, if the physical properties of the manipulator are selected such that $r_{11} = r_{22}$, i.e.

$$\frac{I_1 + m_1 h_1^2 + m_2 L_1^2}{I_2 + m_2 h_2^2} = \frac{L_1}{L_2}\frac{K_{m1}}{K_{m2}} \tag{5.22}$$

then the two eigenvalues will become equal and the ellipsoid converges to a sphere. In that case, the capability of the manipulator in transforming the input energy to the acceleration of the end effector will be the same in all directions.

The aspect ratio that was previously defined for the force ellipsoid and the generalized ellipsoid of inertia can be expressed here as

$$\zeta_A = \frac{R_{min}}{R_{max}} = \sqrt{\frac{\rho_1}{\rho_2}}$$

Similar to the previous ellipsoids, the minimum value of the aspect ratio for the acceleration ellipsoid occures at the singularity circles, and its maximum occurs at the home circle. A relatively large aspect ratio means that the manipulator has a better capability for transforming the input energy into the acceleration of the end effector. Figure 5.7 shows the loci of the points with constant aspect ratios. The loci coincide with the solid configuration circles, however, as mentioned in the similar previous cases, their slight deviation from perfect circles at some points of the work volume is due to the approximations made by the contour tracing software.

- Similar to the case of the generalized ellipsoid of inertia, $r_{12} = 0$ on the home circle while r_{11} and r_{12} determine the orientation of the acceleration ellipsoid. With reference to the orientation of a general ellipsoid given in Equation D.3, the slope of the major axis of the acceleration ellipsoid can be obtained as

$$\phi_A = tan^{-1}\left(\frac{\rho_1 - D_{11}}{D_{12}}\right)$$

Substituting for the members of the matrix $\mathbf{D}$ from the Equation 5.19 gives

$$\phi_A = tan^{-1}\left(\frac{\rho_1 - r_{11}C_2^2 - r_{22}C_1^2}{r_{11}S_2C_2 + r_{22}S_1C_1}\right) \qquad (5.23)$$

If $r_{11} < r_{22}$ then Equation 5.21 gives $\rho_1 = r_{11}$. Substituting for this value of ρ_1 in the above equation gives $\phi_A = \theta_2$. This means that the major axis of the acceleration ellipsoid falls along the longitudinal axis of the upper arm of the manipulator. Figure 4.3-a shows this case. Similarly, if $r_{11} > r_{22}$ then the minor axis of the ellipsoid will coincide with the longitudinal axis of the upper arm as depicted in the Figure 4.3-b.

It was mentioned earlier that for a PUMA type manipulator it is usual to have $I_{11} > I_{22}$. For such robots it is also usual to expect that $L_1 \leq L_2$ and $K_{m1} = K_{m2}$. This leads to $r_{11} > r_{22}$. As a result it can be concluded that, in the vicinity of the home circle, the capability of a PUMA type manipulator in accelerating from rest is maximum in a direction perpendicular to the longitudinal axis of the upper arm.

- Equations 5.21 and 5.23 indicate that at any point on the singularity circles the acceleration ellipsoid degenerates into a line which is infinitely long and is oriented along the tangent to the singularity circles.

5.6 Dynamic Output-Demand Relation

Earlier in this chapter it was verified that for a given amount of energy supplied to the joint motors of a manipulator under stall condition, the acceleration capability of the end effector can be portrayed by the acceleration ellipsoid. It was also proven that the effect of gravity can be transformed into the generalized gravitational acceleration vector acting at the end effector. Considering the acceleration ellipsoid as the output and the generalized gravitational acceleration as the demand, the static output-demand model that was presented in Chapter 4 to study the static behavior of the robot arms can be extended to the dynamic case. The magnitude index in this case may be defined as the ratio of the magnitude of the generalized gravitational acceleration to the radius of the acceleration ellipsoid along the generalized gravitational acceleration at that configuration. Considering the vector $\vec{OA}$ in Figure 4.4 as the generalized gravitational acceleration and the vector $\vec{OB}$ as the corresponding

radius of the acceleration ellipsoid, the magnitude index can be expressed as

$$\eta_m = \frac{|\mathbf{G}|}{|\mathbf{A}|} = \frac{|\vec{OA}|}{|\vec{OB}|}$$

where $|\mathbf{G}|$ indicates the magnitude of the generalized gravitational acceleration and $|\mathbf{A}|$ represents the acceleration that the end effector can attain in the direction of $\mathbf{G}$. Replacing the vector $\mathbf{W}$ and the matrix $\mathbf{B}$ in Equation 4.19 by $\mathbf{G}$ and $\mathbf{D}$ respectively, gives the magnitude index as

$$\eta_m = \sqrt{\frac{\{\mathbf{G}\}^T [\ \mathbf{D}\ ] \{\mathbf{G}\}}{P}}$$

Substituting for $\mathbf{G}$ from Equation 5.15 and for $\mathbf{D}$ from Equation 5.19 proves that the magnitude index in the present case is identical to the one derived for the force ellipsoid. Consequently the contour map shown in Figure 4.5 can also represent the present case.

The direction index can be obtained by replacing the members of the matrix $\mathbf{B}$ and its first eigenvalue by those of the matrix $\mathbf{D}$ and substituting for the components of the vector $\mathbf{W}$ by those of the vector $\mathbf{G}$. The result would be

$$\eta_d = \frac{1 + \frac{e_1 - D_{11}}{D_{12}} \frac{G_2}{G_1}}{\sqrt{\left[1 + \left(\frac{e_1 - D_{11}}{D_{12}}\right)^2\right] \left[1 + \left(\frac{G_2}{G_1}\right)^2\right]}}$$

Figure 5.8 shows the contour map of the direction index for the dynamic output-demand model.

5.7 Effect of Gravity on the Output

In the previous section it was assumed that the gravity had no effect on the acceleration ellipsoid. To include the effect of gravity, the torque in Equation 5.5 should be replaced by the sum of the vector of the joint torques τ_m and the vector τ_g which represents the torques applied on the system due to the effect of gravity. The resulting expression becomes

$$\left[\ \mathbf{I}\ \right]\left[\ \mathbf{J}\ \right]^{-1}\left\{\mathbf{A}\right\} = \left\{\ \tau_m\ \right\} + \left\{\ \tau_g\ \right\} \tag{5.24}$$

The vector τ_g can be related to the generalized weight W through the transformation given by Equation 4.4 as

$$\left\{\ \tau_g\ \right\} = \left[\ \mathbf{J}\ \right]^{T}\left\{\mathbf{W}\right\}$$

Substituting for M from Equation 5.7 into Equation 5.14, and substituting the result into the above equation gives

$$\left\{\ \tau_g\ \right\} = \left[\ \mathbf{I}\ \right]\left[\ \mathbf{J}\ \right]^{-1}\left\{\mathbf{G}\right\}$$

Substituting this value of τ_g into Equation 5.24 and rearranging yields

$$\left[\ \mathbf{I}\ \right]\left[\ \mathbf{J}\ \right]^{-1}\left\{\mathbf{A}-\mathbf{G}\right\} = \left\{\ \tau_m\ \right\}$$

If the vector τ_m from the above equation is substituted into Equation 4.2 the following quadratic form will result

$$\left\{\mathbf{A}-\mathbf{G}\right\}^{T}\left[\ \mathbf{D}\ \right]\left\{\mathbf{A}-\mathbf{G}\right\} = P$$

The above expression represents an ellipsoid with its center shifted to the end of the generalized gravitational acceleration vector G. Figure 5.9 portrays some acceleration ellipsoids shifted to the end of the local generalized gravitational acceleration vectors.

With a reasoning similar to that of the force ellipsoid, it can be shown that in presence of the effect of gravity, the maximum and minimum values of the acceleration that the end effector can achieve due to a given input energy can not be found, as argued by Yoshikawa, from the principal axes of the acceleration ellipsoid. As illustrated in Figure 4.9, the true maximum and minimum values can be found by drawing perpendicular lines from the end effector to the surface of the acceleration ellipsoid. The longest and the shortest distances will indicate the maximum and the minimum accelerations respectively.

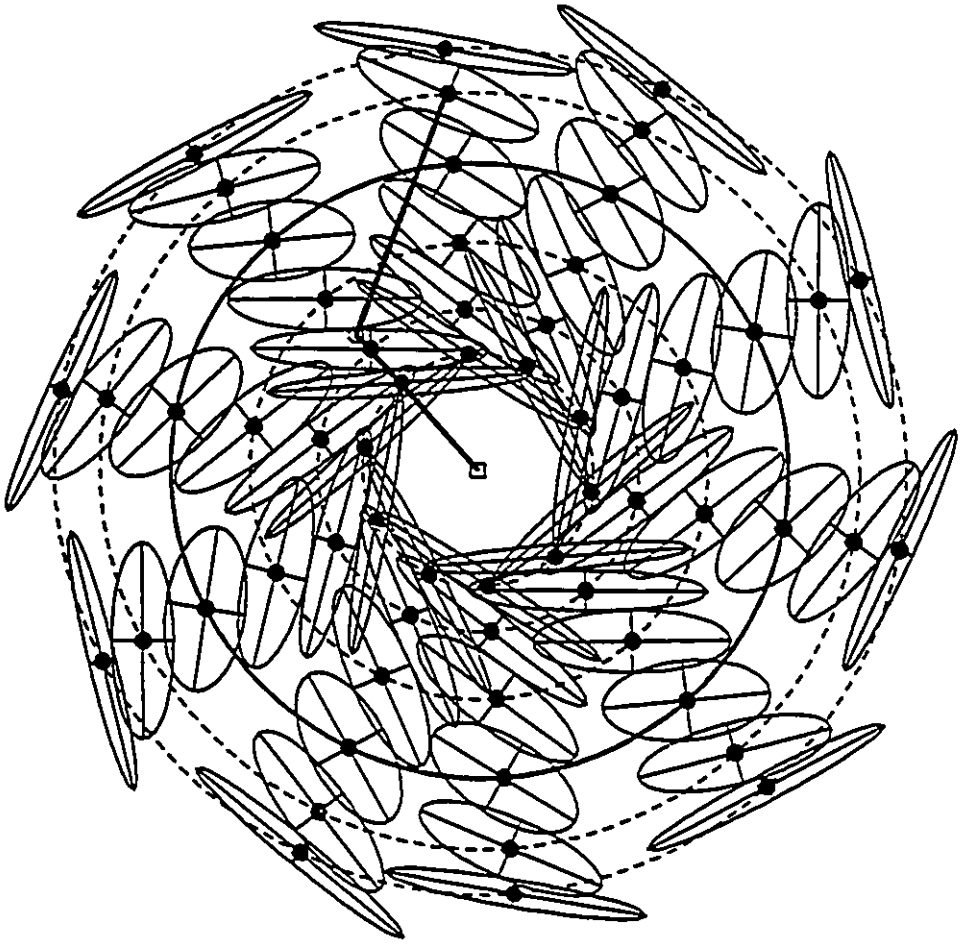

Figure 5.1: Generalized ellipsoids of inertia.

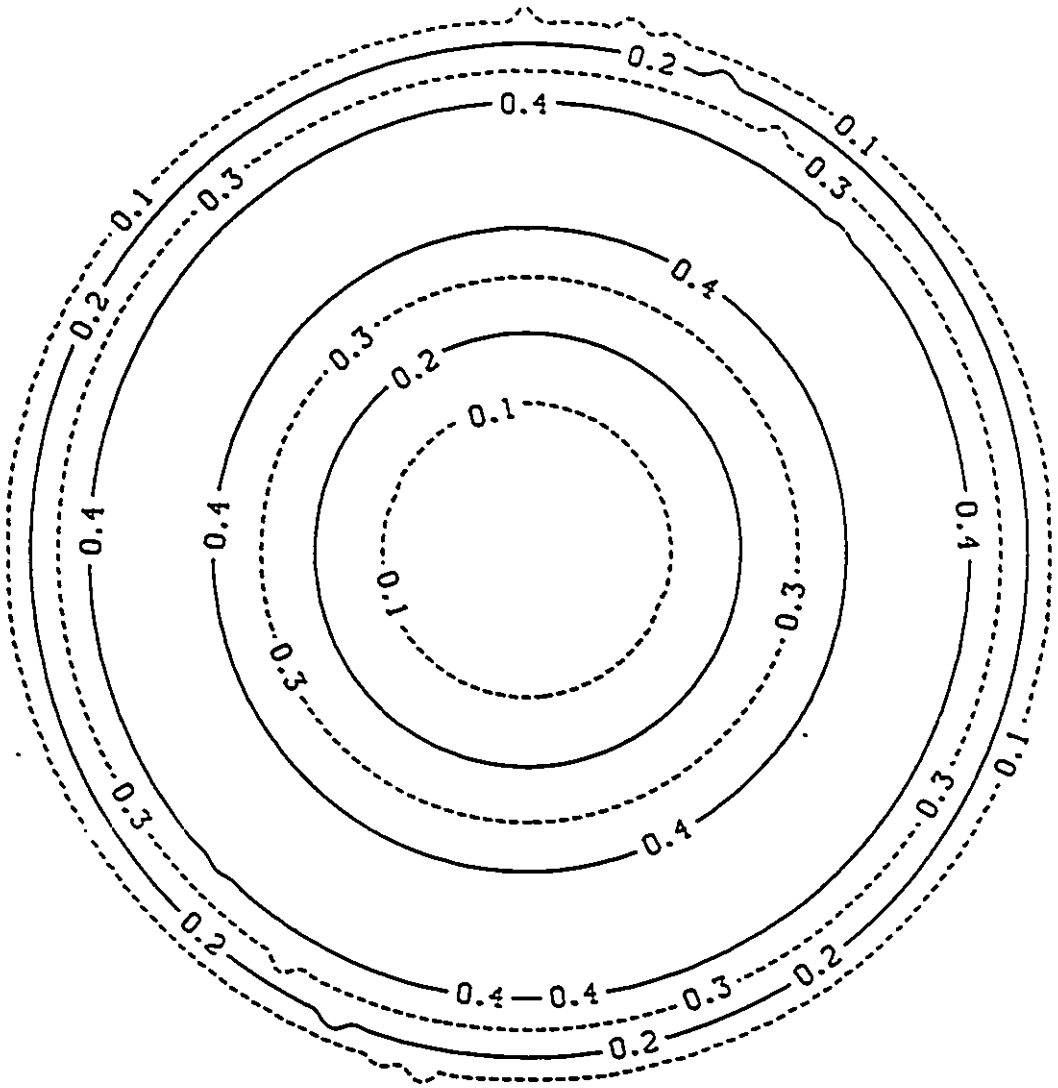

Figure 5.2: Contour map of aspect ratio for generalized ellipsoid of inertia.

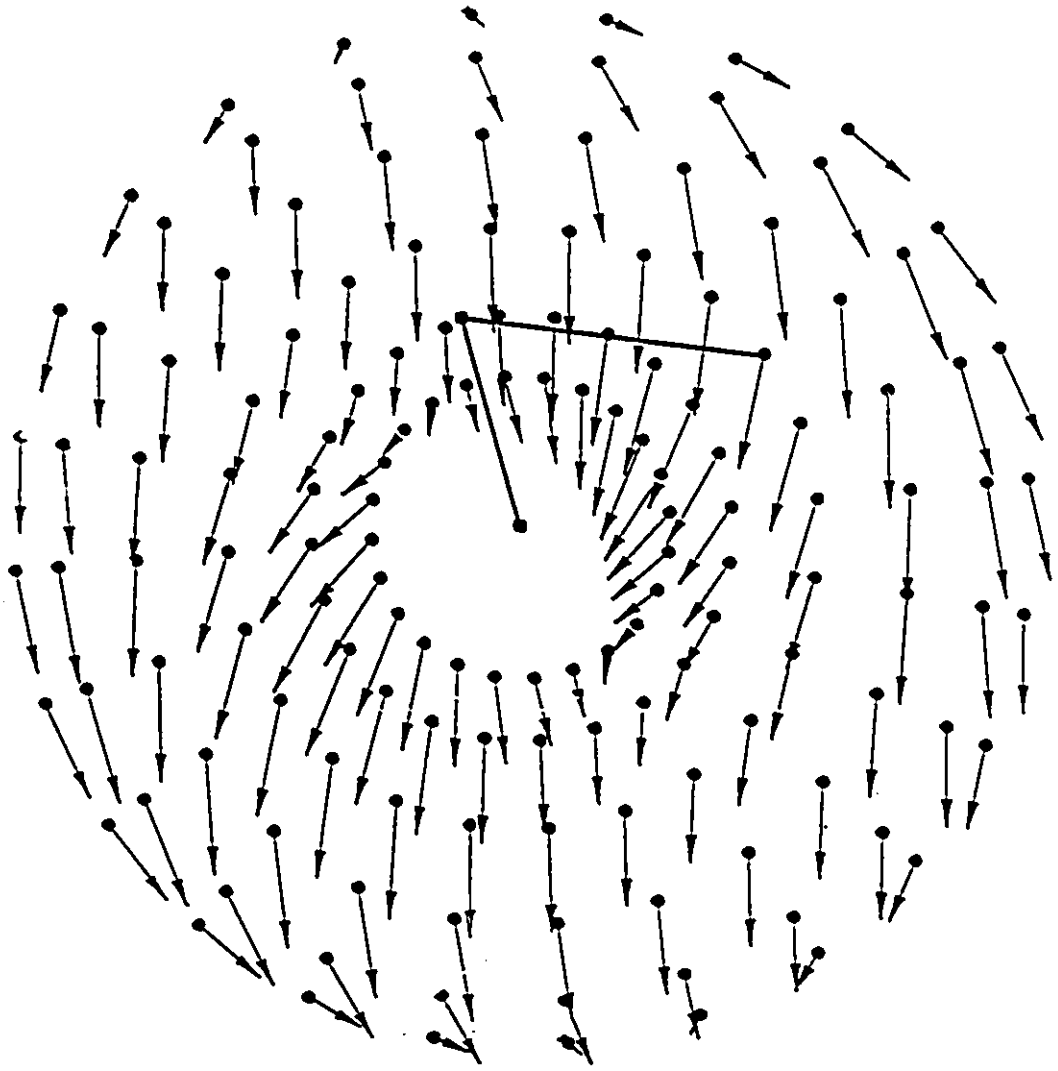

Figure 5.3: Generalized gravitational acceleration field.

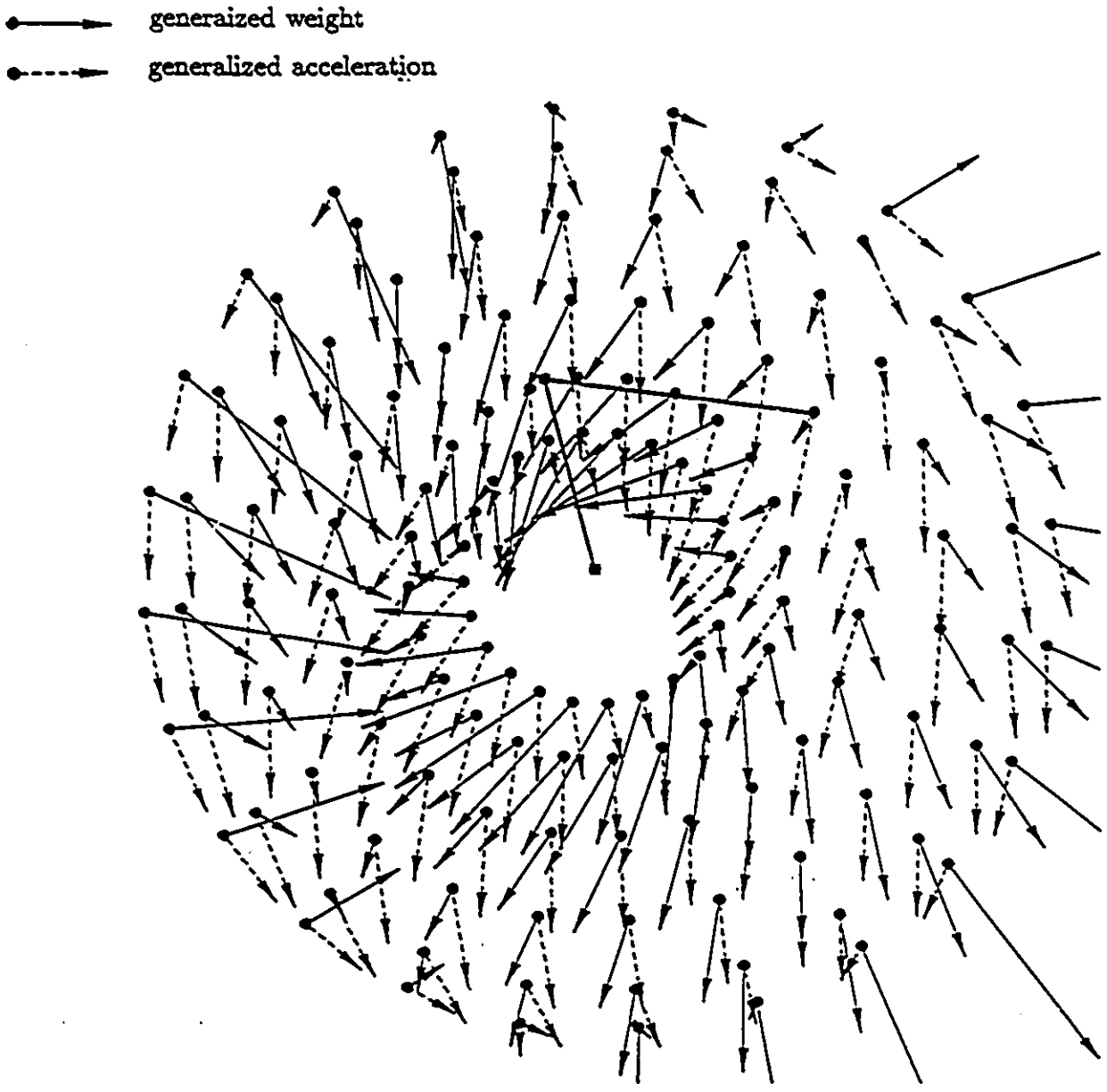

Figure 5.4: Generalized weight and generalized gravitational acceler ation fields.

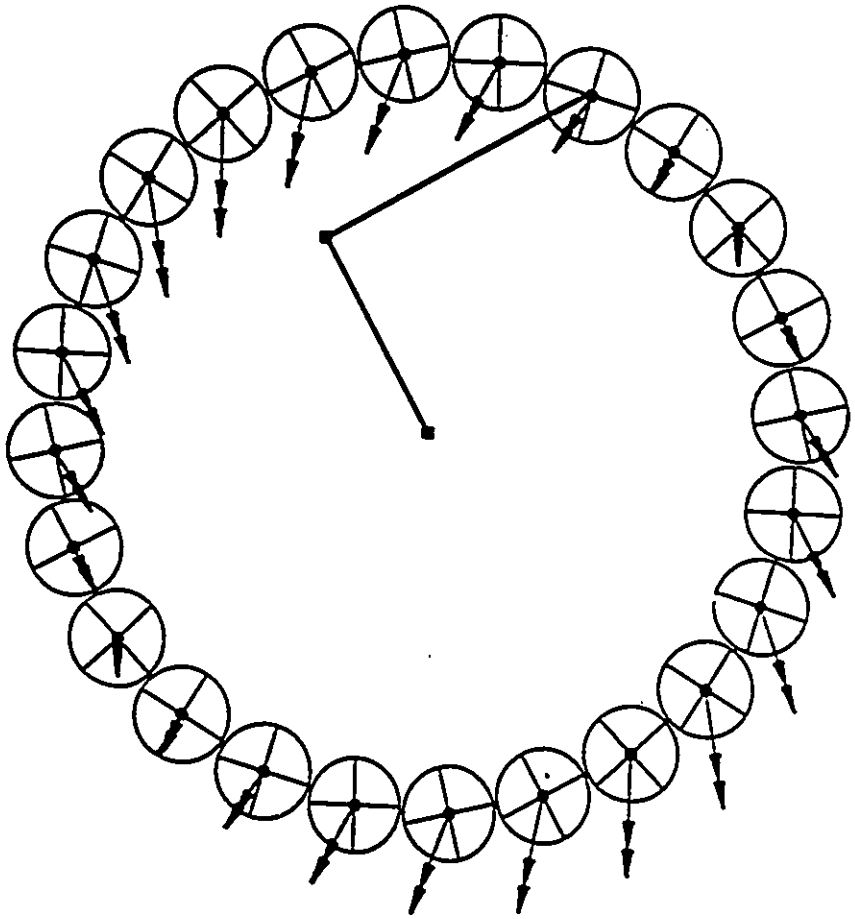

Figure 5.5: Generalized ellipsoid of inertia, generalized weight and generalized gravitational acceleration on the home circle.

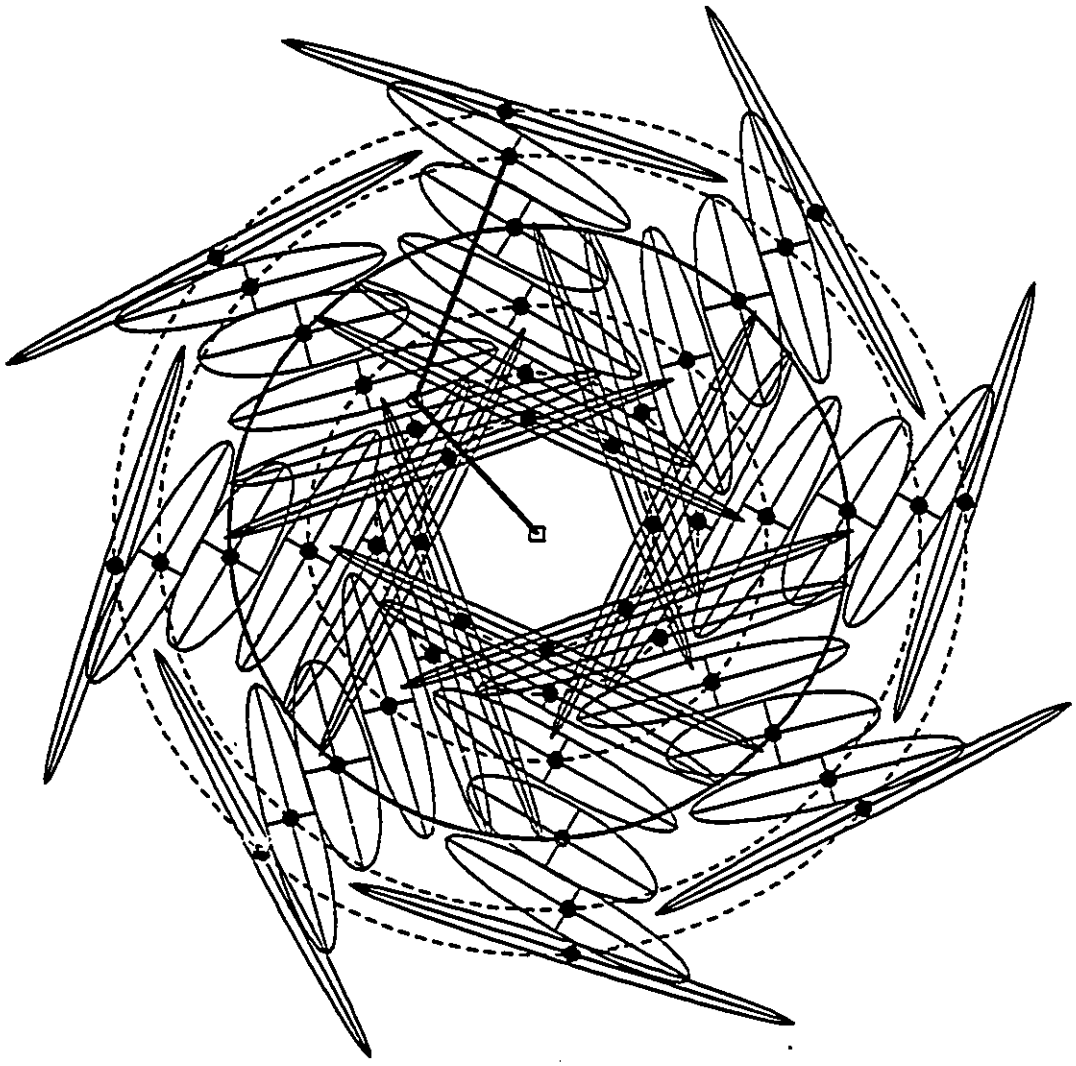

Figure 5.6: Acceleration ellipsoids.

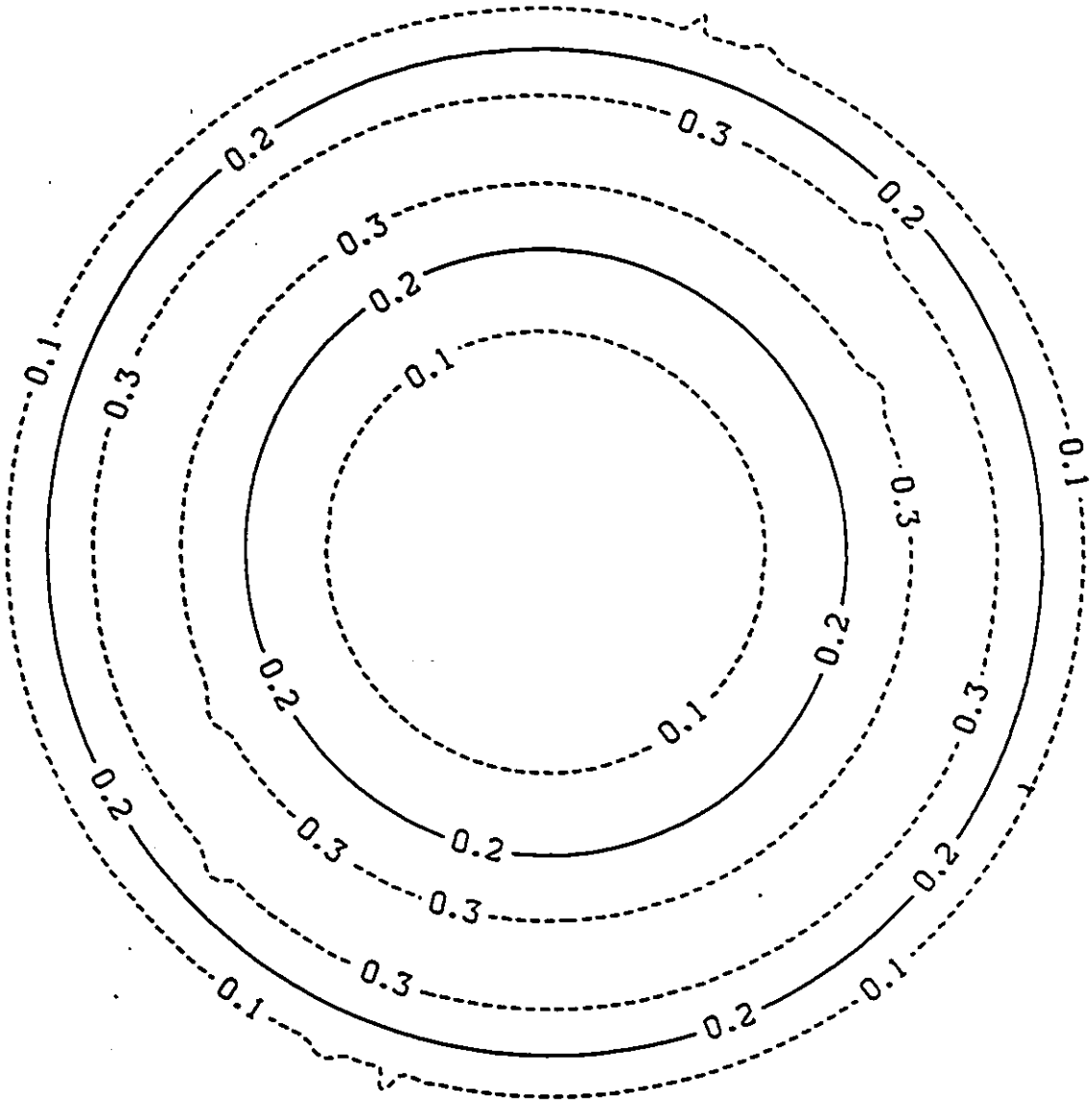

Figure 5.7: Contour map of aspect ratio for the acceleration ellipsoids.

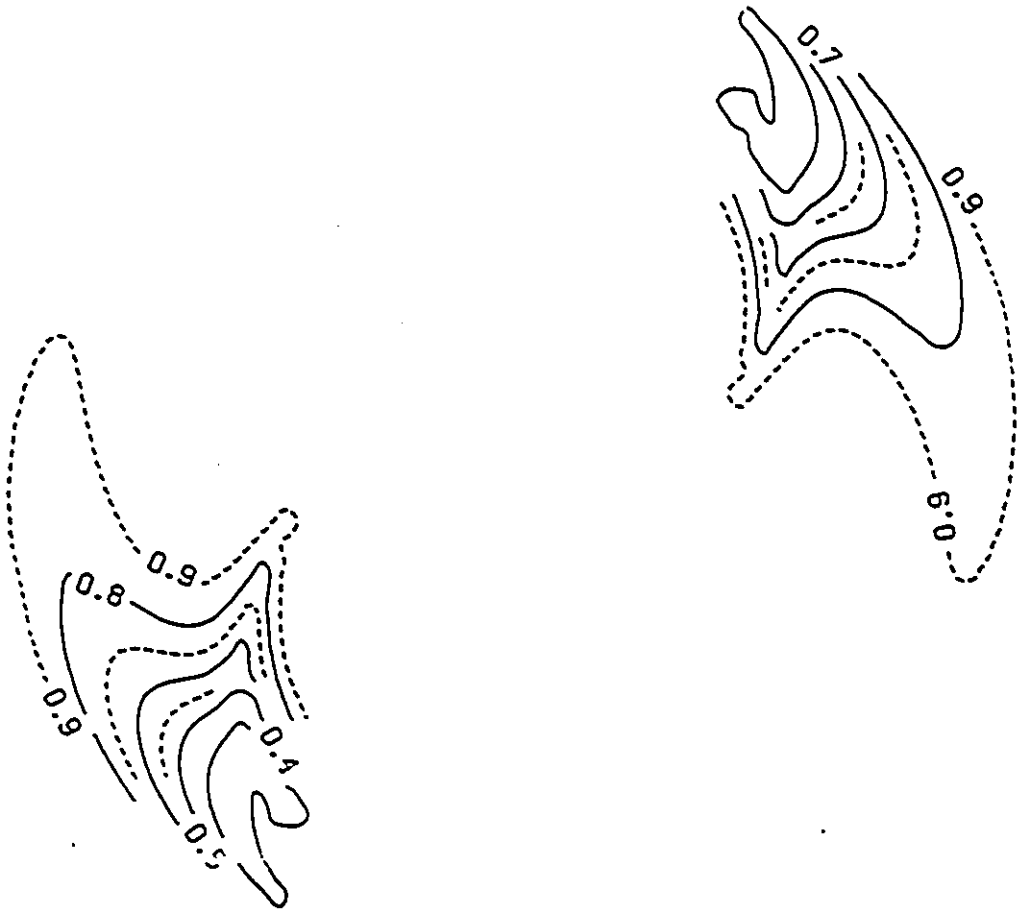

Figure 5.8: Contour map of direction index for dynamic output-demand model.

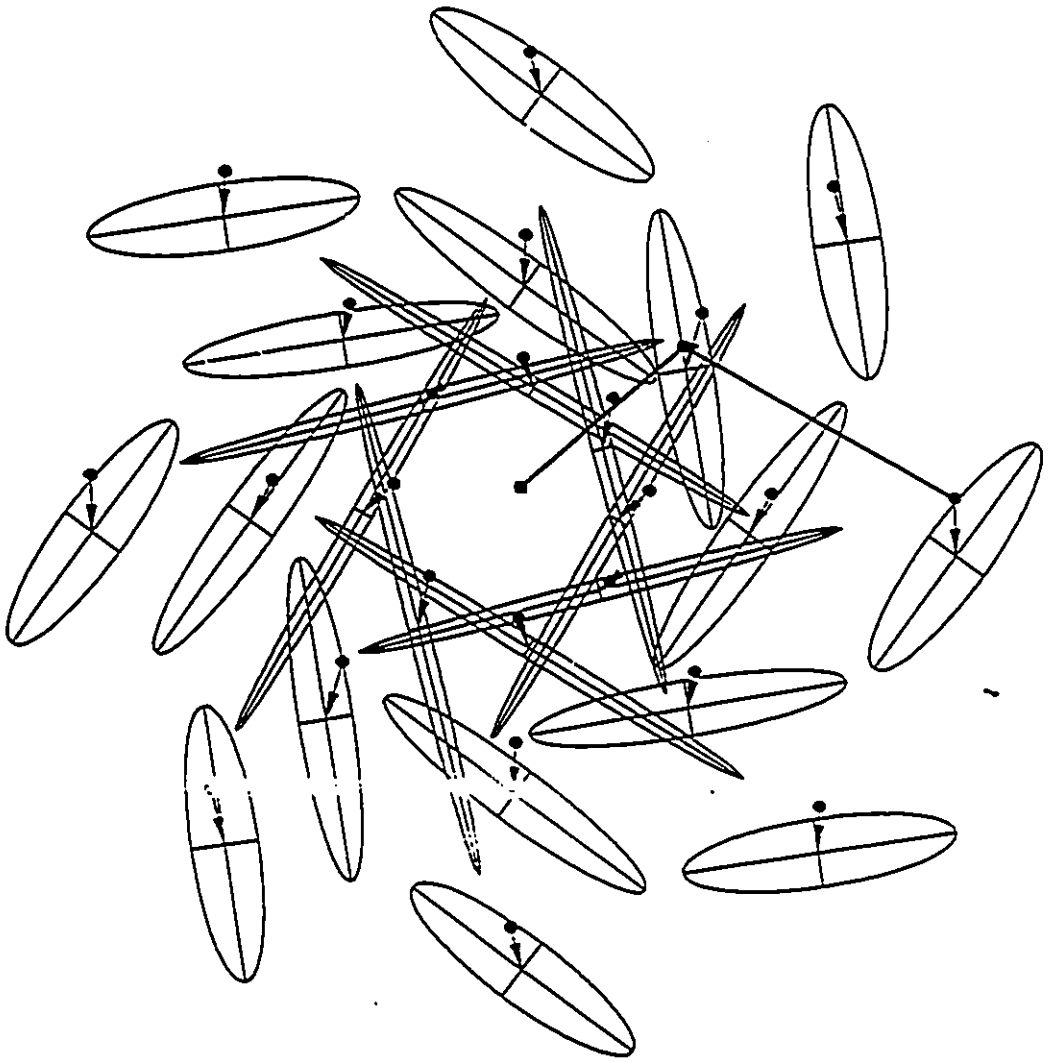

Figure 5.9: Acceleration ellipsoids in shifted positions.

Chapter 6

Effect of Change of Physical Properties of the Arm on its Static and Dynamic Behavior.

6.1 Introduction

The material discussed so far in this study has been exemplified only through a typical PUMA manipulator whose schematic diagram and physical properties were given in Figure 3.4. The aim of this chapter is to investigate how the gravitational field and other generalized characteristics of a manipulator will vary as a result of a change in one or more of its physical properties. The base link which is usually oriented along the direction of gravitational acceleration, does not contribute to the static behavior of the manipulator and has little effect on its dynamic performance. With the exception of the base link, a unique feature of the GGF is that it depends on

all the physical properties of the manipulator's links as well as those of the payload. Consequently, it can be said that any change in any of the physical properties of the links, except those of the base link, will be reflected on the structure of the GGF. Therefore, it is possible to categorize the manipulators according to the shape of their GGF.

The shape of the generalized gravitational field of a manipulator is a function of many parameters. In order to study the relation between these parameters and the shape of the GGF, two measures are defined. The first measure relates the physical properties of the arm to the local conformation of the GGF. The second one quantizes the overall contortion of the field. The static and dynamic behavior of several manipulators with various physical properties will then be considered. It will be shown that for a special case the equipotential lines of the GGF will be straight horizontal lines. In consequence the generalized weight of the arm will be the same at all points of the work volume. It will also be shown that in such a case, the shape of the lines are independent of the magnitude of the payload.

6.2 Classification of Manipulators Based on their Generalized Gravitational Field Conformation.

In order to contemplate the shape of the GGF of manipulators, two quantitative measures are defined. The first measure which directly involves the local slope of the equipotential lines is called here the *local field index* , and is designated by φ_l. The

second one, denoted by φ_g , takes into account the overall contortion of the field, and is called the *global field index*.

The local field index groups all the physical parameters of the arm's links and the payload in a dimensionless quantity given as

$$\varphi_l = \frac{\frac{a_1}{L_1}}{\frac{a_2}{L_2}} \tag{6.1}$$

Substituting for a_1 and a_2 from Equation 3.4 into the above equation and combining the resulting expression with Equation 3.2 leads to

$$\varphi_l = \frac{\frac{m_2}{m_1} + \frac{h_1}{L_1} + \frac{m_p}{m_1}}{\frac{m_2}{m_1}\frac{h_2}{L_2} + \frac{m_p}{m_1}} \tag{6.2}$$

From Equation 3.7 the slope of the equipotential lines in Cartesian space can be expressed as

$$\frac{dx_2}{dx_1} = -\frac{w_1}{w_2} = -\frac{\frac{a_2}{L_2} - \frac{a_1}{L_1}}{\frac{a_2}{L_2}tan\theta_1 - \frac{a_1}{L_1}tan\theta_2}$$

Combining this expression with Equation 6.1 yields

$$\frac{dx_2}{dx_1} = \frac{1 - \varphi_l}{\varphi_l tan\theta_2 - tan\theta_1} \tag{6.3}$$

Equation 6.3 indicates that the slope of the equipotential lines at a given point of the work volume is only a function of the local field index φ_l.

Referring to Figure 3.5 the global field index φ_g can be defined as the ratio of the energy level u_{dis} of the first equipotential line that curls down to osculate the inner singularity circle, to the maximum energy level u_{max} . Equation 3.6 shows that the limit for continuity in equipotential lines is reached when the expression under

the radical becomes zero, i.e. when $x_1^2 + x_2^2 = r^2$. Substituting this into Equation 3.6 gives $u_{dis} = a_1 - a_2$. The global field index can therefore be expressed as

$$\varphi_g = \frac{a_1 - a_2}{a_1 + a_2} = a_1 - a_2 \tag{6.4}$$

or as a function of φ_l as

$$\varphi_g = \frac{\varphi_l - \frac{L_2}{L_1}}{\varphi_l + \frac{L_2}{L_1}} \tag{6.5}$$

Equation 6.4 shows that the global field index varies from -1 to $+1$ such that its value coincides with the energy level of the first equipotential line that osculates the inner singularity circle at its lowest point. On the other hand, since the field is symmetrical, the equipotential line with energy level $-u_{dis}$ will be the last line in contact with the inner singularity circle and its osculating point will be the uppermost point of the circle. As a result, a large φ_g indicates that a large number of the equipotential lines will come in contact with the inner singularity circle, and vice versa. As an example, for the field shown in the Figure 3.5, Equation 6.4 gives $\varphi_g = 0.4$. Therefore the first and the last equipotential lines to osculate the inner singularity circle will have an energy level of 0.4 and -0.4 respectively. It can be concluded that a higher global index refers to a more contorted field, and conversely, a small global index is associated with a more flattened field.

In later sections three types of manipulators with global indices equal to -1, 0, and $+1$, with the addition of a manipulator with a completely flat field are studied. Important features such as GGF, generalized weight field, generalized ellipsoid of inertia, etc. for each manipulator will be presented and discussed. The similarities and differences will be highlighted and explained accordingly. The length of the links will be kept constant in all cases to keep the working volume the same for all

manipulators.

As it can be seen from Equation 4.15, the force ellipsoids are only functions of the length of the links and the joint motors specifications. Keeping these values constant the force ellipsoids will remain the same for all manipulators under investigation in this chapter.

6.3 Manipulators with Minimum Global Index

Figure 6.1 shows the schematic diagram and physical properties of a manipulator with $\varphi_g = -1$. The local index for this manipulator can be found from Equation 6.1 as $\varphi_l = 0$. For this value of φ_l Equation 6.1 yields $a_1 = 0$. Substituting this result in Equation 3.4 and making use of the Equation 3.2 leads to

$$A_1 = m_1 h_1 + (m_2 + m_p) L_1 = 0$$

The above relation is satisfied when the first link balances the second link and the payload about the first joint. Such a state of balancing makes the total potential energy of the manipulator insensitive to the orientation of the first link. Therefore $\tau_1 = 0$ for all configurations of the arm. This can be verified from Figure 6.3 where the GGF of the arm in joint space is shown. For the example arm of Figure 3.4. the equipotential lines in joint space as shown in Figure 3.6, are conformed into some concentric ellipsoidal shapes. In the limit these shapes have flattened into horizontal lines as shown in Figure 6.3.

The corresponding field in Cartesian space and the generalized weight field for

this manipulator are shown in Figures 6.2 and 6.4 respectively. It can be seen in the last two figures that the strength of the field is smallest near the lower right region of the work volume. This is the area in which most of the overhang type manipulators work. Unlike the typical manipulator shown in Figure 3.4 in which the total potential energy of the arm was maximum or minimum at only one point, in present case the total potential energy is maximum or minimum along a full line. The home circle shown in Figure 6.2 represents the locus of the points associated with minimum field strength in Cartesian space. This circle will map onto a straight line in joint space as it can be seen from Figure 6.3.

The generalized ellipsoid of inertia for the manipulator under discussion is depicted in Figure 6.5. Not much difference can be observed between this figure and Figure 5.1 which shows the generalized ellipsoid of inertia for the typical robot of the Figure 3.4. This is due to the fact that the total moment of inertia of the links have not changed much. This is true for almost all the other cases to be discussed later.

Figures 6.6 and 6.7 illustrate the generalized gravitational acceleration field and acceleration ellipsoids respectively.

6.4 Manipulators with Absolutely Flat Fields

As the magnitude of the global field index increases the equipotential lines flatten. This trend continues until the condition

$$\varphi_g = \frac{\frac{L_1}{L_2} - 1}{\frac{L_1}{L_2} + 1}$$

is reached. This condition corresponds to $\varphi_l = 1$. Equation 6.3 shows that for this

value of φ_l the slope of the equipotential lines is zero everywhere. The generalized gravitational field in Cartesian space for this case is shown in Figure 6.9. The equipotential lines are parallel and the spacing between them are the same throughout the work volume.

It was proved in Section 3.4 that the GGF is, in general, conservative but not solenoidal. It can be proved that for the present special case the field is also solenoidal everywhere. Substituting unity for the value of φ_l in Equation 6.1 gives

$$\frac{a_1}{L_1} = \frac{a_2}{L_2} \tag{6.6}$$

Combining this result with Equation 3.11 shows that the divergence of the field is zero throughout the work volume. This indicates that an absolutely flat generalized field is similar to the ordinary gravitational field in every respect. The generalized weight field for this case shown in the Figure 6.11 justifies this conclusion.

The relation between the physical parameters of the manipulator that causes the GGF in Cartesian space become absolutely flat can be obtained by substituting for a_1 and a_2 from Equation 3.4 in Equation 6.6 and combining the result with Equation 3.2. This will lead to

$$\frac{m_2}{m_1} = \frac{\frac{h_1}{L_1}}{\frac{h_2}{L_2} - 1} \tag{6.7}$$

It is interesting to note that this condition is independent of the payload. Any variation of the payload will only change the magnitude of the generalized weight of the arm. This can be further clarified by finding the components of the generalized weight from Equation 3.7 under the condition given by the Equation 6.6. Combining that relation with Equation 3.7 gives the normalized components of the generalized

weight as

$$\begin{cases} w_1 = 0 \\ w_2 = -\frac{a_1}{L_1} = -\frac{a_2}{L_2} \end{cases} \tag{6.8}$$

The actual components of the generalized weight can now be obtained by multiplying w_1 and w_2 by normalization factor $A_1 + A_2$. Performing the multiplication and substituting for a_1 and a_2 from the Equation 3.4 yields

$$\begin{cases} W_1 = 0 \\ W_2 = -\frac{A_1}{L_1} = -\frac{A_2}{L_2} \end{cases} \tag{6.9}$$

Substituting for A_1 or A_2 from Equation refeq:A1,A2 in the above relation gives

$$\begin{cases} W_1 = 0 \\ W_2 = -(\frac{h_2}{L_2} m_2 + m_p) g \end{cases} \tag{6.10}$$

This expression shows that for all values of the physical parameters of the manipulator, including the payload, the horizontal component of the generalized weight is zero. However the vertical component which constitutes the strength of the flat field, is a function of the physical properties of the upper arm as well as that of the payload.

The generalized gravitational field in joint space is shown in Figure 6.10. The ellipsoidal shape of the equipotential lines are clearly formed in comparison with the field lines of the previous case. It can be seen that with the increase of the global field index the equipotential lines of the joint space are compressed in horizontal direction and elongated in vertical direction.

Figure 6.12 illustrates the generalized ellipsoid of inertia for the flat field manipulator. As it was mentioned in previous section, this characteristic of the manipulators

does not change much because the variation in moments of inertia of the links are small.

The generalized gravitational acceleration field is shown in the Figure 6.13. Although the generalized weight field for the present case is uniform both in magnitude and direction throughout the work volume, the acceleration field is not necessarily so. This is due to the fact that the components of the generalized mass of the manipulator, as indicated by Equation 5.9, are functions of the space. However, the magnitude of the field is more or less uniform across the working space.

The acceleration ellipsoids are depicted in the Figure 6.14. Again not much of a change is seen in comparison with the same figure for the manipulator of the previous case. The reason given for the generalized ellipsoid of inertia also applies here.

6.5 Manipulators with Zero Global Index

As the field index is increased further, the equipotential lines in the Cartesian space start to curl up and the contortion of the field increases. The corresponding lines in the joint space continue to shrink in the horizontal direction and elongate in the vertical direction. The trend goes on until the special case where $\varphi_g = 0$ is reached. At this instance the equipotential line associated with zero energy level in Cartesian space will be the only line to osculate the inner singularity circle. The field then seems to be in its most unwarped shape, with no discontinuities. The Cartesian field for this case is shown in Figure 6.16. The equipotential lines in joint space, as shown in Figure 6.17 are now axisymmetric with respect to positions at which $\theta_1 = \theta_2 = \pm 90°$.

The generalized weight field for this case is shown in Figure 6.18. The generalized ellipsoids of inertia, as it can be seen in Figure 6.19, have basically remained the same. The generalized gravitational acceleration field shown in the Figure 6.20 shows more strength in the upper right quadrant and less in the lower right quadrant. The acceleration ellipsoids are depicted in the Figure 6.21. In comparison with previous cases it seems that for the present case the ellipsoids are thinner.

6.6 Manipulators with Maximum Global Index

With further increase of the global field index above zero, higher level equipotential lines in Cartesian space lose continuity and osculate the inner singularity circle. Accordingly the lines in joint space elongate more in vertical direction. This trend can be tracked by noticing the generalized gravitational field of the typical arm that was subject of study in Chapters 3, 4, and 5. That manipulator has a global field index of 0.4 and as it can be seen from Figure 3.5, its Cartesian field is more contorted than that of the previous case. Its equipotential lines in joint space, as shown in Figure 3.6, are elongated more in the vertical direction.

The limit to this trend comes when $\varphi_g = 1$. Similar to the case in which the global field index was at its minimum, Once again all equipotential lines in Cartesian space osculate the singularity circles as it can be seen from the Figure 6.23. However, the concavity of the equipotential lines in the present case is opposite to that of the other case. Furthermore, the Cartesian field in the present case is strong at regions where the other field is weak and vise versa. However, similar to the other case the home circle shown in Figure 3.5 represents the locus of the points associated with

minimum field strength in Cartesian space. The corresponding locus in joint space is a straight line as shown in the Figure 6.24.

The value of the local field index φ_l becomes infinitely large in this case. Equation 6.1 then yields $a_2 = 0$. Substituting this in Equation 3.4 and combining the result with Equation 3.2 leads to

$$A_2 = (m_2 h_2 + m_p L_2) = 0$$

The above relation is satisfied when the center of gravity of the second link is located at a point where it balances the mass of the payload with respect to the second joint. As a result of this balancing condition the total potential energy of the manipulator becomes insensitive to the orientation of the second link. Therefore $\tau_2 = 0$ for all configurations of the arm as can be seen from the Figure 6.24. This is in agreement with the trend with which the shape of the equipotential lines in joint space has been changing. The lines have been elongated more and more in the vertical direction until the limit at which they all have become vertical straight lines.

Figure 6.25 shows the strength of the Cartesian field at various points of the work volume. The generalized ellipsoids of inertia, the generalized gravitational acceleration field and the acceleration ellipsoids are shown in Figures 6.26, 6.27 and 6.28 respectively for completeness.

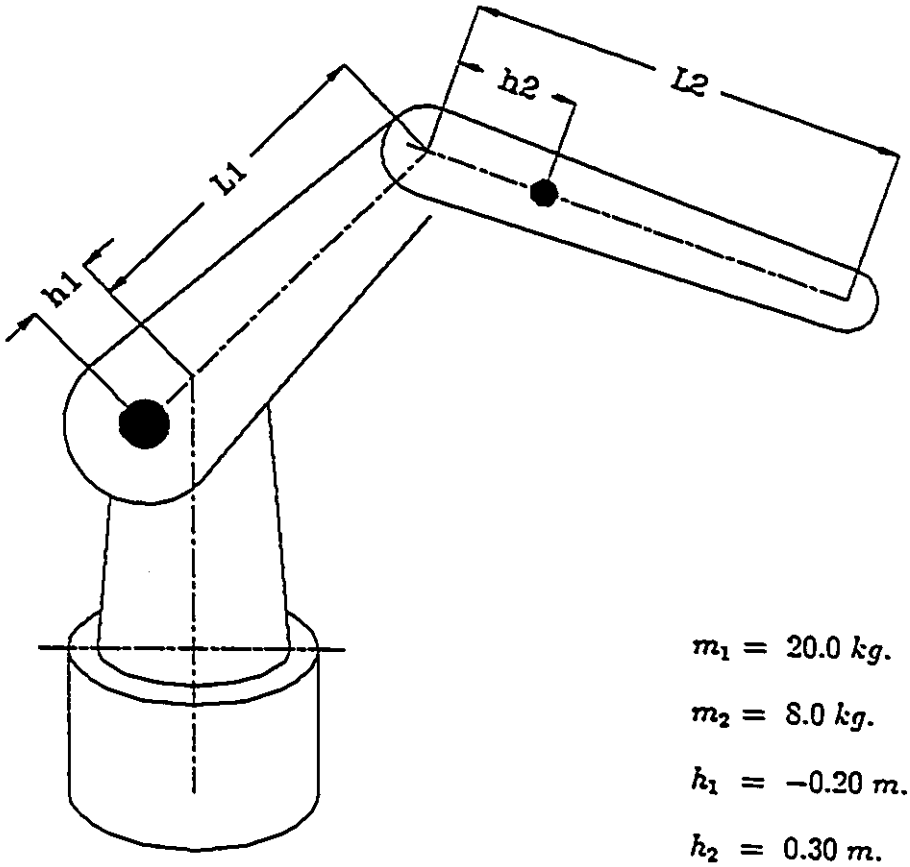

$m_1 = 20.0\ kg.$

$m_2 = 8.0\ kg.$

$h_1 = -0.20\ m.$

$h_2 = 0.30\ m.$

$L_1 = 0.50\ m.$

$L_2 = 0.70\ m.$

$\varphi_g = -1.0$

Figure 6.1: Schematic diagram of a manipulator with minimum global field index.

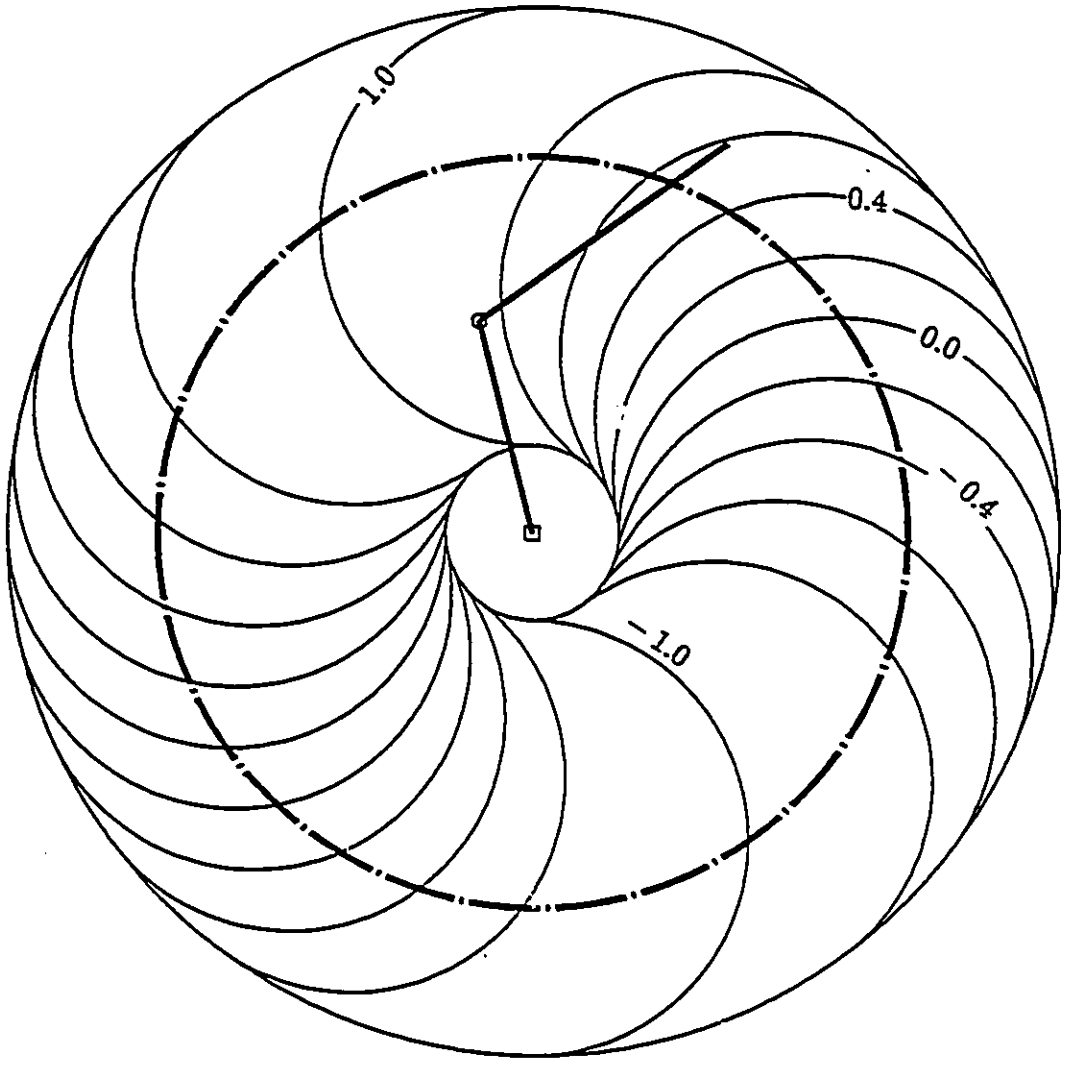

Figure 6.2: Generalized gravitational field in Cartesian space for a Manipulator with minimum global field index.

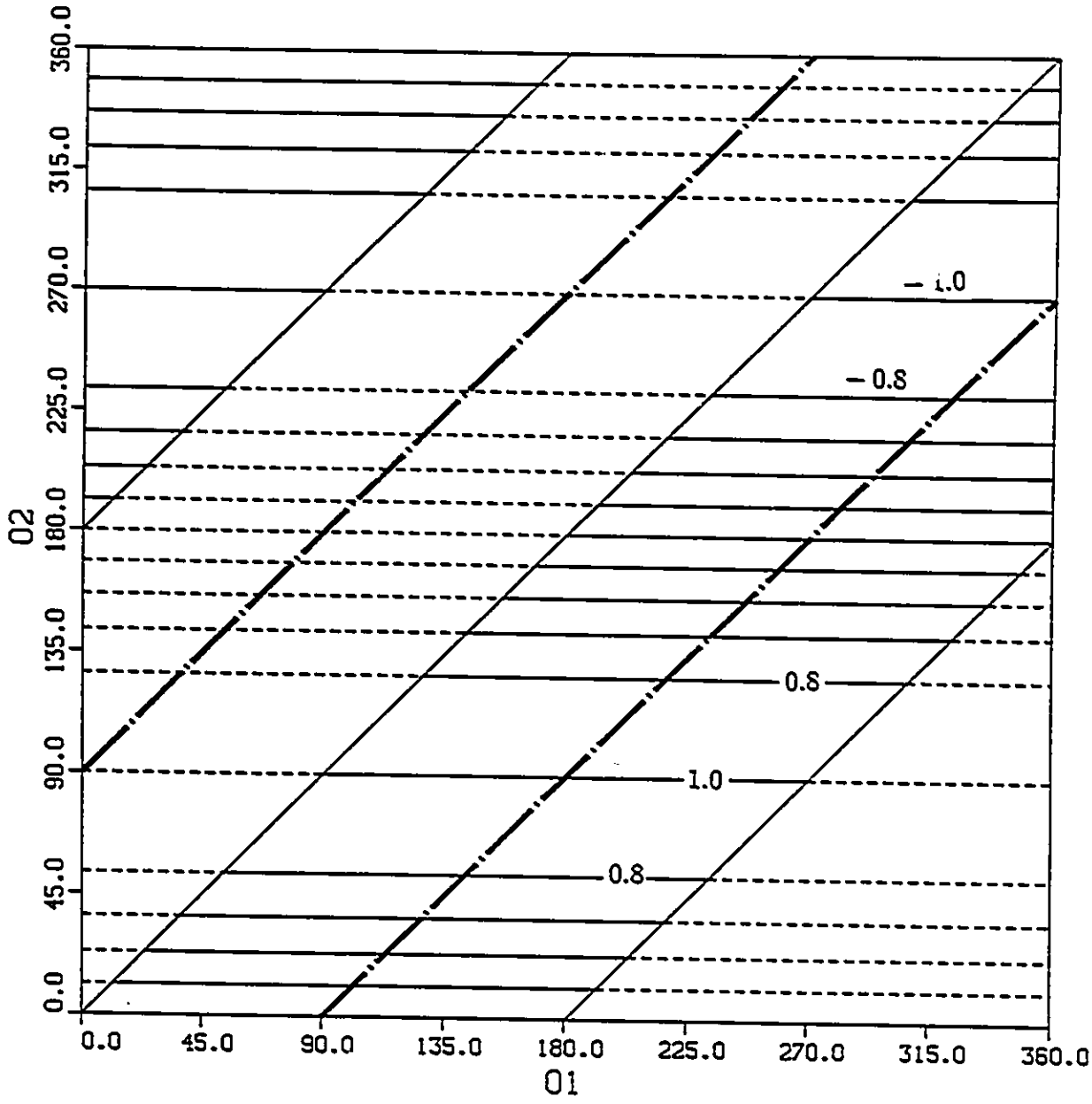

Figure 6.3: Generalized gravitational field in joint space for a manipulator with minimum global field index.

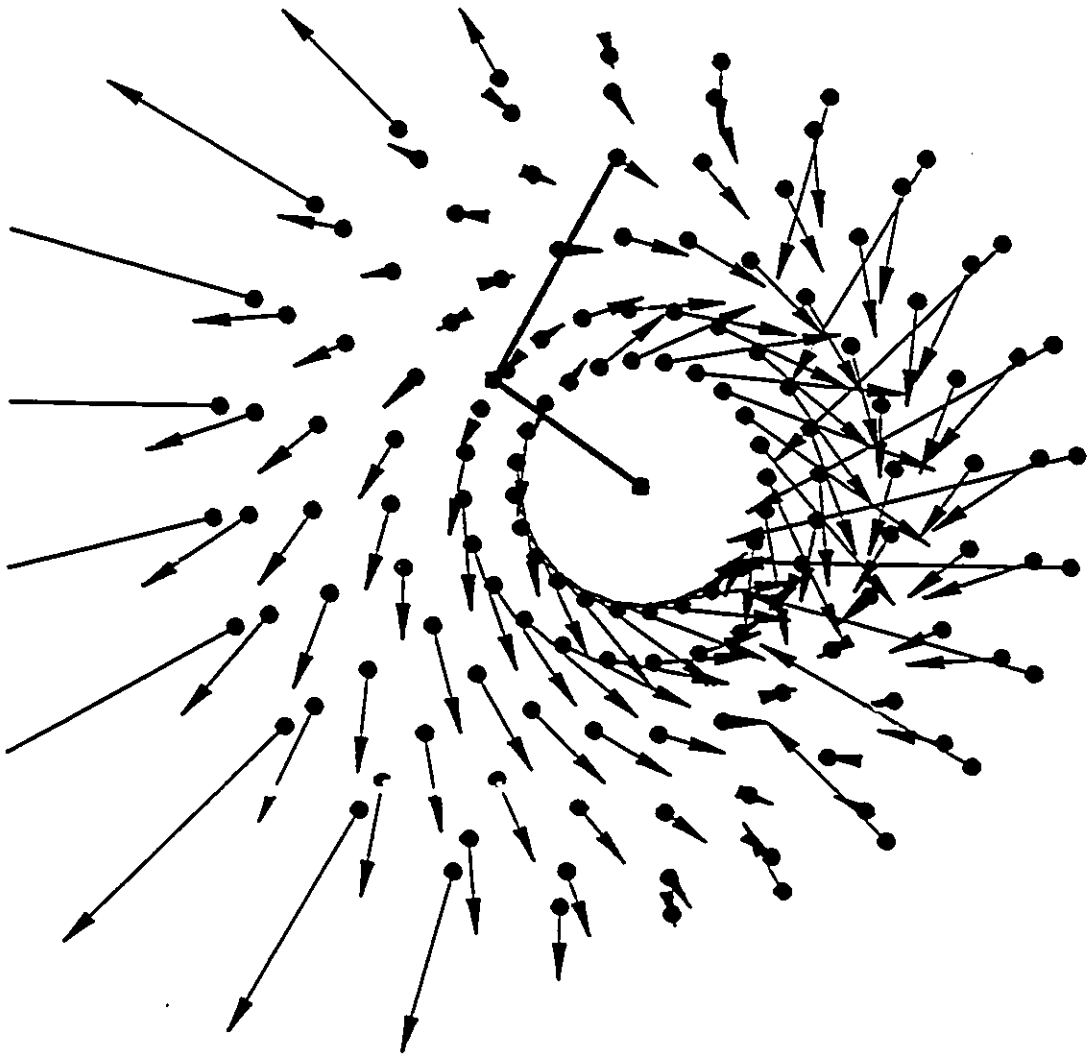

Figure 6.4: Generalized weight field for a manipulator with minimum global field index.

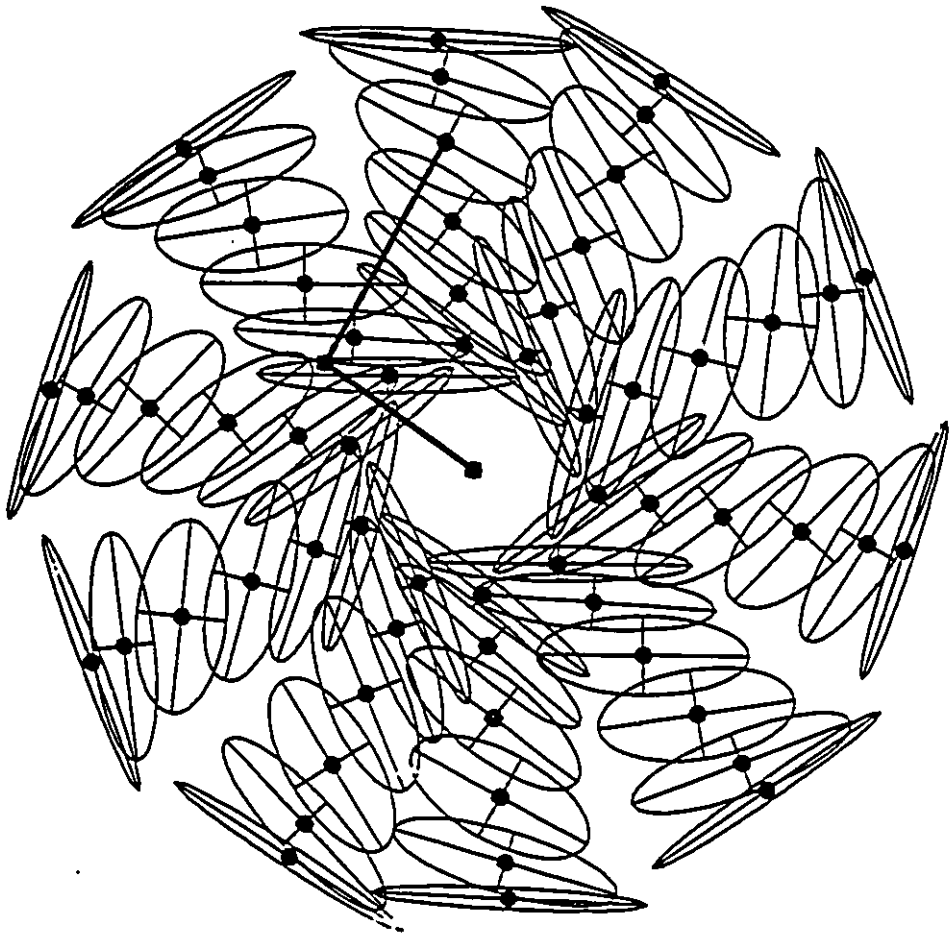

Figure 6.5: Generalized ellipsoid of inertia for a manipulator with minimum global field index.

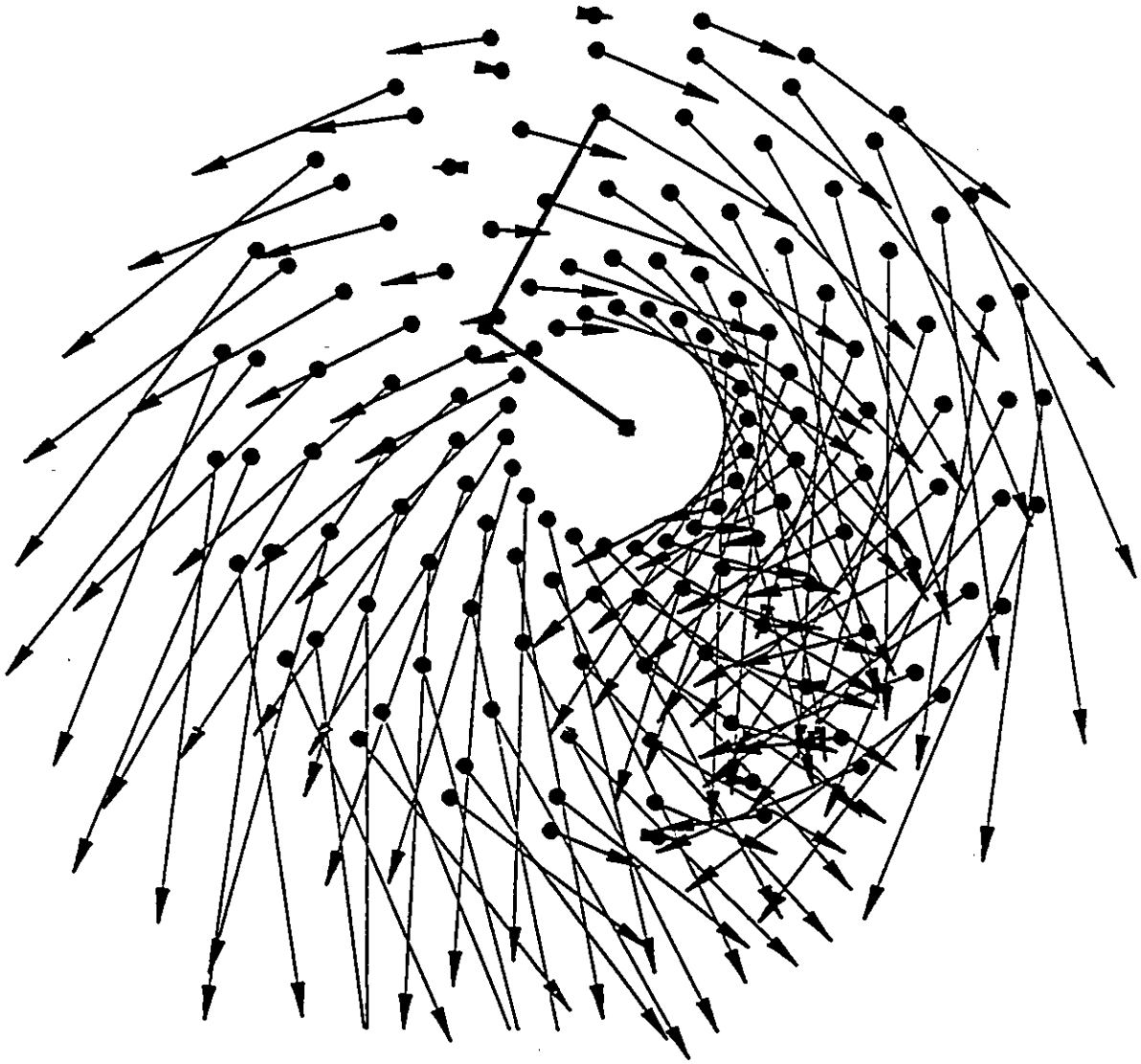

Figure 6.6: Generalized gravitational acceleration field for a manipulator with minimum global field index.

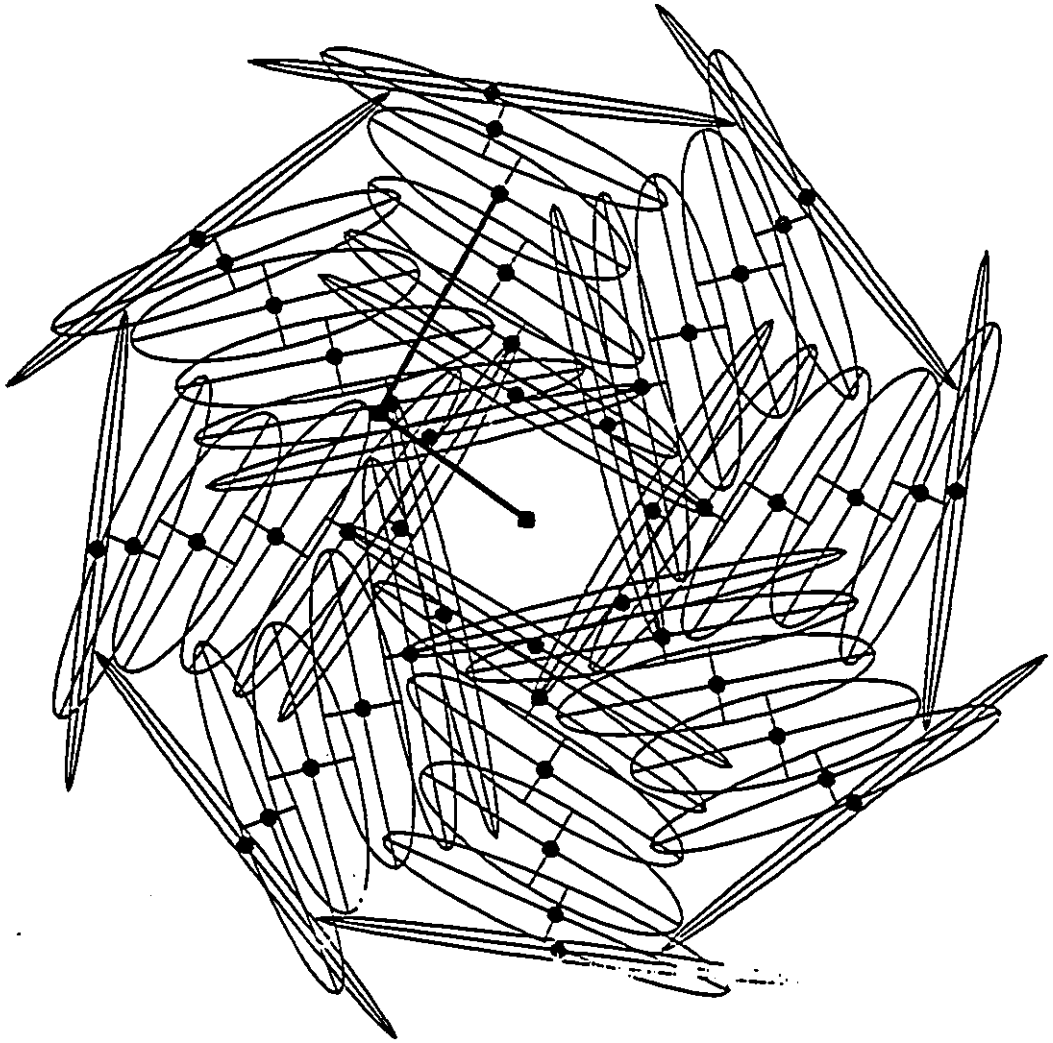

Figure 6.7: Acceleration ellipsoids for a manipulator with minimum global field index.

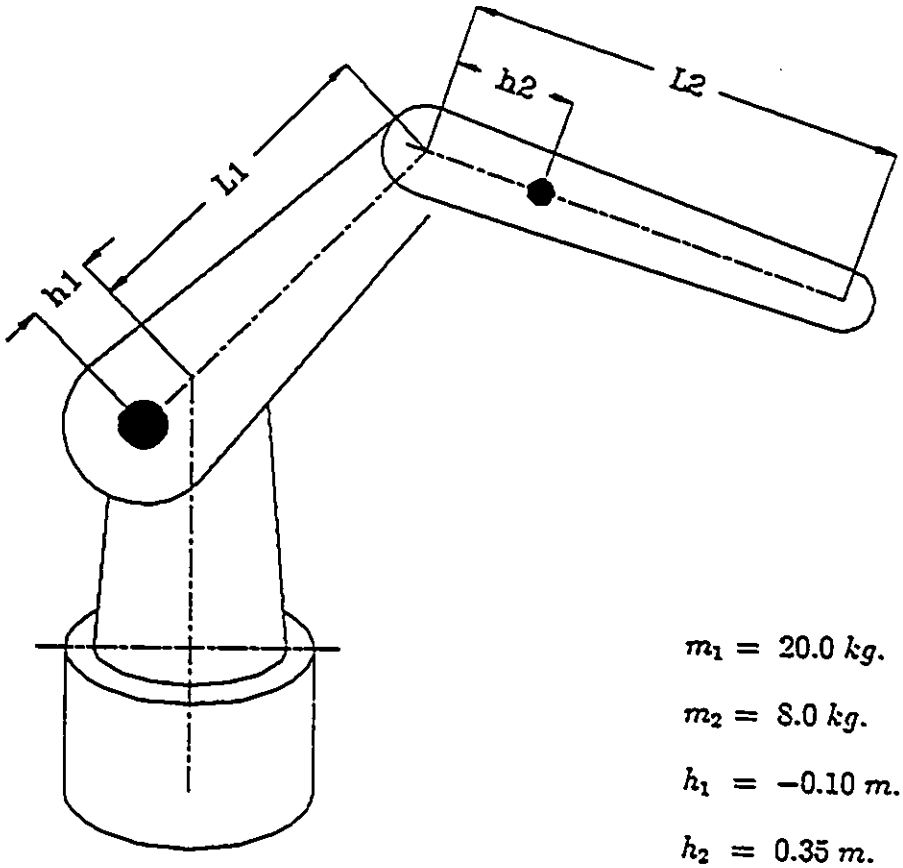

$m_1 = 20.0\ kg.$

$m_2 = 8.0\ kg.$

$h_1 = -0.10\ m.$

$h_2 = 0.35\ m.$

$L_1 = 0.50\ m.$

$L_2 = 0.70\ m.$

$\varphi_g = \frac{-1}{6}$

Figure 6.8: Schematic diagram of a manipulator with flat field.

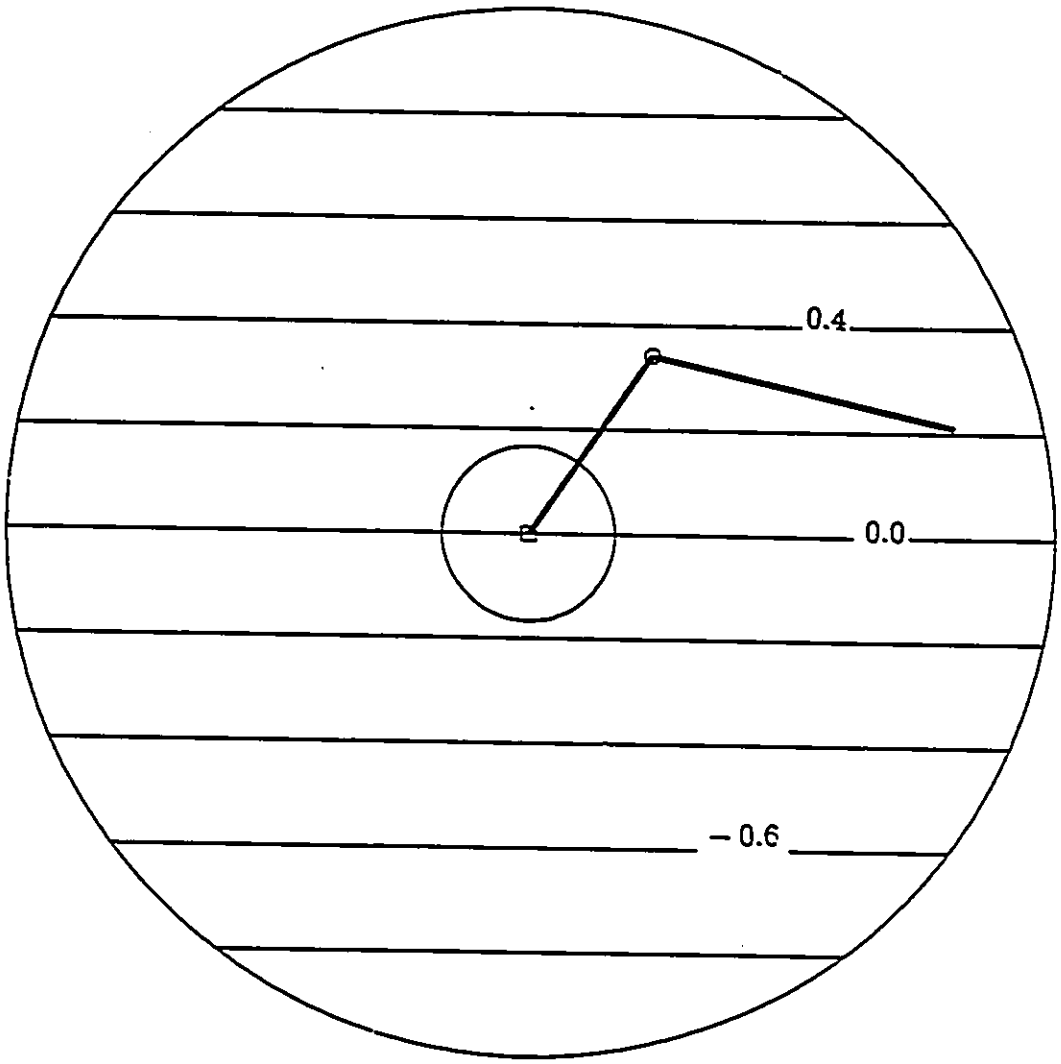

Figure 6.9: Generalized gravitational field in Cartesian space for a manipulator with flat field.

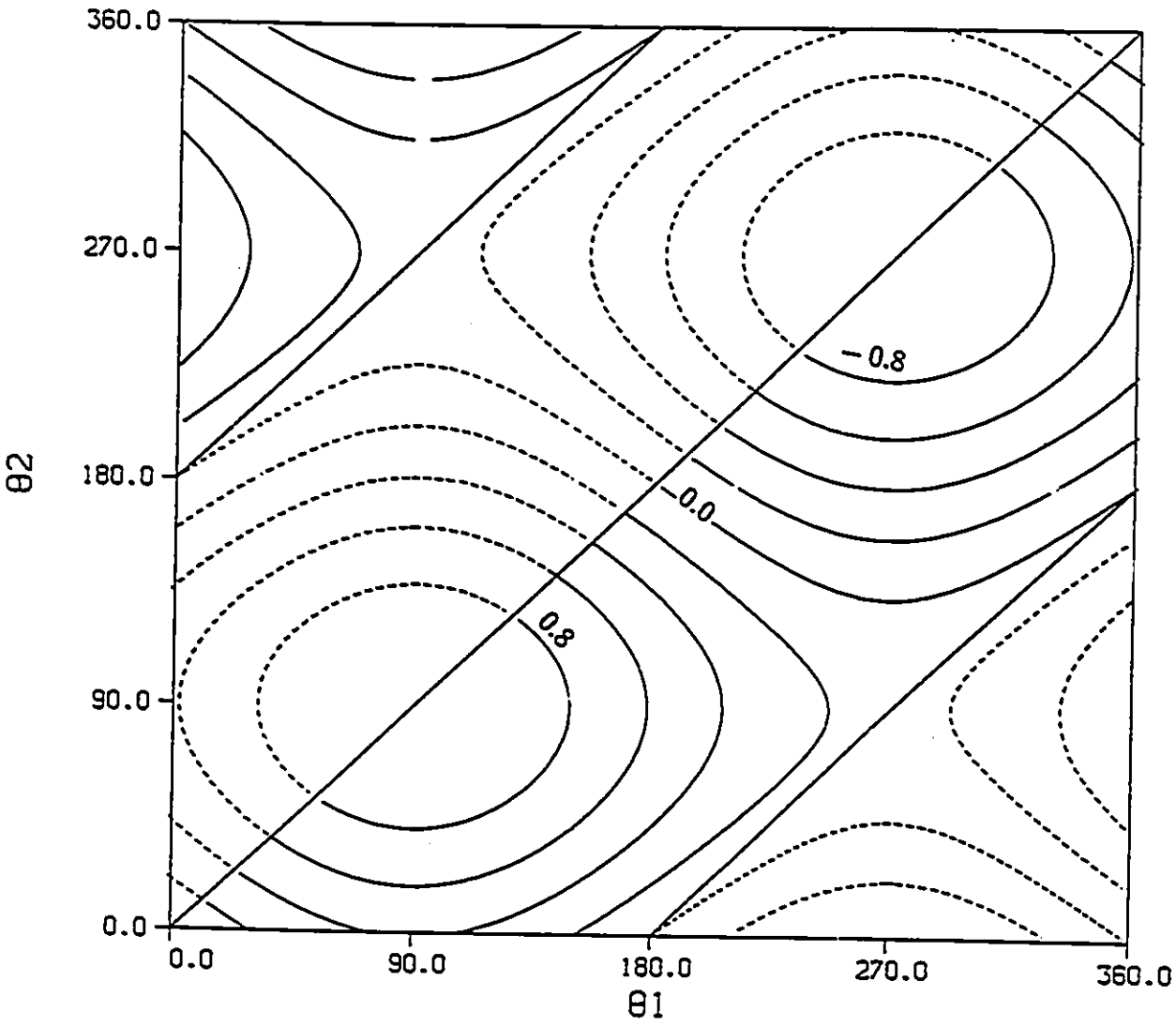

Figure 6.10: Generalized gravitational field in joint space for a manipulator with flat field.

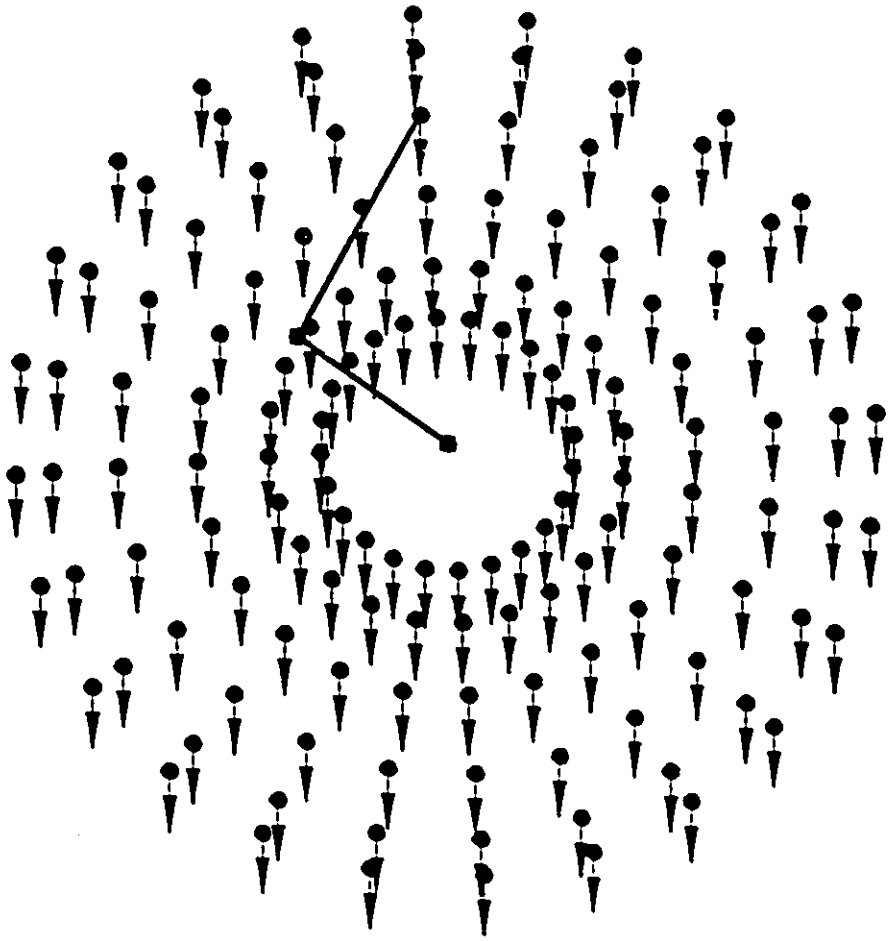

Figure 6.11: Generalized weight field for a manipulator with flat field.

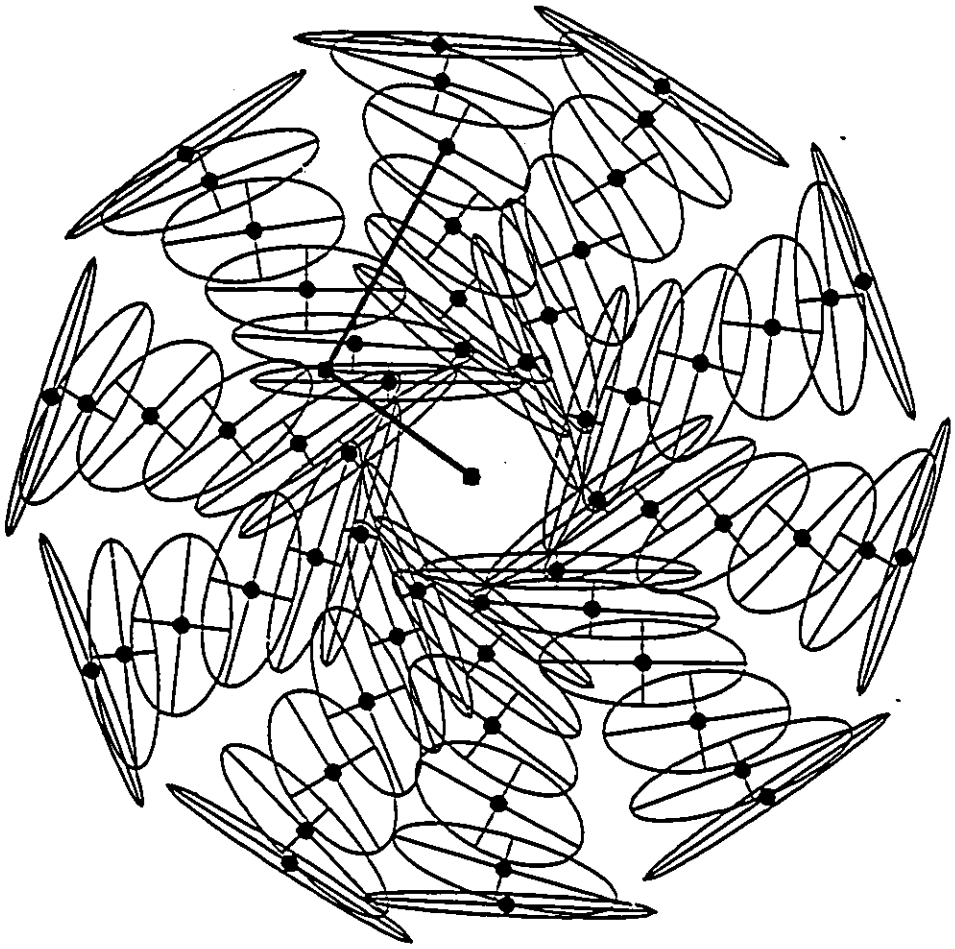

Figure 6.12: Generalized ellipsoid of inertia for a manipulator with flat field.

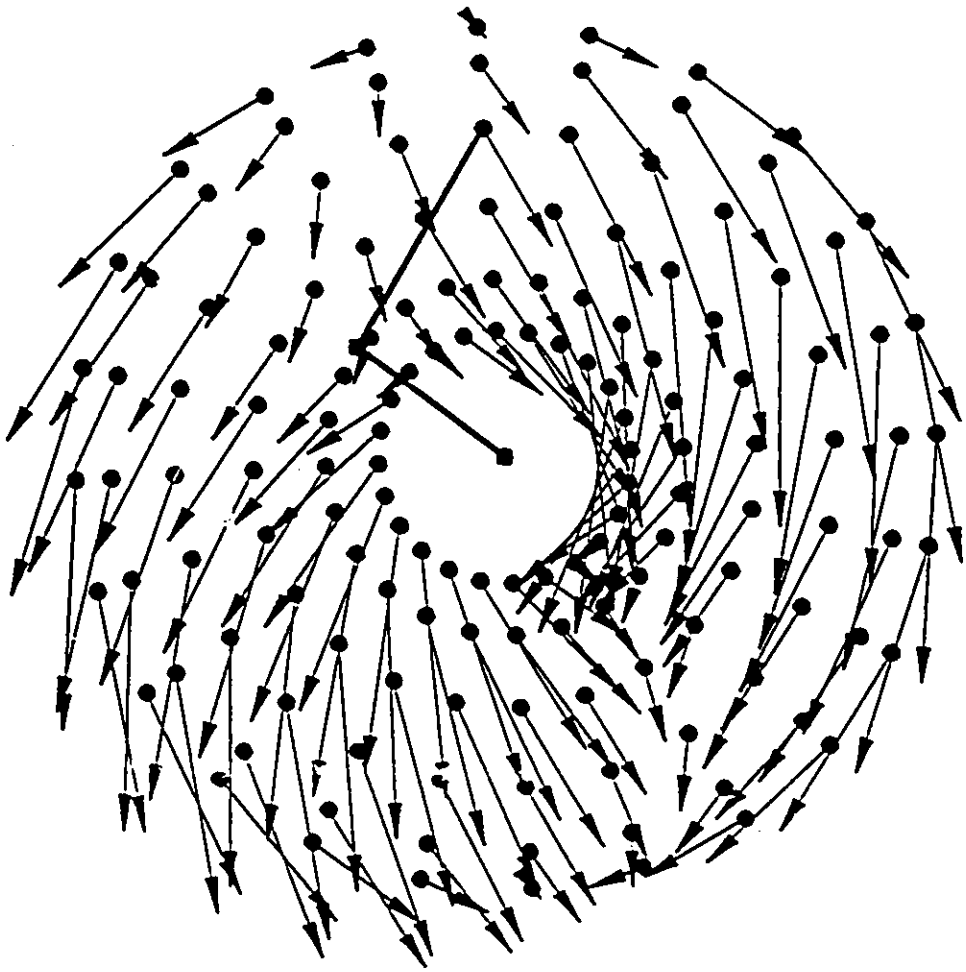

Figure 6.13: Generalized gravitational acceleration field for a manipulator with flat field.

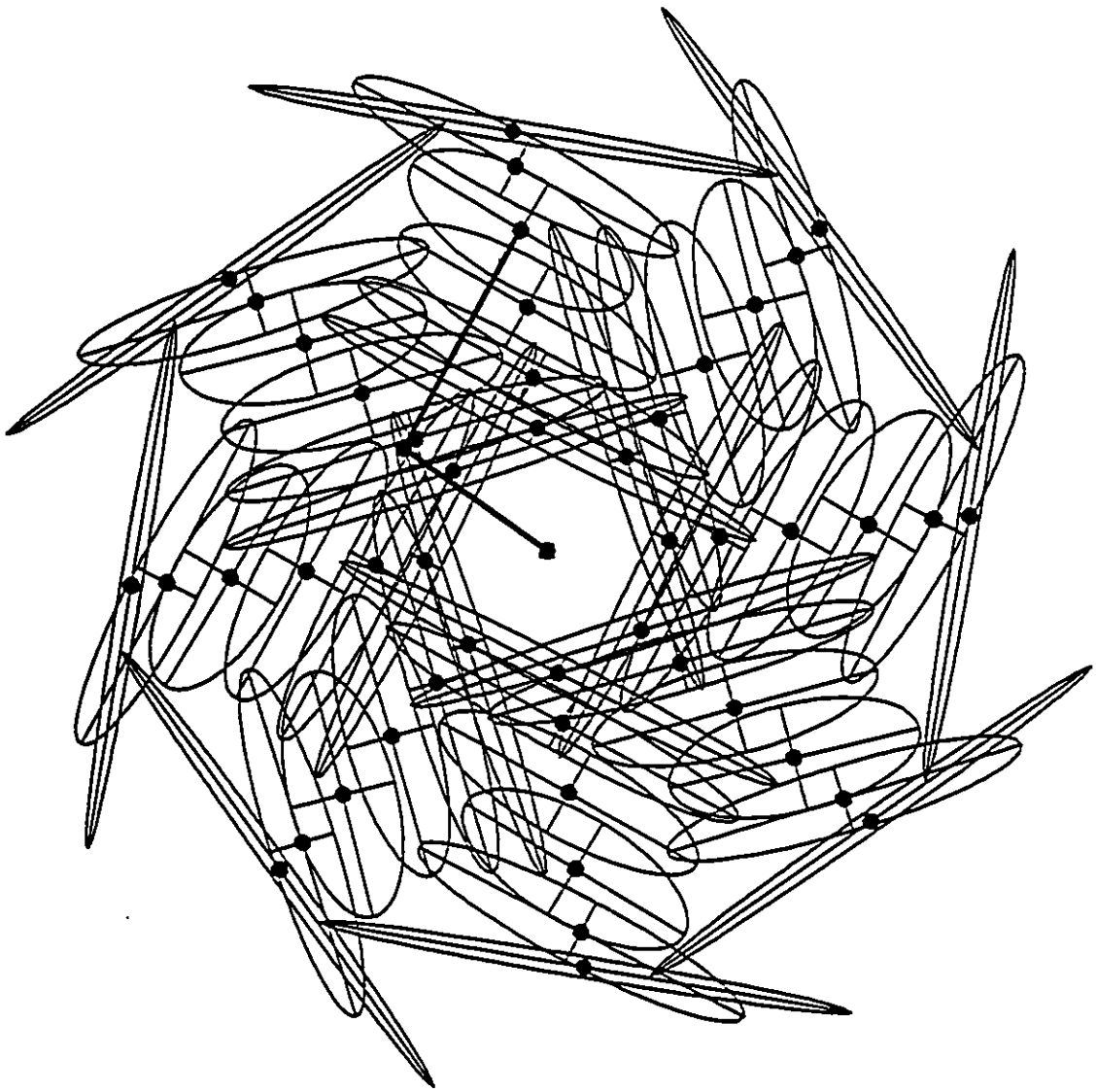

Figure 6.14: Acceleration ellipsoids for a manipulator with flat field.

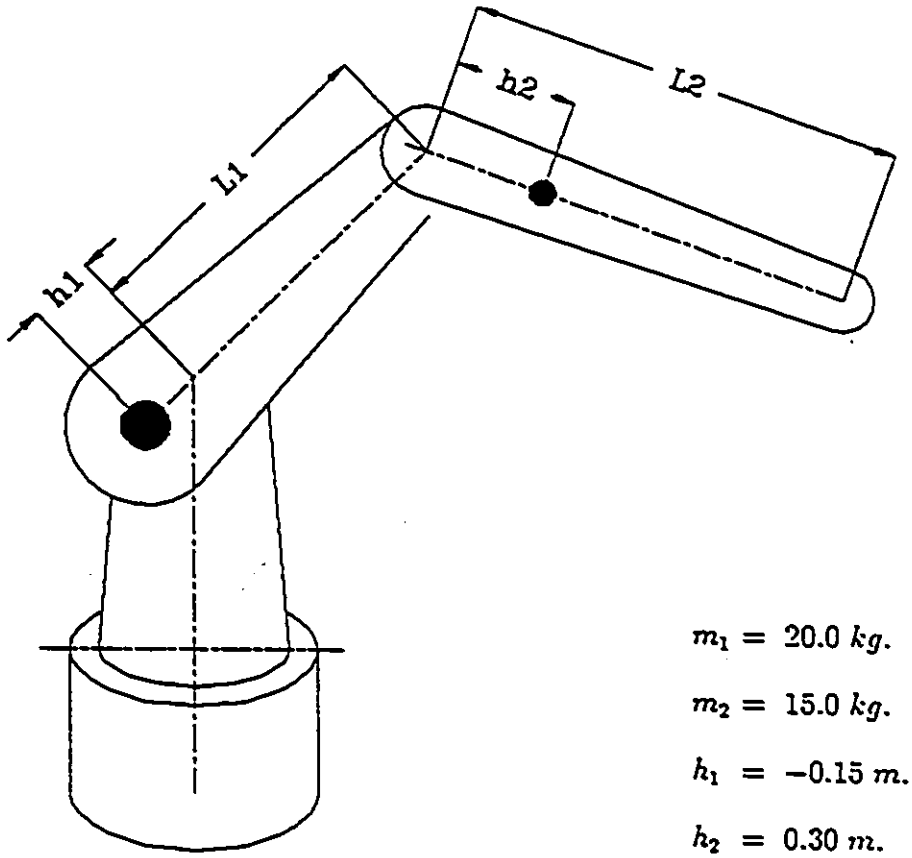

$m_1 = 20.0\ kg.$

$m_2 = 15.0\ kg.$

$h_1 = -0.15\ m.$

$h_2 = 0.30\ m.$

$L_1 = 0.50\ m.$

$L_2 = 0.70\ m.$

$\varphi_g = 0.0$

Figure 6.15: Schematic diagram of a manipulator with zero global field index.

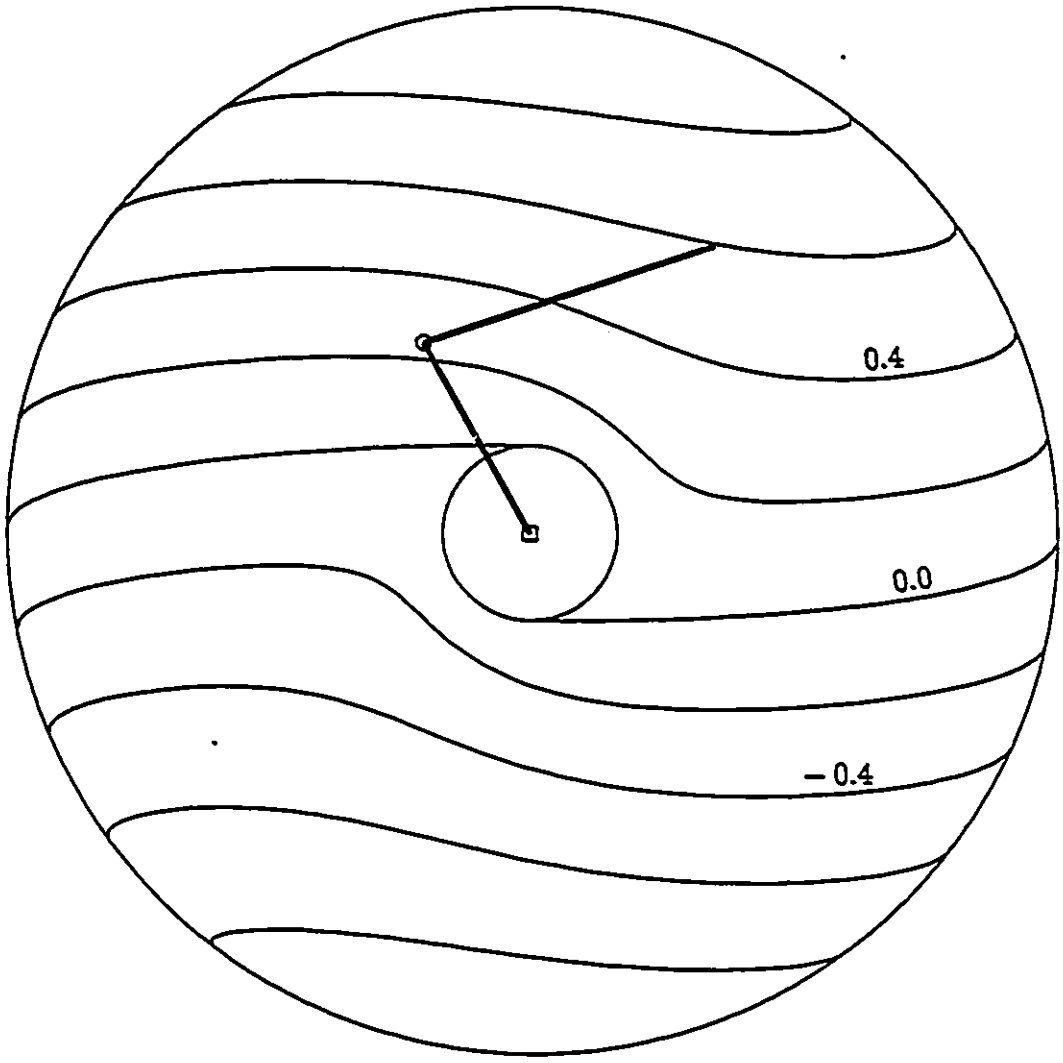

Figure 6.16: Generalized gravitational field in Cartesian space for a manipulator with zero global field index.

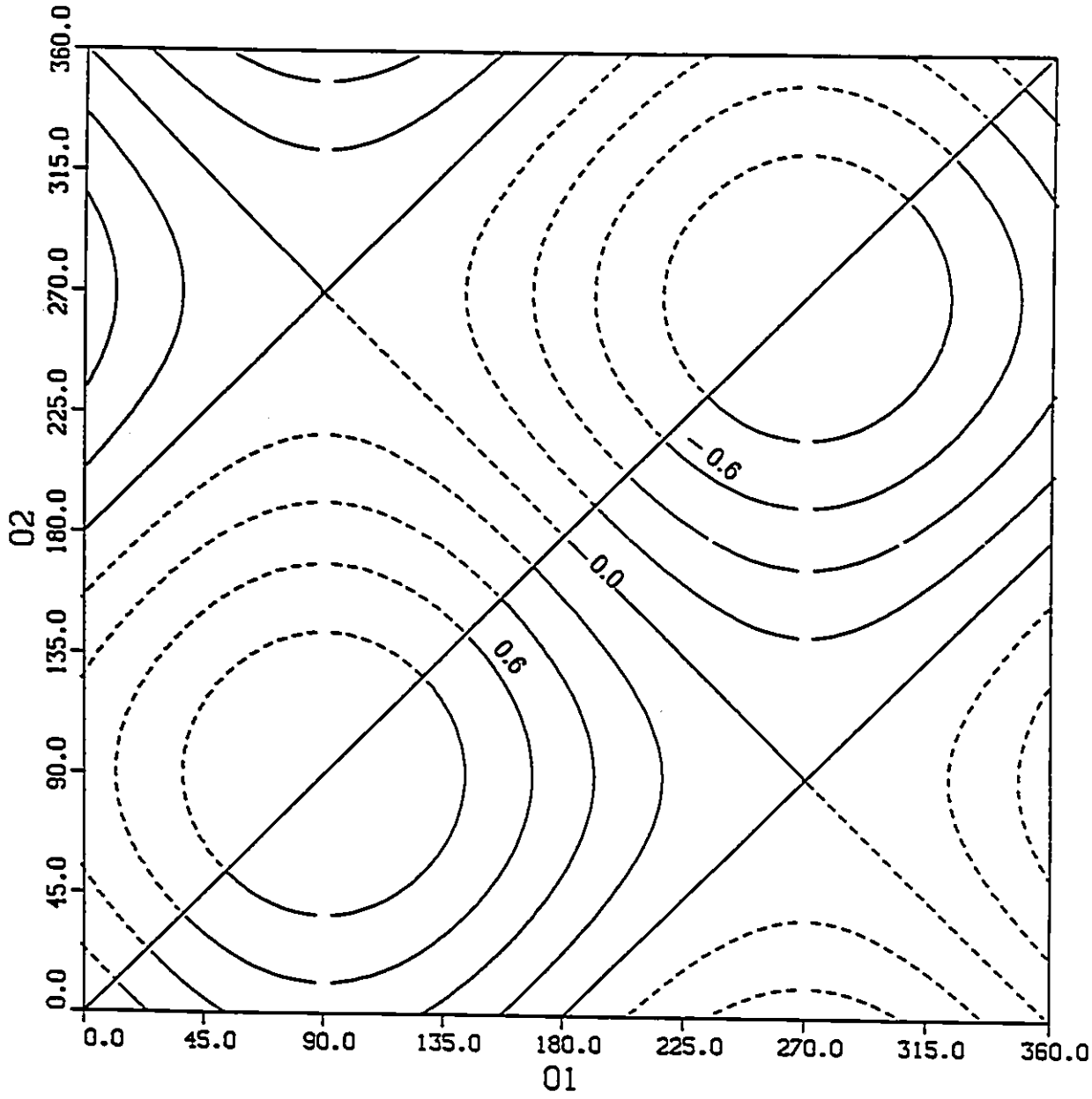

Figure 6.17: Generalized gravitational field in joint space for a manipulator with zero global field index.

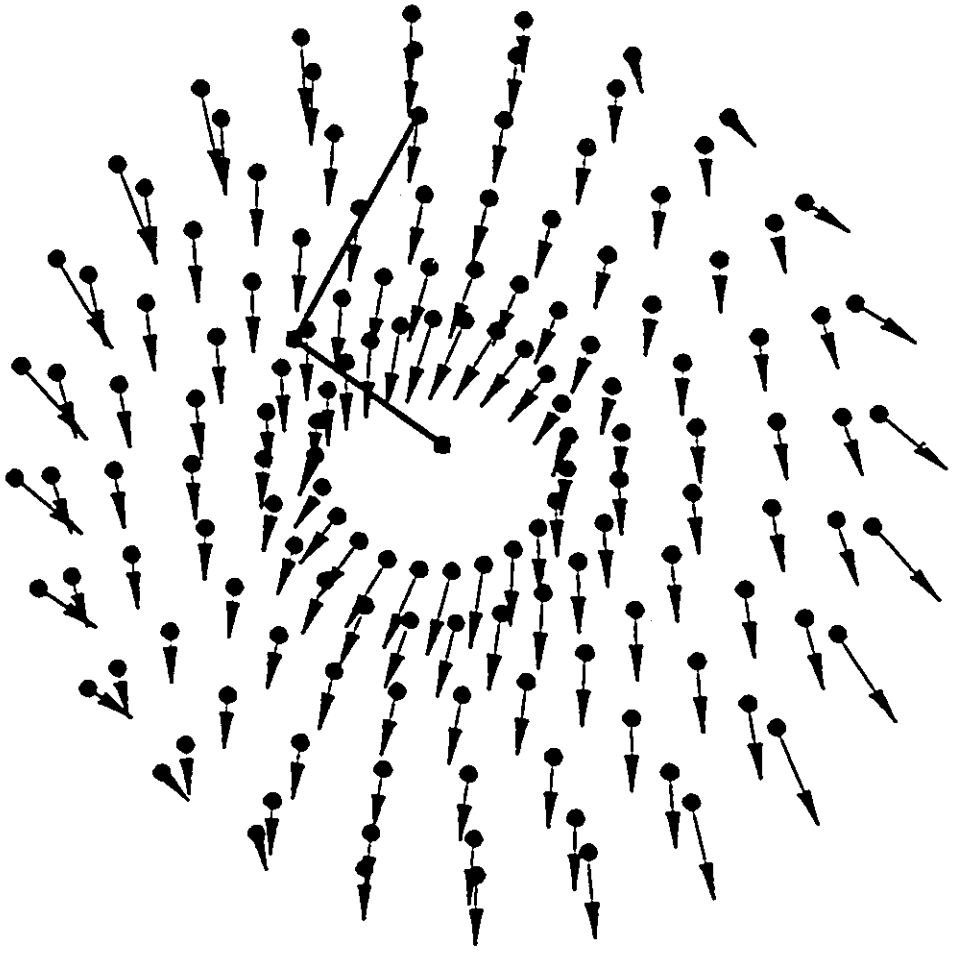

Figure 6.18: Generalized weight field for a manipulator with zero global field index.

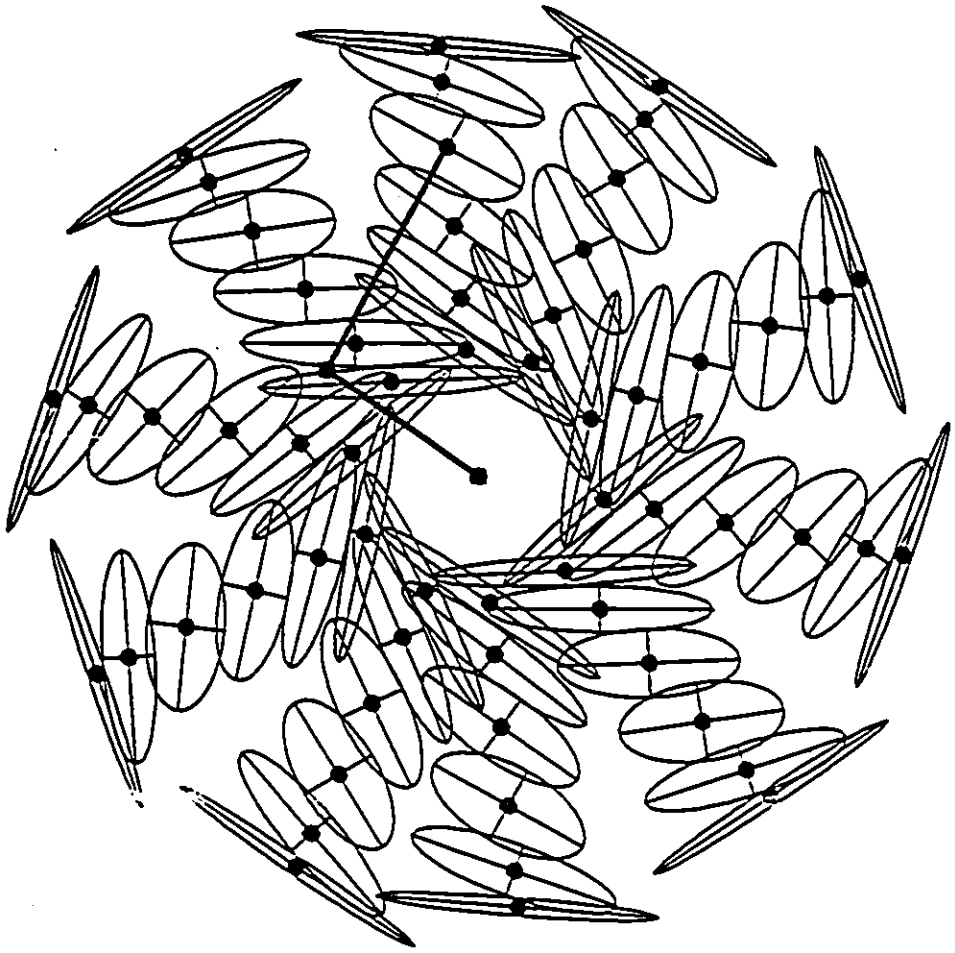

Figure 6.19: Generalized ellipsoid of inertia for a manipulator with zero global field index.

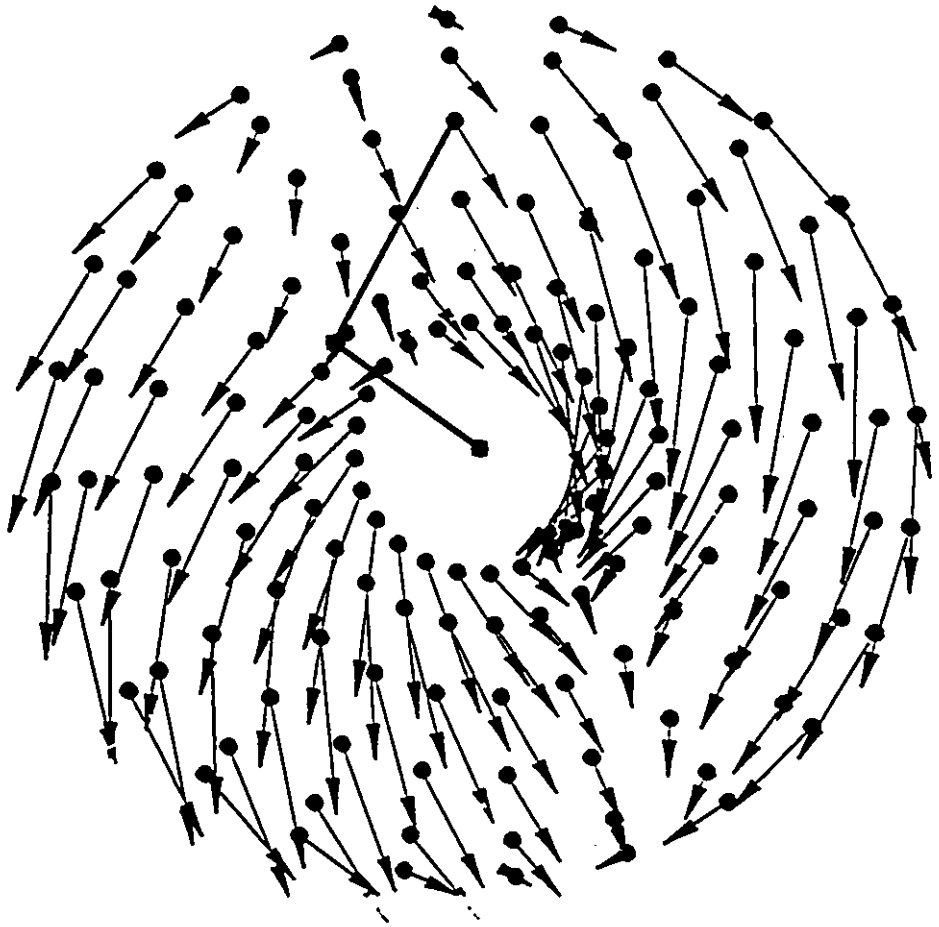

Figure 6.20: Generalized gravitational acceleration field for a manipulator with zero global field index.

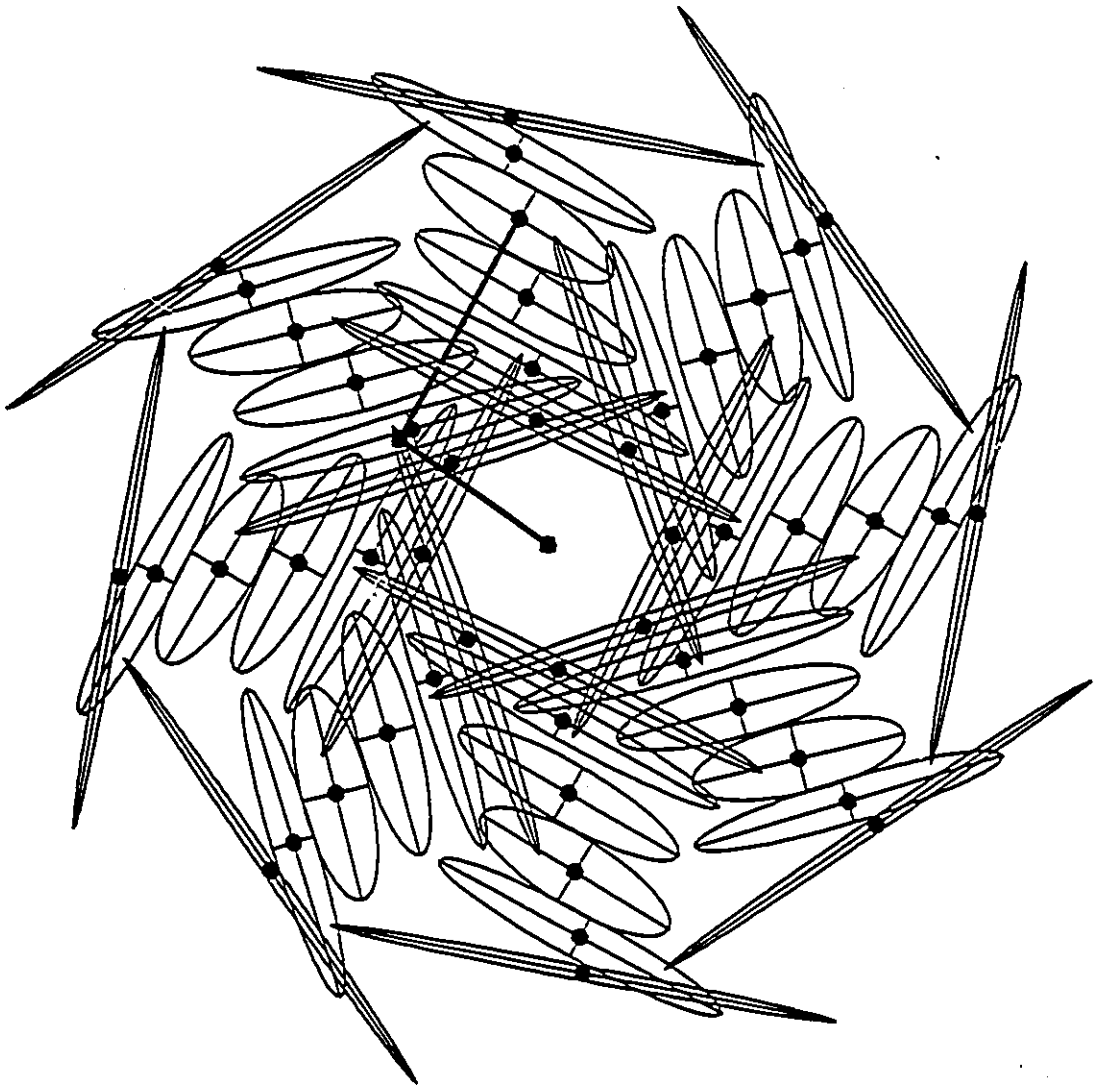

Figure 6.21: Acceleration ellipsoids for a manipulator with zero global field index.

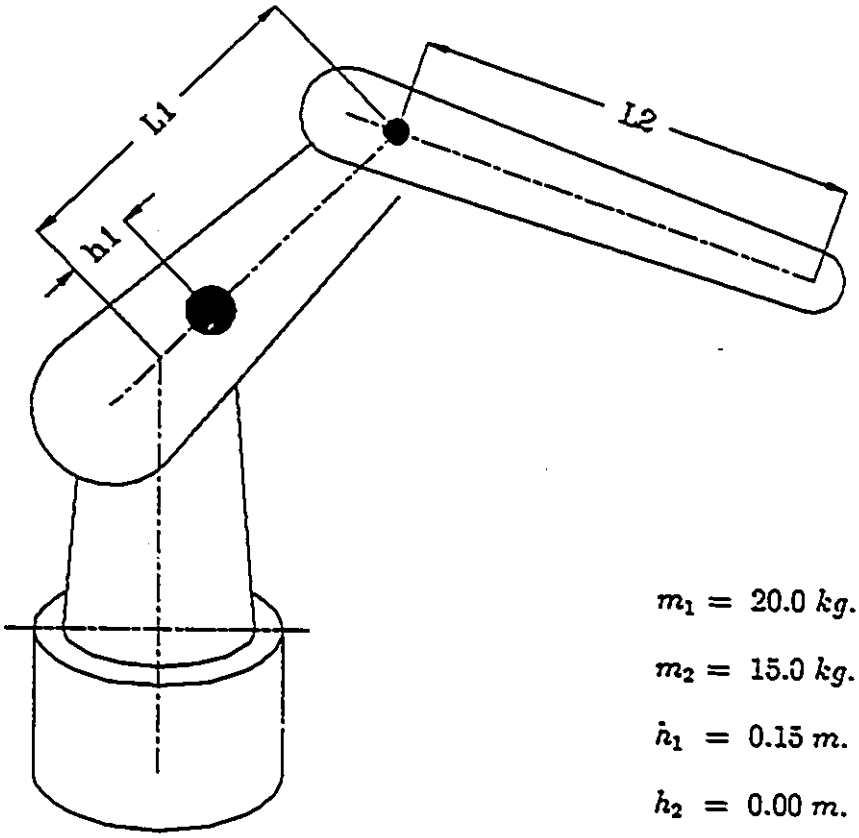

$m_1 = 20.0\ kg.$

$m_2 = 15.0\ kg.$

$h_1 = 0.15\ m.$

$h_2 = 0.00\ m.$

$L_1 = 0.50\ m.$

$L_2 = 0.70\ m.$

$\varphi_g = 1.0$

Figure 6.22: Schematic diagram of a manipulator with maximum global field index.

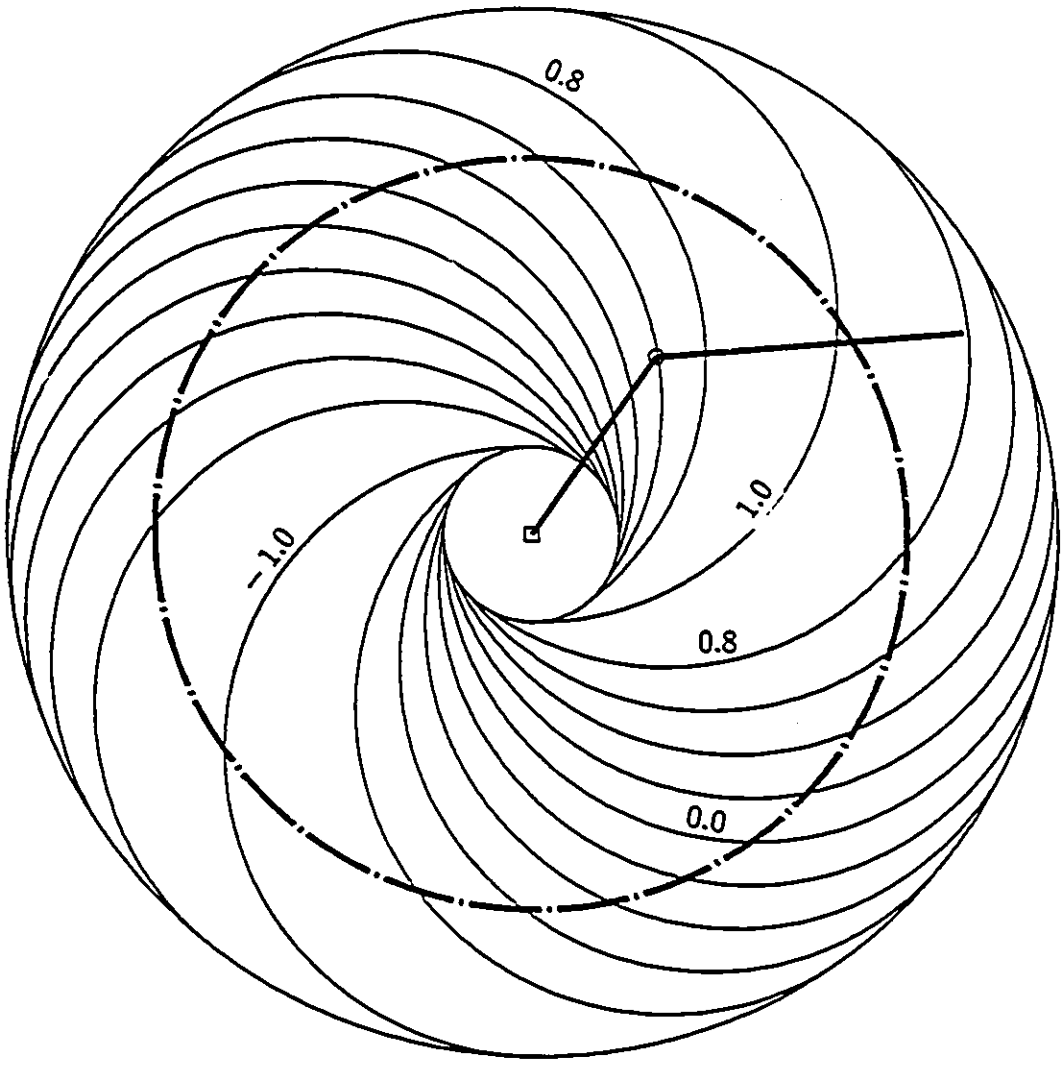

Figure 6.23: Generalized gravitational field in Cartesian space for a manipulator with maximum global field index.

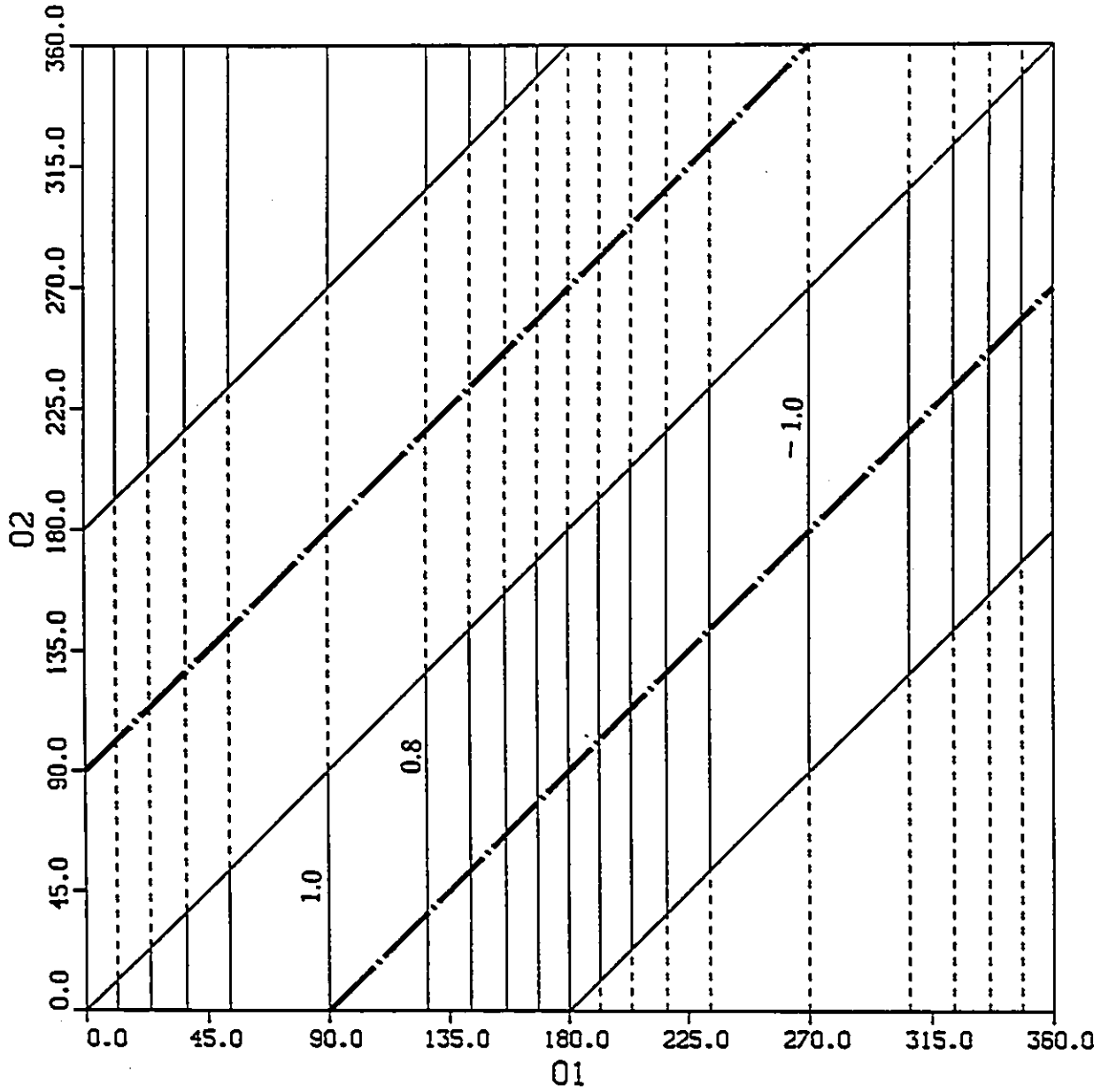

Figure 6.24: Generalized gravitational field in joint space for a manipulator with maximum global field index.

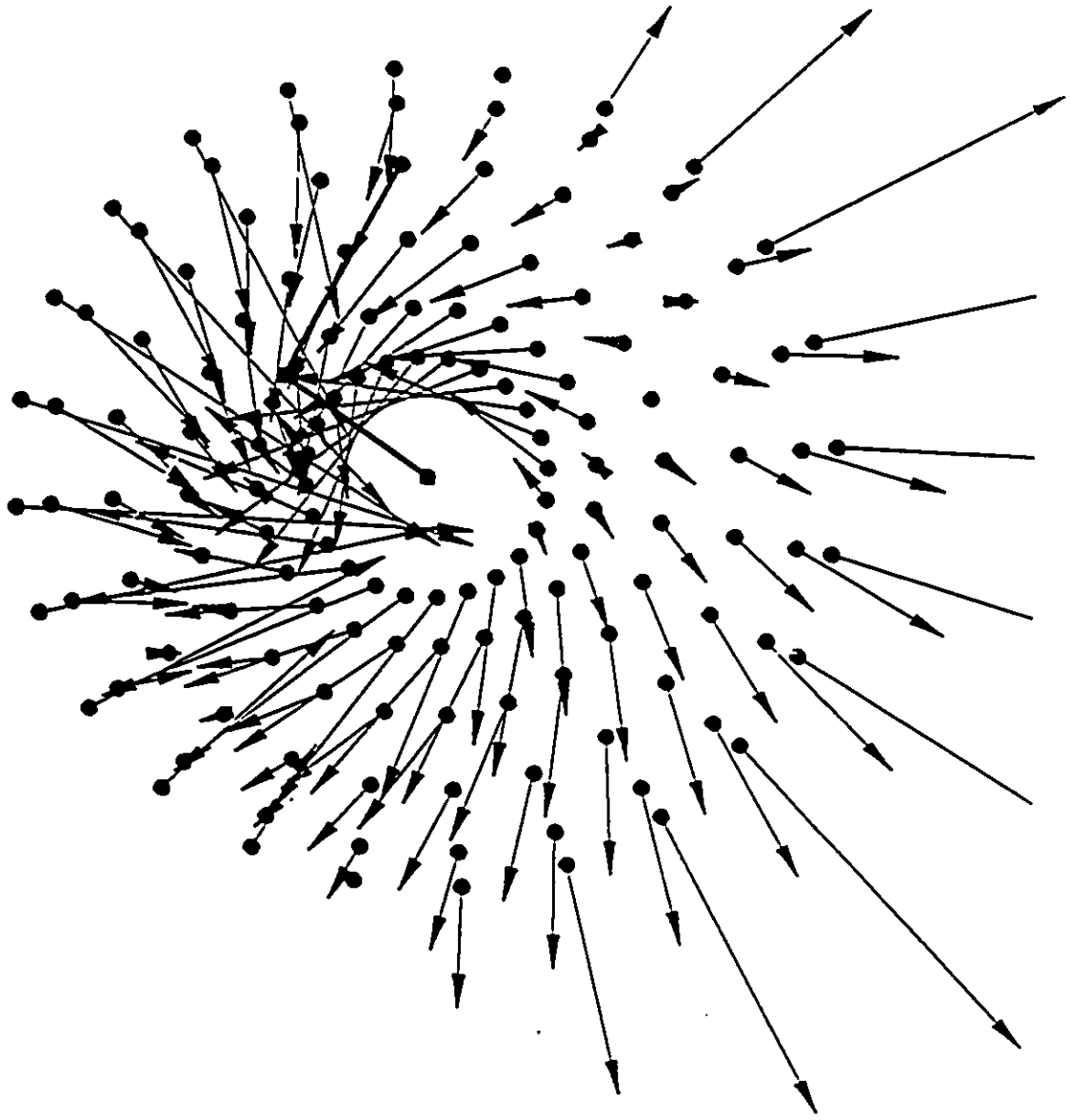

Figure 6.25: Generalized weight field for a manipulator with maximum global field index.

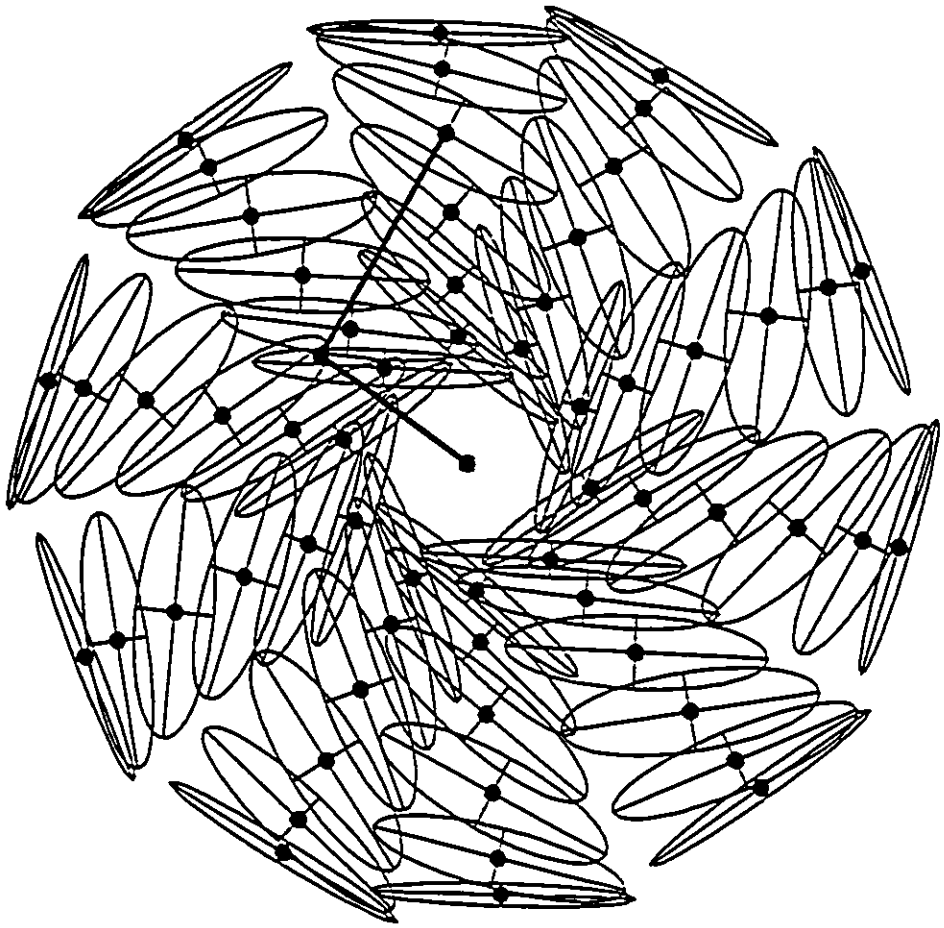

Figure 6.26: Generalized ellipsoid of inertia for a manipulator with maximum global field index.

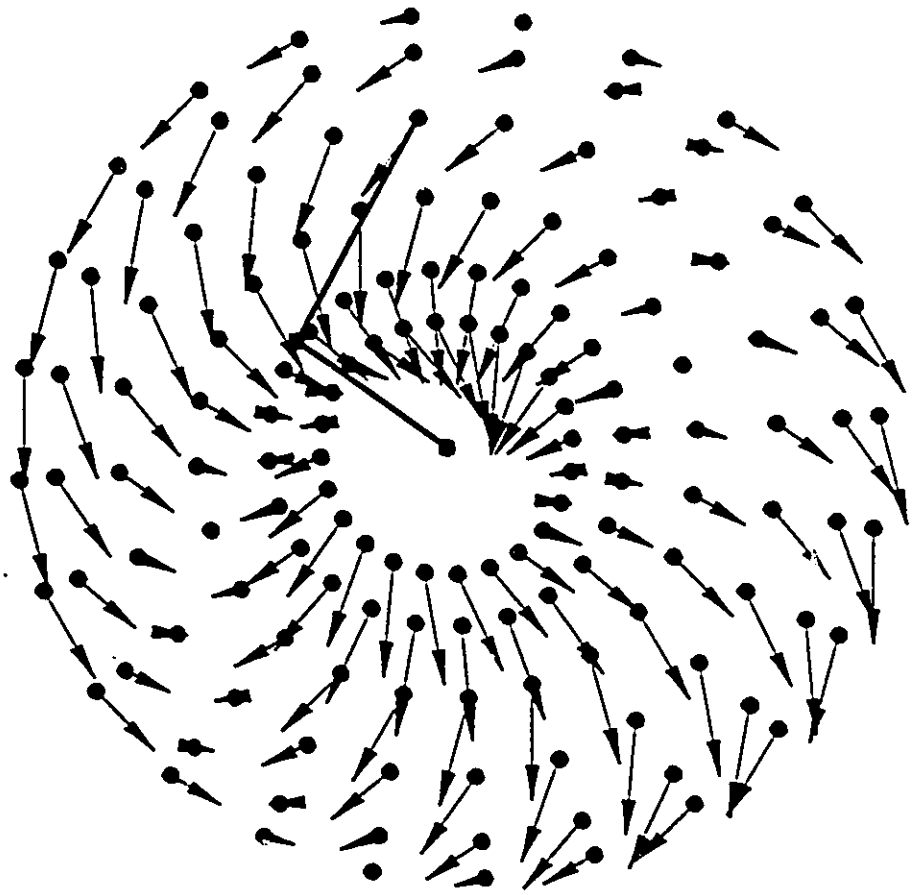

Figure 6.27: Generalized gravitational acceleration field for a manipulator with maximum global field index.

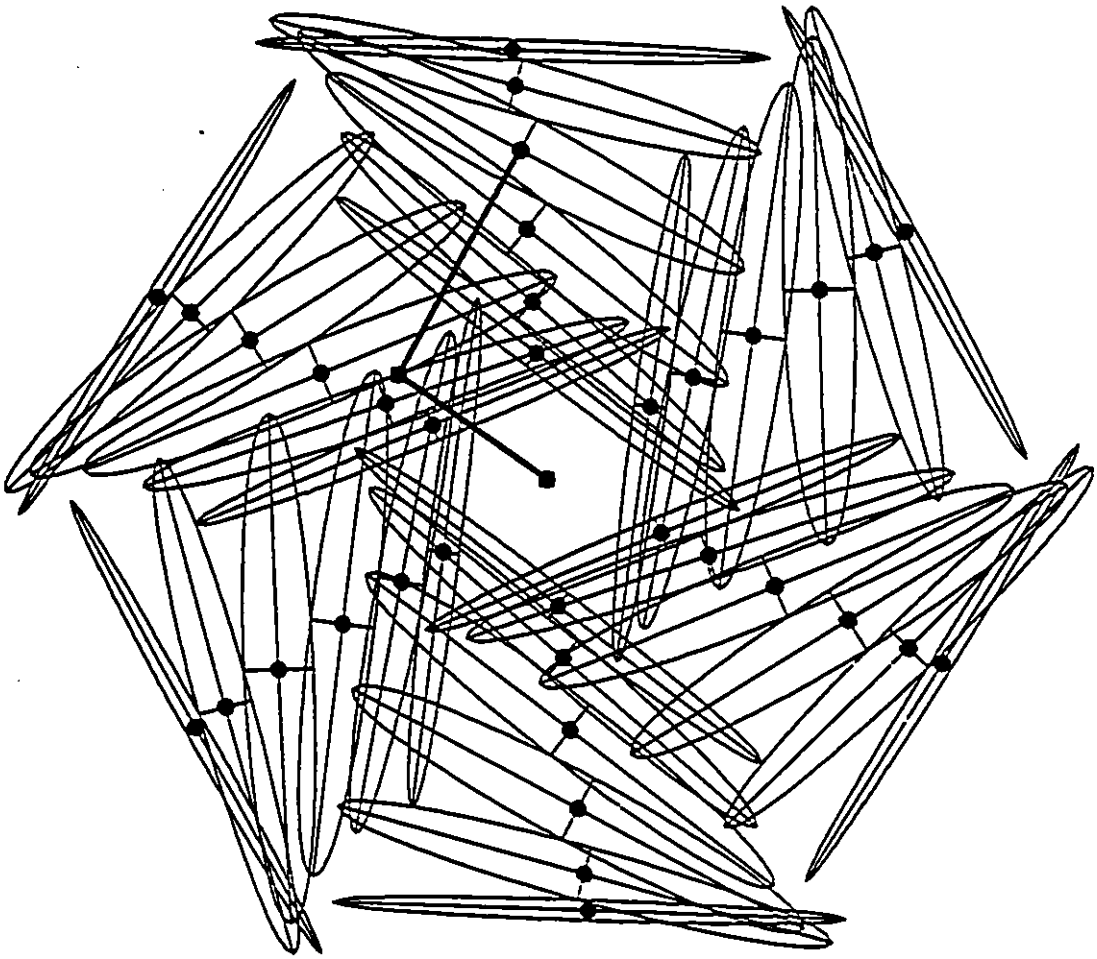

Figure 6.28: Acceleration ellipsoids for a manipulator with maximum global field index.

Chapter 7

Conclusion and Future Work

7.1 Conclusion

The purpose of this work is to propose a new approach in studying the effect of gravity on static and dynamic behavior of robot arms. In Chapter 1 a summary of pertinent literature was presented. In Chapter 2 the importance of the effect of gravity on the joint motors of robot arms was highlighted through the dynamic and quasistatic simulation of a 6 DOF PUMA manipulator. Effect of variation in the speed of the end effector was also monitored.

It was shown in Chapter 3 that replacing the secondary links of a manipulator by an equivalent mass lumped at the end point, greatly simplifies the static and dynamic analysis of manipulators without introducing any significant error. The concept of the Generalized Gravitational Field (GGF) was then introduced. The gravity induced force field acting on individual links was replaced by a single force field acting at the

tip of the manipulator's arm. This force field, the strength of which was designated as the generalized weight of the arm, was shown to be the gradient of the generalized gravitational field obtained from the total potential energy of the links. The field was found to be conservative but nonsolenoidal.

The equipotential lines for a typical two link arm were plotted and the strength distribution of the field was investigated. Due to the nonsolenoidal nature of the field, only qualitative results for the field strength could be inferred from the spacing between the equipotential lines.

Study of the static behavior of manipulators through the generalized gravitational field was the subject of Chapter 4. The force ellipsoid, introduced by other researchers as a tool for the evaluation of the capability of manipulators in applying static force to their environment was reviewed. It was shown that the size and the relative orientation of the force ellipsoids with respect to the manipulator remain constant along the circumference of the solid configuration circles. It was proven, in Chapter 5, that this fact is also true about the generalized ellipsoid of inertia and the acceleration ellipsoid.

The force ellipsoid, considered as the output of the system, was integrated with the generalized weight as the demand at various configurations of the arm. The static force capability of the arm was then related to the generalized weight through the magnitude index and the direction index. The contour maps of the two indices were then drawn across the manipulator's work volume.

The main goal of Chapter 4 was the inclusion of effect of gravity in the static force capability of the manipulators. It was shown that the true capability of the

arm is obtained only when the force ellipsoid is translated, with no rotation, to the tip of the vector of the generalized weight. The maximum and minimum values of the task force were then redefined accordingly.

Study of the dynamics of the manipulators based on the generalized gravitational field was the subject of Chapter 5. The generalized inertia tensor, introduced by other researchers, was redetermined through the application of the generalized weight. The generalized gravitational acceleration field was introduced as the acceleration induced at the tip of the arm due to the effect of gravity. The generalized ellipsoid of inertia which is constructed on the generalized tensor of inertia was reviewed and its relation with the generalized weight and the generalized gravitational acceleration explained.

The acceleration ellipsoid was also reviewed. It was shown that the true acceleration capability of the end effector can be demonstrated only when the acceleration ellipsoid is translated to the tip of the vector of the generalized gravitational acceleration. The true maximum and minimum acceleration that the end effector can attain was then illustrated.

Effect of change of physical properties of the arm on its static and dynamic behavior was investigated in Chapter 6. Manipulators were categorized based on the shape of their generalized gravitational fields. The global and local field indices were introduced in order to facilitate the process of categorization. Static and dynamic behavior of each type was then explained through their generalized properties. It was shown that under a special condition the generalized potential field would become similar to an ordinary gravitational field.

The contribution of this study in the field of robotics can be highlighted as follows.

- An alternative method to the use of Jacobian matrix in forward and inverse kinematic analysis of the manipulators is employed. This method can be used to verify the results of the other methods based on the application of Jacobian matrix.

- The Newton-Euler equations used in the dynamic analysis of manipulators are presented in a form that they comprise only matrices.

- A whole new meaning has been given to the effect of gravity on robotic manipulators. The generalized gravitational field can demonstrate the global effect of gravity in a clear geometrical way. The generalized gravitational acceleration field can show the magnitude and direction of the acceleration that the end effector can attain due to the effect of gravity at any point of the work volume.

- The generalized weight field was integrated with the force ellipsoid to demonstrate the correct capability of the manipulators in applying static force to their environment. In a similar way the generalized gravitational acceleration field was superimposed on the acceleration ellipsoid to demonstrate the true acceleration capability of the arm's tip.

- The generalized ellipsoid of inertia that characterizes the dynamic behavior of the manipulator at any point of the work volume is related to the generalized weight and the generalized gravitational acceleration. It was shown that the ratio of the generalized weight to the generalized gravitational acceleration along the pricipal axes of the generalized ellipsoid of inertia is equal to the magnitude of the eigenvalue of generalized inertia tensor in the same direction.

- It was shown here that the size and orientation with respect to manipulator of the force ellipsoids, the generalized ellipsoids of inertia and the acceleration ellipsoids are fixed along the solid configuration circles. This fact greatly simplifies the process of drawing information through these ellipsoids at various points of the work volume.

- The global and local field indices defined in Chapter 6 relate the field's conformation to all physical properties of the manipulator's links as well as those of the payload. In consequence, they can be used to establish a methodology for the mechanical design of manipulators based on the type of the interaction that they must have with their environments.

7.2 Future Work

The effect of gravity is an important factor in the design of manipulators. No attempt has been made in present study to consider the design process. However, based on the method that has been introduced here, a comprehensive methodology for the mechanical design of manipulators can be founded. Once the task of a manipulator has been determined and the preliminary decisions about its physical parameters are made, the effect of gravity on the system as a whole can be studied. The necessary adjustments can then be done to optimize the manipulator.

The interest in research on cooperation of robots has been growing in recent years. The versatility associated with the cooperative task execution is an important issue in complicated jobs such as space operations currently performed by astronauts.

Laroussi et al (1988) have investigated the modeling and control of two planar manipulators cooperating in displacement of objects. Lee (1989) extended the notion of manipulability ellipsoid mentioned earlier in this work to study the behavior of two manipulators working together. Effect of gravity on the system of robots in cooperation can be significant. Generalized gravitational field and the generalized weight field can be utilized to study the effect of gravity on the system of robots. The regions of the working volume in which the effect of gravity is a minimum can be detected by integrating the generalized potential field of individual robots and superimposing the strength of the individual fields.

In studying the forward and inverse kinematics of the manipulators it is common practice to make use of the manipulators Jacobian matrix and its inverse. The direct differentiation method which was utilized in Chapter 3 of this study can be elaborated into a more efficient alternative method.

The method that was used to study the effect of gravity on the torques of the joint motors in Chapter 3 can be repeated for the effect of Coriolis and other nonlinear terms. The path that was used for the end effector in present study was selected to represent the average working practice of usual industrial manipulators. To get a better idea about the effect of various force terms affecting the joint torques several other paths, including random generated paths should be examined.

The generalized gravitational field was proven to be conservative both in Cartesian and joint spaces. Equation 3.11 shows that the divergence of the field is identically zero if either $a_1 - \frac{L_2}{L_1}a_2$ or x_1 are zero. The first condition refers to an absolutely flat field which was discussed in Section 6.4. The second condition indi-

cates that the field is solenoidal along the line $x_1 = 0$ in the work volume. The implication to this conclusion is not clear and it is worth study. It might have some peculiar effect on the static behavior of the arm. The gradient of generalized gravitational field in joint space is the vector of the torques working at the joints. Therefore it is necessary to gain a deeper understanding of that field.

A classic problem in calculus of variations is the so called Brachistochrone problem attributed to Johann Bernoulli. It is the curve of fastest descent for a massive particle moving in a gravitational field with constant strength. Perhaps a similar problem can be formulated for the case of generalized gravitational field introduced in this study.

The generalized gravitational field can also be studied for the case of manipulators with redundancy and manipulators with serial drive mechanism.

The ordinary gravitational acceleration, normally denoted by g, is considered as the gradient of a scalar potential field. In a similar way it may be possible to find out wether the generalized gravitational acceleration $\mathbf{G}$ given by Equation 5.15 can be the gradient of any scalar field. The differential equation of the vector field can easily be obtained from the components of $\mathbf{G}$. If the resulting equation is exact then the scalar field does exist and can be found. The scalar field might exist under some particular condition that can be reflected into a relation between the physical parameters of the arm. Once the scalar field is found the acceleration capability of the end effector due to the effect of gravity at any point of the work volume can readily be determined. This investigation is justified by the fact that it is much easier to deal with scalar fields than vector fields. A comparison between Figures 3.5 and

3.7 proves this argument.

As it was shown earlier in the text, there is a close relation between the generalized weight and the generalized gravitational acceleration fields in one hand and the generalized ellipsoid of inertia on the other. It was pointed out that the base matrix of the generalized ellipsoid of inertia is the same as the transformation matrix between the two fields. More investigation on this relation can lead to a deeper understanding of the dynamic behavior of manipulators.

Bibliography

J. S. Albus. Robotics. In M. Brady et al., editors, *NATO ASI Series. Vol. F11, Robotics and Artificial Intelligence*, Springer-Verlag, 1984.

G. B. Andeen, editor. *Robot Design Handbook.* McGraw-Hill, 1988.

H. Asada. A geometrical representation of manipulator dynamics and its application to arm design. *ASME J. of Dynamic Systems, Measurement and Control*, 105, 1983.

H. Asada and J. A. Cro-Granito. Kinematic and static characterization of wrist joints and their optimal design. In *Proc. IEEE Int. Conf. Robotics and Automation, St. Louis*, 1985.

H. Asada and H. Ro. A linkage design for direct drive robot arms. *ASME J. of Mech., Trans. and Automation in Design*, 107, 1985.

H. Asada and J. Slotine. *Robot Analysis and Control.* John Wiley, 1986.

H. Asada and H. West. Design and analysis of braced manipulators for improved stiffness. In O. D. Faugeras and G. Giralt, editors, *Proc. Robotics Research: The 3rd Int. Symp.*, MIT Press, 1986.

H. Asada and K. Youcef-Toumi. Analysis and design of a direct drive arm with five bar link parallel drive mechanism. *ASME J. of Dynamic Systems, Measurement and Control*, 106, 1984.

H. Asada and K. Youcef-Toumi. Development of a direct drive arm using high torque brushless motors. In M. Brady and R. P. Paul, editors, *Proc. Robotics Research: The 1st Int. Symp.*, MIT Press, 1984.

H. Asada and K. Youcef-Toumi. *Direct Drive Robots: Theory and Practice.* MIT Press, Cambridge, 1987.

C. G. Atkeson et al. Estimation of inertial parameters of manipulator loads and links. *The Int. J. of Robotics Research*, 5(3), 1986.

S. K. Biswas and R. D. Klafter. Dynamic modeling and optimal control of flexible robot manipulators. In *1989 IEEE Int. Conf. on Robotics and Automation*, 1989.

W. J. Book. New concepts in lightweight arms. In H. Hanafusa and H. Inoue, editors, *Proc. Robotics Research: The 2nd Int. Symp.*, MIT Press, 1985.

M. Brady et al., editors. *Robot Motion: Planning and Control.* MIT Press, Cambridge, 1984.

N. G. Chalhoub and A. G. Ulsoy. Control of a flexible robot arm: experimental and theoretical result. *ASME J. of Dynamic Systems, Measurement and Control*, 109(3), 1987.

P. Chedmail and J. C. Bardiaux. Experimental validation of a plane flexible

robot modelling. In *Proc. IFAC /IFIP/IMACS 1st Symp. on Theory of Robots, Austria*, 1986.

S. L. Chiu. Task compatibility of manipulator postures. *The Int. J. of Robotics Research*, 7(5), 1988.

W. K. Chung and H. S. Cho. Sensitivity analysis of balanced robotic manipulators. *Robotica*, 6, 1988.

W. K. Chung et al. On the dynamic characteristics of balanced robotic manipulators. In *Proc. Japan-USA Symp. on Flexible Automation, Japan*, 1986.

W. K. Chung et al. Performance of robotic manipulators with an automatic balancing mechanism. In *Proc. ASME Winter Annual Meeting, New Orleans*, 1984.

A. Cugy and K. Page. *Industrial Robot Specifications.* Hermes Pub. and Kogan Page Ltd, 1984.

R. W. Daniel. Two key problems in robotics research. In H. Hanafusa and H. Inoue, editors, *Proc. Robotics Research: The 2nd Int. Symp.*, MIT Press, 1985.

T. M. Depkovich and R. M. Stoughton. A general approach for manipulator system specification, design, and validation. In *1989 IEEE Int. Conf. on Robotics and Automation*, 1989.

K. Desoyer et al. Flexible robots - a survey. In *Proc. IFAC /IFIP/IMACS 1st Symp. on Theory of Robots, Austria*, 1986.

S. Dubowsky and D. L. Des Forges. The application of model-referenced adaptive control to robotic manipulators. *ASME J. of Dynamic Systems, Measurement and Control*, 101, 1979.

A. Fahim and M. P. Fernandez. Performance enhancement of robot arms through active counterbalancing. *The Int. J. of Advanced Manufacturing Technology*, 3(4), 1988.

O. D. Faugeras and G. Giralt, editors. *Robotics Research: The 3rd Int. Symp.* MIT Press, 1986.

R. Featherstone. The calculation of robot dynamics using articulated-body inertias. *The Int. J. of Robotics Research*, 2(1), 1983.

M. P. Fernandez. *Active Counterbalancing of Robot Arms.* Master's thesis, University of Ottawa, 1987.

J. B. Fraleigh and R. A. Beauregard. *Linear Algebra.* Addison-Wesley, 1987.

H. Goldstein. *Classical Mechanics.* Addison-Wesley, 1959.

A. Gosiewski. Dynamic interactions in 3-main-axes-robot and their influence on cp control. In *Proc. IFAC /IFIP/IMACS 1st Symp. on Theory of Robots, Austria*, 1986.

T. J. Graettinger and B. H. Krogh. The acceleration radius: a global performance measure for robotic manipulators. *IEEE J. of Robotics and Automation*, 4(1), 1988.

D. T. Greenwood. *Principles of Dynamics.* Prentice-Hall, 1965.

Y. F. Gvozdev. New balancing mechanisms for the links of manipulator arms. *Soviet Engineering Research*, 3(8), 1983.

H. Hanafusa and H. Inoue, editors. *Robotics Research: The 2nd Int. Symp.* MIT Press, 1985.

J. M. Hollerbach. Dynamic scaling of manipulator trajectories. *ASME J. of Dynamic Systems, Measurement and Control*, 106, 1984.

J. M. Hollerbach. Dynamics. In M. Brady et al., editors, *Robot Motion Planning and Control*, MIT Press, 1984.

M. Javid and P. M. Brown. *Field Analysis and Electromagnetics.* McGraw-Hill, 1963.

G. Jumarie. On the use of time-varying inertia links to increase the versatility of manipulators. *Robotica*, 4, 1986.

G. Jumarie. Trajectory control of manipulators with time varying inertia links. *Robotica*, 6, 1988.

H. Kawasaki and K. Nishimura. Terminal-link parameter estimation of robotic manipulators. *IEEE J. of Robotics and Automation*, 4(5), 1988.

O. Khatib. The operational space formulation in the analysis, design and control of robot manipulators. In O. D. Faugeras and G. Giralt, editors, *Proc. Robotics Research: The 3rd Int. Symp.*, MIT Press, 1986.

O. Khatib and J. Burdick. Dynamic optimization in manipulator design: the operation space formulation. In *Proc. ASME Winter Annual Meeting, Miami,*

1985.

P. K. Khosla. Categorization of parameters in the dynamic robot model. *IEEE J. of Robotics and Automation*, 5(3), 1989.

P. K. Khosla and T. Kanade. An algorithm to determine the identifiable parameters in the dynamic robot model. In *Proc. IEEE Int. Conf. on Robotics and Automation, San Francisco*, 1986.

A. Kiedrzynski and M. Becquet. Light structure modular design using honeycomb links. In *Proc. 18th Int. Symp. on Industrial Robots, Switzerland*, 1988.

H. L. Langhaar. *Energy methods in applied mechanics*. John Wiley, 1962.

K. Laroussi et al. Coordination of two planar robots in lifting. *IEEE Transactions on Robotics and Automation*, 4(1), 1988.

C.S.G. Lee. Robot arm kinematics, dynamics, and control. *Computer*, 15(12), 1982.

S. Lee. Dual redundant arm configuration optimization with task-oriented dual arm manipulability. *IEEE Transactions on Robotics and Automation*, 5(1), 1989.

A. Liegeois. *Robot Technology Volume 7: Performance and Computer-Aided Design*. Prentice-Hall, 1985.

A. Liegeois et al. Model-reference control of high velocity industrial robots. In *Proc. of the 1980 Joint Automatic Controls Conference, San Fransisco, Calif.*, 1980.

S. Lipschutz. *Theory and Problems of Linear Algebra.* McGraw-Hill. 1987.

J. Y. S. Luh et al. Newton-euler formulation of manipulator dynamics for computer control. In *Proc. 2nd IFAC/IFIP symposium on Information Control Problems in Manufacturing Technology, Stuttgart, W Germany*, 1979.

M. T. Mason. Compliance and force control for computer controlled manipulators. *IEEE Transactions on Systems, Man and Cybernetics*, 11(6), 1981.

M. T. Mason. On the scope of quasi-static pushing. In O. D Faugeras and G. Giralt, editors, *Proc. Robotics Research: The 3rd Int. Symp.*, MIT Press, 1986.

R. B. McQuistan. *Scalar and Vector Fields: A Physical Interpretation.* John Wiley, 1965.

L. Meirovitch. *Methods of Analytical Dynamics.* McGraw-Hill, 1970.

S. Y. Nof, editor. *Handbook of Industrial Robotics.* John Wiley, 1985.

D. E. Orin and S. Y. Oh. Control of force distribution in robotic mechanisms containing closed kinematic chains. *ASME J. of Dynamic Systems, Measurement and Control*, 102, 1981.

S. P. Patarinsky et al. Robot-balancing manipulator cooperation for handling of heavy parts. In *Proc. 15th Int. Symp. on Industrial Robots, Japan*, 1985.

A. G. Patwarkhan and A. H. Soni. Motion simulation of an articulated robotic arm subjected to static forces. *ASME J. of Mechanical Design*, 104(2), 1982.

R. P. Paul. *Robot manipulators: Mathematics, Programming and Control.* MIT Press, 1983.

E. D. Rainville and P. E. Bedient. *Elementary Differential Equations* Macmillan Pub. Co., 6 edition, 1981.

E. I. Rivin. *Mechanical Design of Robots.* McGraw-Hill, 1988.

A. Robson. *An Introduction to Analytical Geometry.* Volume 1, Cambridge University Press, 1949.

L. Rossol. Technological barriers in robotics: a perspective from industry. In M. Brady and R. P. Paul, editors, *Proc. Robotics Research: The 1st Int. Symp.*, MIT Press, 1984.

B. Roth. Control and mechanics of simple manipulator systems. In H. Hanafusa and H. Inoue, editors, *Proc. Robotics Research: The 2nd Int. Symp.*, MIT Press, 1985.

B. Roth. Overview on advanced robotics: manipulation. In *Proc. Int. Conf. on Advanced Robotics, Japan*, 1985.

B. Roth. Robots: state of the art in regard to mechanism theory. *ASME J. of Mech., Trans. and Automation in Design*, 105, 1983.

Gompertz R. S. and Yang D. C. H. Feasibility evaluation of dynamically linearized kinematically redundant planar manipulators. In *1989 IEEE Int. Conf. on Robotics and Automation*, 1989.

J. K. Salisbury and J. J. Craig. Articulated hands: force control and kinematic issues. *The Int. J. of Robotics Research*, 1(1), 1982.

F. E. Saner. *PITTMAN Servo Motor Application Notes.* PITTMAN Co., Harleysville, PA 19438, 1987.

H. M. Schey. *Div, Grad, Curl, and All That: An Informal Text on Vector Calculus.* W. W. Norton and Co. Inc., NY, 1973.

W. P. Seering. Directions on robot design. *ASME J. of Mech., Trans. and Automation in Design*, 105, 1983.

M. Shahinpoor. *A Robot Engineering Textbook.* Harper and Row, NY, 1987.

J. G. Simmonds. Moment potentials. *American J. of Physics*, 52(9), 1984.

I. S. Sokolnikoff and R. M. Redheffer. *Mathematics of Physics and Modern Engineering.* McGraw-Hill, 1958.

G. Strang. *Linear Algebra and its Applications.* Academic Press, 1976.

K. M. W. Tang and V. D. Tourassis. Systematic simplification of dynamic robot models. In *Proc. of the Midwest Symp. on Circuits and Systems, Syracuse, N.Y.*, 1987.

M. Thomas and D. Tesar. Dynamic modelling of serial manipulator arms. *ASME J. of Dynamic Systems, Measurement and Control*, 104, 1982.

M. Togai. Manipulability and sensitivity for design and evaluation of industrial robots: kinematic consideration. In *Proc. 15th Int. Symp. on Industrial Robots, Japan*, 1985.

V. D. Tourassis. Principles and design of model-based controllers. *Int. J. of Control*, 47(5), 1988.

V. D. Tourassis. Robot dynamic emulation. In M. Jamshidi et al., editors, *Robotics and Manufacturing: Recent Trends in Research, Education, and Applications*, ASME Press, 1988.

V. D. Tourassis and C. P. Neuman. The inertial characteristics of dynamic robot models. *Mechanism and Machine Theory*, 20(1), 1985.

C. O. Tuckey and W. Armistead. *Coordinate Geometry*, Longmans Green and Co, 1953.

M. Uchiyama et al. Performance evaluation of manipulators using the jacobian and its application to trajectory planning. In H. Hanafusa and H. Inoue, editors, *Proc. Robotics Research: The 2nd Int. Symp.*, MIT Press, 1985.

P. B. Usoro et al. Control of lightweight flexible manipulators: a feasibility study. In *Proc. American Control Conference, San Diego*, 1984.

P. B. Usoro et al. A finite element/lagrange approach to modelling lightweight flexible manipulators. *ASME J. of Dynamic Systems, Measurement and Control*, 108, 1986.

K. Wang and T. K. Lien. Structure design and kinematics of a robot manipulator. *Robotica*, 6(4), 1988.

L. T. Wang and B. Ravani. Dynamic load carrying capacity of mechanical manipulators - part i : problem formulation. *ASME J. of Dynamic Systems, Measurement and Control*, 110(1), 1988.

L. T. Wang and B. Ravani. Dynamic load carrying capacity of mechanical

manipulators - part ii : computational procedure and applications. *ASME J. of Dynamic Systems, Measurement and Control*, 110(1), 1988.

H. West and H. Asada. Kinematic analysis and mechanical advantage of manipulators constrained by contact with the environment. In *Proc. ASME Winter Annual Meeting, Miami*, 1985.

H. West and H. Asada. A method for the control of robot arms constrained by contact with the environment. In *Proc. American Control Conference, Boston*, 1985.

D. E. Whitney. Historical perspectives and state of the art in robot force control. In *Proc. IEEE Int. Conf. Robotics and Automation, St. Louis*, 1985.

D. C. H. Yang and S. W. Tzeng. Simplification and linearization of manipulator dynamics by the design of inertia distribution. *The Int. J. of Robotics Research*. 5(3), 1986.

T. Yoshikawa. Analysis and control of robot manipulators with redundancy. In *Proc. Int. Symp. Robotics Research, Bretton Woods, NH*, 1983.

T. Yoshikawa. Analysis and design of articulated robot arms from the viewpoint of dynamic manipulability. In O. D. Faugeras and G. Giralt, editors, *Proc. Robotics Research: The 3rd Int. Symp.*, MIT Press, 1986.

T. Yoshikawa. Dynamic manipulability of articulated robot arms. In *Proc. 15th Int. Symp. on Industrial Robots, Japan*, 1985.

T. Yoshikawa. Dynamic manipulability of robot mechanisms. In *Proc. IEEE Int. Conf. Robotics and Automation, St. Louis*, 1985.

T. Yoshikawa. Manipulability of robotic mechanisms. In H. Hanafusa and H. Inoue, editors, *Proc. Robotics Research: The 2nd Int. Symp.*, MIT Press, 1985.

T. Yoshikawa. Manipulability of robotic mechanisms. *The Int. J. of Robotics Research*, 4(2), 1985.

K. Youcef-Toumi and H. Asada. The design of arm linkages with decoupled and configuration-invariant inertia tensors. In *Proc. ASME Winter Annual Meeting, Symp. on Robotics and Manufacturing Automation, Miami*, 1985.

K. Youcef-Toumi and H. Asada. The design of open-loop manipulator arms with decoupled and configuration-invariant inertia tensors. *ASME J. of Dynamic Systems, Measurement and Control*, 109(3), 1987.

Appendix A

Specifications of the PUMA Robot

LINK .	L (m)	h (m)	m - (kg)	I_{xx} (kgm^2)	I_{yy} (kgm^2)	I_{zz} (kgm^2)
1	0.5	0.2	20.0	1.0	0.4	1.0
2	0.5	0.2	20.0	0.5	1.4	1.2
3	0.7	0.3	15.0	1.0	1.0	0.3
4	0.2	0.1	2.0	0.2	0.2	0.2
5	0.2	0.0	1.0	0.1	0.1	0.1
6	0.2	0.1	1.0	0.15	0.15	0.1

Table A.1: Physical properties of the links.

JOINT	$\theta_i(deg)$	$a_i(m)$	$d_i(m)$	$\alpha_i(deg)$
1	θ_1	0.0	0.0	−90.0
2	θ_2	0.5	0.2	0.0
3	θ_3	0.0	0.0	90.0
4	θ_4	0.0	0.7	−90.0
5	θ_5	0.0	0.0	90.0
6	θ_6	0.0	0.1	0.0

Table A.2: Link parameters of the PUMA manipulator

JOINT	1	2	3	4	5	6
UPPER BOUND(deg)	160	45	225	170	100	266
LOWER BOUND(deg)	-160	-225	-45	-110	-100	-266
MAX SPEED(r/s)	2.1	2.1	2.1	2.1	2.1	2.1

Table A.3: Limits of the joint angles and joint speeds.

Appendix B

Recursive Newton-Euler Equations

B.1 Kinematics

The absolute acceleration of a particle P whose motion is monitored by a viewer fixed in a noninertial reference frame R is given by

$$\mathbf{a}_P = \mathbf{a}_O + \dot{\Omega}\times\mathbf{r} + \Omega\times(\Omega\times\mathbf{r}) + \ddot{\mathbf{r}} + 2\Omega\times\dot{\mathbf{r}} \tag{B.1}$$

where

$\mathbf{a}_P$ = Absolute acceleration of the particle.

$\mathbf{a}_O$ = Absolute acceleration of the point O fixed in R.

Ω = Absolute angular velocity of frame R.

$\dot{\Omega}$ = Absolute angular acceleration of frame R.

$\mathbf{r}$ = Position vector of the particle with respect to point O.

$\dot{\mathbf{r}}$ = Velocity of the particle with respect to frame R.

$\ddot{\mathbf{r}}$ = Acceleration of the particle with respect to R.

The above equation can be used to obtain the acceleration of center of mass of the links of robot arms. Figure B.1 shows the schematic diagram of three successive links of a typical revolute manipulator. In that figure $\mathbf{P}_i$ represents the position vector of the origin of the frame i with respect to the origin of the frame $i-1$, and $\mathbf{U}_i$ represents the position vector of the C.M. of link i with respect to the origin of frame i. A coordinate system is rigidly attached to each link and numbered accordingly.

Denoting the absolute angular velocity of the links i and $i-1$ by $\mathbf{\Omega}_i$ and $\mathbf{\Omega}_{i-1}$ respectively, the following relation is true

$$\mathbf{\Omega}_i = \mathbf{\Omega}_{i-1} + \dot{\theta}_i \mathbf{k}_{i-1} \tag{B.2}$$

where $\dot{\theta}_i$ represents the angular velocity of the link i with respect to frame $i-1$ and k_{i-1} is the unit vector along the z axis of the coordinate system $i-1$. This equation can be expressed in frame i as

$$\left\{\Omega_i\right\} = \begin{bmatrix} R_i \end{bmatrix}^T \left(\left\{\Omega_{i-1}\right\} + \begin{Bmatrix} 0 \\ 0 \\ \dot{\theta}_i \end{Bmatrix} \right) \tag{B.3}$$

where $[R_i]^T$ represents the transpose of the 3×3 transformation matrix that relates the frame i to frame $i-1$.

Denoting the absolute angular acceleration of the links i and $i-1$ by $\dot{\mathbf{\Omega}}_i$ and $\dot{\mathbf{\Omega}}_{i-1}$ respectively, the absolute angular acceleration of link i can be expressed as

$$\dot{\mathbf{\Omega}}_i = \dot{\mathbf{\Omega}}_{i-1} + \ddot{\theta}_i \mathbf{k}_{i-1} + \mathbf{\Omega}_{i-1} \times \dot{\theta}_i \mathbf{k}_{i-1} \tag{B.4}$$

where $\ddot{\theta}_i$ represents the angular acceleration of the link i with respect to the frame $i-1$.

Equation B.4 can be expressed in frame i as

$$\left\{\dot{\Omega}_i\right\} = \begin{bmatrix} R_i \end{bmatrix}^T \left(\left\{\dot{\Omega}_{i-1}\right\} + \begin{Bmatrix} 0 \\ 0 \\ \ddot{\theta}_i \end{Bmatrix} + \left\{\Omega_{i-1}\right\} \times \begin{Bmatrix} 0 \\ 0 \\ \dot{\theta}_i \end{Bmatrix} \right) \tag{B.5}$$

It is convenient to transform the vector cross product on the right hand side of Equation B.5 into a product of two matrices. The cross product of the two vectors A and B can be expressed in matrix form as

$$\mathbf{A} \times \mathbf{B} = \begin{bmatrix} 0 & -A_z & A_y \\ A_z & 0 & -A_x \\ -A_y & A_x & 0 \end{bmatrix} \begin{Bmatrix} B_x \\ B_y \\ B_z \end{Bmatrix}$$

or in a more compact form as

$$\mathbf{A} \times \mathbf{B} = \left[dev\mathbf{A} \right] \left\{ \mathbf{B} \right\} \tag{B.6}$$

where $[dev\mathbf{A}]$ represents the vector A developed into a 3×3 matrix. As a result, Equation B.5 can be expressed as

$$\left\{\dot{\Omega}_i\right\} = \begin{bmatrix} R_i \end{bmatrix}^T \left(\left\{\dot{\Omega}_{i-1}\right\} + \begin{Bmatrix} 0 \\ 0 \\ \ddot{\theta}_i \end{Bmatrix} + \left[dev\Omega_{i-1} \right]^T \begin{Bmatrix} 0 \\ 0 \\ \dot{\theta}_i \end{Bmatrix} \right) \tag{B.7}$$

In order to find the acceleration of C.M. of link i, first it is necessary to find the acceleration of the origin of frame i. This can be done by making use of Equation B.1 and realising, from Figure B.1, the fact that $\mathbf{r} = \mathbf{P} = const.$, i.e. $\dot{\mathbf{r}} = \ddot{\mathbf{r}} = 0$. Substituting for these quantities in Equation B.1 yields

$$\dot{\mathbf{V}}_i = \dot{\mathbf{V}}_{i-1} + \dot{\Omega}_i \times \mathbf{P}_i + \Omega_i \times (\Omega_i \times \mathbf{P}_i)$$

Transferring $\dot{\mathbf{V}}_{i-1}$ to frame i and expressing the cross products of the above equation in matrix form leads to

$$\left\{\dot{\mathbf{V}}_i\right\} = \left[\ R_i\ \right]^T \left\{\dot{\mathbf{V}}_{i-1}\right\} + \left[dev\dot{\Omega}_i\right]\left\{\mathbf{P}_i\right\} + \left[dev\Omega_i\right]\left[dev\Omega_i\right]\left\{\mathbf{P}_i\right\} \qquad \text{(B.8)}$$

This equation can be expressed in a more compact form by introducing a grouping matrix $[\Delta_i]$ defined as

$$\left[\ \Delta_i\ \right] = \left[dev\dot{\Omega}_i\right] + \left[dev\Omega_i\right]^2 \qquad \text{(B.9)}$$

Equation B.8 thus becomes

$$\left\{\dot{\mathbf{V}}_i\right\} = \left[\ R_i\ \right]^T \left\{\dot{\mathbf{V}}_{i-1}\right\} + \left[\ \Delta_i\ \right]\left\{\mathbf{P}_i\right\} \qquad \text{(B.10)}$$

The acceleration of the center of mass of the link i can now be expressed as

$$\mathbf{a}_i = \dot{\mathbf{V}}_i + \dot{\Omega}_i \times \mathbf{U}_i + \Omega_i \times (\Omega_i \times \mathbf{U}_i)$$

or in matrix form as

$$\left\{\mathbf{a}_i\right\} = \left\{\dot{\mathbf{V}}_i\right\} + \left[\ \Delta_i\ \right]\left\{\mathbf{U}_i\right\} \qquad \text{(B.11)}$$

B.2 Kinetics

According to Newton's second law, the equation of motion of the center of mass of a rigid body is

$$\mathbf{F} = m\mathbf{a} \qquad \text{(B.12)}$$

where m is mass of the body, a represents the absolute acceleration of the center of mass of the body, and $\mathbf{F}$ is the sum of the external forces acting on the body.

Assuming the coordinate system C be rigidly attached to the body with its origin at the center of mass of the body, the equation of rotational motion of the body can by given as

$$\left\{\mathbf{N}\right\} = \left[\ \mathbf{I}\ \right]\left\{\dot{\boldsymbol{\Omega}}\right\} + \left\{\boldsymbol{\Omega}\right\} \times \left(\left[\ \mathbf{I}\ \right]\left\{\boldsymbol{\Omega}\right\}\right) \tag{B.13}$$

In this relation

$\mathbf{I}$ = Tensor of inertia of the body with respect to C.

$\boldsymbol{\Omega}$ =Absolute angular velocity of the body defined in C.

$\dot{\boldsymbol{\Omega}}$ =Absolute angular acceleration of the body defined in C.

$\mathbf{N}$ =Sum of the external torques and the moments of the external forces about the C.M. of the body, also defined in C.

Figure B.2 shows the free body diagram of the link i. In this figure $\mathbf{f}_i$ and $\mathbf{n}_i$ represent the force and the torque applied by the link $i-1$ to the link i. Similarly, $\mathbf{f}_{i+1}$ and $\mathbf{n}_{i+1}$ represent the force and the torque applied by link i to the link $i+1$. The total external force acting on the body becomes[1]

$$\mathbf{F}_i = \mathbf{f}_i - \mathbf{f}_{i+1}$$

[1]It is convenient to exclude the effect of gravity from the freebody diagram and include the acceleration of gravity in the absolute acceleration of the link zero. See for example Luh et al. (1979)

Transferring $\mathbf{f}_{i+1}$ to frame i and rearranging yields

$$\left\{\mathbf{f}_i\right\} = \begin{bmatrix} \\ R_i \\ \\ \end{bmatrix}^T \left\{\mathbf{f}_{i+1}\right\} + \left\{\mathbf{F}_i\right\} \tag{B.14}$$

Taking the moment of the forces about the center of mass of the body, the total external torque acting on the body can be expressed as

$$\mathbf{N}_i = \mathbf{n}_i - \mathbf{n}_{i+1} - (\mathbf{P}_i + \mathbf{U}_i) \times \mathbf{f}_i - \mathbf{U}_i \times (-\mathbf{f}_{i+1})$$

Transferring $\mathbf{f}_{i+1}$ and $\mathbf{n}_{i+1}$ to frame i, substituting for $\mathbf{f}_i$ from Equation B.14, and rearranging gives

$$\left\{\mathbf{n}_i\right\} = \begin{bmatrix} \\ R_i \\ \\ \end{bmatrix}^T \left\{\mathbf{n}_{i+1}\right\} + \left[dev\mathbf{P}_i\right] \begin{bmatrix} \\ R_i \\ \\ \end{bmatrix}^T \left\{\mathbf{f}_{i+1}\right\} + \left[dev\mathbf{Q}_i\right] \left\{\mathbf{F}_i\right\} + \left\{\mathbf{N}_i\right\} \tag{B.15}$$

where $\mathbf{Q}_i = \mathbf{P}_i + \mathbf{U}_i$.

The torque applied by the ith actuator can be found from

$$\tau_i = \left\{\mathbf{n}_i\right\}^T \begin{bmatrix} \\ R_i \\ \\ \end{bmatrix}^T \begin{Bmatrix} 0 \\ 0 \\ 1 \end{Bmatrix} \tag{B.16}$$

B.3 Summary of Equations

1- FORWARD EQUATIONS $i = 1, 2, ..., n$

Angular velocity of link i

$$\left\{\Omega_i\right\} = \left[\ R_i\ \right]^T \left(\left\{\Omega_{i-1}\right\} + \left\{ \begin{matrix} 0 \\ 0 \\ \dot{\theta}_i \end{matrix} \right\} \right)$$

Angular acceleration of link i

$$\left\{\dot{\Omega}_i\right\} = \left[\ R_i\ \right]^T \left(\left\{\dot{\Omega}_{i-1}\right\} + \left\{ \begin{matrix} 0 \\ 0 \\ \ddot{\theta}_i \end{matrix} \right\} + \left\{dev\Omega_{i-1}\right\} \left\{ \begin{matrix} 0 \\ 0 \\ \dot{\theta}_i \end{matrix} \right\} \right)$$

grouping matrix

$$\left[\ \Delta_i\ \right] = \left[dev\dot{\Omega}_i\right] + \left[dev\Omega_i\right]^2$$

Acceleration of the origin of frame i

$$\left\{\dot{\mathbf{V}}_i\right\} = \left[\ R_i\ \right]^T \left\{\dot{\mathbf{V}}_{i-1}\right\} + \left[\ \Delta_i\ \right] \left\{\mathbf{P}_i\right\}$$

Acceleration of the center of mass of link i

$$\left\{\mathbf{a}_i\right\} = \left\{\dot{\mathbf{V}}_i\right\} + \left[\ \Delta_i\ \right] \left\{\mathbf{U}_i\right\}$$

Total external force acting on link i

$$\left\{\mathbf{F}_i\right\} = m_i\left\{\mathbf{a}_i\right\}$$

Total external torque acting on link i

$$\left\{\mathbf{N}_i\right\} = \left[\begin{array}{c} I_i \end{array}\right]\left\{\dot{\Omega}_i\right\} + \left[dev\Omega_i\right]\left[\begin{array}{c} I_i \end{array}\right]\left\{\Omega_i\right\}$$

2- BACKWARD EQUATIONS $\quad i = n, n-1, \ldots, 1$

Total force applied by link $i-1$ to link i

$$\left\{\mathbf{f}_i\right\} = \left[\begin{array}{c} R_i \end{array}\right]^T\left\{\mathbf{f}_{i+1}\right\} + \left\{\mathbf{F}_i\right\}$$

Total torque applied by link $i-1$ to link i

$$\left\{\mathbf{Q}_i\right\} = \left\{\mathbf{P}_i\right\} + \left\{\mathbf{U}_i\right\}$$

$$\left\{\mathbf{n}_i\right\} = \left[\begin{array}{c} R_i \end{array}\right]^T\left\{\mathbf{n}_{i+1}\right\} + \left[dev\mathbf{P}_i\right]\left[\begin{array}{c} R_i \end{array}\right]^T\left\{\mathbf{f}_{i+1}\right\} + \left[dev\mathbf{Q}_i\right]\left\{\mathbf{F}_i\right\} + \left\{\mathbf{N}_i\right\}$$

Torque applied by the actuator on link i

$$\tau_i = \left\{\mathbf{n}_i\right\}^T\left[\begin{array}{c} R_i \end{array}\right]^T\left\{\begin{array}{c} 0 \\ 0 \\ 1 \end{array}\right\}$$

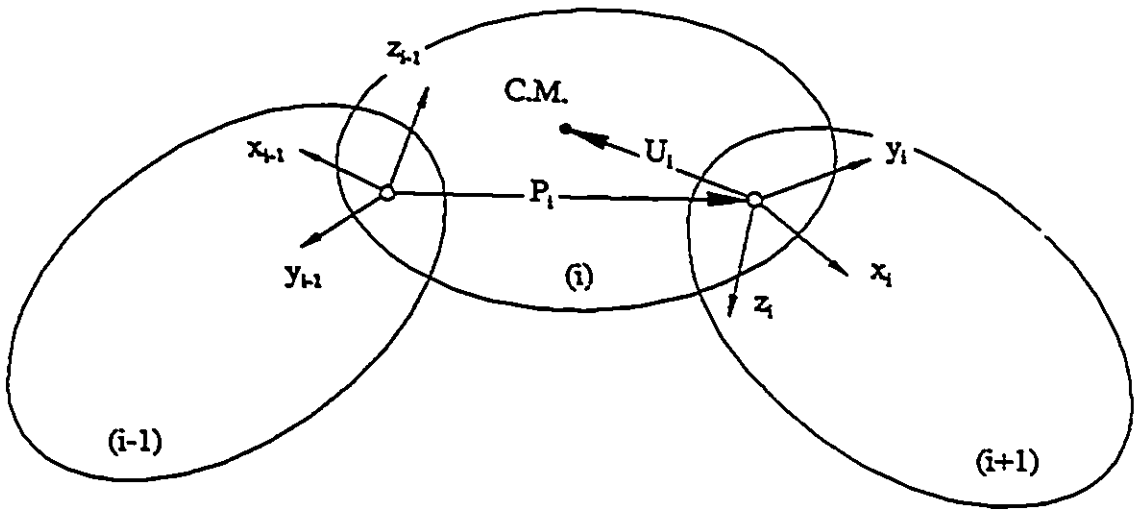

Figure B.1: Three successive links of a revolute manipulator.

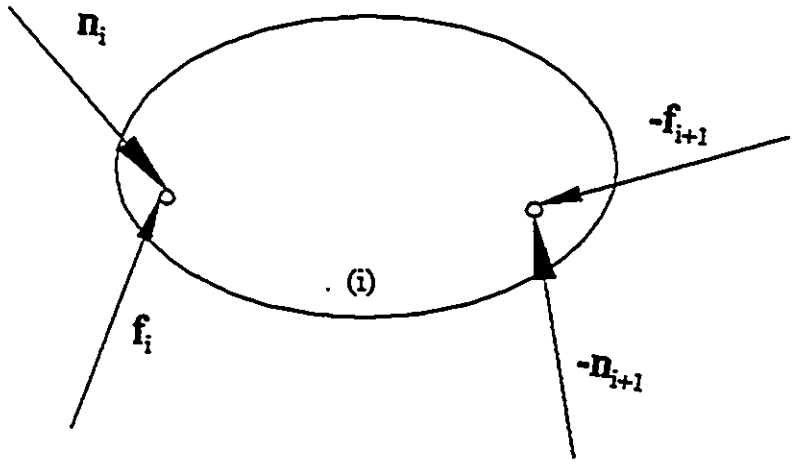

Figure B.2: Free body diagram of link i

Appendix C

Serial Drive and Parallel Drive Arms

Manipulators with revolute primary links are categorized as serial drive or parallel drive depending on the type of the mechanism with which the torque is applied to their links. If the reaction torques cascade down to the base from one motor to the next, the manipulator is referred to as serial drive. On the other hand if the reaction torque of the joint motors is somehow directly transmitted to the ground then the manipulator is called parallel drive. In either case it is possible to select the joint coordinates either with respect to an inertial reference frame as shown in Figure C.1 or with respect to a frame attached to the previous link as Figure C.2 illustrates. However, care must be taken in selection of the joint coordinates such that the relation

$$\tau_i = \frac{\partial U}{\partial \theta_i} \tag{C.1}$$

is satisfied. In this equation τ_i is the joint torque due the effect of gravity, U represents the total gravitational potential energy and θ_i is the corresponding joint coordinate. The following classification clarifies the difference between the various selections.

C.1 Links orientation measured with respect to an inertial frame

The total potential energy for the arm of the Figure C.1 can be expressed as

$$U = A_1 sin\theta_1 + A_2 sin\theta_2$$

where A_1 and A_2 are given by the Equation 3.2.

Partial differentiation of the above equation with respect to θ_1 and θ_2 gives

$$\begin{cases} \frac{\partial U}{\partial \theta_1} = A_1 cos\theta_1 \\ \frac{\partial U}{\partial \theta_2} = A_2 cos\theta_2 \end{cases} \tag{C.2}$$

Referring to the Figure C.3 the joint torques for the serial drive arm can be obtained as

$$\begin{cases} \tau_{1ser} = A_1 cos\theta_1 + A_2 cos\theta_2 \\ \tau_{2ser} = A_2 cos\theta_2 \end{cases} \tag{C.3}$$

For the parallel drive arm the joint torques can be found from Figure C.4 as

$$\begin{cases} \tau_{1par} = A_1 cos\theta_1 \\ \tau_{2par} = A_2 cos\theta_2 \end{cases} \tag{C.4}$$

Comparing Equations C.3 and C.4 with Equation C.2 reveals that for the present selection of joint coordinates the serial drive arm invalidates Equation C.1. However, from the kinematics point of view this selection is advantageous as the trace of the matrix JJ^T can be shown to be independent of the configuration of the arm for both serial and parallel drive arms.

$$\left[\begin{array}{c} \mathbf{J} \end{array}\right] = \left[\begin{array}{cc} -L_1 sin\theta_1 & -L_2 sin\theta_2 \\ L_1 cos\theta_1 & L_2 cos\theta_2 \end{array}\right]$$

$$\left[\begin{array}{c} \mathbf{JJ^T} \end{array}\right] = \left[\begin{array}{cc} sin^2\theta_1 + sin^2\theta_2 & -sin\theta_1 cos\theta_1 + sin\theta_2 cos\theta_2) \\ -sin\theta_1 cos\theta_1 + sin\theta_2 cos\theta_2) & cos^2\theta_1 + cos^2\theta_2 \end{array}\right]$$

The trace of the above matrix is 2.

C.2 Links orientation measured with respect to previous links

Referring to Figure C.2 the potential function for this case can be written as

$$U = A_1 sin\theta_1 + A_2 sin(\theta_1 + \theta_2)$$

therefore

$$\begin{cases} \frac{\partial U}{\partial \theta_1} = A_1 cos\theta_1 + A_2 cos(\theta_1 + \theta_2) \\ \frac{\partial U}{\partial \theta_2} = A_2 cos(\theta_1 + \theta_2) \end{cases} \tag{C.5}$$

Referring to Figure C.3 the joint torques for the serial drive arm can be expressed as

$$\begin{cases} \tau_{1ser} = A_1 cos\theta_1 + A_2 cos(\theta_1 + \theta_2) \\ \tau_{2ser} = A_2 cos(\theta_1 + \theta_2) \end{cases} \tag{C.6}$$

For the parallel drive arm the Figure C.4 can be used to obtain the joint torques as

$$\begin{cases} \tau_{1p} = A_1 cos\theta_1 \\ \tau_{2p} = A_2 cos(\theta_1 + \theta_2) \end{cases} \tag{C.7}$$

Comparison of Equations C.6 and C.7 with Equation C.1 shows that for the present choice of the joint coordinates the parallel drive arm invalidates the Equation C.1. The trace of the matrix JJ^T in this case is a function of the configuration irrespective of the type of the arm's drive.

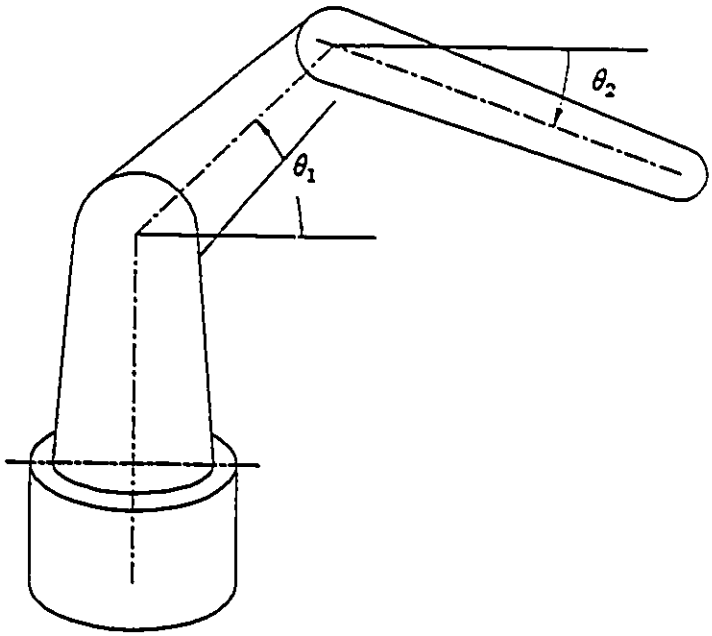

Figure C.1: Joint coordinates when the orientation of each link is meaured with respect to an inertial frame.

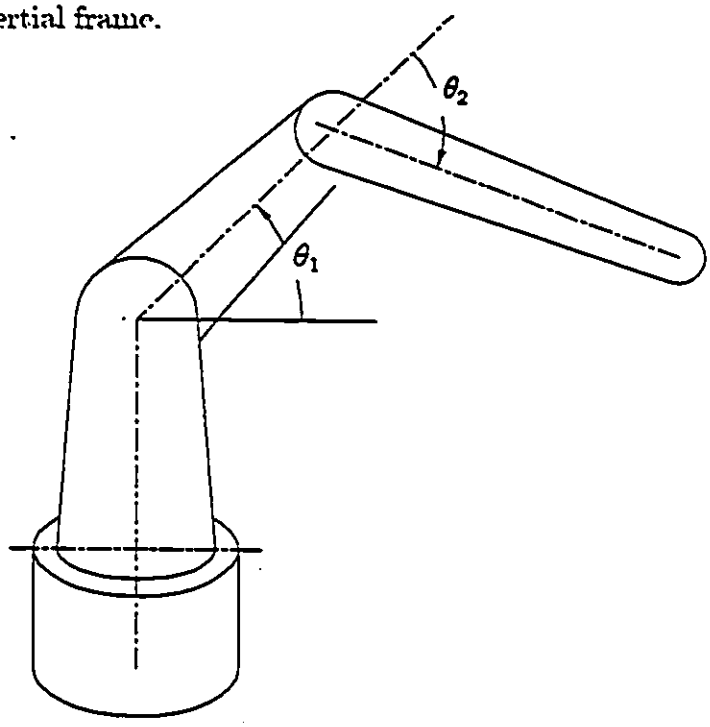

Figure C.2: Joint coordinates when the orintation of each link is measured with respect to the previous link.

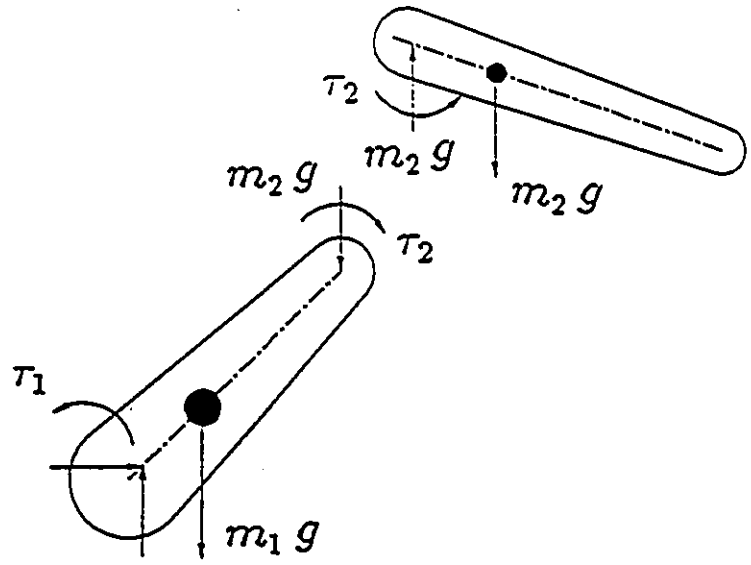

Figure C.3: Free body diagram of the links for a serial drive arm.

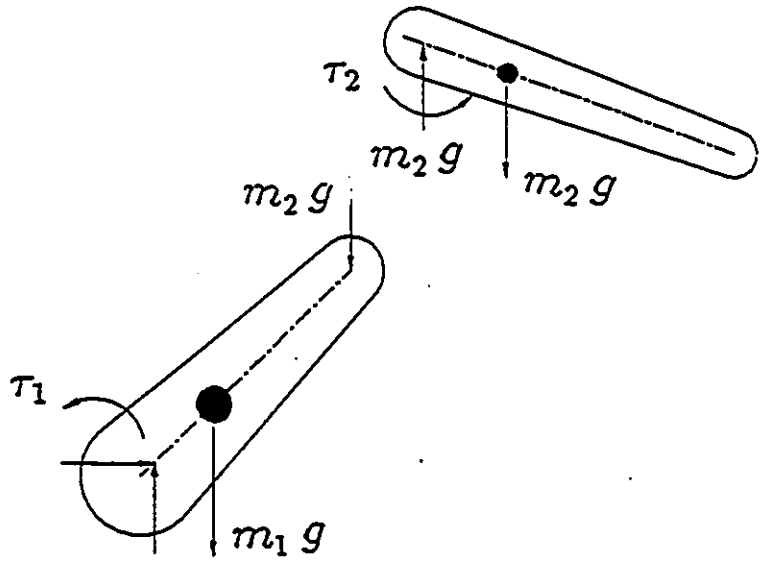

Figure C.4: Free body diagram of the links for a parallel drive arm.

Appendix D

Orientation of the Ellipsoids with Respect to the Arm

The aim of this appendix is to derive the conditions under which the three ellipsoids introduced in the text, i.e. the force ellipsoid, the generalized ellipsoid of inertia, and the acceleration ellipsoid, maintain their orientation with respect to the manipulator along the circumference of the solid configuration circles. Figure D.1 shows the schematic diagram of a manipulator and a dummy ellipsoid with defining matrix **Z** which may represent any of the three ellipsoids. As it can be seen in that figure, the angle β that determines the orientation of the dummy ellipsoid with respect to the manipulator may be expressed as:

$$\beta = \phi_Z - \theta_2$$

where ϕ_Z is the angle that the major axis of the ellipsoid makes with the horizontal. The orientation of the dummy ellipsoid with respect to the manipulator will remain

unchanged if $\frac{\partial\beta}{\partial\theta_1}$ (or $\frac{\partial\beta}{\partial\theta_2}$) vanish. Differentiating both sides of the above equation with respect to θ_1 gives

$$\frac{\partial\beta}{\partial\theta_1} = \frac{\partial\phi_Z}{\partial\theta_1} - \frac{\partial\theta_2}{\partial\theta_1}$$

Setting the left hand side of the last equation equal to zero leads to

$$\frac{\partial\phi_Z}{\partial\theta_1} - \frac{\partial\theta_2}{\partial\theta_1} = 0 \tag{D.1}$$

On the other hand, along the circumference of the solid configuration circles

$$\theta_1 - \theta_2 = const.$$

From the above equation it can be seen that $\frac{\partial\theta_2}{\partial\theta_1} = 1$. Substituting this in Equation D.1 yields

$$\frac{\partial\phi_Z}{\partial\theta_1} = 1 \tag{D.2}$$

The normalized eigenvectors of the matrix $\mathbf{Z}$ are given as the column vectors of the following matrix

$$\begin{bmatrix} 1 & \frac{\xi_2 - Z_{22}}{Z_{21}} \\ \frac{\xi_1 - Z_{11}}{Z_{12}} & 1 \end{bmatrix}$$

where ξ_1 and ξ_2 represent the eigenvalues of $\mathbf{Z}$. The angle ϕ_Z can therefore be given as

$$\phi_Z = tan^{-1}\left(\frac{\xi_1 - Z_{11}}{Z_{12}}\right) \tag{D.3}$$

Differentiating with respect to θ_1 and combining the results with Equation D.2 gives

$$\xi_1^2 - \left(2Z_{11} - \frac{\partial Z_{12}}{\partial \theta_1}\right)\xi_1 + Z_{11}^2 + Z_{12}^2 - Z_{11}\frac{\partial Z_{12}}{\partial \theta_1} + Z_{12}\frac{\partial Z_{11}}{\partial \theta_1} = 0 \qquad \text{(D.4)}$$

On the other hand, the eigenvalues of the matrix $\mathbf{Z}$ can be found from its charachteristic equation. Setting the determinant of the matrix $[\mathbf{Z} - \xi\mathbf{I}]$ equal to zero gives the characteristic equation of the matrix $\mathbf{Z}$ as

$$\xi^2 - (Z_{11} + Z_{22})\xi + Z_{11}Z_{22} - Z_{12}^2 = 0 \qquad \text{(D.5)}$$

Equations D.4 and D.5 will have identical roots if the coefficients of their corresponding terms are equal. Equating the coefficients and rearranging the resulting equations gives the conditions under which the orientation of the dummy ellipsoid is insensitive to variations of θ_1 or θ_2 as

$$\frac{\partial Z_{11}}{\partial \theta_1} = -2Z_{12}$$
$$\frac{\partial Z_{12}}{\partial \theta_1} = Z_{11} - Z_{12}$$

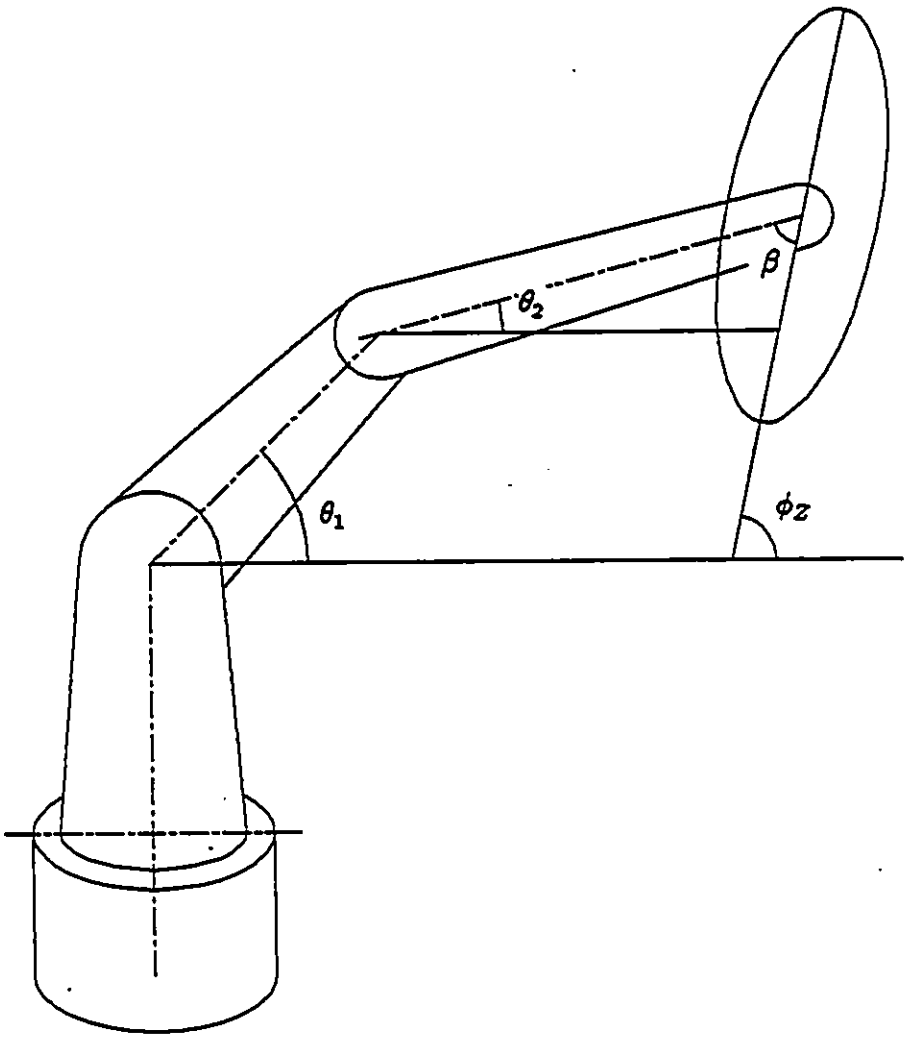

Figure D.1: Orientation of the dummy ellipsoid with respect to the arm.